

OIL RETENTION AND ITS EFFECTS ON PRESSURE DROP AND HEAT TRANSFER IN
MICROCHANNEL EVAPORATORS OF AIR CONDITIONING AND REFRIGERATION
SYSTEMS

By

SARATH KUMAR MULUGURTHI

Bachelor of Technology in Mechanical Engineering

Vellore Institute of Technology

Vellore, India

2008

Submitted to the Faculty of the
Graduate College of the
Oklahoma State University
in partial fulfillment of
the requirements for
the Degree of
MASTER OF SCIENCE
December, 2015

OIL RETENTION AND ITS EFFECTS ON PRESSURE DROP AND HEAT TRANSFER IN
MICROCHANNEL EVAPORATORS OF AIR CONDITIONING AND REFRIGERATION
SYSTEMS

Thesis Approved:

Dr. Lorenzo Cremaschi

Thesis Adviser

Dr. Christian Bach

Dr. Daniel Fisher

ACKNOWLEDGEMENT

Master's thesis was one of the challenging journeys I have ever faced in my life. First, I would like to express the deepest appreciation to my Thesis Adviser Dr. Lorenzo Cremaschi for giving me an opportunity to work under him in this research. Without his guidance, and help this research would not have been possible.

I would like to thank my committee members, Dr. Christian Bach and Dr. Daniel Fisher for their support and advice. I would also like to thank Ardiyansyah Yatim, Stefano Dell'orto, and Carlo Andres who helped me with this research work for construction of various setup, experiments, and Data analysis. I would also like to thank my friends Pedro Perez, Jeremy Smith, Xiaoxiao Wu, Thiam Wong, Gennaro Criscuolo, Andrea Bigi, Ellyn Harges for helping in the lab for training, construction, troubleshooting and all the fun we had together last two years. Special thanks to Gary Thacker, the ATRC building manager, for spending time and effort in the electronic and safety connections.

Last but not least, I would like thank Catherine Kinast, my best friend whose support and motivation during my ups and downs helped me to move forward in this research. Most of all, I am fully indebted to my family for their patience, enthusiasm, and encouragement and for pushing me farther than I thought I could go.

Name: SARATH KUMAR MULUGURTHI

Date of Degree: DECEMBER, 2015

Title of Study: OIL RETENTION AND ITS EFFECTS ON PRESSURE DROP AND HEAT TRANSFER IN MICROCHANNEL EVAPORATORS OF AIR CONDITIONING AND REFRIGERATION SYSTEMS

Major Field: MECHANICAL AND AEROSPACE ENGINEERING

Abstract: In Air-conditioning and Refrigeration systems, a small portion of the compressor oil circulates with the refrigerant through the cycle components. The oil circulating with the refrigerant flow retains in heat exchangers and affects its performance in terms of increased pressure losses and decreased heat transfer capacity.

The purpose of this thesis is to experimentally investigate the oil retention and its effects on heat transfer and pressure drop of refrigerants and oil mixtures in microchannel type evaporators. In this work two different louvered-fin aluminum microchannel heat exchangers were tested in evaporator mode. The refrigerants R-410A and R-134a with Polyolester (POE) were considered with oil mass fraction ranging from 0.5 wt.% to 5.5 wt.%. The tests were run at a range of saturation temperatures which was divided into two sets; one set for air-conditioning application ranging from 33 to 48°F (0.5 to 9°C) and the second set for coolers and refrigeration systems with evaporation temperature ranging from 0 to 33°F (-18 to 0.5°C). Refrigerant entered the evaporator as saturated liquid and exited as superheated vapor ranging from 5° F to 25° F (2.8°C to 13.9° C). Refrigerant mass flow rates were varied from 150 lb_m/hr to 400 lb_m/hr (0.019 kg/s to 0.05 kg/s).

The results showed that the oil retention was strongly depended on the OMF and, at same OMF and saturation temperature, the oil retention increased if the refrigerant mass flux decreased. In addition, at same inlet conditions oil retention in microchannel evaporators increased if the superheat on the outlet side increased. The oil retention volume in the microchannel evaporators was measured up to 13 % of estimated internal volume of the evaporators. The oil decreased the heat transfer rate and increased the pressure drop. Its impact was also depended on oil mass fraction and the refrigerant mass flux. The effect of oil on heat transfer capacity was insignificant for OMF less than 1 wt. %. The refrigerant-side pressure drop across the microchannel evaporators increased by 10 to 25 percent when oil was present inside the heat exchangers and the OMF was in the range of 0 to 1 wt.%.

TABLE OF CONTENT

Chapter	Page
LIST OF FIGURES	viii
1. INTRODUCTION	1
1.1 Introduction	1
1.2 Thesis Organization.....	3
2. LITERATURE REVIEW.....	5
2.1 Overview of oil circulation in air conditioning and refrigeration systems.....	5
2.2 Effect of oil on evaporators and condenser heat exchangers	6
2.3 Effect of oil on two phase evaporation, condensation, and flow pattern	9
2.4 Review of properties of refrigerant and lubricant mixtures.	11
2.5 Review of Oil return characteristics in Air-conditioning and Refrigeration systems	12
2.6 Review of Oil retention in heat exchangers, and suction lines of refrigeration and air-conditioning system.....	13
2.7 Studies of Microchannel heat exchangers and lubricant related issues in microchannel heat exchangers	19
3. OBJECTIVES	21
3.1 Objectives.....	21
3.2 Scope of thesis work.....	22
4. EXPERIMENTAL METHODOLOGY	24
4.1 Introduction	24
4.2 Microchannel Evaporators that were tested in the thesis work	25
4.3 Experimental Setup	28
4.4 Test Conditions and flow rates for the evaporators tests.....	69
4.5 Further Details of the Equipment and Instrumentation of the Experimental Facility	70
4.6 Instrumentation and Data Acquisition System	76

5. DATA REDUCTION AND UNCERTAINTY ANALYSIS.....	89
5.1 Data Reduction.....	89
5.2 Uncertainty Analysis	101
6. EXPERIMENTAL RESULTS AND DISCUSSION.....	108
6.1 Oil retention volume in the evaporators	108
6.2 Heat transfer factors (HTFs) for microchannel evaporators	127
6.3 Pressure drop factor of microchannel evaporators	141
6.4 Thermodynamic and heat transfer analysis of the experimental results of HTF for the microchannel evaporator A.....	151
6.5 Thermodynamic and heat transfer analysis of the evaporator A by using the present simulation tool in order to test several hypotheses of why of the possible increase of HTFs.....	154
7. OIL RETENTION MODEL VALIDATION.....	160
7.1 Summary of the Model for Microchannel Evaporators.....	160
7.2 Experimental Validation of the Microchannel Evaporator Model.....	161
8. CONCLUSIONS AND RECOMMENDATIONS FOR FUTURE WORK.....	166
8.1 Conclusions from the thesis work	166
8.2 Recommendations for Future Work on this Research Topic	169
NOMENCLATURE	171
APPENDICES	180
Appendix A Oil retention volume results summary.....	180
Appendix B PDF and HTF results summary.....	184

LIST OF TABLES

Table	Page
Table 4.1 Dimensions of the Microchannel Heat Exchanger-Evaporators That Were Tested in the Present Project.....	27
Table 4.2: Range of the differential pressure transducers used in the experimental setup	35
Table 4.3 Test matrix for typical air conditioning systems, water/wine coolers, vending machines and refrigeration systems	70
Table 4.4 Main equipment and sensors of the psychrometric chamber used in this project	71
Table 4.5 Specification of the components used in the oil retention tests	78
Table 4.6 Specifications of Resistance Temperature Detectors.....	81
Table 4.7 Specifications of the Thermocouples.....	81
Table 4.8 Specifications of the Absolute Pressure Transducers	83
Table 4.9 Specifications of the Differential Pressure Transducers	83
Table 4.10 Specifications of the Relative Humidity Sensors	84
Table 4.11 Specifications of the Air flow Nozzles	84
Table 4.12 Specifications of the Very Low Differential Pressure Transducers	85
Table 4.13 Specifications of the Refrigerant Mass Flow Meter	86
Table 4.14 Specifications of the Oil-Refrigerant Mixture Injection and Extraction Mass Flow Meter	87
Table 4.15 Specification of the Weighing Scale.....	88
Table 5.1 Accuracy of the main instrumentation for the project	102
Table 6.1 Legend of the letters and symbols used in the figures reporting the tests results of microchannel evaporators with R410A and POE	110
Table 6.2 Legend of the letters and symbols used in the figures reporting the tests results of microchannel evaporators with R410A and POE, for several degree of superheat	111
Table 6.3: Legend of the letters and symbols used in the figures reporting the tests results of microchannel evaporator A with R134a and POE	125
Table 6.4 Variation of the saturation temperature of the refrigerant R134a and POE oil mixture during evaporation with OMF of 0.5 and 1 wt.%	152
Table 6.5 Comparison of the simulation results and experimental data to provide some insights on the HTF and PDF for the microchannel evaporator A.....	155

LIST OF FIGURES

Figure	Page
Figure 2.1: Schematic representation of principle of the oil injection and extraction method (Lee, 2002)	15
Figure 4.1: Microchannel evaporator A (top) actual picture of the first heat exchanger, A, tested in the present project and (bottom) schematic of the heat exchanger A with refrigerant flow direction during the evaporator tests	26
Figure 4.2: Microchannel Evaporator B: (top) schematic of the heat exchanger B with refrigerant flow and air flow directions during the evaporator tests; (bottom left) schematic of the evaporator B with indication of the main dimensions and (bottom right) actual picture of the second heat exchanger, B, tested in the present work	26
Figure 4.3: Schematic of the pump-boiler based experimental setup used the study	30
Figure 4.4: Section of pump boiler loop from exit of oil separators until preheater tubes	33
Figure 4.5: Variable power preheater and constant power preheater tube heat exchangers of the pump boiler loop	33
Figure 4.6: Example of an electric heater wrapped around a refrigerant copper tube and used as preheater for the evaporator tests	34
Figure 4.7: The four differential pressure transducers installed in parallel and used in the evaporator tests	35
Figure 4.8: Photo of the position of sight glass S1 and sight glass S2 with respect to oil separators (the sight glasses S1 and S2 were used as visual aid to see when refrigerant and oil mixture layer first appears in those sight glasses)	37
Figure 4.9: Schematic view of the section near the refrigerant gear pump of the pump- boiler refrigerant loop for the low temperature tests (refrigerant R134a was redirected to a low temperature direct expansion refrigeration system before entering the gear pump)	38
Figure 4.10: Schematic of Auxiliary refrigeration booster system	40
Figure 4.11: Auxiliary low temperature refrigeration system and vertical receiver cylinder	41
Figure 4.12: Test sections and Air sampling device in front of test section	42
Figure 4.13: Thermocouple grid arrangement during Evaporator A installation	43
Figure 4.14: Air dehumidification unit and air duct setup for the low temperature test	44
Figure 4.15: Example of air dehumidification process for the low temperature tests plotted on a psychrometric chart	45
Figure 4.16: Schematic representation of oil extraction system used in present work (Deokar, 2013)	47
Figure 4.17: Infrared Image of microchannel evaporator A for one medium temperature test; this image indicates refrigerant flowing vertically from bottom to top of the heat exchanger and fairly uniform refrigerant flow distribution	49

Figure 4.18: Examples of a measurement of the time at which the oil reached the sight glass; a digital chronometer was video recorded next to the sight glass to synchronize the data (the uncertainty of the measured time was of max 2 seconds).....	51
Figure 4.19: Schematic of test section with the pump-boiler loop pipelines inside and outside of the psychrometric chamber	52
Figure 4.20: Example of time for the oil to travel along the pipeline versus OMF.....	55
Figure 4.21: Mass of oil measured when injected at the outlet of the test section ($M_{(OMF\%@outlet)}$) versus OMF and for two locations of the fight glasses.....	58
Figure 4.22: Screenshot of the Labview graphic interface DAQ displaying the psychrometric conditions of the air at the inlet of microchannel evaporator.....	59
Figure 4.23: Example of a case in which frost formation on the microchannel evaporator A occurred during the experiments (the test was interrupted, the evaporator was defrosted, and then the test was repeated in frost-less conditions).....	60
Figure 4.24: Display of the Labview graphic interface DAQ for the air blower and for the flow nozzles used to measure the air flow rate during the heat transfer experiments.....	61
Figure 4.25: Screenshot of labview DAQ real time graphic interface indicating fluctuations in flow rate after discharging refrigerant from the system	64
Figure 4.26: Sight glass that shows the flow in receiver of auxiliary loop.....	65
Figure 4.27: Comparison between oil retention measurements in the condenser by using the two equivalent experimental techniques of the present project.	67
Figure 4.28: Comparison between oil retention measurements in the condenser by using the two equivalent experimental techniques of the present project.	69
Figure 4.29: Air flow loop inside the psychrometric chamber at Oklahoma State University.....	73
Figure 4.30: Front side of the microchannel evaporator exposed to the ambient air (air flow direction is entering the heat exchanger as indicated by the blue dashed arrow)	74
Figure 4.31: Schematic representation of flow Dynalene in from chiller to condenser	76
Figure 4.32: LabVIEW control and graphic interface for oil retention tests	77
Figure 4.33: Relation between the flow meter accuracy and the mass flow rate (Deokar, 2013) ...	88
Figure 5.1: Modified (Baker, 1954) map adopted from (Radermacher et al., 2006).....	92
Figure 5.2: Liquid film entrainment model (adopted from Sethi, 2011)	95
Figure 5.3: Uncertainty of ORV with $t \pm 2$ seconds	105
Figure 5.4: Oil layer observed for various OMFs.....	105
Figure 6.1: Oil retention volume (ORV_N) in microchannel evaporator A with R410A and POE oil	114
Figure 6.2: Oil retention volume (ORV_N) in microchannel evaporator A with respect to sight glass S1, sight glass S2, and effect of the variation of the observed time by 2 seconds (the results for series H).....	114
Figure 6.3: Oil retention volume (ORV_N) in microchannel evaporator B with R410A and POE oil	117
Figure 6.4: Oil retention volume (ORV_N) in microchannel evaporator A with R410A and POE oil for several degree of superheat	120
Figure 6.5: Oil retention volume (ORV_N) in microchannel evaporator B with R410A and POE oil for several degree of superheat	122
Figure 6.6: Schematic representation two phase evaporation length along the microchannels for various exiting degree of superheat.....	123
Figure 6.7: Oil retention volume for R134a+POE oil in microchannel evaporator A.....	126

Figure 6.8: Heat transfer factor in microchannel evaporator A with R410A and POE oil.....	131
Figure 6.9: Simulation results of the local convective heat transfer coefficient in one microchannel tube of evaporator A with R410A and POE oil mixture.....	131
Figure 6.10: Heat transfer rate measured from the air-side ($Q_{evap, A}$) in microchannel evaporator A with R410A and POE oil at OMF at 0.5%	132
Figure 6.11: $Q_{evap, A}$ in microchannel evaporator A with R410A and POE oil at OMF 1%.....	132
Figure 6.12: $Q_{evap, A}$ in microchannel evaporator A with R410A and POE oil at OMF 3%.....	132
Figure 6.13: $Q_{evap, A}$ in microchannel evaporator A with R410A and POE oil at OMF 5%.....	132
Figure 6.14: Heat transfer factor in microchannel evaporator B with R410A and POE oil.....	134
Figure 6.15: Heat transfer factor in microchannel evaporator A with R410A and POE oil several degree of exit superheat	136
Figure 6.16: Heat transfer factor in microchannel evaporator B with R410A and POE oil.....	137
Figure 6.17: Heat transfer factor in microchannel evaporator A with R134a and POE oil.....	139
Figure 6.18: Air flow rate (CFM) for microchannel evaporator A with R134a and POE oil at saturation temperature 7° F (series N) and OMF 1 wt. %. This figure shows air flow rate did not change	140
Figure 6.19: Air inlet temperature (° F) for microchannel evaporator A with R134a and POE oil at saturation temperature 7° F (series N) and OMF 1 wt. %. This figure shows air inlet temperature was constant.....	140
Figure 6.20: Air outlet temperature (° F) for microchannel evaporator A with R134a and POE oil at saturation temperature 7° F (series N) and OMF 1 wt. %. This figure shows air outlet temperature decreases during injection.....	140
Figure 6.21: Pressure drop factor in microchannel evaporator A with R410A and POE oil.....	144
Figure 6.22: Pressure drop factor in microchannel evaporator B with R410A and POE oil.....	146
Figure 6.23: Pressure drop factor in microchannel evaporator A with R410A and POE oil.....	148
Figure 6.24: Pressure drop factor in microchannel evaporator A with R410A and POE oil.....	149
Figure 6.25: Pressure drop factor in microchannel evaporator A with R134a and POE oil.....	150
Figure 6.26: Local heat transfer coefficient (from modeling results) of refrigerant R134a and of refrigerant R134a and POE oil mixture in the microchannels at OMFs ranging from 0.5 to 5 wt. %	154
Figure 6.27: Effect of oil on local heat transfer coefficient (htc) for (sim-1) OMF=0, (sim-2) OMF = 0.5, (sim-3) OMF =1, (sim-4) OMF = 1 and (h=value from htc correlation*1.5), (sim-4) OMF = 1 and 25% flow blockage, and (sim-6) OMF = 1 and 25% flow blockage and (h=value from correlation*1.5).....	157
Figure 6.28: Comparison of the HTFs of the microchannel evaporator A between the model simulation results and the experimental data in order to tests 3 hypothesis for possible increase of heat transfer capacity when small amount of oil was retained in the evaporator	159
Figure 7.1: Comparison between experimental data and predicted results for the heat transfer capacity (a) and pressure drop (b) of the microchannel evaporator A with refrigerant R410A but with no oil (i.e. in oil free conditions of the baseline R410A tests).....	161
Figure 7.2: Comparison between experimental data and predicted results for the heat transfer capacity (a) and pressure drop (b) of the microchannel evaporator A with refrigerant R134a but with no oil (i.e. oil free conditions for baseline R134a tests).....	162
Figure 7.3: Comparison between experimental data and predicted results for the oil retention volume (ORV) of the microchannel evaporator A with refrigerant R410A and POE oil mixture	

	(a) and with refrigerant R134a and POE mixture (b).....	163
Figure 7.4:	Comparison between experimental data and predicted results for the heat transfer capacity (Q) of the microchannel evaporator A with refrigerant R410A and POE oil mixture (a) and with refrigerant R134a and POE mixture (b)	164
Figure 7.5:	Comparison between experimental data and predicted results for the pressure drop (Δp) of the microchannel evaporator A with refrigerant R410A and POE oil mixture (a) and with refrigerant R134a and POE mixture (b).....	164
Figure 7.6:	Simulation results for the HTF (a) and PDF (b) of the microchannel evaporator A with refrigerant R410A and POE oil mixture at saturation temperature ranging from 33 to 48° F (0 to 9° C) (see Table 6.1 for details on symbols and letters).....	165
Figure 7.7:	Simulation results for the HTF (a) and PDF (b) of the microchannel evaporator A with refrigerant R134a and POE oil mixture at saturation temperature ranging from 33 to 48° F (0 to 9° C) (see Table 6.1 for details on symbols and letters)	165

CHAPTER I

1. INTRODUCTION

1.1 Introduction

In vapor compression air-conditioning and refrigeration systems, the compressor needs oil to lubricate its moving parts. Oil is also used for preventing surface-to-surface contact, to limit the heating and to dispose the debris created by wear. Thus, oil is essential for proper maintenance of compressor. Small portion of oil is carried out of the compressor by vapor refrigerant and circulates through the cycle components. The oil amount carried with the refrigerant typically ranges from 0.5 to 1 percent of the refrigerant flow rate, but in worse case situation it can reach up to 3 percent (Thome, 2007). Unfortunately, the quantity of oil returned to compressor is less than the quantity of oil carried out of the compressor. This means that oil might be missing from the compressor because it can retain in the liquid lines, heat exchangers and suction lines during actual operation of the systems.

One of the concerns in air-conditioning and refrigeration systems for proper maintenance of compressor is oil return. Thus, abundant literature can be found on oil return. First research paper on oil return was published by Jacobs et al., 1976 emphasizing on minimum mass flux required for proper oil return in vertical suction liners. Oil return in vertical suction lines are considered for oil return because in vertically upward flow refrigerant vapor needs to overcome gravity to carry the oil. Oil return characteristic in vertical upward flows was also experimentally and theoretically investigated by Mehendale & Radermacher, 2000 whereof the critical mass flow rates for preventing oil film reversal in a vertical pipe were estimated. Fung & Sundaresan, 1994 showed that in display

case refrigeration system, R-404A/POE (Polyol ester) showed significantly better oil return characteristics when compared to R-404A/MO (Mineral oil). While studies of oil return and oil transport in suction lines are quite numerous in the literature, measurements of oil retention in condensers and evaporators for air conditioning and refrigeration systems are rather sporadic in the open domain state-of-the-art work.

Although most of the oil circulated in the system returns to the compressor, a small portion of the oil is retained in heat exchangers. Oil retention depends on thermodynamic and transport properties of the refrigerant-oil mixture, and operating conditions of the system. Geometrical aspects, flow configuration and surface roughness also affects the oil retention characteristics in heat exchangers. The circulating oil can exist in the form of homogenous mixture with liquid refrigerant or it can exist in the form of separated liquid layer with vapor refrigerant in the tubes and headers of the heat exchangers. Cremaschi et al., 2005 showed that increase in oil mass fraction increases oil retention in evaporator and condenser of an air-conditioning system. Lee, 2002 showed that oil retention volume in evaporator and gas cooler of a CO₂ air-conditioning system increased if oil mass fraction was increased. They also showed that oil retention volume in evaporator decreased if refrigerant mass flux was increased.

In air-conditioning and refrigeration systems, evaporators operate at low pressure and temperature when compared to rest of the system components, which makes it more sensitive to the presence of oil when compared to high pressure side i.e. condenser side. During in-tube flow evaporation the local concentration of oil in liquid refrigerant mixture increased as the refrigerant vapor quality increased. At high vapor qualities the local oil concentration in liquid mixture can reach up to 20% when circulating oil mass fraction is 1 wt.%. In high vapor quality sections of evaporator, the properties of refrigerant and oil mixture is significantly different from properties of pure refrigerant. Therefore in evaporators, at high quality regions the presence of oil increases the pressure losses and results in an additional thermal resistance to the heat exchange process. Hu et al., 2008a have studied effect of oil on heat transfer characteristics of R410A flow boiling in conventional and small size microfin tubes. They reported that oil enhances the local heat transfer coefficient at vapor qualities lower than 0.7, but decreases drastically for qualities higher than 0.8. Ding et al., 2009

studied two-phase frictional pressure drop of R410A-oil mixture in 5 mm micro fin tubes. They reported that presence of oil increases frictional pressure drop in higher vapor qualities where oil concentration is high. Schlager et al., 1987 showed that in two phase flow boiling presence of oil can increase pressure drop. They reasoned that increase in pressure drop was due to presence of relatively thick oil film which can reduce potential flow area and induce additional shear stresses.

In summary, there appears to be a growing number of studies on the oil effects on heat exchanger performance for conventional heat exchangers. However, studies of the effects of oil on microchannel type heat exchangers are still limited in the open domain literature. The objective of this project is to measure the oil retention and its effects on heat transfer and pressure drop in microchannel evaporators used in air conditioning and refrigeration applications.

1.2 Thesis Organization

Objective of this thesis is to measure oil retention in microchannel evaporators and its effects on pressure drop and heat transfer. Present thesis report is divided into eight chapters. Chapter 1 provides introduction and background of the problem investigated in this thesis. Chapter 2 discusses the literature in detail and highlights the main lessons learned from the previous studies. Chapter 3 describes the experimental methodology chosen for this research and explains the test facility and its components details. This chapter describes the geometry of microchannel heat exchangers tested in the present study, test matrix, test objectives and test procedures. Instrumentation and data acquisition system are also covered in this chapter. Chapter 4 discusses data processing, data reduction and uncertainty analysis of the present study. Chapter 5 discusses the experimental results of the present study. Figures, plots, and charts obtained for tests listed in the test matrix are given and technical analysis of the experimental data is presented. Chapter 7 describes the validation of the oil retention model with experimental data obtained in this thesis work. The validation of existing heat transfer and pressure drop correlations with the experimental data of the present work is also

presented in this chapter. Chapter 8 describes the conclusions drawn from the thesis work, and recommendations for future potential research in microchannel heat exchangers.

CHAPTER II

2. LITERATURE REVIEW

It is estimated that in HVAC systems, the energy usage is at least 20% of total consumption in USA (Pérez-Lombard et al., 2008). Prime importance is given to improve efficiency of those systems for economic and environmental impact, and it has been continuous focus point of research from past six decades. Among the important considerations in improvement of air-conditioning and refrigeration systems efficiency is studies of lubricant related impacts on those systems and their efficiency. In open literature there are large number of publications available on effect of oil on performance of refrigeration systems, compressors, and heat exchangers. Following is brief review of those studies:

2.1 Overview of oil circulation in air conditioning and refrigeration systems

In Air-conditioning and refrigeration systems the compressor needs lubricant oil to provide lubrication to its moving parts. The other purpose of lubricants are to provide sealing to the vapor compression circuit inside the compressor, to prevent surface-to-surface contact, and limit the heating of refrigerant in the compressor. During vapor compression small amount of oil is carried away by refrigerant vapor in the form entrained droplets or sometimes oil forms an equilibrium mixture with refrigerant, or some oil is simply dragged out of compressor due to high refrigerant vapor velocity (Kesim et al., 2000). The working fluid in these systems is not pure refrigerant instead it is mixture of refrigerant and oil. Many of these systems have oil separators installed downstream of discharge line of compressor to separate the oil from refrigerant, temporarily store the oil, and then returned back to the compressor crank case. Oil separators are not 100 % effective. At the same time the separated oil is not pure oil, instead it is a mixture of lubricant and refrigerant. The oil that

bypassed the oil separators is dragged by high refrigerant vapor velocity and enters the condenser as viscous liquid mixture which is rich in oil. During the two phase condensation process oil starts to dissolve in liquid refrigerant due to miscible characteristics, while some oil retains in condenser itself. The liquid that exits condenser is typically mixture of liquid refrigerant and oil. Some researchers consider the exit of condenser as reference point to define oil circulation ratio (OCR) (e.g. Choi et al., 2009, and Sethi, 2011). Amount of oil hold up in liquid lines are proportional to OCR (Cremaschi et al., 2005). After the expansion valves the liquid refrigerant and oil mixture enters evaporators. Here the liquid mixture during in-tube flow boiling starts to evaporate and as the vapor quality of the mixture increases the local oil concentration in liquid refrigerant-oil mixture starts to increase because typically oil is non-volatile component and has bubble point around 300°C which is considerably higher than bubble point temperatures of liquid refrigerant. At high vapor qualities oil retains in the evaporators due to high viscosity of liquid mixture which is predominantly due to oil. The fluid that exits evaporator is separated flow of annular oil rich liquid film and core refrigerant vapor. In suction lines the refrigerant superheated vapor drags liquid film whose thickness depends on refrigerant vapor Reynolds number, liquid mixture weber number, liquid mixture refrigerant Reynolds number and orientation of suction lines. In this manner the escaped oil from compressor can retain in various parts of the system. Often missing oil from compressor can cause draining of oil level from compressor which leads to mechanical failure of compressor. Therefore it is essential that most of the escaped oil from compressor is returned back to the oil sump. Apart from compressor lubricant is not required in other parts of air-conditioning or refrigeration system. For proper functioning of compressor the lubricant rich mixture must have high viscosity in order to provide proper lubrication. At the same time the oil/ refrigerant mixture must not have high viscosity so that the escaped lubricant does not form separate layers in other parts. This ensures that the escaped oil returned to compressor (Kruse & Schroeder, 1985).

2.2 Effect of oil on evaporators and condenser heat exchangers

In air-conditioning and refrigeration systems, the condenser, evaporators and suction lines operate at different temperatures and pressures. Thus the effect of oil varies from component to component. There are many

publications studied the effect of oil on individual components of the system or system as whole. Following is brief review of studies related to effects of oil.

McMullan et al., 1988a; McMullan et al., 1988b have developed an experimental rig which allowed them to study the effects of lubricating oil on the performance of refrigeration plant. They have studied evaporator heat transfer rate for various degree of superheat ($^{\circ}\text{C}$) for oil free and with oil conditions. For oil free tests, their results indicated that as the degree of super heat ($^{\circ}\text{C}$) decreases, the evaporator heat transfer increases linearly. But when oil was present and oil mass fraction was 1.9 %, their results indicated that for high degree of superheat the effect of oil on heat transfer rate had negligible effect. When degree of superheat is further decreased, at a particular point there is maximum heat transfer rate. Further decrease in superheat reduces the heat transfer process and falls down suddenly. For this case where the maximum heat transfer rate was observed at 4°C superheat. Hughes et al., 1980 have experimentally investigated the effect of oil on heat transfer, pressure drop and refrigerant flow in an evaporator. They had studied the effect of oil for oil mass fraction of 0, 3 and 6 wt. %. Their results indicated that the heat transfer coefficient was affected due to the presence of oil at various quality in the evaporator. The trend of variation of heat transfer coefficient with respect to quality was similar to that of oil free conditions but the presence of oil decreased the heat transfer coefficient. Due to presence of oil the pressure drop is highest for higher vapor quality and higher refrigerant mass flow rate. Lottin et al., 2003a have modeled vapor compression refrigeration system which takes into account the fact that the oil used in the system effects the system performance. This model focused on R410A and new synthetic oil developed for it. Their results showed if OMF is less than 0.5 % the parameters in simulations were unaffected but evaporator and condenser capacity increased and the COP of refrigeration system reduced in same proportion. The effect of oil on heat transfer becomes important when OMF is above 0.5%. The decrease in condenser heat transfer is small when compared to evaporator where it losses the capacity by 13% when OMF is above 5%. The authors argued that the reduction in evaporator capacity is due to presence of high quantity of remaining liquid at the exit of evaporator heat exchanger. The pressure drop at the high pressure side is not significant but the pressure drop at low pressure side that is at the evaporator

is more significant for OMF above 2.5 %. They suggested that for systems optimal performance in presence of oil can be achieved by controlling apparent super heat at evaporator outlet. It should be noted that the term ‘super heat’ is irrelevant when oil is present in the system because oil does not evaporate in the range of temperatures of refrigeration and air-conditioning system. So the apparent superheat should be used in this context. Lottin et al., 2003b plotted evolution of local oil concentration in liquid phase along the length of evaporation. Those plots suggested that the amount of oil present in the outlet of evaporator does not vary much when amount of oil in the system increases that is when OCR increases. But when OCR increases above 5% the amount of oil at evaporator outlet increases significantly due to change in pressure at the exit of evaporator. Since evaporator has lowest pressure and temperature, the solubility of oil in those points are highest and liquid exiting evaporator contains 32.5% to 40% of refrigerant. They also reported that frictional pressure drops in condenser are always found to be negligible due to high pressure applications. The pressure losses in evaporator is not significant when amount of oil is present below 0.5% wt.%. But it becomes significant when amount of OMF is above 0.5%. When using other low pressure refrigerants, for example R134a, the pressure drop can be multiplied because evaporation pressure is significantly low when compared to R410A. Youbi-Idrissi et al., 2003 studied the effect of refrigerant–oil solubility on an evaporator performances. The working fluids were R407C/POE oil mixtures with same viscosity grade oils but different solubility properties. Their results indicate that for similar conditions with same viscosity grade oil but with different refrigerant-oil solubility, the evaporator performance decreases when refrigerant oil solubility increases. In the same study authors have studied the effect of OMF and superheat on R_h . It is a ratio of enthalpy change of refrigerant with oil and without oil. R_h can be expressed as follow.

$$R_h = \frac{\Delta h_{r,oil}}{\Delta h_{r,only}} \quad (2-1)$$

$$\text{Where } \Delta h = h_{evap\ out} - h_{evap\ in} \quad (2-2)$$

Their results showed that R_h value decreased as OMF increased. For higher apparent superheats the ratio remains less than one showing that oil has always detrimental effect. They also showed that for less soluble

oil R_h is bigger. They have also shown that Non-Evaporated refrigerant quantity (NEQ) at evaporator outlet decreases as superheat increases but becomes stable at higher superheats. NEQ is more sensitive to solubility. More the solubility higher is NEQ. Furthermore, Youbi-Idrissi et al., 2004 validated their model with experiments. Their experimental and numerical results found to be in agreement with maximum deviation about 2.2%.

2.3 Effect of oil on two phase evaporation, condensation, and flow pattern

In refrigeration systems lubricating oils can have dramatic effect on two phase heat transfer coefficient and two phase pressure drops in direct expansion heat exchangers. Most of the research papers showed that pressure drop in two phase increases due to presence of oil but there is no unanimous agreement on effect of oil in two phase heat transfer.

Zürcher et al., 1997 carried out experiments to measure heat transfer coefficient of R134a and oil mixture in plain tubes. Their results showed that for mass flux of R134a at 200 Kg/m²-s and OMF 0.5 wt. %, the effect of oil on heat transfer were positive for qualities ranging from 0.2 to 0.8. Kattan et al., 1998 performed some experimental measurements to calculate local heat transfer coefficients for R134a and oil mixture. They have conducted experiments for fixed mass flux 100 and 300 kg/m²-s and at fixed saturation pressure of 342.7 kPa. Their results suggests that at low mass flux oil enhanced heat transfer coefficient for qualities ranging from low to intermediate when compared to oil-free condition. Possible reason for increase in heat transfer could attributed foaming and/or increase in wetting properties. But the enhancements were found to be smaller when mass flux was increased. They also found that at qualities above 0.7 the oil decreases heat transfer coefficient.

Hu et al., 2008a experimentally investigated effect of oil on two phase heat transfer of R140A inside 7 mm outside diameter microfin tube. Their results showed that at lower vapor qualities less than 0.4, the presence of oil increases heat transfer process when mass flux was increased from 200 Kg/m²-s to 400 Kg/m²-s. Their results also suggested that heat transfer coefficient decreases in high quality regions sharply as local oil

concentration is high. Hu et al., 2008b conducted heat transfer experiments to study the heat transfer coefficient of R410A and POE oil mixture during flow boiling in a 7 mm diameter smooth tube. Their analysis showed that decreasing the mass flux of R410A/POE mixture at particular quality and oil concentration resulted in diminished local heat transfer coefficient. Hu et al., 2014 measured flow boiling heat transfer coefficient of R410A-oil mixture inside three microfin tubes (Outer diameter 4.0-5.0 mm) with different microfin structures. Authors suggested that the reduction in tube diameter may reduce the detrimental effect of oil on heat transfer at intermediate and high vapor qualities. Nidegger et al., 1997 calculated mean heat transfer coefficient for R134a and oil mixture for which OMF ranged from 0.5% to 5% in microfin tube subsection. The quality was from 0.045 to 0.12 in this subsection. They found that as quality increases from lower qualities the heat transfer coefficient increases until a peak at high quality range. After the peak heat transfer coefficient decreases significantly when compared to no oil conditions. This shows onset of retarding dry condition during two phase boiling. They have also reported that for higher OMF at higher qualities the heat transfer coefficient is significantly degraded.

Many researchers showed that presence of oil increases two phase pressure drops of refrigerant flow. Schlager et al., 1987 reasoned that increase in pressure drop was due to presence of relatively thick oil film can reduce flow area and induce additional shear stresses. Some researcher reported in change of flow pattern for two phase evaporation refrigeration and oil mixture when compared to pure refrigerant flow pattern. Manwell & Bergles, 1994 and Wongwises et al., 2002 reported that flow patterns in smooth tubes for lower mass flux conditions the flow pattern changed to annular when compared pure refrigerant flow. Sometimes degradation of flow boiling heat transfer can be attributed to increase in mixture viscosity. Due to increase in viscosity of liquid mixture there will be reduction in convective heat transfer process. Hambraeus, 1995 studied the effect of oil on flow boiling for three different lubricants mixed with R134a. They reported that the worst degradation of flow boiling of refrigerant was due to the lubricant which had the largest viscosity.

2.4 Review of properties of refrigerant and lubricant mixtures.

Since the working fluid in vapor compression refrigeration and air-conditioning systems is mixture of refrigerant and lubricant oil, the properties of working fluid are not same as those of pure refrigerant or pure oil. One of the challenges arises while determining the properties of fluid to estimate capacity of heat exchangers and COP of whole system. Many researchers have been investigating the changes in density, viscosity, surface tension, enthalpy, specific heats of refrigerants due to presence of oil. There are two methods in open literature to estimate the properties of the refrigerant-oil mixture. First method, mentioned by Tichy et al., 1985 estimated the properties of mixture by using pure refrigerant properties. In order to consider the effect of oil he used correction factors. Another method is to develop empirical and semi-empirical correlations for refrigerant and oil mixture.

In 1989 an international treaty called 'Montreal Protocol on Substances that Deplete the Ozone Layer' have started phasing out production of various products that caused ozone depletion which includes CFCs and HCFCs. Since then CFCs and HCFCs were replaced with HFCs like R410A and R134a. Prior to introduction of HFCs, Mineral oils were used for lubrication of compressors because of their excellent miscibility with CFCs and HCFCs. Mineral oils showed poor miscibility (Yokozeki et al., 2000) and poor oil return characteristics with HFCs like R410A (Sundaresan et al., 1996). Due to this reason retrofit lubricants were developed for compatibility with HFCs. Since then miscible oil like POE, PAG etc. were developed for HFCs. Sunami et al., 1994 pointed out that R134a/ POE mixture showed better miscibility and solubility properties when compared to R134a and alkylbenzene oil mixture. Due to poor miscibility properties of R134a with alkylbenzene oil mixture, it showed higher viscosities and poor oil return characteristics. Martz & Jacobi, 1994 reported the effect of POE lubricant on equilibrium pressure, liquid density, and viscosity of various HFCs (R134a, R22, R125) at varying concentrations and temperatures. Marsh & Kandil, 2002 reviewed some recent work on thermodynamic properties of refrigerant-oil mixtures.

Many researchers reported properties of refrigerant and oil mixture by conducting experiments and correlating properties with available information like temperature and pressure of the mixture. Often these empirical correlations are limited to the range of conditions where experiments were conducted. Hughes et al., 1980 thermodynamically developed pressure-enthalpy charts for refrigerant – oil mixture for range of oil concentrations. Based on developed properties he performed modeling for performance on evaporator. Yokozeki, 1994 proposed thermodynamic model to calculate solubility of refrigerant-oil mixtures. He also proposed simple mixing rule to calculate the viscosity of refrigerant-oil mixture. Neto & Barbosa, 2012 modeled properties of refrigerant-oil mixtures and studied effect on oil circulation.

In current research it was important to have information on how much refrigerant dissolved in POE lubricant. Solubility of oil refers to how much refrigerant is dissolved in pure oil. For current research work the solubility data for R410A and POE ISO 32 mixture was borrowed from Cavestri & Schafer, 2000. For R134a and ISO VG 32 was borrowed from Cavestri, 1993; Cavestri, 1995.

2.5 Review of Oil return characteristics in Air-conditioning and Refrigeration systems

It is crucial to make sure that in vapor compression refrigeration and air-conditioning systems proper care should be taken for returning the oil back to compressor crank case. Due to oil loss from compressor can lead to its mechanical failure. Especially during part load the refrigerant vapor velocity is reduced and more oil is retained in evaporators and suction lines when compared to full load conditions. This leads to significant reduction in amount of oil returned to compressor.

Jacobs et al., 1976 (j_g empirically determined for R12 and 150 SUS oil) was first to publish oil return in suction lines. He conducted experiments by injecting oil at bottom of the vertical suction lines. The flow of the mixture in those line was monitored through sight glass. He decreased the refrigerant flow rate until he observed oil reversal in the sight glass. This data through visualization process then later used to predict minimum mass flow rate of refrigerant in order to prevent oil reversal in vertical suction lines.

$$G = \left(j_g^{*\frac{1}{2}} \right)^2 \left(\rho_g g D (\rho_f - \rho_g) \right)^{0.5} \quad (2-3)$$

Mehendale & Radermacher, 2000 investigated oil return characteristics in vertical suction lines and studied minimum mass flow rates required for proper oil return. They studied oil return for R22, R407C, and R410A with Mineral Oil and POE. They also compared their results with predicted values from Jacobs et al., 1976. The authors proposed model to estimate minimum refrigerant mass flow rate for oil return which accounts for local oil concentration and viscosity of mixture which Jacobs (1976) did not account. Sundaresan et al., 1996 showed that newly introduced HFCs such as R134a, R410A, and R407C were immiscible with mineral oils like alkyl benzene. Due to this reason the liquid film were highly viscous and showed poor oil return characteristics. They also reported that synthetic lubricants were highly miscible in HFCs and displayed good oil return characteristics.

Kesim et al., 2000 have developed semi-empirical correlation to estimate minimum refrigerate velocity in vertical pipelines in order to prevent downward flow liquid film. When refrigerant needs to entrain the oil there are two forces that are responsible for oil entrainment. Gravity and shear force between oil and refrigerant interface in the pipelines. When the flow is in vertically upward gravity acts against entrainment, so shear force has to be strong enough to entrain the oil layer.

$$V_{ref-min} = \left(\frac{ag\rho_{oil}D_i^{1.25}}{0.1582a\rho_{ref}v_{ref}^{0.25} - 0.402D_i\rho_{ref}v_{ref}^{0.25}} \right)^{\frac{1}{1.75}} + \frac{0.1a^2g}{v_{oil}} \left(\frac{D_i}{0.1582a - 0.402D_i} \right) \quad (2-4)$$

2.6 Review of Oil retention in heat exchangers, and suction lines of refrigeration and air-conditioning system.

Industries of refrigeration and air-conditioning systems needs to estimate the amount of oil escaped and retained in the rest of the system. This information is pertinent for proper oil management in order to maintain proper functioning of compressors and achieve optimum performance of heat exchangers.

2.6.1 Oil retention measurements methods

In open literature domain there are two distinct methods to measure oil retention in various parts of the refrigeration and air-conditioning systems. First method is destructive method and other method is non-intrusive or non-destructive method. Peuker & Hrnjak, 2010 used three different methods to measure amount of oil retained in different components of an automotive system with R134a. Those three methods were based on separating oil from that particular component by means of valves used on its inlet and outlet lines. After the component was separated then measurements were performed.

Wujek et al., 2010 proposed similar method to measure oil contained in a component of an air-conditioning system. Their method also involved by isolating the component by means of closing valves. Next step is to remove the refrigerant from the component. Then a predetermined amount of solvent, usually liquid refrigerant itself, is used for filling the component completely. Then the oil free pump is used to circulate the solvent. The concentration of oil in the solvent is determined. Then total amount of oil contained in the component is determined by following equations. Online measurements or sampling methods can be used to determine the concentration of the oil concentration in solvent.

$$\omega = \frac{m_{oil}}{m_{oil} + m_{solvent}} \quad (2-5)$$

For measuring oil retention or oil hold-up using destructive method the components has to be separated from rest of the system. This procedure takes longer time and the experiments has to be repeated multiple times in order to show repeatability.

Lee, 2002 used oil injection and extraction method in a CO₂ air-conditioning system with vapor compression cycle which is non-intrusive method to measure oil retention in individual components of refrigeration systems. Using this method they have measured oil retention in components of the CO₂ air-conditioning system. Their test setup consisted closed refrigerant loop with an oil separator at discharge line to collect oil and send it back to compressor. The refrigerant loop consisted variable speed compressor to achieve required mass flow rate. Besides from refrigerant loop, the test setup also consisted oil loop for injecting oil before the

test section. A variable speed gear pump was used in oil loop to inject oil at desired mass flow rate to achieve required OCR from oil reservoir. The mass flow rate of oil injection and refrigerant flow rate in refrigerant loop was measured with corresponding Coriolis mass flow meter. The oil loop consists of helical oil separator to separate oil from vapor refrigerant. The extracted oil is directed in an oil accumulator cylinder using gravity which consists of a level sensor. The level sensor was used for measuring the rate of oil extraction. Plots were made for oil injection volume and oil extraction volume vs. time as shown in figure. There was time delay between oil injection and oil extraction start because of oil retention between injection and connecting pipelines until oil extractor. In the figure the vertical distance between oil injection volume and oil extraction volume is oil retention volume. Cremaschi et al., 2005 used same procedure to measure oil retention in condensers, evaporators, and suction lines of an air-conditioning system. Yatim et al., 2014 used similar method to determine amount of oil retention in microchannel condenser.

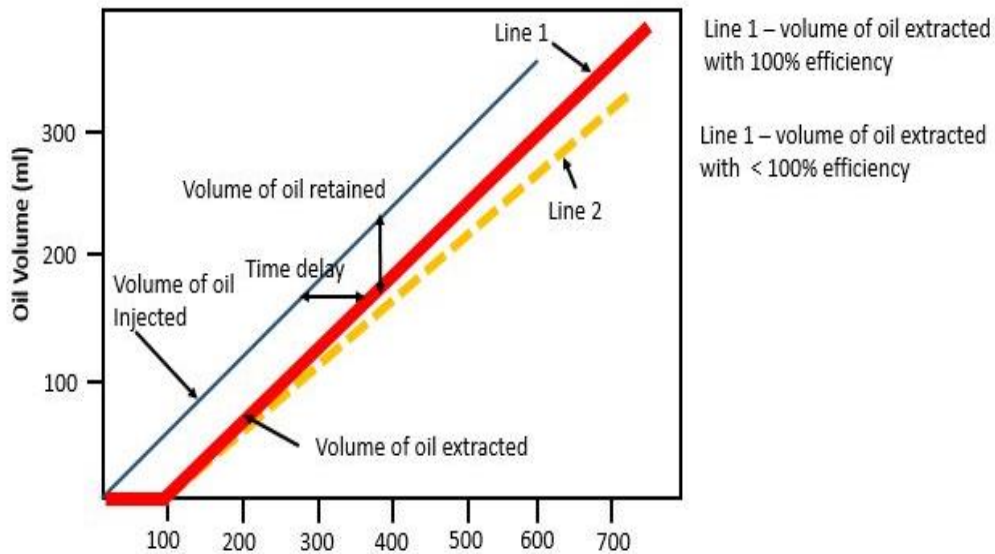


Figure 2.1: Schematic representation of principle of the oil injection and extraction method (Lee, 2002)

2.6.2 Oil retention in air-conditioning and refrigeration systems and its effects on pressure drop and heat transfer:

Lee, 2002 have studied oil retention in gas coolers and evaporators in CO₂ air-conditioning systems using oil injection and extraction method described in section 2.3.1. OCR was varied from 1 % to 5 %. Refrigerant

flow rate was varied from 14 g/s to 27 g/s. When OCR increased from 1 % to 5 % for flow rate of 14 g/s, Oil retention increased from 8 ml to 16 ml. When mass flow rate decreased and OCR was kept constant oil retention volume decreased. When mass flow rate decreased from 20 g/s to 27 g/s, the oil retention volume was similar. That means minimum oil retention volume may exist. They also reported that at same mass flow rate more oil was retained in evaporator than gas cooler. Lee also found that as quality at evaporator increases from 0.75 to 0.85 the oil retention volume increases. Presence of oil also has effect on pressure drop. As OCR increased pressure drop increased. Cremaschi, 2004 developed model to estimate oil retention in condenser, evaporator and liquid lines of vapor compression systems. His simulation results predicted oil retention in evaporator with same as found in his experimental data. His model predicted 72% of data points within 29% relative error. Oil retention profile for evaporator shows that in evaporator oil retention is maximum at the end part of the heat exchanger. Simulations for condenser predicted oil retention which were in agreement with his experimental results. In liquid line he used simple homogenous model to estimate oil retention. Cremaschi et al., 2005 carried out experimental studies on parametric study of oil retention in air-conditioning system. If OMF increased from 1 wt.% to 5 wt.% then oil retained in major components of air conditioning system also increased up to 30% when compared to initial oil charge respectively. The effect of mass flow rate on oil retention has different magnitude in different parts. When mass flux was increased the oil retention in evaporator decreased by 15% but there was no change in condenser. The effect of miscibility of refrigerant and oil mixture was also studied on effect of oil retention. The poorly miscible R410A/MO mixture showed increase in Oil retention by 60% when compared good miscible mixture R410A/ POE mixture. Yatim et al., 2014 have studied oil retention in microchannel condenser which predecessor of this research project. Results indicated that as OMF increases oil retention volume in microchannel condenser also increases. In air-conditioning application OMF ranged from 0.5 wt.% to 1 wt.%. In this range of OMF, oil retention volume was found up to 5% of total volume of microchannel condenser. The effect of mass on oil retention was different for different saturation temperature. Oil increased pressure drop in across the microchannel condenser when compared to oil free conditions. Pressure drop factor increased as OMF increased. It was

also evident that pressure drop increased when mass flux increased at same OMF. The effect of oil on heat transfer capacity of microchannel condenser had shown different trend at different saturation temperature.

Crompton et al., 2004 studied oil hold up in smooth and microfin tubes under adiabatic conditions. They observed that as qualities of refrigerant were low, the concentration of oil effected significantly on oil hold up. She also found that as mass flow rate decrease the oil hold up increases. Alonso et al., 2010 also studied experimentally the oil hold up in during refrigerant two phase condensation and evaporation in smooth tubes, axially fined tubes, and helically fined tubes with R134a and POE mixture. Tests were conducted at saturation temperature of 25° C and mass flux from 100 to 300 kg/m²-s. The qualities were varied from 0.2 to 0.95 and OMF from 3 to 5.5 wt.%. Their results indicated that as quality increase from low quality range to medium qualities the oil hold up decreases but it reaches minimum at intermediate qualities. As quality increases further oil hold up starts to increase and it was highest at high qualities. Similar trends were found for enhanced tubes but oil hold up was more when compared to smooth tubes. The effect of oil hold up in condensation seems to decrease nearly all qualities. But evaporation heat transfer seems to increase at low mass flux in smooth tubes for quality below 0.9. At high mass fluxes heat transfer is reduced due to oil for qualities above 0.5. Zürcher et al., 1998 studied oil hold up in microfin tubes. They observed oil hold up in higher qualities and if mass flux was decreased the oil hold up increased. Schlager et al experimentally studied amount of oil retained in smooth and micro-fined tubes during two phase evaporation and condensation of refrigerant and oil mixture. They showed that oil retention was effected significantly by OMF, mass flux, and vapor quality at evaporator outlet.

2.3.2 Oil retention in suction lines

In large building air-conditioning and refrigeration systems, suction lines can have highest amount of oil retention. Due to lowest pressure and low temperature conditions in suction lines the oil rich liquid film have high viscosity when compared to discharge lines. In particularly part load or low load the amount of oil

retained in suction lines could be high due to low vapor velocities. It is crucial to have high refrigerant vapor velocity in suction lines in order to prevent oil reversal flow in suction lines.

Lee et al., 2001 measured oil accumulation in vertical suction lines and observed flow pattern for R134a/Mineral oil, R134a/Alkyl benzene and R134a/Polyol ester mixtures with two different refrigerant mass flux. They used oil injection and extraction method to measure oil accumulation in suction lines. Their results showed that mineral oil resulted larger oil accumulation due to higher viscosity. They observed that flow pattern was churn flow when refrigerant flow rate was 0.1 g/s and flow pattern was annular flow for refrigerant flow rate 0.37 and 0.57 g/s that forced film to flow upward. Lee, 2002 studied oil retention in suction lines of a CO₂ air-conditioning system. Their results showed that oil retention in suction lines increased if OMF increased. They also suggested empirical correlation to estimate liquid film thickness in horizontal and vertical lines. The correlation for interfacial friction factor was expressed in terms of oil film ratio and gas Reynolds number in CO₂ air-conditioning system. Cremaschi et al., 2005 experimentally measured oil retention in suction lines of air-conditioning system using oil injection-extraction method. Their parametric analysis showed that increase in mass flow flux of refrigerant from 150 to 206 kg/m²-s decreased oil retention volume by 30%. Oil retention volume increased by more 50% when orientation of suction line changed from horizontal to vertical while keeping other parameters constant. This augmentation was due to gravitational force acting on oil film. They also showed that when viscosity of mixture was changed by changing refrigerant oil mixture oil retention volume increased for higher viscosity oil. Radermacher et al have proposed fluid mechanics based semi-empirical model to estimate oil retention in horizontal and vertical suction lines of air-conditioning system. Lee, 2002 and Cremaschi et al., 2005 have shown that oil retention in suction lines are highest when cumulative oil retention was plotted for whole system. They also reported that oil retention in the system is decreases if mass flux of the refrigerant oil mixture increases.

Ramakrishnan, 2012 experimentally measured Oil Retention and its effect on pressure drop in horizontal and vertical suction lines for R134a, R1234yf and R410A with POE 32 and POE 100. They observed that oil retention in vertical suction lines increased if mass flux was decreased. They also observed that when oil was

changed from POE 32 to POE 100 the oil retention in suction lines increased up to 30% due to increase in viscosity of oil. In similar study Sethi and Hrnjak experimentally measured oil retention in suction lines for R134a, R1234yf with POE 32. They also proposed empirical correlation to estimate oil film thickness. Their results suggested that as systems capacity is decreased to part load, oil retention in suction lines increases.

2.7 Studies of Microchannel heat exchangers and lubricant related issues in microchannel heat exchangers

Tuckerman & Pease, 1981 introduced the concept of compact heat sinks for VLSI for high efficiency and compactness. Since then microchannels and microchannel heat exchangers were studied extensively. Microchannel heat exchangers are light weight, and compact which meets requirements of decreasing characteristics dimensions and increasing heat transfer efficiency. Jiang & Garimella, 2001 When compared to conventional heat exchangers the heat transfer coefficient per unit volume can increased in order of 1-2. Hasan et al., 2009 carried out numerical simulation of counter flow microchannel heat exchangers. He studied effect of size and shape of various channels on its performance. He reported that for same volume of a heat exchanger, increasing the number of channels can lead to increase in efficiency at the same time it leads to increase in pressure drop. Among various shapes of channels circular shape showed to have best performance. Jiang & Garimella, 2001 compared the performance of round-tube and flat fin geometries with microchannel heat exchangers. They showed that 30% to 50% size reduction of indoor and outdoor units can be achieved in residential application of air-conditioning systems by utilizing microchannel heat exchangers. They also showed that inventory of refrigerant can reduced by 20% by using microchannel heat exchangers in replacement of conventional round-tube heat pump. Qi et al., 2010 introduced two retrofit microchannel heat exchangers for mobile air-conditioning systems (MAC). They compared performance of enhanced MAC system that utilizing microchannel heat exchangers with conventional MAC system. Their experimental results showed that enhanced MAC system provided more cooling capacity. They also showed that COP of enhanced MAC system increased up to 8% when compared to conventional MAC system. Park & Hrnjak, 2008 studied two R-410A residential air-conditioning systems in which one system utilized microchannel

condenser and other system used conventional tube condenser. In their experimental study both condenser had similar packaging volume. Their results showed that COP and cooling capacity of system with microchannel condenser was considerably higher than that of conventional system. COP of the system with microchannel condenser was 13.1% higher than that with round tube condenser.

Characteristics of hydraulic diameters of microchannels can lead to potential blockage due to presence of lubricant oil in refrigerant. Very few previous works addressed studies of flow boiling and condensation of refrigerant oil mixture in microchannels and microchannel heat exchangers. Zhao et al., 2002 studied flow boiling heat transfer of CO₂ with miscible oil in horizontal triangular microchannels with a hydraulic diameter of 0.86 mm. Their experimental results indicated that oil concentration less than 3 wt.% with lower vapor qualities can enhance heat transfer coefficient when compared to oil free conditions. For higher oil concentration can lead to decrease in heat transfer coefficient. They argued that augmentation in heat transfer coefficient could be due to formation of foaming which could lead to increase in wetting conditions. However, at higher refrigerant qualities separate oil layer was formed which attributed to degradation in heat transfer coefficient. Li & Hrnjak, 2014a; Li & Hrnjak, 2014b studied lubricant effect on microchannel evaporator of a typical MAC system. They reported increase in capacity of microchannel evaporators at OCR 2% due to increase in distribution due to presence of oil. Bigi et al., 2014 developed a model to study oil retention in microchannel condenser. Their model utilized local thermodynamic properties of R140A and POE mixture. Their simulation data were in agreement with experimental data of Yatim et al., 2014 and showed deviation of $\pm 20\%$ with heat transfer rate data.

CHAPTER III

3. OBJECTIVES

3.1 Objectives

The goal of this research was to measure the quantity of oil retained in two microchannel type heat exchangers, and to investigate the effect of oil on heat transfer and pressure drop of refrigerant during flow boiling in microchannels. The overall objectives were

1. To develop experimental procedure to measure oil retention in microchannel evaporators by measuring oil travel time using observational sight glasses.
2. To measure the quantity of oil retained in two microchannel heat exchangers, for R410A air conditioning and R134a coolers applications, operating in evaporator modes.
3. To experimentally determine the impact of the oil that was retained inside the microchannel heat exchanger on the heat transfer capacity degradation and refrigerant side pressure drop
4. To isolate and possibly quantify the effect of following parameters on oil retention, pressure drop and heat transfer rate of microchannel heat exchangers
 - i. Nominal oil mass fraction (OMF) circulating in the microchannel evaporator
 - ii. Refrigerant flow rates
 - iii. Refrigerant saturation temperatures
 - iv. Refrigerant degree of superheat at exit of microchannel evaporator

3.2 Scope of thesis work

In the thesis work, two different louvered-fin aluminum microchannel heat exchangers were tested in evaporator mode. These heat exchangers were commercially available and they were used in commercially available heat pump systems. The experiments were conducted in a custom-made test facility built ad-hoc for this project in order to replicate the real life operating conditions of the heat exchangers of air conditioning and refrigeration systems at Oklahoma State University (OSU) laboratory. The OSU test facility controlled the amount of oil released to the heat exchangers and it measured the corresponding oil retention, the heat transfer rates, and the pressure drops. The test conditions were selected based on typical applications of refrigerant R410A in air conditioning systems and of refrigerant R134a in vending machines and water/wine coolers, and refrigeration systems. The oil used in the present work was synthetic polyol ester (POE) with viscosity grade of VG 32 (that is, Emkarate RL32-3MAF POE oil). The saturation temperatures for evaporator applications was divided to two sets; one set for air conditioning applications ranging from 33 to 48°F (0.5 to 9°C) and the second set for coolers and refrigeration systems with evaporation temperature ranging from 0 to 33°F (-18 to 0.5°C).

Tests were conducted for two refrigerant mass fluxes at each saturation temperature. The first mass flux was representative of the mass flux for full load design conditions of the heat exchangers. The second mass flux was representative of the mass flux for part load conditions of the heat exchangers and it was intentionally selected between 50 to 67 percent of the first mass flux in order to isolate the effect of mass flux on the oil retention. For each refrigerant mass flux, the oil mass fraction, (abbreviated as to OMF), was controlled and varied in a parametric fashion from 0 to 5 weight percent (abbreviated as to wt.%). The mass flux of the refrigerant was controlled by a variable speed gear pump. A series of electrical heating tape and a low temperature chiller served as the hot and cold reservoirs, respectively. This allowed to control the saturation pressure in the microchannel evaporator. The degree of vapor superheat at the outlet of the heat exchanger was controlled to 5° F to 25° F (2.8°C to 13.9° C).

Furthermore, to experimentally validate the oil retention model, including the predicted heat transfer rates and pressure drops for refrigerant and oil mixtures, with the data of the present work. The oil retention model was developed by Andrea Bigi, a PhD candidate at Oklahoma State University, and Stefano Dell'Orto, an exchange student at Oklahoma State University.

CHAPTER IV

4. EXPERIMENTAL METHODOLOGY

4.1 Introduction

The oil retention experiments were conducted using pump-boiler type closed loop refrigeration system in which the refrigerant was circulated by using a gear pump. Oil was injected in the refrigeration loop by using a variable frequency drive (VFD)-controlled gear pump and the oil was injected at two locations, namely the inlet and the outlet of the microchannel evaporator (referred to as test section in this thesis). To calculate the oil retention in the microchannel evaporator, the oil injection flow rate injected at the inlet and outlet of the test section and the time that the oil was observed in the sight glass installed downstream the microchannel evaporator for each injection were measured. The amount of oil retention in each test was calculated from numerical integration of the oil injection flow rate over the corresponding time. The amount of the oil retention at the microchannel heat exchanger was obtained from the difference between oil retained during oil injection at the inlet and the outlet of the microchannel evaporator. In addition, oil mass retention in connecting pipelines between oil injection ports and the test section (at inlet and outlet) were estimated and subtracted from amount of oil retention measured.

During the period for the oil injection at the inlet of the test section, the heat transfer capacity and the refrigerant-side pressure drop of the microchannel evaporator were measured. The heat transfer capacity was experimentally measured from the air side of the heat exchanger. Calibration tests were performed for the same system running with only refrigerant at the same flow rates and saturation pressure at the inlet of the test section. The results were then used as baseline data of heat transfer capacity and pressure drop of the test

section when no oil was present in the system, i.e., in oil free conditions. The heat transfer rate and pressure drop during the tests with oil were then compared to that of the corresponding baseline data. Because the baseline data in oil free conditions and the experimental data with oil shared same total mixture flow rate, i.e. the refrigerant flow rate for the baseline data was equal to the mixture (refrigerant plus oil) flow rate for the experiments with oil. Same saturation pressure, same inlet refrigerant temperature, and same air side inlet temperature and velocity were maintained between the experiments with oil and the reference baseline tests without oil. The results of the comparison provided heat transfer factors and pressure drop factors that isolated the effect of oil on the heat transfer rate and pressure drop of the microchannel evaporator.

4.2 Microchannel Evaporators that were tested in the thesis work

Two louvered-fin aluminum microchannel heat exchangers were experimentally tested as evaporator and they are referred throughout this report to as evaporator A and evaporator B. Evaporator A was a single pass heat exchanger while evaporator B was a double pass heat exchanger as shown schematically in Figure 4.1 and Figure 4.2. Both evaporators were installed in a cross flow configuration relative to the air flow direction. The dimensions of the evaporators are given in Table 4.1.

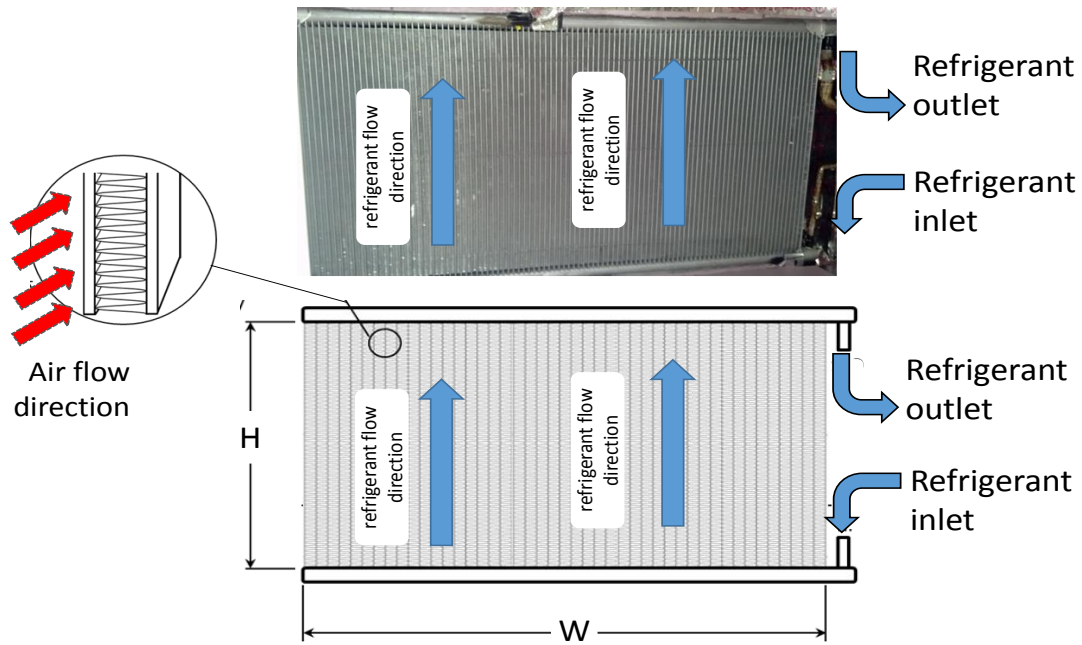


Figure 4.1: Microchannel evaporator A (top) actual picture of the first heat exchanger, A, tested in the present project and (bottom) schematic of the heat exchanger A with refrigerant flow direction during the evaporator tests

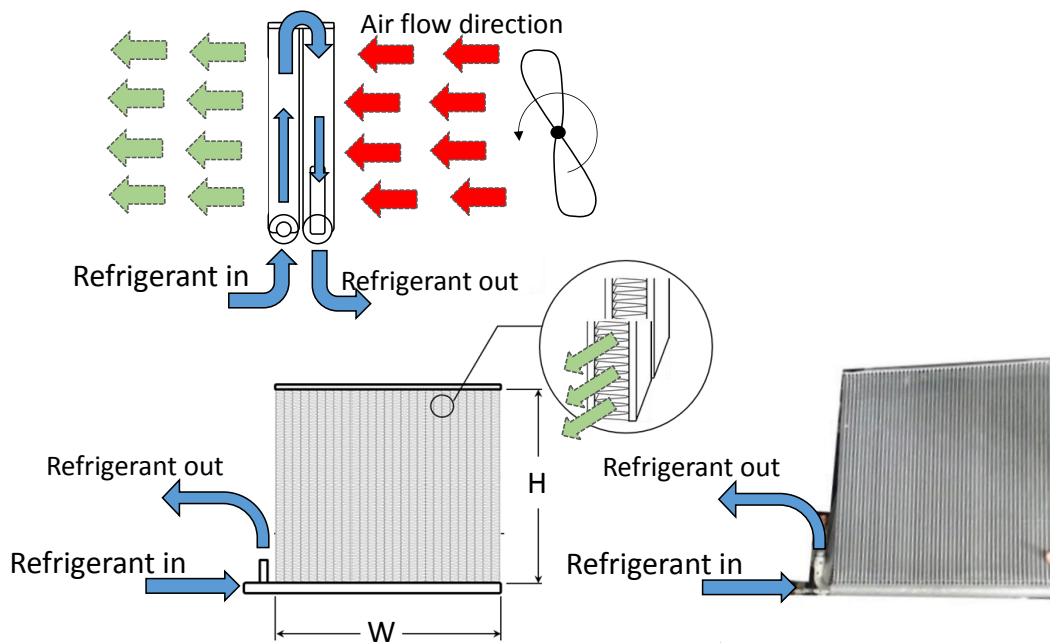


Figure 4.2: Microchannel Evaporator B: (top) schematic of the heat exchanger B with refrigerant flow and air flow directions during the evaporator tests; (bottom left) schematic of the evaporator B with indication of the main dimensions and (bottom right) actual picture of the second heat exchanger, B, tested in the present work.

Table 4.1 Dimensions of the Microchannel Heat Exchanger-Evaporators That Were Tested in the Present Project

Parameter	Evaporator A*	Evaporator B*
Material	Aluminium	Aluminium
Fin type	Louvered	Louvered
Number of tube	98	50
Height (H)	0.438 m (17.2 in)	0.546 m (21.5 in)
Width (W)	0.884 m (34.8 in)	0.501 m (19.7 in)
Number of slab / passes	1	2
Sectional cross flow area of one entire tube (A_{flow})	18.5 mm ² (0.0286 in ²)	22 mm ² (0.034 in ²)#
Wetted perimeter in one entire tube (P_{wet})	50.72 mm (2.00 in)	99.2 mm (3.91 in)#
Hydraulic diameter of one entire tube (D_h)	1.46 mm(0.057 in)	0.88 mm (0.0035 in)
Microchannel tube height	1.4 mm (0.055 in)	2 mm (0.079 in)
Microchannel tube depth, in the direction of air flow, or depth of one microchannel heat exchanger slab	25.4 mm (1.00 in)	30.5 mm (1.20 in)
Microchannel tube spacing, space between adjacent tubes	7.44 mm (0.29)	7.62 mm (0.30)
Microchannel tube thickness	0.35 mm (0.014 in)	0.4 mm (0.016)
Fin Pitch	0.79 fin/mm (20 fpi)	0.63 fin/mm (16 fpi)
Fin Height	7.44 mm (0.29 in)	7.62 mm (0.30 in)
Fin Type	Louvered	Louvered
number of louvers on the fin	16	16
Louver length	6 mm (0.236 in)	6 mm (0.236 in)
louver height from the fin plane	0.2 mm (0.008 in)	0.2 mm (0.008 in)
Louver pitch	0.89 n.louv./mm (22.6 n.louv./in)	0.89 n.louv./mm (22.6 n.louv./in)
Louver angle measured from fin plane	30 deg.	30 deg.
Inlet header diameter (measured as envelope diameter)	31.75 mm (1.25 in)	33 mm (1.30 in)
Outlet header diameter (measured as envelope diameter)	31.75 mm (1.25 in)	33 mm (1.30 in)

Internal volume of the microchannel evaporators used to normalize the oil retention measurements	1,890 cm ³ (115 in ³)	1,250 cm ³ (76 in ³)
--	--	---

*Note: The dimensions of the microchannel evaporator sample were not provided by the manufacturers. The dimensions were estimated by conducting a limited number of measurements on the sample at Oklahoma State University Research Laboratory.

#the sectional cross flow area, A_{flow} , and the wetted perimeter, P_{wet} , for one entire tube were provided by the manufacturer of this microchannel heat exchanger. The hydraulic diameters for microchannel evaporators were calculated as $D_h = 4 A_{\text{flow}}/P_{\text{wet}}$.

4.3 Experimental Setup

The microchannel evaporator A and evaporator B were installed inside a thermally controlled enclosure and the inlet air psychrometric conditions were regulated by the large-scale climate control psychrometric chamber (Cremaschi & Lee, 2008). The psychrometric chamber allowed user to control the temperature, humidity, and velocity of the air entering the microchannel heat exchangers during the oil retention experiments. The temperature range of the room was from 10°F to 130°F (-12° to 54°C), and the relative humidity range was from 10% up to 95% R.H. In addition, the velocity and temperature of air supplied to microchannel heat exchangers was uniform. More details about the facility design, construction, and specifications can be found in (Cremaschi & Lee, 2008).

Pressure transducers and inline thermocouples were installed to monitor the refrigerant conditions along the test section and a dedicated differential pressure transducer was used to measure the refrigerant side pressure drop. The heat transfer capacities of the microchannel evaporators were measured from the air side heat transfer and the air flow rate measured and calculated according to ANSI/ASHRAE 41.2 Standard (1987). Heat balance tests were conducted when the refrigerant outlet was in superheated vapor conditions for the evaporator tests. The error of heat transfer capacities measured from the refrigerant side and the air side were within ±5%.

4.3.1 Oil Retention Measurement in Microchannel Evaporators

The oil retention in microchannel evaporators were measured for two different refrigerant and oil mixtures and two different microchannel evaporators. Refrigerant R410A and POE oil mixture was used to study microchannel evaporators in air conditioning applications while refrigerant R134a and POE oil mixture was

used to investigate microchannel evaporators for AC systems, water/wine coolers, vending machines applications, and refrigeration systems. All the test conditions carried out for the microchannel evaporators are given in Table 4.3. Experiments were carried out for saturation temperatures above and below freezing point of water i.e. at 32° F (0° C). Throughout this report, when the saturation temperature was above 32°F (0°C), the experiments are referred to as “medium” temperature series (or “medium” temperature tests conditions) and for refrigerant saturation temperature below 32°F (0°C), the experiments are referred as “low” temperature series (or “low” temperature tests conditions). Refrigerant R410A and POE oil mixture was studied for medium temperature tests conditions in both microchannel evaporator A and microchannel evaporator B while the R134a and POE oil mixture was investigated for medium and low temperature tests conditions but only for the microchannel evaporator A.

The pump-boiler based test apparatus used to experimentally measure the oil retention, heat transfer rate, and pressure drop of microchannel condensers (Deokar, 2013) was modified to accommodate the tests for microchannel evaporators. This section provides an overview of the test apparatus used for measuring oil retention, and the effects of oil on pressure drop, and heat transfer capacity in microchannel evaporators. The experimental setup consisted of four main sections as follows:

1. Pump-boiler refrigerant side loop (also referred in this report to as “refrigerant loop”),
2. Air flow loop,
3. Oil loop, which consisted of the oil injection and oil extraction devices,
4. All remaining auxiliary hydronic systems used to control the test parameters and the test setup operating conditions.

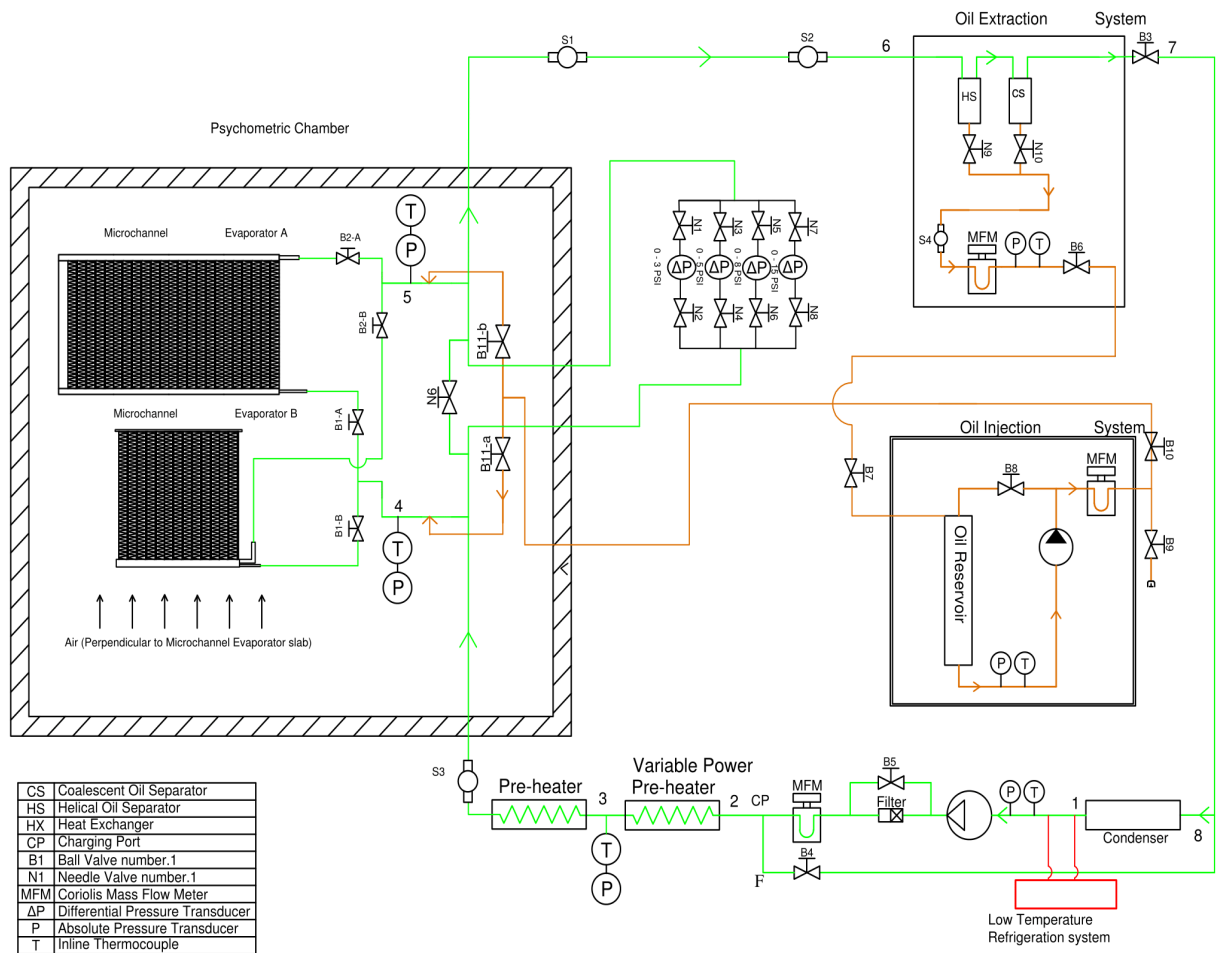


Figure 4.3: Schematic of the pump-boiler based experimental setup used the study

The schematic of the pump-boiler based test setup for the oil retention measurements in microchannel evaporators is shown in Figure 4.3. A series of electric tape heaters were installed along the refrigerant pipelines before the microchannel evaporators. These heaters controlled the degree of subcooling of the liquid refrigerant at the inlet of the evaporator. Furthermore, to guarantee sub-cooled liquid refrigerant at the inlet of the gear pump, a large plate-heat exchanger, labeled as condenser in the Figure 4.3, was installed. A low temperature chiller was used to cool the refrigerant to below saturation temperature before it entered the refrigerant gear pump. Liquid refrigerant from the pump was circulated to a Coriolis mass flow meter and

then was heated slightly with a series of electric heaters in a preheater. With reference to Figure 4.3 the preheater had two sections: the first section was a variable electric power heater from point 2 to 3 and the second section was a constant electric power heater from 3 to s3. Both heaters were made of smooth copper tube with electric tape heaters wrapped around them. The first heater section had electric tape heaters that were controlled by a variable transformer in order to adjust the heat transfer rate to refrigerant flow. In the variable power heater, the liquid refrigerant was heated up to about 5 to 10 degree of subcooling and at the exit of the first variable power preheater, pressure and temperature of the liquid refrigerant were measured in order to determine its enthalpy. Then, in the second heater, the refrigerant liquid was heated to near saturation liquid temperature, that is, to slightly subcooled liquid state with only 1 to 2°F (0.5 to 1°C) of subcooling at the inlet of the test microchannel evaporators. The second heater in the preheater section was very well insulated and the electric power was measured during the tests by using a voltmeter. Thus, from the inlet enthalpy in state 3, mass flow rate, and heat transfer rate measured from the second section of the preheater, the refrigerant inlet conditions at the inlet of the test section (microchannel evaporator A or microchannel evaporator B) were experimentally determined. The refrigerant at the inlet was slightly subcooled liquid with temperature of 1 to 2°F (0.5 to 1°C) below the thermodynamic refrigerant saturation temperature of evaporation. This meant that refrigerant near to saturated liquid state entered the microchannel evaporators. This approach was intentionally chosen to promote uniform distribution of the refrigerant among the vertical microchannel tubes in the test evaporators. A sight glass (component s3 in Figure 4.3) was installed between the second preheater and the inlet of test section to visually confirm the liquid phase of the refrigerant at the inlet of the test evaporators.

In the test section (i.e., the microchannel evaporator A or the microchannel evaporator B), the refrigerant evaporated in the microchannel tubes and exited as superheated vapor. The degree of superheat at the outlet of the evaporators was controlled to 5° F to 25° F (2.8°C to 13.9° C) by adjusting the air temperature of the air flow entering the heat exchanger and the refrigerant flow rate. The test section was installed inside a psychrometric chamber, which controlled the inlet air temperature, humidity, and air speed. Two sight

glasses, referred as to components S1 and S2 in Figure 4.3 were installed along the refrigerant pipelines downstream the test section. Since refrigerant was in vapor phase in this part of the loop, these two sight glasses were used to visually detect the instant at which oil arrived to the sight glasses. This technique was used to determine the oil retention in the microchannel evaporators. Then, the refrigerant vapor and oil mixture was directed to the oil separators in the oil extraction device. In this component, oil was separated from the refrigerant vapor and it was collected in the oil reservoir. The refrigerant vapor was circulated to the condenser and cooled down to subcooled liquid before it was recirculated back to the refrigerant gear pump.

4.3.1.1 Pump-boiler loop

The schematic of the pump-boiler loop for the oil retention measurements in microchannel evaporators for “medium” temperature series is shown in Figure 4.3 as light green solid line loop. The same system was slightly modified for “low” temperature series in order to provide additional cooling to the refrigerant.

Pump-boiler loop for medium temperature tests

This section provides an overview of the pump-boiler system that was used for medium temperature tests. With reference to Figure 4.4, subcooled liquid refrigerant from condenser was fed into pump suction. The pump suction pressure and temperature (before component 1 in Figure 4.4) showed how much subcool was at pump suction. The liquid refrigerant at the pump suction had over 10°F (~5°C) of sub-cooling in order to prevent cavitation of gear pump. From the refrigerant pump, the refrigerant circulated to a Coriolis mass flow meter and then was directed to the preheaters. The actual image in Figure 4.4 shows the positioning of condenser, pump, mass flow meter, and the direction of refrigerant flow.

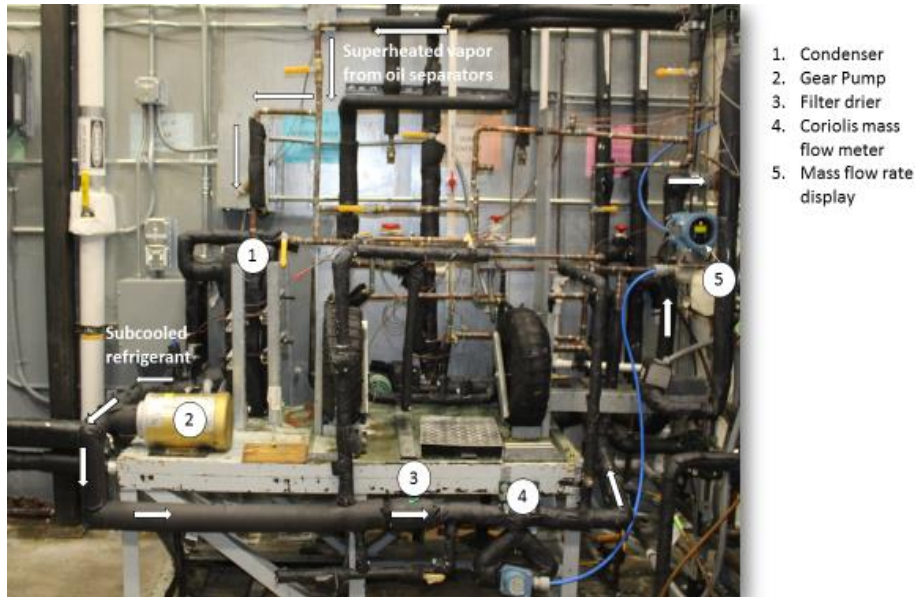


Figure 4.4: Section of pump boiler loop from exit of oil separators until preheater tubes

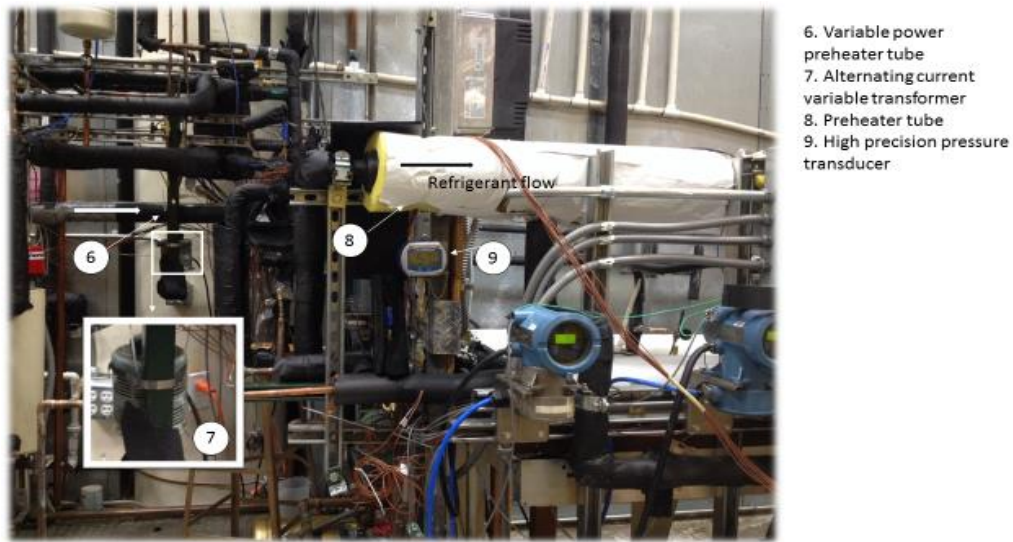


Figure 4.5: Variable power preheater and constant power preheater tube heat exchangers of the pump boiler loop

The subcooled refrigerant from the pump was heated in preheater tube (from point 2 to S3 in Figure 4.3) to near saturated liquid conditions. The preheater consisted of three electrical tape heaters installed around the refrigerant pipelines (from point 3 to S3 in Figure 4.3). The first electrical tape heater (from point 2 to 3 in Figure 4.3) was coupled with variable AC transformer (VARIAC). Constant power supplies were connected to the second and third electrical tape heaters (from point 3 to S3 in Figure 4.3). The power supply to the first

electrical tape heater varied from 0 to 500 Watts using the VARIAC, which was manually adjusted to control the temperature of the refrigerant at the test section inlet. The second and third electrical tape heaters were of constant power of 300 Watts each. The temperature and pressure readings (indicated with the symbols T and P at point 3 in Figure 4.3) indicated how much subcooled the liquid refrigerant was in this location of the refrigerant loop. This helped to estimate how much power supply was needed to bring the subcooled liquid refrigerant in 3 to near saturated liquid conditions at the inlet of the test section.

Figure 4.6 shows how one of the electrical tape heaters of preheater was installed on refrigerant pipelines before entering the test section. The second and third electrical tape heater (from point 3 to 3s in Figure 4.3) was heavily insulated with fiberglass insulation. The component 8 in Figure 4.5 shows the exterior of fiberglass insulation on preheater. This insulation guaranteed that most of the heat from electrical tape heater was directed into the liquid refrigerant circulating inside the pipelines.



Figure 4.6: Example of an electric heater wrapped around a refrigerant copper tube and used as preheater for the evaporator tests

In order to measure the pressure drop across the test section, the inlet and outlet of the test section were connected to the differential pressure transducer bank that was located outside the psychrometric chamber. With reference to Figure 4.3 and Figure 4.7 the differential pressure bank consisted four differential pressure transducers connected in parallel to each other. Each differential pressure transducer had different range from each other. Table 4.2 shows the range of each differential pressure transducer in the bank. The proper

differential pressure transducer was selected and connected in parallel with the test section based on the actual pressure drop measured during the experiments. For example, after having reached the test conditions but before commencing the test, the actual pressure drop was measured with the differential pressure transducer DP4. If the actual pressure drop in the test section was about 0.8 psid, the DP4 was close and isolated and DP1 was opened and put in parallel to the test section. Then, DP1 was used during the recording period of the experiment.

Table 4.2: Range of the differential pressure transducers used in the experimental setup

Differential Pressure Transducer	Pressure differential range
DP1	0 to 20 kPa (0 to 3 psid)
DP2	20 to 34.5 kPa (3 to 5 psid)
DP3	34.5 to 55.2 kPa (5 to 8 psid)
DP4	55.2 to 103 kPa (8 to 15 psid)

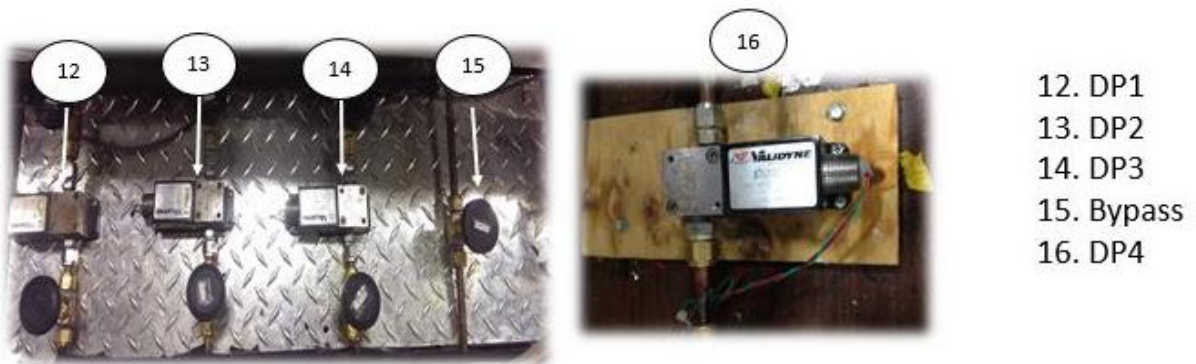
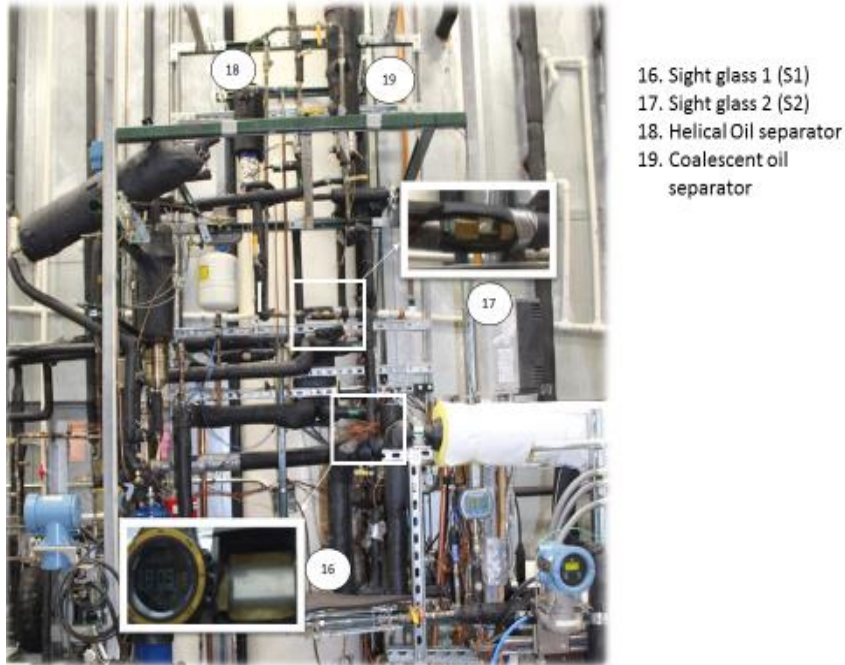


Figure 4.7: The four differential pressure transducers installed in parallel and used in the evaporator tests

The inlet of test section was connected to two absolute pressure transducers. One pressure transducer at point 4 in Figure 4.3 had 0 to 500 psia range. The second absolute pressure transducer had a range from 0-150 psia and it had higher precision and sensitivity than the first one. This transducer was installed outside the chamber and it was connected to inlet of the microchannel test evaporators by using a long pressure line made by port ¼ inch diameter copper tubing. This high precision pressure transducer was used in order to improve the accuracy of the measurements of the inlet absolute pressure, especially during the low temperature tests.

During the oil injection tests in microchannel evaporator A, the ball valve B1-A and B2-A (see between points 4 to 5 in Figure 4.3) were opened and ball valves B1-B and B2-B were closed. This configuration directed the refrigerant flow to the microchannel test evaporator A. During the oil injection tests with the microchannel test evaporator B, the ball valves B1-A and B2-A were closed, and B1-B and B2-B were opened. As the refrigerant entered the test section (either microchannel test evaporator A or microchannel test evaporator B), it evaporated in the microchannel tubes and exited as superheated vapor. The superheated refrigerant from test section outlet exited the psychrometric chamber and entered the oil separators. There were two sight glasses S1 and S2 installed before oil separators (indicated with the symbols S1 and S2 in Figure 4.3). The actual photo in Figure 4.8 shows the position of sight glass S1 and sight glass S2 with respect to oil separators. The sight glasses S1 and S2 were used as visual aid to see when refrigerant and oil mixture layer first appears in those sight glasses. In the oil separators oil was separated from the refrigerant vapor. After that the refrigerant from oil separator entered the condenser (see points 7 to 8 in Figure 4.3). The condenser was a large plate-heat exchanger used to cool refrigerant below its saturation temperature. The condenser was served with a glycol solution (Dynalene HC-40) from a low temperature chiller, and more details on the low temperature chiller are presented in section 4.5.2.



- 16. Sight glass 1 (S1)
- 17. Sight glass 2 (S2)
- 18. Helical Oil separator
- 19. Coalescent oil separator

Figure 4.8: Photo of the position of sight glass S1 and sight glass S2 with respect to oil separators (the sight glasses S1 and S2 were used as visual aid to see when refrigerant and oil mixture layer first appears in those sight glasses)

4.3.1.2 Additional components in the pump-boiler setup for the low temperature tests

In the low temperature tests, the saturation temperature of the refrigerant R134a in the test section ranged from 0 to 10° F (-18° C to -12° C). An additional large brazed plate heat exchanger was added after the condenser to provide further cooling to the refrigerant. This brazed plate heat exchanger was a direct expansion evaporator of an auxiliary low temperature refrigeration system. This low temperature refrigeration system is discussed in section 4.3.1.3. In the low temperature tests, refrigerant R134a at the condenser outlet of the refrigerant loop (see point 1 Figure 4.3 and in Figure 4.9) was redirected to the brazed plate heat exchanger of the auxiliary low temperature refrigeration system.

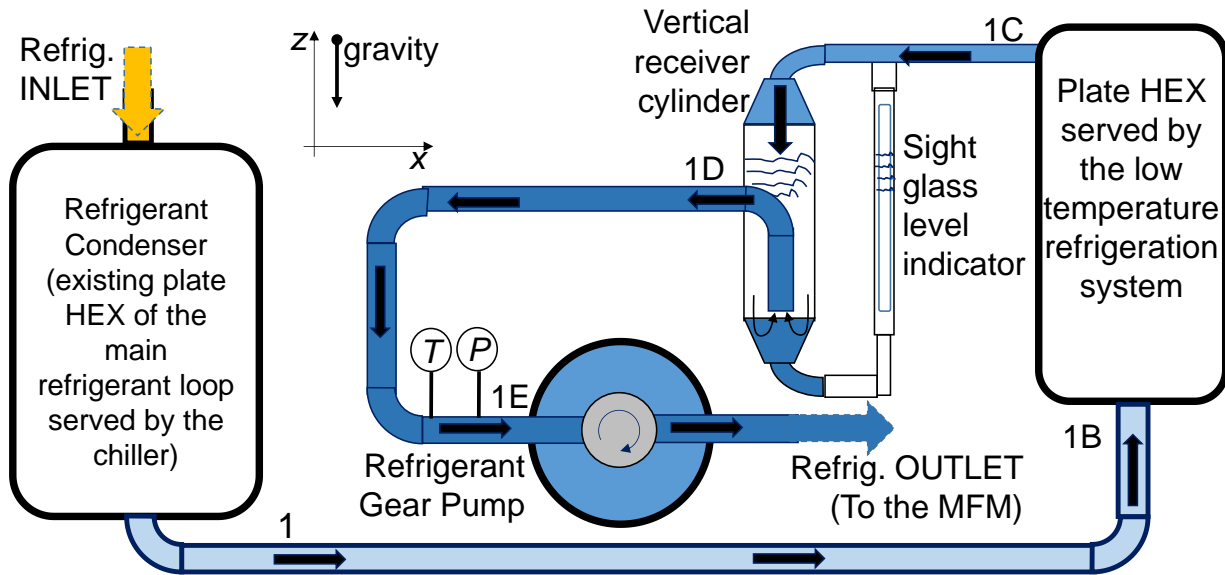


Figure 4.9: Schematic view of the section near the refrigerant gear pump of the pump- boiler refrigerant loop for the low temperature tests (refrigerant R134a was redirected to a low temperature direct expansion refrigeration system before entering the gear pump)

In the low temperature tests, refrigerant R134a was cooled down to very low temperature of about -24°F (-31°C) in the plate heat exchanger of the low temperature refrigeration system, and from point 1B to 1C in Figure 4.9. After the plate heat exchanger, the refrigerant R134a entered a custom-made large receiver cylinder at the point 1C and only liquid refrigerant exited the receiver from point 1D. A sight glass level indicator was installed in parallel to vertical receiver cylinder. The entire assembly of the receiver and sight glass level indicator is shown in Figure 4.9 between the points 1C and 1D. The receiver promoted that only liquid refrigerant exited the cylinder and was supplied to the gear pump suction (which is point 1E in Figure 4.9).

4.3.1.3 Auxiliary low temperature refrigeration system used for the low temperature tests

The auxiliary low temperature refrigeration system was installed to supply additional cooling to the pump-boiler refrigerant loop during the low temperature tests. The unit was water cooled, it had refrigerant R404A, and the refrigeration capacity was about 3,000 Btu/hr (0.9 kW) at -40°F (-40°C). This low temperature refrigeration system consisted of the following components:

1. A brazed plate heat exchanger used as direct expansion evaporator (this heat exchanger was installed in counter flow configuration)
2. A brazed plate heat exchanger used a refrigerant-to-water condenser (the condenser was installed in counter flow configuration)
3. An hermetic reciprocating compressor, manufacturer: Tecumseh, model number: AWA2460ZXD, Compressor, hermetic, low temp, 1 1/2 HP, POE, R404A, 208-230/1/60, 1 1/4" RL - 7/8" S x 3/8" S, Rated capacity at rated -10°F (-23°C) evaporator / 120°F (49°C) condensing: 6,300 Btu/hr (1.8 kW).
4. A suction line accumulator
5. A gas bulb switch for low temperature limit
6. Two metering valves of different sizes in parallel as expansion devices
7. A filter drier
8. A refrigerant receiver

The auxiliary low temperature refrigeration system was custom-build for low temperature tests. Pressure and temperature sensors and the main components of the vapor compression refrigeration cycle of this system are reported in the schematic in Figure 4.10. A photo of the low temperature refrigeration system with all its components is shown in Figure 4.11. From the compressor, refrigerant R404A circulated in the water cooled condenser and the temperature of the entering cooling water ranged between 50° to 60°F (10° to 15°C). Then, the refrigerant was throttled to the evaporator by using the smallest metering valve in the system; this metering valve was a nominal ¼ inch pipe diameter in line precision metering valve. In the brazed plate heat exchanger (used as DX-evaporator for R404A) of the low temperature system, R404A entered with saturation temperature that ranged from -48° F to -25° F (-45.5° C to -32° C). Refrigerant R404A absorbed heat from the refrigerant R134a circulating on the other side of this brazed plate heat exchanger. Refrigerant R404A evaporated, exited the brazed plate heat exchanger, and then it entered the suction line accumulator. The degree of superheat at the compressor suction was controlled between 4 to 20 °F (2 to 11°C) by adjusting the power level of a flexible band electric heater wrapped around the suction line and by adjusting the opening

of the metering expansion valve. With this low temperature refrigeration system, the temperature of the liquid refrigerant R134a circulating in the pump-boiler loop was as low as -24°F ($\sim -32^{\circ}\text{C}$). This resulted in about 20°F ($\sim 11^{\circ}\text{C}$) of subcooling at the gear pump inlet, which was the minimum degree of subcooling required with the refrigerant R134a in order to avoid cavitation of the pump. Thus, at the lowest temperature, the saturation temperature in the microchannel heat exchanger was 0°F (-18°C).

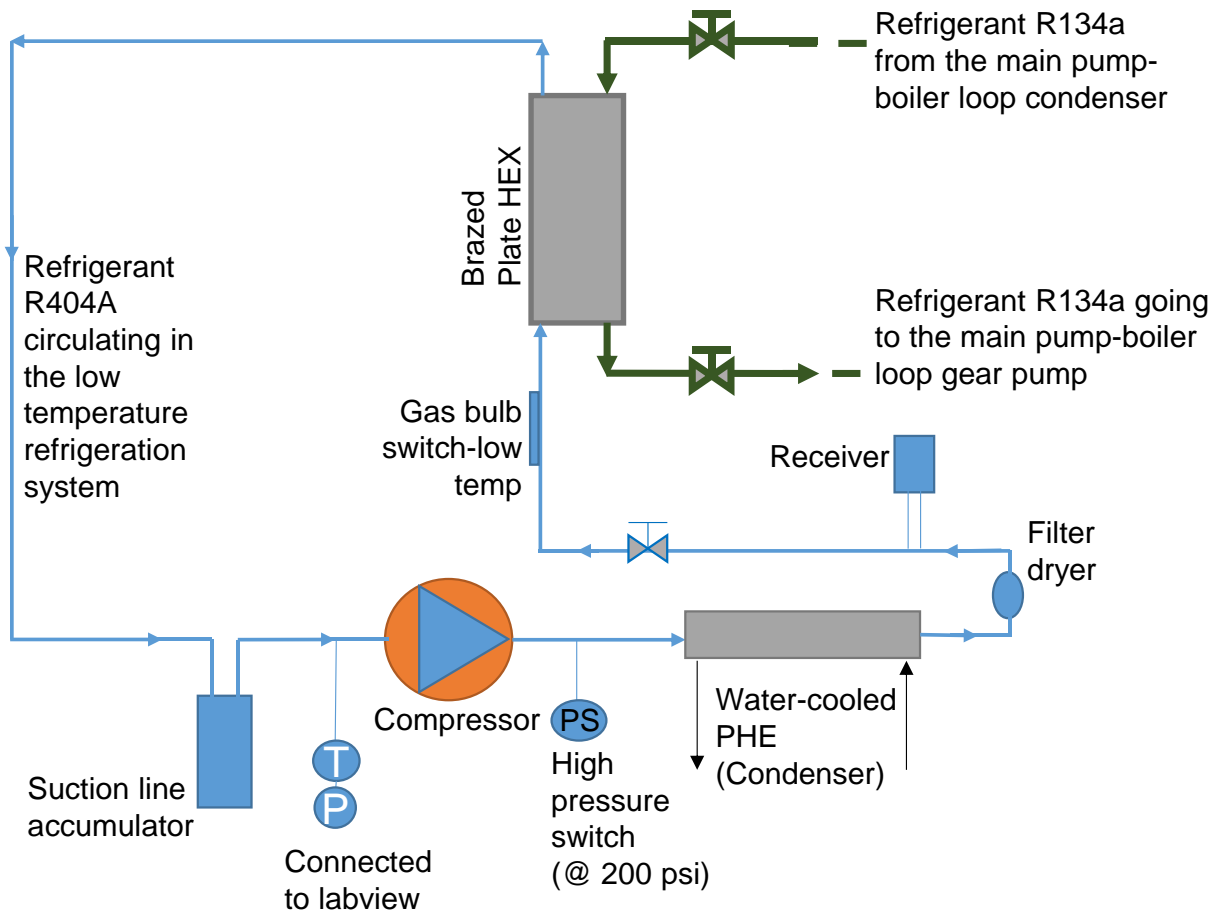


Figure 4.10: Schematic of Auxiliary refrigeration booster system

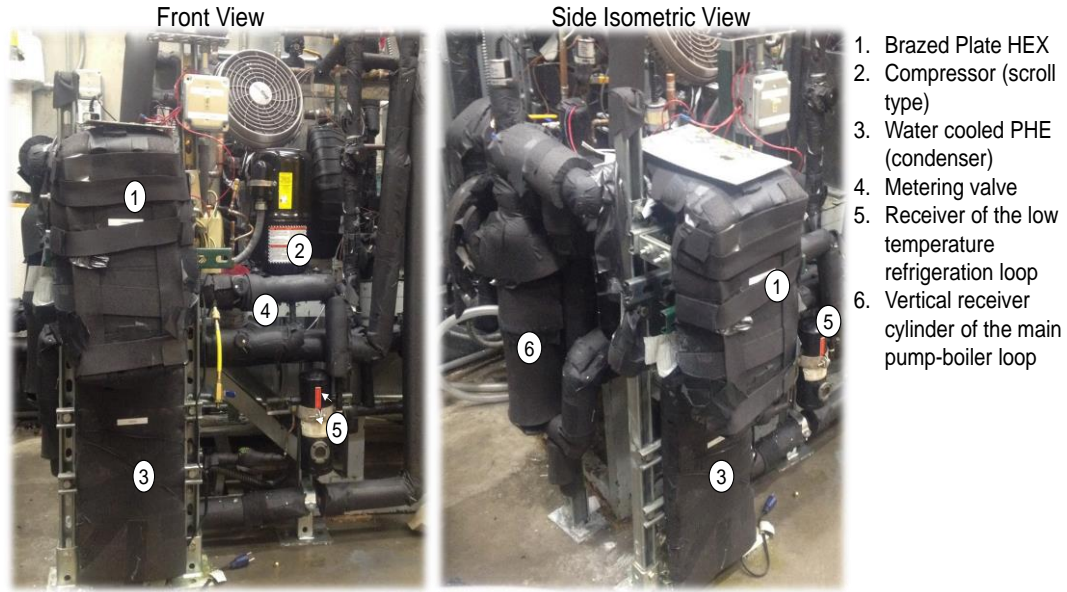


Figure 4.11: Auxiliary low temperature refrigeration system and vertical receiver cylinder

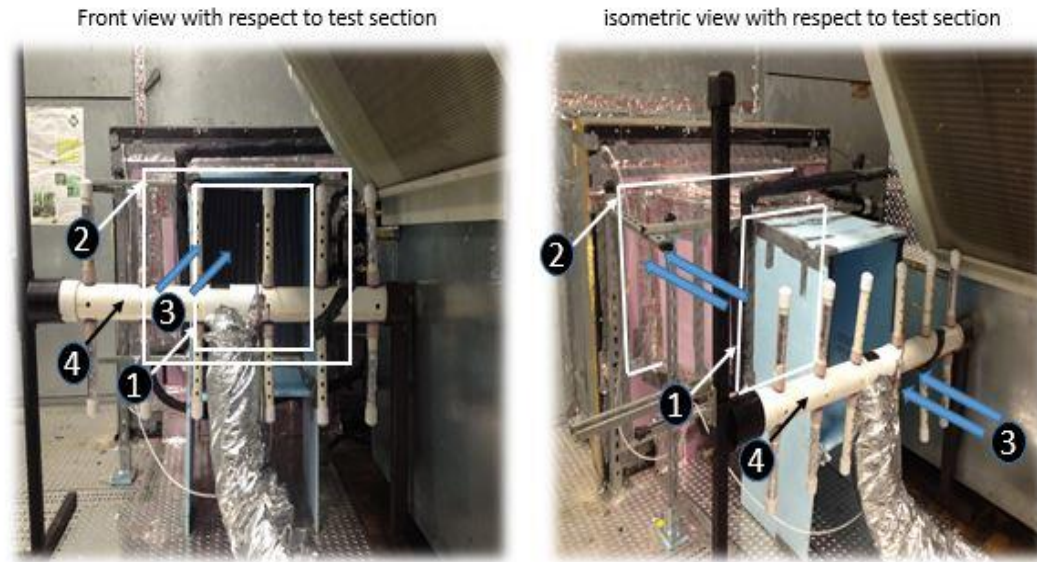
4.3.1.4 Air flow loop

A large-scale psychrometric chamber was used to control the temperature, humidity, and velocity of the air entering the microchannel heat exchangers during the oil retention experiments.

After the completion of medium temperature tests, the air flow loop was slightly modified for the low temperature evaporator tests. An additional dehumidification system was used to further remove the moisture from the air stream entering the microchannel test evaporator. Lowering the air dew point temperature was critical to prevent frost formation when the saturation temperature of the refrigerant inside the microchannel test evaporator ranged from 0°F to 32°F (-18°C to 0°C). This was achieved by controlling the air dew point temperature of the entering air stream to below the refrigerant saturation temperature inside the microchannel test evaporator. Thus, the temperature of the heat transfer surfaces (both fins and microchannel tubes) of the evaporator was above the air dew point temperature and condensation and frosting of the fins were eliminated. This condition is referred as dry fins testing condition because during the oil retention experiments, the latent loads of the evaporators, if any present, were very small compared to the measured sensible load of the evaporators.

4.3.1.4.1 Air flow loop for medium temperature tests of the microchannel evaporators

After completion of testing in microchannel evaporator A, the microchannel evaporator B was installed in front of it (component 1 and 2 in Figure 4.12).



1. Microchannel Evaporator B
2. Microchannel Evaporator A
3. Air direction
4. Air sampling device

Figure 4.12: Test sections and Air sampling device in front of test section

With reference to Figure 4.12, the air entered microchannel evaporators via a small tunnel in front of microchannel evaporator B. The air was sampled before the microchannel evaporators through a mechanical air sampling probe. The sampled air dry bulb and wet bulb temperatures were measured by using RTDs in a standard dry/wet bulb probe device.

Air entered into microchannel evaporator B slabs and then entered into intermediate tunnel between microchannel evaporator A and B (between 1 and 2 in Figure 4.12). As air passes through the test section (evaporator A or evaporator B), the temperature of air decreases. The temperature of the air after the test section was measured using thermocouples and the mechanical sampling dry bulb probe. Figure 4.13 shows

5 out of 20 thermocouples that were installed at the outlet of the evaporators. Thermocouples were installed on a plastic thin wire forming grid of 5 rows and 5 columns and they were used to measure the local temperature of the air exiting the microchannel evaporator A.

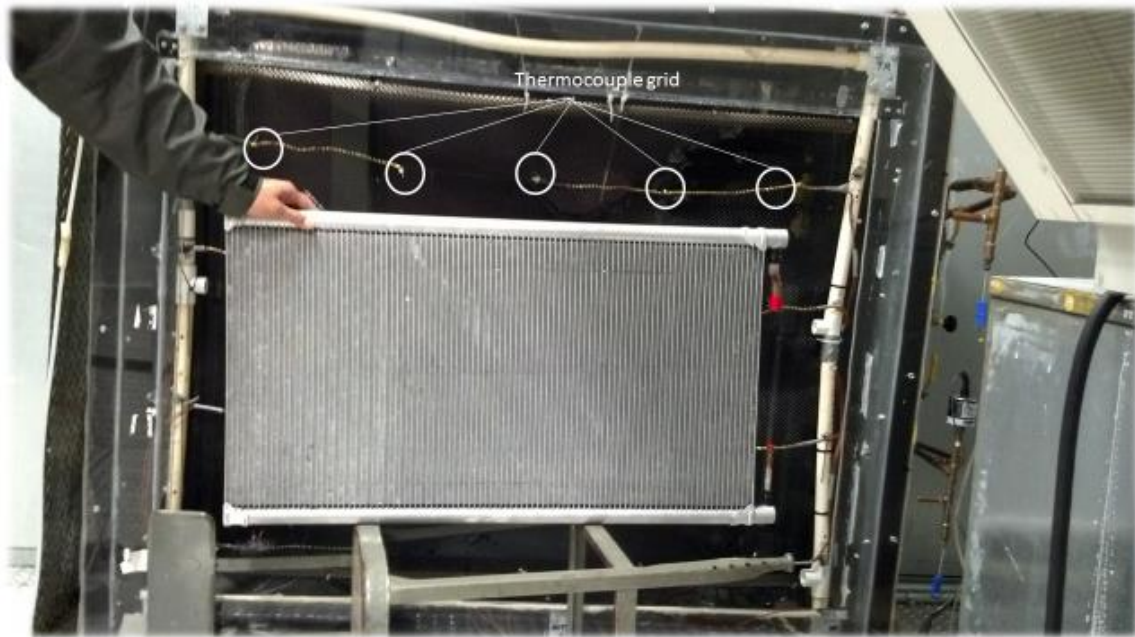


Figure 4.13: Thermocouple grid arrangement during Evaporator A installation

4.3.1.4.2 Air flow loop for low temperature tests of the microchannel test evaporator A

The only difference between air flow loop used in medium temperature series and low temperature series was that a dedicated dehumidification unit was installed in front of the microchannel test evaporator A. The dehumidification unit and the corresponding air duct is shown in Figure 4.14. The air sampling probe (component 4 in Figure 4.12) was not used because the space in the air duct was limited. Furthermore the wet bulb RTD sock froze if the temperature of the air was below 32° F (0°C). Instead a 5 thermocouples were installed in a mesh located at the front of the microchannel evaporators.

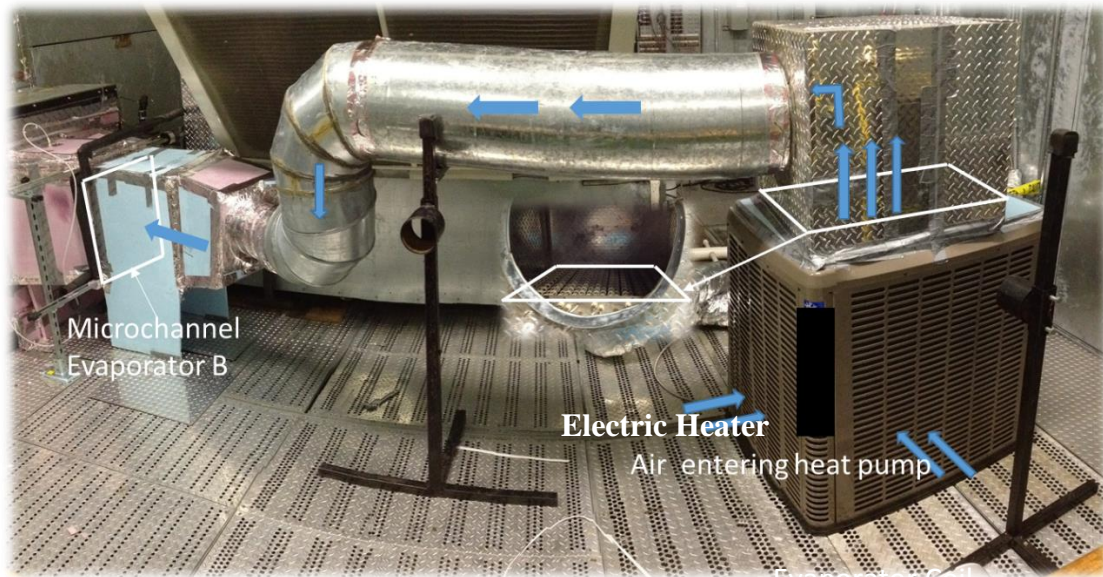


Figure 4.14: Air dehumidification unit and air duct setup for the low temperature test

The dehumidification system consisted an evaporator coil of a low temperature heat pump unit, a custom-made air electric heater, and a tunnel to direct the air flow to the test section. The low temperature heat pump unit cooled the air in the room to very low temperature. During this cooling period, frost accumulated on the heat pump unit and defrost cycles were executed several times. The test evaporator was off and isolated during the period of cooling and dehumidification of the air inside the room. After few frost and defrost cycles of the heat pump unit, most of the moisture was removed from the air inside the chamber and the time to defrost of the heat pump unit became as long as 5 to 6 hours. This period was long enough to conduct one or two experiments with the microchannel evaporator A. The air in the room entered the heat pump unit and its temperature decreased further when flowing across the heat pump unit evaporator coil (direction of the air before the heat pump is indicated by the blue arrows in Figure 4.14). The electric heater was installed inside the box at the top of the unit and positioned downstream with respect to the evaporator coil of the heat pump unit. Right before starting the actual experiment, the electric heater was turn on and the air dry bulb temperature increased to about the same temperature of the room. However, the moisture content of the air inside the metal duct and approaching the microchannel test evaporator was significantly diminished. This dehumidification process is shown in the psychrometric chart in Figure 4.15. By using the electric heater after

the heat pump unit, the air was heated up before entering the microchannel test evaporator in order to control the degree of refrigerant vapor superheat at the outlet of the microchannel test evaporator to between 7 and 20°F (4 and 11°C).

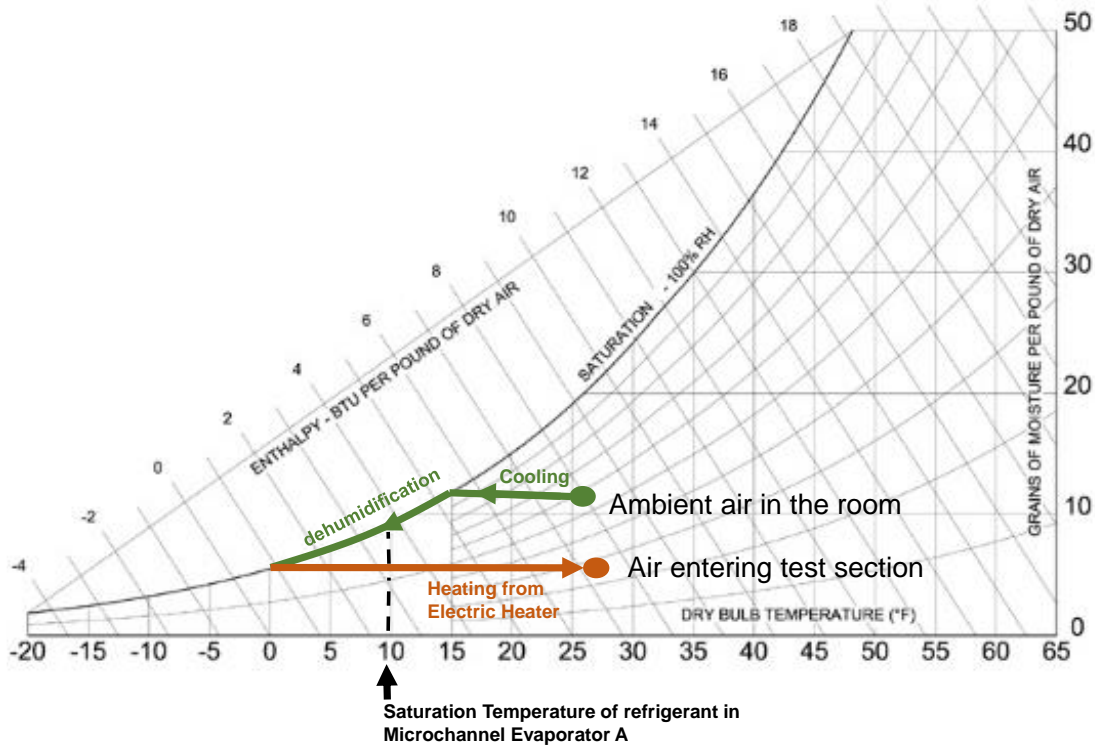


Figure 4.15: Example of air dehumidification process for the low temperature tests plotted on a psychrometric chart

Figure 4.15 illustrates an example of the process of dehumidification of ambient air by using the dehumidification unit for the low temperature tests. In this psychrometric chart it is shown that saturation temperature of the refrigerant in the microchannel evaporator was 10°F (-12°C) and dew point of ambient air was initially about 15°F (-9°C). After flowing through the evaporator coil of the heat pump unit, the dew point of the air was reduced to about 0°F (-18°C). Thus, the fins temperature of the microchannel test evaporator was above the dew point temperature of the entering air stream, avoiding frost formation on the heat transfer surfaces. The electric heater warmed up the air back to about 25°F (~-4°C) dry bulb temperature before the air entered the microchannel test evaporator. The air inlet dry bulb temperature controlled the

degree of superheat of the refrigerant at the outlet of the microchannel evaporator. Once the operating conditions were sufficiently steady state, the oil retention experiment started. Heat transfer rates were recorded for this dry fins test conditions with and without oil in the microchannel test evaporator A. The tests continued until the dehumidification heat pump unit entered the defrost cycle. Then, the oil retention tests were terminated for the day and the room was cooled and dehumidified again overnight. The next day, the dehumidification heat pump unit was restarted again and the procedure to achieve dry fins testing conditions was repeated.

4.3.1.5 Oil injection and extraction systems

The experimental equipment used for oil extraction system was the same as that of the previous work done by Deokar, 2013 and Yatim et al., 2014 in microchannel condenser tests. This section discusses briefly about oil injection and extraction system used in present thesis work.

Oil injection system:

The oil injection system consisted of an oil reservoir and a gear pump. Before the injection, refrigerant vapor, taken at high pressure, was used to pressurize the oil at the top of the oil reservoir and to assist the oil pump during the injection of the oil into the test section. The temperature and pressure of the oil reservoir were measured to determine the solubility of refrigerant in the oil that was released to the test section. This solubility was also experimentally measured with random periodic samples taken from the oil reservoir and analyzed according to the ASHRAE Standard 41.4 (1996). From the oil reservoir (see Figure 4.3), oil was metered into the test section using a variable speed gear pump coupled by a variable-frequency drive. Additional fine tuning of the oil flow was provided by a bypass metering valve. A Coriolis mass flow meter was used to measure the injected oil mass flow rate. When the oil was released to the test section, it formed a mixture with refrigerant and circulated in the refrigerant loop. Then the oil entered the oil separators where it was separated from the refrigerant stream and extracted from the refrigerant loop.

Oil extraction system:

The oil extraction system consisted of two customized refrigerant oil separators that were placed in series, a mass flow meter and oil tanks as depicted in Figure 4.16. The first oil separator was a helical-type separator of large capacity and it separated the main oil stream from the refrigerant flow. A second oil separator was a coalescence-type separator installed downstream to remove all residual oil, if present. Both oil separators originally had internal floating valves in the oil compartment but the valves were removed to promote stable and continuous flow of the oil that was extracted from the refrigerant loop. A sight glass was mounted in the oil line of the oil separators to visually observe the extracted oil flow. A special refrigerant dye was mixed with the oil to help the detection of the oil and visualization of the flow.

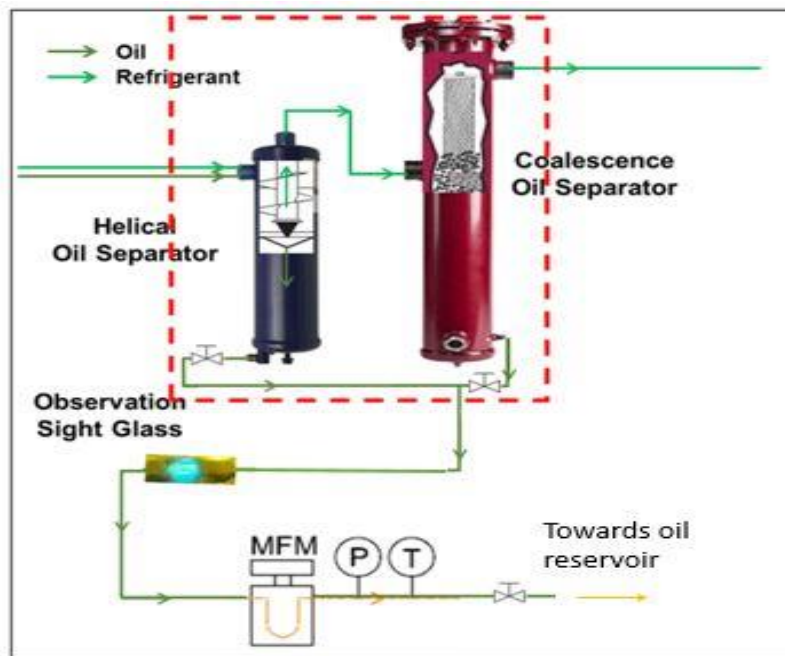


Figure 4.16: Schematic representation of oil extraction system used in present work (Deokar, 2013)

The oil injection and extraction (see section 2.6.1) method that was used for oil retention measurement in condenser test was not feasible in the evaporator tests. During the injection of oil in evaporator tests it was observed that there was not enough free flow of oil after the oil extractors. This was observed through sight

glass that was located at the bottom of the oil extractors (see sight glass S4 in Figure 4.3 and observation sight glass in Figure 4.16) and the flow meter located below the oil separators (see MFM located below the HS and CS in Figure 4.3 and Figure 4.16). In other words, there was not enough pressure difference to drive the oil from the oil separators to the oil reservoir of the oil extractor system when the test section functioned as microchannel evaporator. This meant that measuring the flow rate of the extracted oil from the refrigerant loop was not possible for the microchannel evaporator tests. An alternative method was developed to estimate the oil retention in the microchannel evaporators. This alternative method was verified for condenser tests (Yatim, 2015) and it provided equivalent results of oil retention (as it will be presented later in the report). The alternative method to measure oil retention in microchannel evaporators is described in detail next.

4.3.1.6 Oil retention measuring methodology for the microchannel evaporator tests

The methodology to measure the oil retention for the microchannel evaporator tests is explained briefly in this section. Liquid refrigerant from the pump was directed to a Coriolis mass flow meter and then flowed to the preheater tubes. In the preheater, the refrigerant was heated to near saturation conditions before entering the microchannel test evaporators.

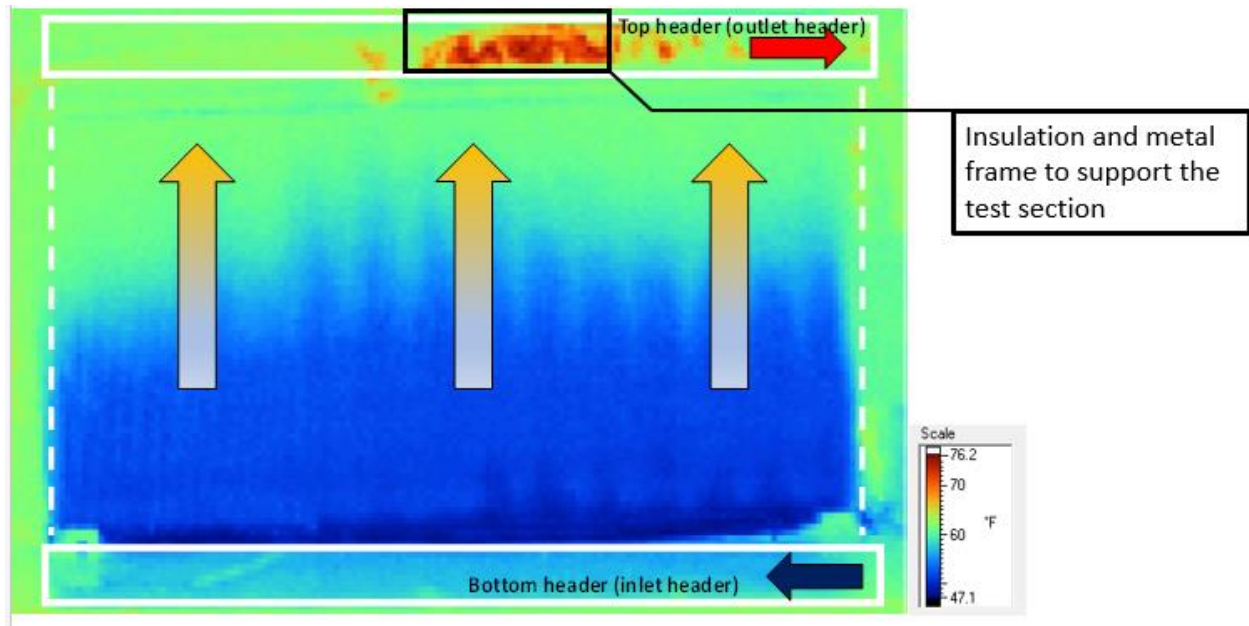


Figure 4.17: Infrared Image of microchannel evaporator A for one medium temperature test; this image indicates refrigerant flowing vertically from bottom to top of the heat exchanger and fairly uniform refrigerant flow distribution

The refrigerant inlet conditions were controlled at near saturated liquid conditions with the aim to promote uniform distribution of refrigerant and of the refrigerant and oil mixture. Infrared thermal images of the microchannel evaporator A were taken to confirm that the distribution was uniform. An example is shown in Figure 4.17, in which the color appears uniform along the horizontal sections. The liquid refrigerant entered at the bottom (dark blue color in Figure 4.17), evaporated in the vertical microchannel tubes, and exited as superheated vapor refrigerant at the top. Two sight glasses (indicated by the symbols S1 and S2 in Figure 4.3) were installed at the outlet of the test section. The refrigerant vapor circulated toward the oil separators in the oil extraction device. From the outlet of the oil separators, the refrigerant circulated to the condenser and was brought to subcooled liquid conditions before it circulated back to the gear pump.

After achieving the required mass flow rate of refrigerant and test condition in pump boiler system, oil was injected at the inlet port of the test section by opening ball valve B10 (component B10 in Figure 4.3). The time ' t_0 ' is noted when injection of the oil was started. During the oil injection at the inlet of the test section, the oil mixed with refrigerant and flowed through the test section (either microchannel evaporator A or

microchannel evaporator B) and proceeded to the outlet and then passed through the sight glasses (see again S1 and S2 in Figure 4.3). As the oil was released to the test section, the oil filled the test section and connecting pipelines until it reached the sight glass S1. A liquid film layer of lubricant appeared clearly visible at the walls of the sight glass S1. During each test for the evaporators, the sight glasses S1 and S2 were monitored by using video recordings of the flow. These videos helped to measure the time at which the oil was first observed on each sight glass.

Figure 4.18 shows an example of a measurement of the time at which the oil reached the sight glass. At the top image, the sight glass was clear and only refrigerant vapor was present. In the center image, a first drop of oil appeared at the inlet of the sight glass. When a first complete layer of oil covered the sight glass S1 the time t_1 was recorded. This was the scenario in the bottom image of Figure 4.18. Similarly, the time t_2 was noted when a first layer of oil was observed to cover completely the sight glass S2. After oil was detected in both sight glasses S1 and S2, oil was continuously metered to the test section for additional 15 minutes to record the effect of oil on heat transfer rate and refrigerant-side pressure drop. After completion of one test, the test section was flushed with two phase refrigerant which collected the residual oil in the test section and connecting pipelines between test section and the oil separators. Two phase refrigerant flow throughout the test section was achieved by simply reducing the air flow rate in the air flow loop.

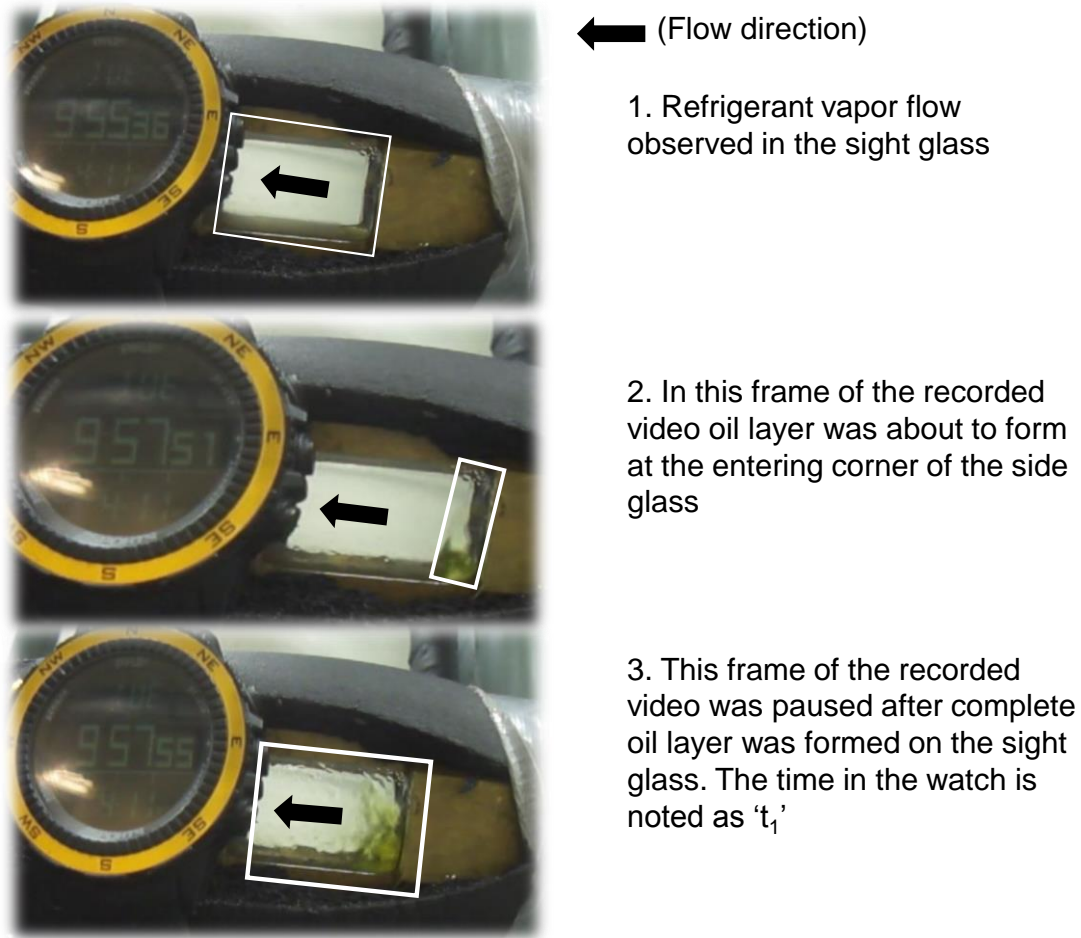


Figure 4.18: Examples of a measurement of the time at which the oil reached the sight glass; a digital chronometer was video recorded next to the sight glass to synchronize the data (the uncertainty of the measured time was of max 2 seconds)

After flushing for about 30 minutes, the oil residual was stored in a tank and the test section was ready for next test. The above procedure was carried out for OMF of 0.5 wt.%, 1 wt.%, 3 wt.%, and 5 wt.%. A similar procedure was repeated when the oil was metered at the outlet of the test section but the OMFs were 0.5 wt.%, 0.8 wt.%, 1 wt.%, 2.5 wt.%, 3 wt.%, and 5 wt.%.

After completion of each test, the time it took the oil to travel from the sight glass S1 to the sight glass S2 was recorded: $\Delta t_{in} = t_{2,in} - t_{1,in}$ (seconds) was defined as time it took the oil to travel from the sight glass S1 to the sight glass S2 when the oil was injected at the inlet of the test section and $\Delta t_{out} = t_{2,out} - t_{1,out}$ sight glass S1 to sight glass S2 when the oil was injected at the outlet of the test section. For same OMF and mass flow rate,

we expected $\Delta t_{in} = \Delta t_{out}$, but our experiments showed that for the same OMF, Δt_{in} was greater than Δt_{out} . In other words, oil travelled from S1 to S2 with slightly lower velocity when the oil was injected at the inlet of the test section compared to when the oil was injected at the outlet of the test section. The reason for higher Δt_{in} as compared to Δt_{out} for same OMF and mass flow rate is that some portion of oil injected during inlet test retains in the test section. Due to oil retention, the OMF or velocity of oil at downstream of the test section reduces slightly when oil layer was observed at one of the sight glasses. For estimation of the oil retention in the test section, the conditions downstream the test section during the injection tests at the outlet of the test section were corrected to replicate the conditions downstream the test section during the injection tests at the inlet of the test section. These conditions included controlling the same temperature, pressure, refrigerant mass flux and same oil velocity. When the outlet conditions were the same between inlet and outlet injection tests, then the oil retention in the test section was measured by taking the difference between two oil masses.

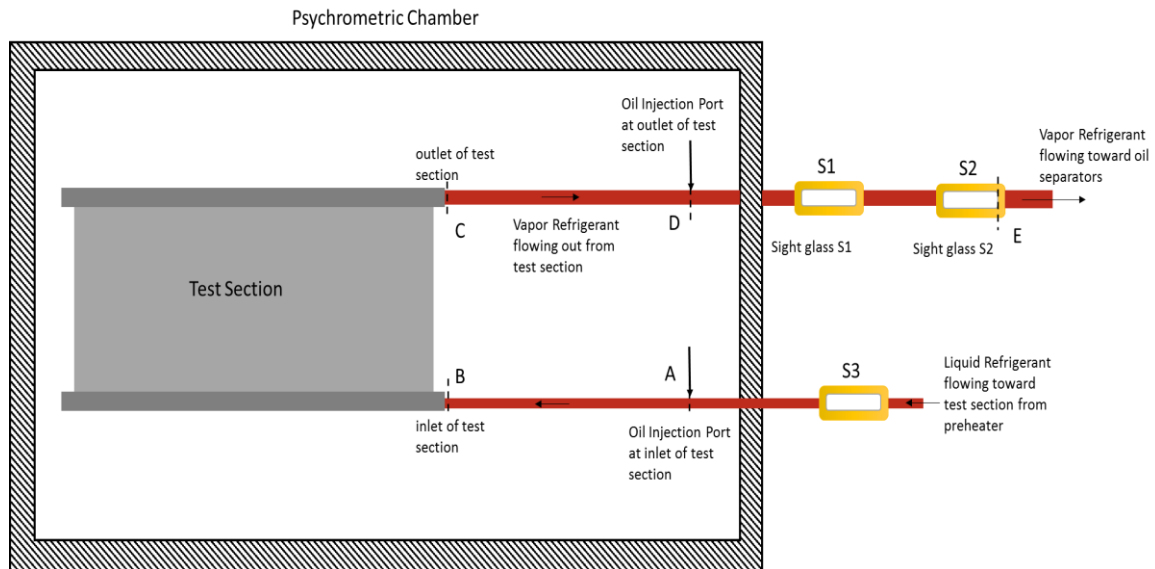


Figure 4.19: Schematic of test section with the pump-boiler loop pipelines inside and outside of the psychrometric chamber

The Figure 4.19 shows schematic representation copper pipeline present between oil injection port at inlet (point A in Figure 4.19) and test section inlet (point B in Figure 4.19), and copper pipeline present between test section outlet (point C in Figure 4.19) and oil injection port at outlet (point D in Figure 4.19). For

convenience these copper pipelines referred throughout this report to as ‘Pipeline A-B’, ‘Pipeline C-D’, and ‘Pipeline D-E’ (from oil injection port at outlet to sight glass s2 in Figure 4.3).

Pipeline A-B = Copper pipeline between inlet inject port (point A in Figure 4.19) and inlet of test section (point B in Figure 4.19)

Pipeline C-D = Copper pipeline between outlet of test section (point C in Figure 4.19) and outlet injection port (point D in Figure 4.19)

Pipeline D-E = Copper pipeline between outlet injection port (point D in Figure 4.19) and Sight glass S2 (point E in Figure 4.19)

The above described method for measuring oil retention in test section does not exclude oil mass retention in Pipeline A-B and Pipeline C-D. The oil mass retention in Pipeline A-B and Pipeline C-D were separately calculated and subtracted from oil retention that was measured by taking the difference between two oil masses. The procedure to estimate oil mass in Pipeline A-B and Pipeline C-D are discussed in section 5.1.1.1 through section 5.1.1.3. The following example clarifies the procedure used to measure the oil retention in test section for one test:

After completion of a test series, Δt_{in} and Δt_{out} were measured as function of OMF as shown in Figure 4.20. In this example at given OMF, it was observed that Δt_{in} were greater than Δt_{out} and a correction was needed. If OMF was equal to 2.4 wt.% then Δt_{out} was 70 seconds while Δt_{in} was 80 seconds. Δt_{in} became 70 seconds if the OMF was slightly higher, that is, of 2.8 wt.%. Therefore when oil was injected at the inlet of the test section with OMF of 2.8 wt.%, then the oil travelled in the pipeline downstream the test section with the same velocity of when the oil was injected at the outlet of the test section with OMF of 2.4 wt.%. During the tests, if oil was injected at the inlet of the test section with OMF equal to x wt.% (for example if $OMF_{@inlet}$ was 2.8 wt.% – see zoom out plot at the bottom of in Figure 4.20), then the measured travel time for the oil to flow from the sight glass S2 to S3 was used to determine OMF of (x -dx) wt.% for the injection at the outlet of the

test section from Figure 4.20 (for example the corresponding $OMF_{@outlet}$ was $(2.8-0.4)=2.4$ wt.%). The reason that the $OMF_{@outlet}$ had to be lower than $OMF_{@inlet}$ by a small quantity (dx) wt.% was to replicate the same thermodynamic and transport flow conditions for the oil and refrigerant mixture in the pipeline downstream of the test section. When investigating possible reasons for this behavior, I considered that it might take some time for the oil to mix with the refrigerant and attain solubility and miscibility equilibrium. During the inlet injection tests, the oil had such time while circulating in the heat exchanger and when it exited from the microchannel heat exchanger the oil is already well mixed and uniformly miscible with the liquid phase of the dissolved refrigerant. During the outlet oil injection tests, the oil was introduced directly to the pipe downstream the heat exchanger but it was not in equilibrium right away, that is, there had to be a certain length of pipe in order for the oil and the refrigerant to mix and behaves of one homogenous mixture. This meant that for some time in which the oil travel along the pipeline it might not be well mixed with the refrigerant, yet. Thus, even if the OMFs were the same, the thermodynamic and transport flow conditions in the pipeline downstream the heat exchanger were not exactly the same when comparing a test with injection at the inlet of the heat exchanger and the corresponding test with injection at the outlet. To correct for this difference in the thermodynamic and transport conditions, I observed that by reducing the OMF by a small quantity dx when metering the oil downstream the test section, I had the same travel time of the oil in the pipeline downstream the test section as that of when I metered the oil at the inlet of the test section with OMF of x wt.%. Cremaschi et al., 2005 studied oil retention in suction lines for various refrigerant and oil mixture. They showed that difference in solubility and miscibility between oil and refrigerant affected amount of oil retained in suction lines. Likewise, difference in solubility of refrigerant and oil mixture at downstream of the test section could be the possible reason for different travel time for oil to go from S2 to S3 as shown in Figure 4.20.

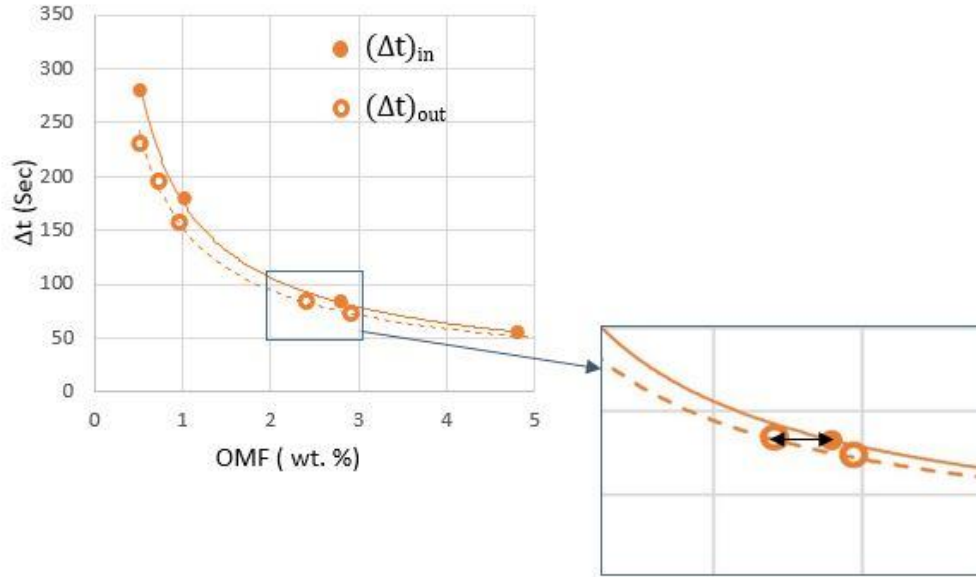


Figure 4.20: Example of time for the oil to travel along the pipeline versus OMF

Now that we found the two OMFs for which the flow conditions in the pipeline downstream the test section were the same, we calculate the oil retention as follow:

Oil retention mass in test section = Oil retention mass in test section plus in the pipeline - Oil retention mass in the pipeline

$$OR_{mass@OMF=2.8wt\%} = Ma_{@OMF=2.8wt\%@inlet} - M_{pipeline}$$

Where Ma is total amount of oil mass injected from starting of oil injection time $t_{0,in}$ at inlet until the time ($t_{2,in}$) when oil layer was observed at sight glass s2. It was calculated as follow:

$$Ma_{(@OMF=2.8wt\%@inlet)} = \int_{t_{0,in}}^{t_{2,in}} \dot{m}_{oil,injected@inlet} dt = 275.0 \text{ grams}$$

Oil retention mass in pipeline ($M_{pipeline}$) was calculated as follow

Oil retention

mass in pipeline = Oil mass in Pipeline A-B + Oil mass in Pipeline C-D + Oil mass in Pipeline D-E

$$M_{\text{pipeline}} = M_{(A-B)@OMF=2.8\text{wt.\%}@inlet} + M_{(C-D)@OMF=2.4\%@outlet} + M_{(D-E)@OMF=2.4\%@outlet}$$

Where $M_{(A-B)@OMF=2.8\text{wt.\%}@inlet}$ is amount of oil (gm) in the Pipeline A-B. In this pipeline section at the inlet, saturated liquid refrigerant and oil mixture was assumed to be homogenous mixture. It is calculated as follow.

$$M_{(A-B)@OMF=2.8\text{ wt\%}@inlet} = \frac{OMF}{100} \cdot \rho_{\text{oil}@68^{\circ}\text{F}} \cdot V_{A-B} = 0.85 \text{ [grams]}$$

Where V_{A-B} is volume of Pipeline A-B.

$M_{(C-D)@OMF=2.4\text{wt.\%}@inlet}$ (or is amount of oil mass (gm) retained in the pipeline C-D. In this section of pipeline which is located downstream of the test section, the refrigerant oil mixture flow was assume to be separated annular flow for feasible calculation of oil mass retention in pipeline C-D. It was calculated using following expression:

$$M_{(C-D)@OMF=2.4\text{ wt\%}@outlet} = \partial \cdot \pi D \cdot L \cdot \rho_{\text{oil}@68^{\circ}\text{F}} \cdot \omega = 2.02 \text{ [grams]}$$

Here ∂ is oil film thickness and ω is local oil concentration in annular liquid film. The methodology of estimating oil film thickness and local oil concentration is described briefly in section 5.1.1.1 through section 5.1.1.3.

$M_{(D-E)@OMF=2.4\%@outlet}$ (or $M_{b(@OMF=2.4\text{wt\%}@outlet)}$) is total amount of oil mass injected at outlet from starting of injection at time $t_{0, \text{out}}$ at inlet until the time $t_{2, \text{out}}$ when oil layer was observed at sight glass s2 in pipeline between oil injection port at outlet and sight glass S2 (from D to E in Figure 4.19). It is calculated as follow:

$$M_{(D-E)@OMF=2.4wt%@outlet} = \int_{t_{0,out}}^{t_{2,out}} \dot{m}_{oil,injected@outlet} dt = M_{b(@OMF=2.4wt%@outlet)} = 98.6 \text{ grams}$$

Where, $\dot{m}_{oil,injected} = \frac{\dot{m}_{oil,injection}}{(1+S)}$ is the mass flow rate of oil injected at the inlet and at the outlet by subtracting the amount of refrigerant dissolved in the oil. The time $t_{0,in}$ and $t_{0,out}$ are the times at which the oil was first released to the inlet (point A in Figure 4.19) and outlet (point D in Figure 4.19). The time $t_{2,in}$ and $t_{2,out}$ are the times at which the oil was detected at the sight glass S2 (point E in Figure 4.19) for oil injection at the inlet and outlet of the test section. The final oil retention mass is calculated as follow:

$$M_{pipeline} = 0.85 \text{ grams} + 2.02 \text{ grams} + 98.6 \text{ grams} = 101.5 \text{ grams}$$

And

$$OR_{mass@OMF=2.8wt.}\% = 275.0 \text{ grams} - 101.5 \text{ grams} = 175.42 \text{ grams}$$

And the oil retention volume was calculated with the following equation:

$$OR_{volume@OMF=2.8wt.}\% = \frac{OR_{mass@OMF=2.8wt.}\%}{\rho_{oil@68^{\circ}F}} = \frac{175.42 \text{ grams}}{0.980 \text{ gram/cm}^3} = 179 \text{ cm}^3$$

Where ρ_{oil} was the density of the oil at reference temperature of 68 °F (20 °C). The oil retention inside the microchannel evaporator A is normalized with respect to the estimated internal volume of the heat exchanger, that is,

$$ORV_{N,@OMF=2.8wt.}\% = \frac{OR_{volume@OMF=2.8wt.}\%}{V_{total,Evap A}} = \frac{180 \text{ cm}^3}{1,890 \text{ cm}^3} = 0.0947 \text{ or } 9.47\%$$

In above calculation it is clear that oil mass retention in Pipeline ($M_{pipeline}$) is mostly dominated by $M_{(D-E)@OMF=2.4wt%@outlet}$. In the sample calculation above, oil retention volume was calculated for Microchannel Evaporator A. In summary, for this example, if the OMF in the evaporator A is 2.8 wt. % then the oil occupies 9.5 percent of the estimated internal volume of the heat exchanger.

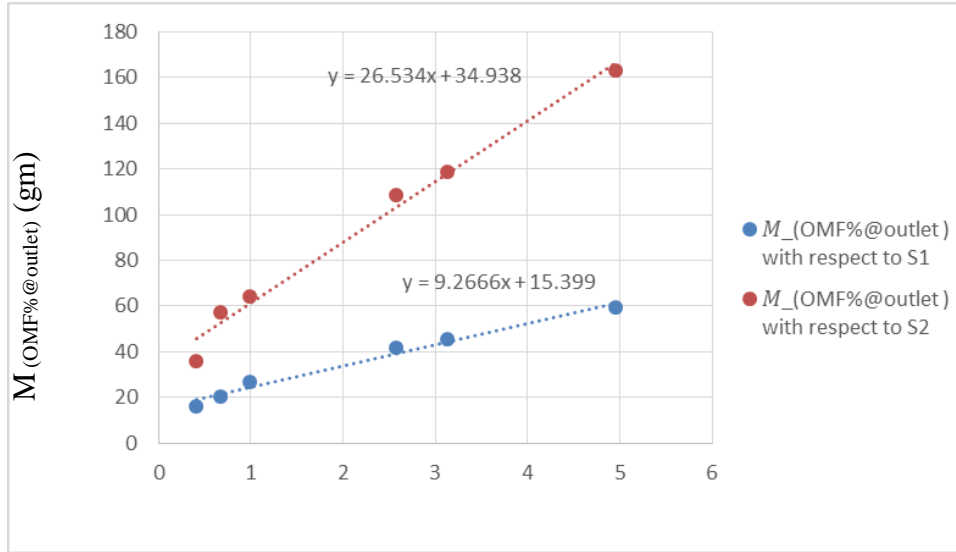
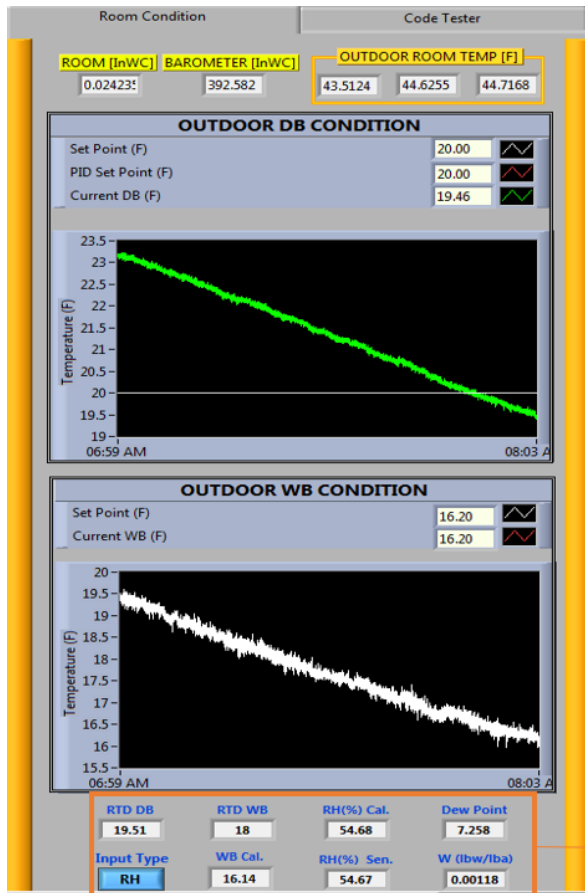


Figure 4.21: Mass of oil measured when injected at the outlet of the test section ($M_{(OMF\%@outlet)}$) versus OMF and for two locations of the flight glasses.

4.3.1.7 Heat transfer experiments with dry fin tests conditions

Dry fin tests conditions were defined as when the moisture in the air did not condensate or did not frost on the microchannel evaporators air-side heat transfer surfaces during the period of the experiments. During the heat transfer experiments, the microchannel evaporators were tested in dry fin tests conditions. The dew point temperature of the entering air stream was lower than the refrigerant saturation temperature inside the evaporators. Figure 4.22 shows an example of the measurements of dry bulb temperature, wet bulb temperature and relative humidity (sensor) of air entering the test section. Dew point temperature was calculated using dry bulb and wet bulb temperatures for above freezing wet bulb temperature and the dry bulb temperature and relative humidity for below freezing wet bulb temperature.



Various Notation for information of air entering Microchannel Evaporator

1. RTD DB – RTD Dry Bulb temperature (°F)
2. RTD WB – RTD Wey Bulb temperature (°F)
3. RH(% Cal. – Relative humidity calculated from Wet bulb and dry bulb (RTDs)
4. RH(% Sen. – Relative humidity measured from sensor
5. WB cal. – Wet bulb calculated using RTD DB and RH(% Sen.
6. Dew Point : Dew point of air entering microchannel calculated from RTD DB and RH(% Sen.

Figure 4.22: Screenshot of the Labview graphic interface DAQ displaying the psychrometric conditions of the air at the inlet of microchannel evaporator

Figure 4.23 shows an example in which frost formation accidentally occurred on the fins of microchannel evaporator A during an experiment. For this case, the saturation temperature of the refrigerant R410A in test section was 32°F (0°C). Since the experiments were conducted at constant blower speed, a gradual but continuous decrease of the air flow rate was symptomatic that frost might have been occurred. The air side air flow rate was continuously monitored live during the experiments by using a Labview graphic interface DAQ for the air flow rate, shown in Figure 4.24. The pressure difference across the nozzle, ΔP_{Nozzle} , was proportional to air flow rate across the evaporators. If frost formed on the fins, then the air flow rate decreased and any variation of the airflow rate was indicated by a decrease in the measured instantaneous ΔP_{Nozzle} . The decrease in ΔP_{Nozzle} was used as used an indicator that frost started to accumulate on the test section. If frost formation occurred, then the test was interrupted and a defrost cycle was initiated. In order to defrost the

microchannel, the saturation temperature of refrigerant in microchannel evaporator A was raised higher than 40° F and the setup was run overnight with warm air that melted the frost. Then the test was repeated.

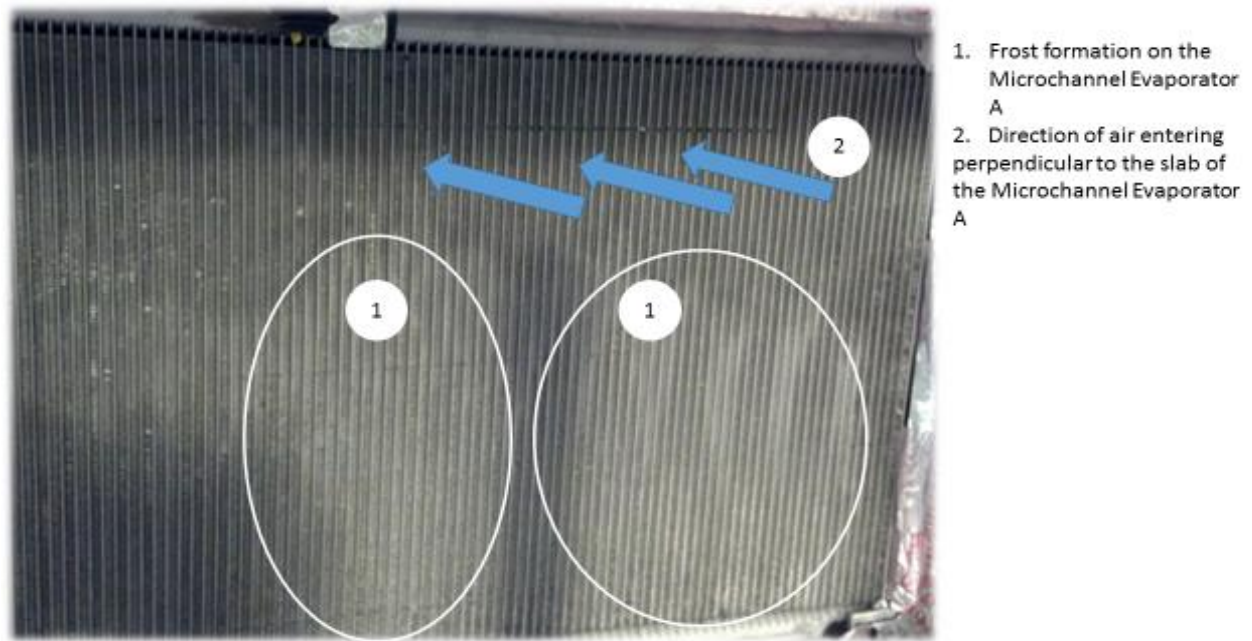


Figure 4.23: Example of a case in which frost formation on the microchannel evaporator A occurred during the experiments (the test was interrupted, the evaporator was defrosted, and then the test was repeated in frost-less conditions)

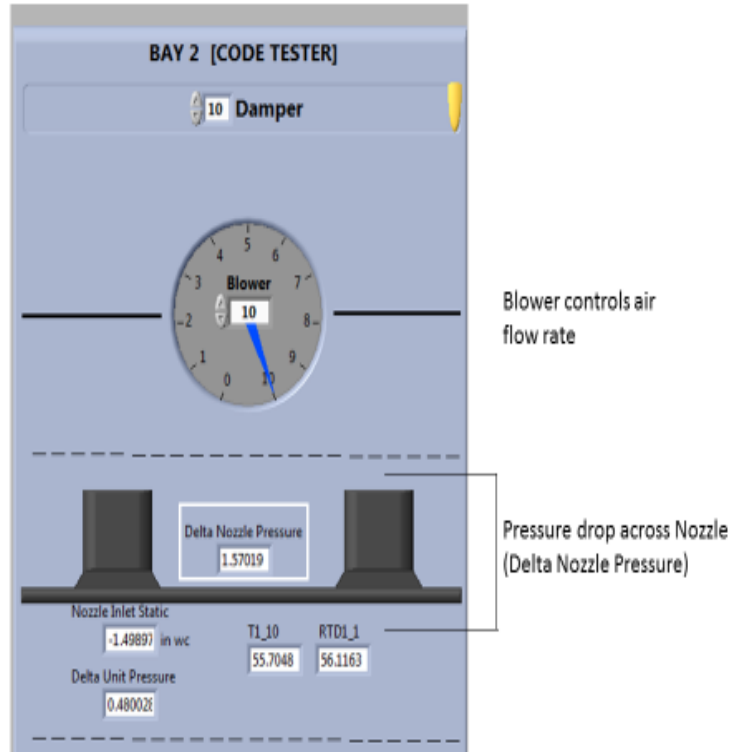


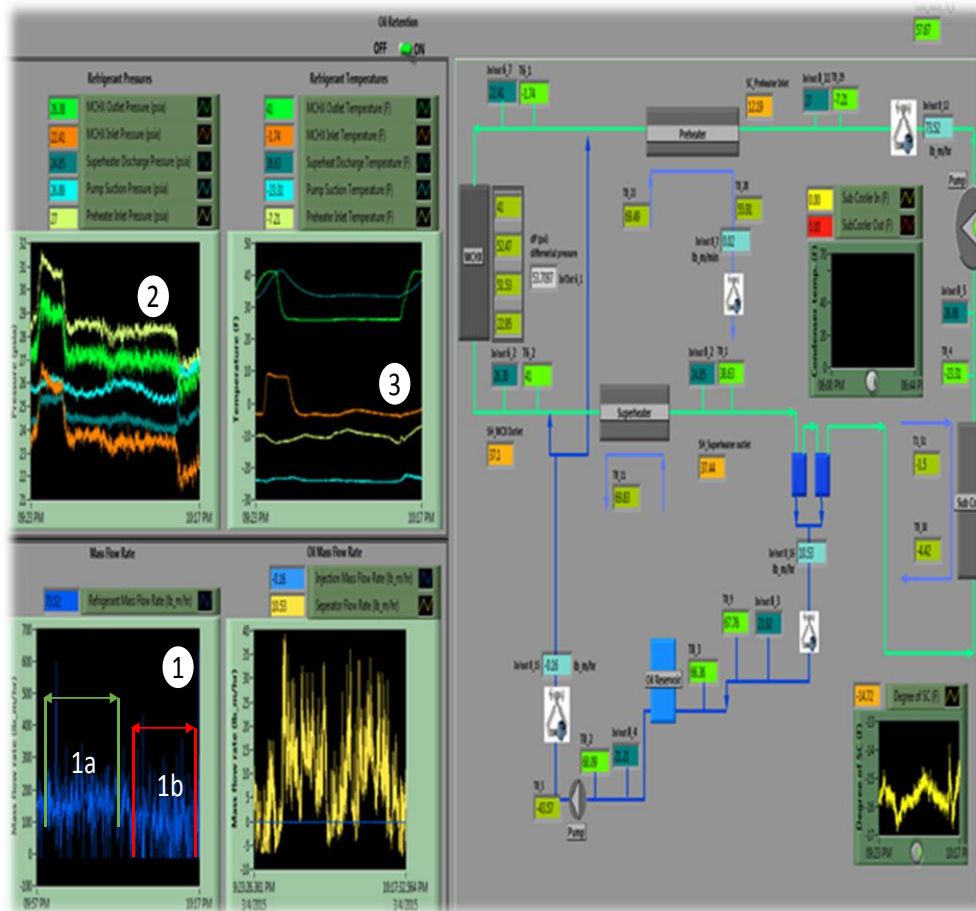
Figure 4.24: Display of the Labview graphic interface DAQ for the air blower and for the flow nozzles used to measure the air flow rate during the heat transfer experiments

4.3.2 Further attempts to reach refrigerant R134a saturation temperatures below 0°F (-18°C) for the microchannel evaporator tests

After completing the low temperature tests of the present work, further attempts were made to conduct evaporator tests at refrigerant R134a saturation temperatures ranging from -20°F to -10°F (-29°C to -23°C) in order to investigate oil retention effect for a wide range of refrigeration systems and applications. Unfortunately, we were not able to achieve saturation temperatures in the microchannel evaporators below 0°F (-18°C) with refrigerant R134a and with the experimental test apparatus of the present work. This section provides a brief description of the challenges encountered during our attempts to reach below 0°F (-18°C) temperatures and the objective of this section is to provide some information that can guide future test apparatus design dedicated to measure oil retention and oil effects on heat transfer and pressure drop in low temperature refrigeration applications.

With the test apparatus of the present work, the lowest refrigerant R134a saturation temperature in the microchannel test evaporators was 15°F (-9°C) when only cooling was supplied to the pump boiler loop and the refrigerant charge in the loop was not modified. To achieve saturation temperatures of 10°F (-12°C), 7°F (-14°C), and 0°F (-18°C) with refrigerant R134a, (see tests no. 16, 17, and 18 in Table 4.3), the overall operating pressure of the pump boiler loop was decreased by taking out some of the refrigerant from the loop. By increasing the cooling of the refrigerant R134a with the auxiliary low temperature refrigeration system and by managing the refrigerant charge in the pump boiler loop, we were able to achieve a saturation temperature of 0°F (-18°C) with refrigerant R134a in the microchannel evaporator A and still preserve enough flow rate to be able to carry the oil along the pipelines between the evaporator and the oil separators. For example, in order to lower the refrigerant saturation temperature from 15 to 5°F (from -9 to -15°C), the amount of refrigerant recovered from the pump boiler loop was about 13 to 15 lb_m (5.9 to 6.8 kg) from the 30 to 40 lb_m (13.6 to 18.1 kg) initially charged in the pump boiler loop for the microchannel test evaporators above 15°F (-9°C). The removal of refrigerant R134a from the pump boiler loop reduced the overall loop operating pressure and consequently lowered the saturation pressure of evaporation in the microchannel heat exchanger. But at the same time it also lowered the degree of subcooling at the refrigerant pump inlet to below 20°F (11°C) and large fluctuations in refrigerant mass flow rate appeared. Figure 4.25 shows an example in which the fluctuations of the refrigerant mass flow rate increased as refrigerant R134a was removed from the loop. During the period in which the fluctuations of the measured refrigerant mass flow rate shown in Figure 4.25 were recorded, the degree of subcooling of the refrigerant R134a at the gear pump inlet ranged 20 to 25 °F (11 to 14°C). Small bubbles were visually observed in the vertical sight glass that was installed in refrigerant receiver cylinder before the pump suction (see receiver and corresponding sight glass at the top of the pump in Figure 4.9). Figure 4.26 shows the sight glass through which such bubbles were observed in the refrigerant flow. The refrigerant R134a was transparent and bubbles were fairly visible in recorded videos of the flow inside this sight glass. Further removal of the refrigerant from the pump-boiler loop increased the fluctuations of mass flow rate and overall lowered the average refrigerant flow rate

circulating in the pump boiler loop. When the saturation temperature became lower than 0°F (-18°C), the pump cavitared and no more refrigerant flow rate was measured in the Coriolis flow meter installed after the pump. We speculated that in order to achieve saturation temperatures of -20°F to -10°F (-29°C to -23°C) with R134a in the microchannel test evaporators, an ultra-low refrigeration system is required to cool down R134a further and control the degree of subcooling at the pump inlet to at least 20 to 25 °F (11 to 14°C). In addition, the refrigerant pump, especially the gaskets and shaft bearings, must be able to handle temperatures below -25°F (-32°C) for long periods of testing. These technical limitations of the equipment used in the present project were the reasons that we were not able to set very low saturation temperatures with refrigerant R134a in the microchannel evaporator tests. However, the three low saturation temperatures investigated in the present work (that is, 10°F (-12°C), 7°F (-14°C), and 0°F (-18°C) with refrigerant R134a) provided clear information about the trends of oil retention and the effects of oil on heat transfer rates and pressure drops for some refrigeration applications.



1. Refrigerant mass flow rate
 - 1a. Acceptable conditions
 - 1b. Too much fluctuations
2. System pressure. (Psia)
 - i. Orange – MCHX inlet
 - ii. Green – MCHX outlet
3. System temperature (°F)
 - i. Orange – MCHX inlet
 - ii. Green – MCHX outlet

Figure 4.25: Screenshot of labview DAQ real time graphic interface indicating fluctuations in flow rate after discharging refrigerant from the system



1. Sight glass
2. Flow direction of refrigerant

Figure 4.26: Sight glass that shows the flow in receiver of auxiliary loop

4.3.3 Verification that the sight glasses visual observation and timing method provided similar results as oil injection and extraction method

Prior to oil retention tests in microchannel evaporators, the test setup of pump boiler loop, oil injection and extraction system were constructed by Deokar, 2013 and Yatim, 2015 for oil retention measurements in microchannel condenser. They measured oil retention in microchannel condenser using oil injection and extraction method described in section 2.6.1. This method required that pressure difference was established between the oil separators and oil reservoir through a complex network of pipelines, metering valves required. In the evaporator tests, it was not practical to establish a similar pressure difference because the evaporator outlet, i.e, the oil separator inlet, was already close to the lowest pressure point of the pump boiler loop. In the microchannel evaporator tests, the pressure difference between the oil separator and the pump suction was not enough to drive the oil down from the oil separator into the oil level reservoir. Therefore, when

using the present refrigerant pump-boiler type test apparatus, the oil injection and extraction method resulted not feasible for oil retention measurements when the heat exchangers were run as evaporators, that is, in the low side pressure section of the test apparatus. The sight glasses visual observation and timing method of the oil flow was introduced and adopted in the present work to overcome the feasibility limitations of using the extraction method. This sight glass visual observation and timing method was based on detecting the oil travel time when the oil was slowly metered in the pipelines, and then carried by the refrigerant flow from oil injection port until the sight glasses (S1 or S2 in Figure 4.3). The oil was practically used as tracer for the flow inside the pipelines. The fact that the oil retention was proportional to the oil travel time and oil mass flow rate metered in the pipeline during the injection tests was an approximation but it provided consistent and repeatable results from the experiments. Thus, the relative comparison of the oil retention data resulting from adopting this method at different OMFs, mass flux, and saturation temperature was still meaningful and useful in order to fulfill the main objectives of this thesis. A brief theoretical analysis of this approximation is given next.

In air-conditioning and refrigeration systems, the velocity of oil layer on the surface of heat exchanger or pipeline is very low which makes it reasonable to assume that oil can be accumulated in various parts of the system. Figure 4.27 shows separated annular two phase flow of refrigerant vapor and oil in a pipe section. According to Newton's law of viscosity, the velocity of oil film layer near to the surface is very low and almost zero due to the non-slip velocity boundary condition at the oil layer and wall surface interface. As distance of oil layer from the surface increases along y-axis as shown in Figure 4.27, the velocity of oil layer increases. For thinner oil films the velocity gradients are higher because it goes from zero velocity at the surface of wall to highest velocity at the interface. As viscous shear stress is directly proportional to the velocity gradient, the viscous shear stress will be higher in thinner oil film and it will be much harder to carry over. Therefore, as OMF in the refrigerant flow increases, the thickness of oil film δ and the corresponding average oil velocity increases. Using equation (5-32 and (5-33, the ratio of average vapor velocity to average oil velocity was calculated for low mass flux (series G in Table 6.1) condition and OMF of 0.5 wt.%, and 5

wt.% respectively. The ratio of refrigerant vapor velocity to liquid oil velocity ranges from 45 to 17 as OMF ranges from 0.5 wt.% to 5 wt.%. Therefore, oil has relatively slower velocity and thus higher traveling time at high OMF. The oil retained in the test section was assumed to be proportional to oil travel time measured from oil injection port until the first oil film appeared at one of the sight glasses (S1 or S2 in Figure 4.3). When oil travel time was higher at given OMF, then the oil retention in the test section and connecting pipelines was also higher. For example, the velocity of oil layer was estimated to be 0.25 ft./s (0.075 m/s) for low mass flux (series G in Table 6.1) at OMF of 0.5 wt.% and 0.62 ft./s (0.191 m/s) for high mass flux (series J in Table 6.1) at OMF of 0.5 wt.%. This meant that oil was observed at sight glass in less time for high mass flux condition when compared to low mass flux condition at same OMFs. Therefore, the oil mass retention for high mass flux case was lower than the corresponding oil mass retention for low mass flux condition and these results are discussed in details in section 6.1.

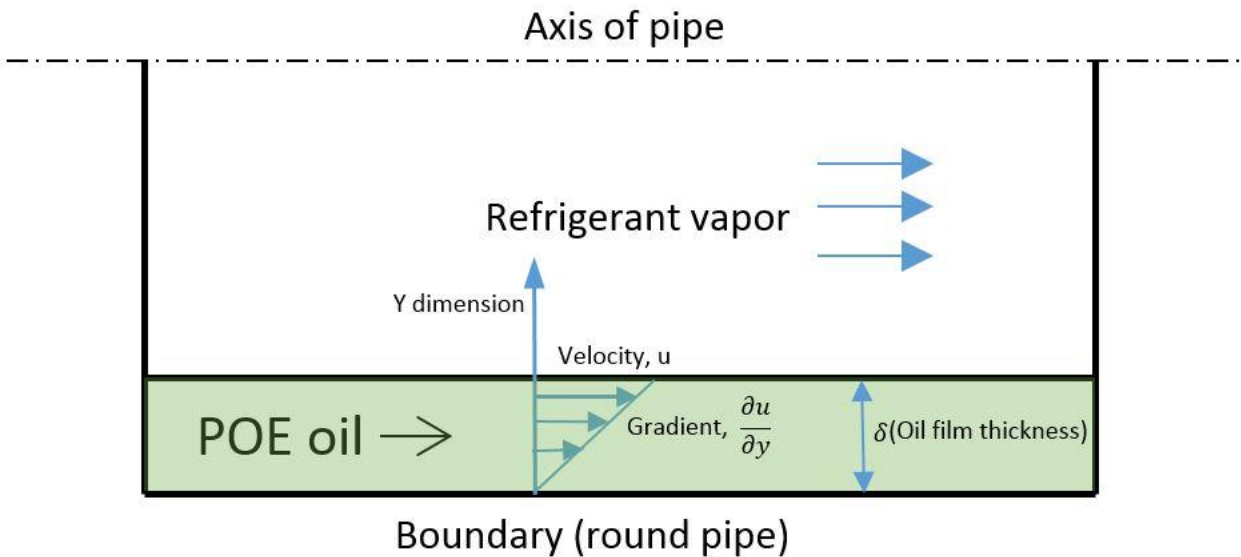


Figure 4.27: Comparison between oil retention measurements in the condenser by using the two equivalent experimental techniques of the present project.

Therefore by measuring oil travel time for inlet and outlet test at same mass flow rate and similar test section downstream conditions during injection of oil at inlet tests gave accurate measurements of oil retention in microchannel evaporator. The steps to calculate oil retention in test section is already discussed in section

4.3.1.6. Several tests were conducted by Yatim, 2015 to verify that two methods (Oil injection-extraction method and sight-glasses visual observation timing method) were equivalent and provided the same oil retention data within the experimental uncertainty. This section explains these verification tests.

First, it is important to emphasize that the efficiency of the oil separators of the pump boiler loop was not affected whether the test section was a condenser or an evaporator. For both condenser tests and evaporator tests, the condition of oil and refrigerant mixture at the inlet of oil separators was always superheated vapor phase and the oil separation process inside the oil separators was similar between the condenser tests and the evaporator tests (Yatim, 2015). Second, the equivalence of the oil retention volume measurements by using the collection of oil method (oil injection and extraction method) in the oil level reservoir and the oil flow visual observation and timing method were performed for condenser tests and the results are shown in Figure 4.28. The data in this figure were obtained for refrigerant R410A at saturation temperature of 105°F (41°C) for OMF of 1.6 and 4.5 wt.%. The results showed that the oil retention volume normalized, ORV_N , for both methods were in good agreement and the two methods provide equivalent oil retention results. The ORV_N for the oil flow visual observation and timing method was slightly lower for both OMFs but the difference of ORV_N values of 0.004 and 0.006 was well within the experimental uncertainty for ORV_N , which was ± 0.01 and it is indicated by the error bars in Figure 4.28. These results provided some confidence that the oil flow visual observation and timing method was accurate enough to be used in the condenser tests by Yatim, 2015 in his PhD work. Because the oil separation process shared similar characteristics between the condenser and evaporator tests, it was assumed that the relation of the ORV_N s between the two methods were valid for the evaporator tests.

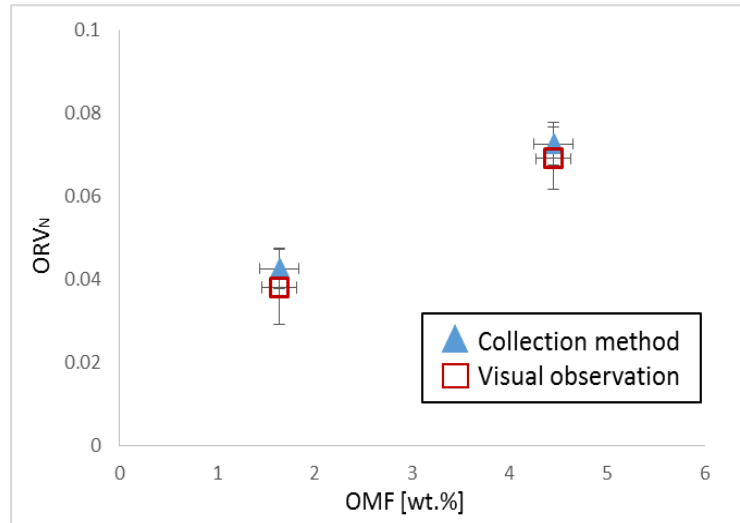


Figure 4.28: Comparison between oil retention measurements in the condenser by using the two equivalent experimental techniques of the present project.

4.4 Test Conditions and flow rates for the evaporators tests

The test conditions were selected based on typical applications for the refrigerants R410A and R134a in air conditioning systems and for refrigerant R134a in vending machines, water/wine coolers, and refrigeration systems. The saturation temperatures varied from 0 to 48°F (-18 to 9°C). Flow rates, OMFs and degree of superheat at test section outlet are summarized in Table 4.3.

Table 4.3 Test matrix for typical air conditioning systems, water/wine coolers, vending machines and refrigeration systems

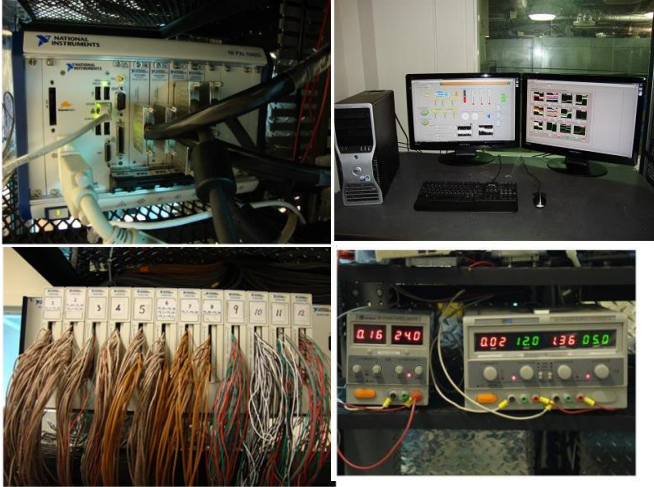

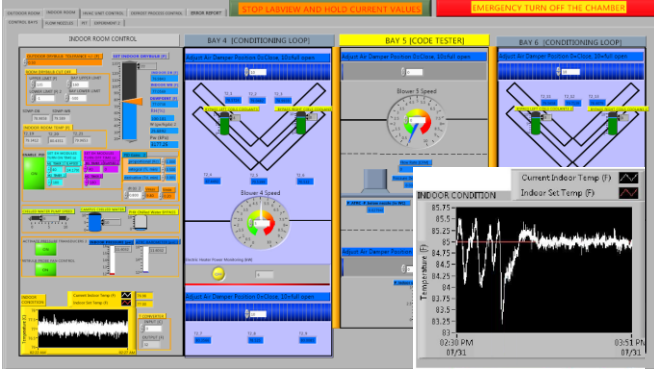

Test No.	Saturation Temp. [°F] (°C)	Refrigerant & Oil	Refrigerant Flow Rate [lb _m /hr] (g/s)	Oil Mass Fraction [wt.%]	Degree of vapor superheat at test section outlet [°F] (°C)	Component function / application
1	48 (9)	R410A/POE	360 (45) 200 (25)	0, 0.5, 1, 3, 5	10°F (5.5°C)	Evaporator A AC unit
2	38 (3.3)	R410A/POE				
3	32 (0)	R410A/POE				
4	39 (3.9)	R410A/POE	360 (45)	0, 1, 3	5°F(2.8°C)	
5	39 (3.9)	R410A/POE			15°F(8.3°C)	
6	39 (3.9)	R410A/POE			25°F(13.9°C)	
7	48 (9)	R410A/POE	360 (45) 200 (25)	0, 0.5, 1, 3, 5	10°F (5.5°C)	Evaporator B AC unit
8	38 (3.3)	R410A/POE				
9	32 (0)	R410A/POE				
10	39 (3.9)	R410A/POE	360 (45)	0, 1, 3	5°F(2.8°C)	
11	39 (3.9)	R410A/POE			15°F(8.3°C)	
12	39 (3.9)	R410A/POE			25°F(13.9°C)	
13	48 (9)	R134a/POE	200 (25)	0, 0.5, 1, 3, 5	10°F (5.5°C)	Evaporator A AC units, vending machines, water/wine coolers
14	38 (3.3)	R134a/POE				
15	33 (0.5)	R134a/POE				
16	10 (-12)	R134a/POE	150 (18.75)	0, 0.5, 1, 3, 5	10°F (5.5°C)	Evaporator A vending machines, water/wine coolers and refrigeration systems
17	7 (-14)	R134a/POE				
18	0 (-18)	R134a/POE				



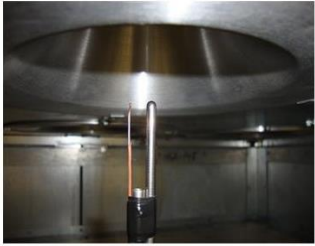
4.5 Further Details of the Equipment and Instrumentation of the Experimental Facility

Table 4.4 provides a brief description of the main equipment and sensors used for the present project. A state-of-the-art data acquisition system from National Instrument with Labview Real Time Controller was used for monitoring the tests, plotting, and recording the data. A designed pump-driven refrigeration system was used to control the saturation temperature of the refrigerant to the test section. A large variable speed fans was used to control the flow rate across the test section and for setting the environmental conditions during the

tests. The heat transfer capacity was measured from the refrigerant side (primary method) and from the air side (secondary method) for redundancy. The main sensors are also shown on the right column of Table 4.4.

Table 4.4 Main equipment and sensors of the psychrometric chamber used in this project

Equipment	Sensors
<p data-bbox="261 464 834 520">Process Control and Data Acquisition System (DAQ) (National Instruments PXI controller platform)</p> 	<p data-bbox="932 464 1414 520">Dry and Wet-bulb temperature probes inside chamber</p> 
<p data-bbox="358 1100 737 1127">Labview and Real Time Controller</p> 	<p data-bbox="954 1100 1393 1220">Dry-bulb and wet-bulb RDTs for air side measurements Dry bulb and wet bulb temperatures are measured according to ASHRAE standard 37 (Ashrae, 1988)</p> 

<p>Variable Speed Fan with VFD control</p> 	<p>Hot wire anemometer for local velocity measurements</p> 
<p>3 tons capacity water cooled heat pump unit. This unit will be used as auxiliary systems for outdoor room temperature below 40 °F</p>	<p>Air Pressure Transducers</p>
<p>5 tons capacity air cooled heat pump unit. This unit will be used as auxiliary systems to dehumidify the inlet air to the microchannel evaporator at low temperature tests</p>	<p>Air flow nozzle with RTD at the inlet of the nozzle. This calibrated nozzle measures the air flow rate according to ASHRAE standard 41.2 (Ashrae, 1987)</p> 

4.5.1 Air Tunnel Apparatus

The microchannel evaporators are placed inside the psychrometric chamber, while the remaining components in the test setup are installed outside the chamber. This section describes the position of the microchannel evaporators inside the chamber, and the instrumentation.

During the heat balance tests the refrigerant outlet was maintained superheated vapor conditions and refrigerant inlet was maintained subcooled liquid conditions. The error of heat transfer capacities measured from the refrigerant side and the air side were within $\pm 5\%$.

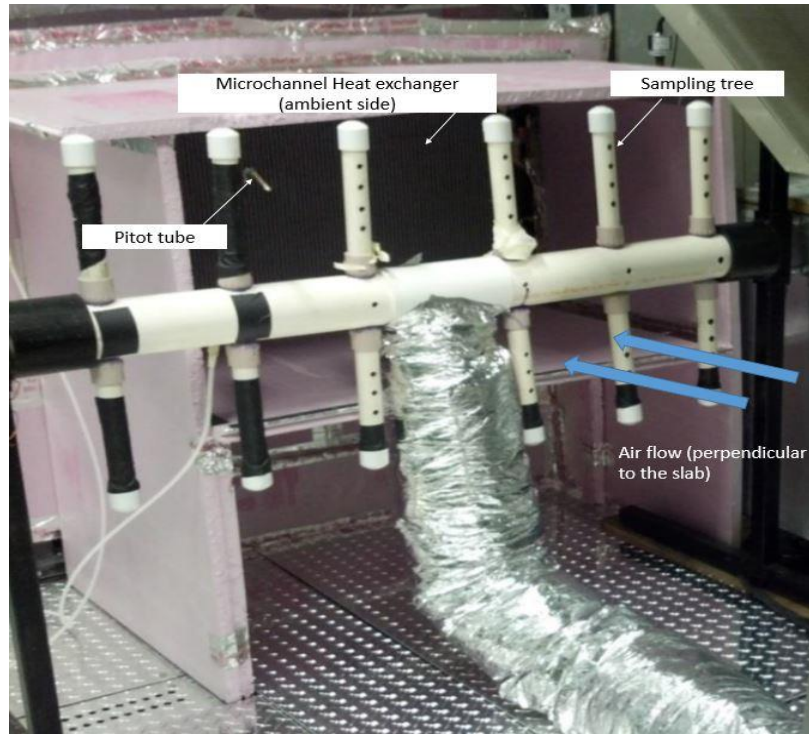


Figure 4.30: Front side of the microchannel evaporator exposed to the ambient air (air flow direction is entering the heat exchanger as indicated by the blue dashed arrow)

The position of the microchannel evaporator in the duct is such that it has the same face velocity of air over its entire slab. A thermocouples grid row was installed downstream to measure the air distribution. The grid consisted of 18 welded thermocouples on the air supply side and was placed 1 in. away from the microchannel evaporator A slab. The grid has 4 horizontal rows; starting from the top each row has 4, 5, 5, and 4 thermocouples.

The air side condition entering the microchannel evaporators was monitored using air sampling devices (see Figure 4.30). The sampling devices on the two sides of the microchannel heat exchanger, one exposed to the ambient air and the other on the side exposed to the supply air (see Figure 4.29), were constructed according

to ANSI/ASHRAE Standard 41.1(2013). The following section gives the description of the components of the sampling device and how they work.

The sampling trees shown that are positioned upstream and downstream of microchannel evaporators (Figure 4.29 and Figure 4.30) were similar in construction. Each sampling tree was constructed of a horizontal 4 in. (10.16 cm) diameter PVC pipe, the ends were capped, and the center was connected to a flexible duct. The horizontal PVC pipe has 12 vertical branches made of 1.5 in. (3.81 cm) diameter PVC pipes. Holes drilled into the branches face the air flow. The construction of the tree helps to mechanically collect small samples of air (collected through these holes) over a large region, mix them in the central horizontal PVC pipe, and then transport the mixture further through the flexible duct.

A flexible duct carries the sampled air from the sampling tree to the relative humidity measurement probe. Further, the sampled air gets carried through a long PVC pipe to the dry bulb and wet bulb temperature-measuring RTDs. The long PVC pipe assists in having a fully developed flow before the air reaches the temperature sensors. The wet bulb probe has its own water reservoir in which its wick is dipped.

A separate in-line centrifugal fan/blower (labeled as 'Fan' in Figure 4.29) helps to overcome the pressure drop in the 4 in. diameter flexible duct and the long PVC pipe from the sampling tree to the dry and wet bulb RTDs, inducing a sufficient air flow velocity of around 1000 ft/min (5 m/s) over the temperature sensors. The in-line centrifugal fan/blower from Suncourt Inc. Centrax (Model #TF104-CRD 4") has a capacity to have a flow rate of 200 cfm at least resistance. The flow rate at the temperature sensors is measured using a differential pressure transducer and a Pitot tube during the calibration phase. The blower then returns the sampled air back to the main airstream (on the downstream side of the sampling tree).

4.5.2 Low temperature chiller and condenser plate heat exchanger

Figure 4.31 is schematic representation of Dynalene supply from chiller to condenser. The chiller supplied Dynalene HC 40 to condenser (component 8 in Figure 4.3) plate heat exchanger of pump boiler loop in counter flow configuration. The supplied chilled fluid cooled down superheated refrigerant vapor from oil

separators to temperature below saturation temperature of the refrigerant in pump boiler loop. The model number of this chiller is CPCW-12LT/TC2-1-9X2 manufactured by Cooling Technology Inc. This low temperature chiller supplies up to 2.0 tons capacity with minimum leaving temperature up to -31.67°C (-25°F). The chiller is equipped with recirculating pump that supply up to 6 to 8 gpm with pressure rise between 25 to 30 psi (172.4 to 206.8 kPa). Chiller also utilized inline heater to control the temperature of Dynalene entering the condenser.

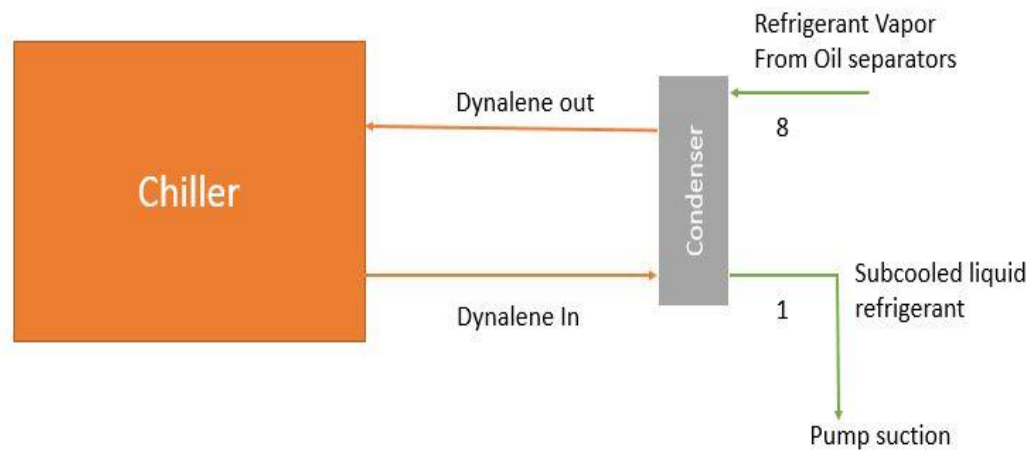


Figure 4.31: Schematic representation of flow Dynalene in from chiller to condenser

4.6 Instrumentation and Data Acquisition System

The oil retention measurement test facility utilized multiple sensors to measure the temperatures, pressures, mass or volume flow rates and other properties of air, refrigerant and oil. These sensors are discussed in brief in the following sections. These sensors were connected to National Instruments Data Acquisition (NI-DAQ) system with Real Time Labview Graphic Software Interface. The readings from the sensors were displayed, plotted, and recorded every 2 seconds. An example of the Labview graphic interface during one oil retention experiment is shown in Figure 4.32.

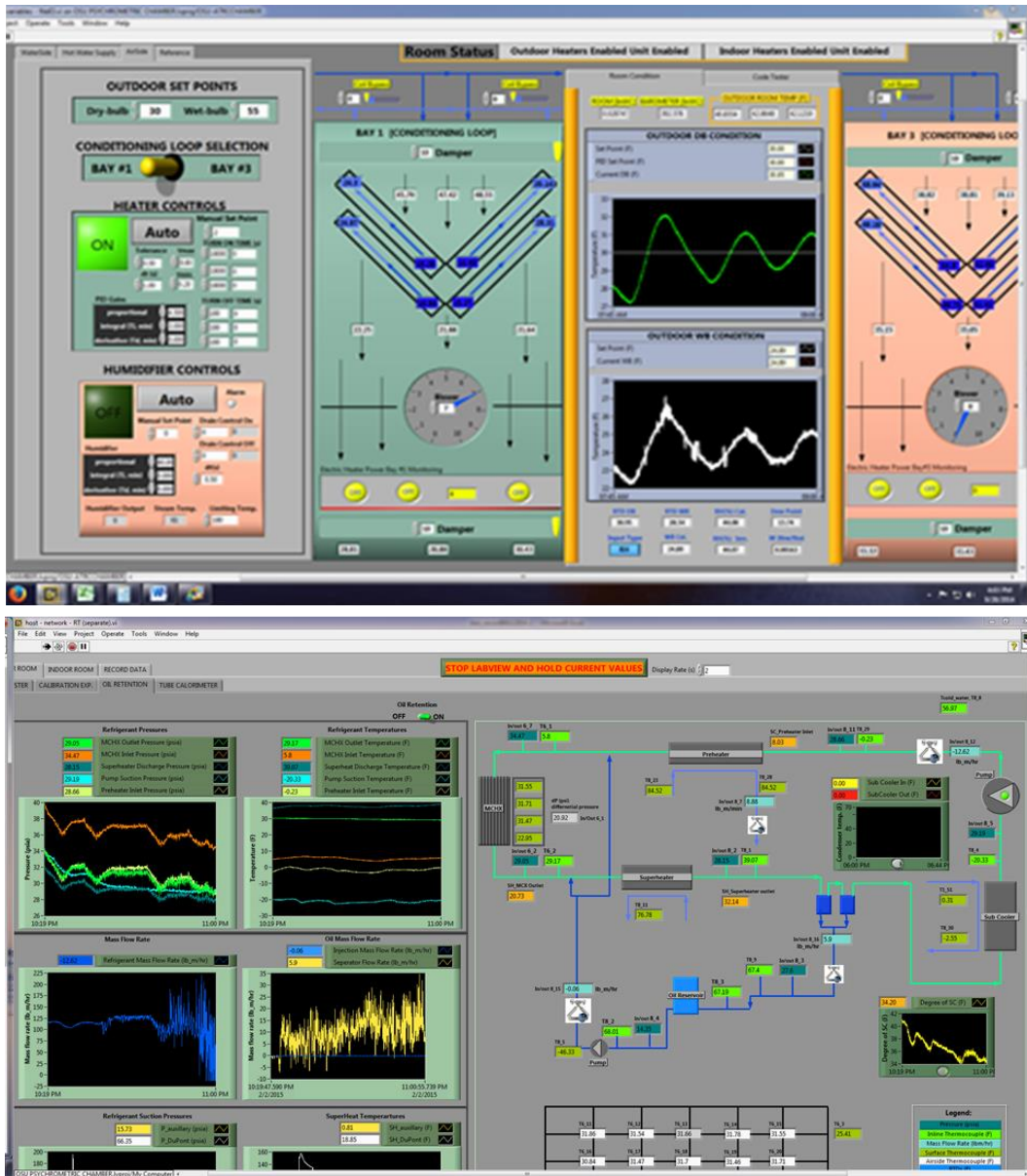


Figure 4.32: LabVIEW control and graphic interface for oil retention tests

The graphic interface consisted of two screens: the control screen (top image in Figure 4.32) was used to provide the inputs to both the air side and refrigerant side control parameters of the test facility. The display screen (bottom image in Figure 4.32) plotted all the readings from the sensors with time, which allowed to identify stable and quasi steady state conditions of the test apparatus before starting the actual oil retention test.

The instrumentation and main equipment used in the test setup for the oil retention test apparatus are listed in, which provides manufacturer, model, and a short description of the specification and functionality of each component.

Table 4.5 Specification of the components used in the oil retention tests

Component	Manufacturer [Model]	Specifications and description of use
Ball Valves, Gate Valves, PVC pipes, Copper pipes and tubes, and fittings	Grainger Inc., Lowe's, McMaster-Carr, Locke Supply Co, United Refrigeration Inc.	Refrigeration system and Hydronic system (water side of the sub cooler, auxiliary heat exchanger and the evaporators).
Centrifugal pump	Taco [1400 – 50 –A]	Input: 230 V, 60 Hz, 1 phase, 2.4 A, 3450 rpm; used to provide necessary head at the sub cooler and the superheater's inline heater.
Check valve	McMaster-Carr [7775K12,7768K14]	One is used on the oil injection line and the other on the pressure equalization line.
Coalescent Separator	Temprite [925R]	Separates up to 0.05 microns particles, height: 28.6 in. (0.73 m), diameter: 4 in. (10.2 cm). The bottom 16.4 in. (41.6 cm) serves as a reservoir, which has sight glass for monitoring purpose. Internal float valve absent.
DAQ wire	Olympic Wire and Cable Corp. [2824]	Multi-conductor 24 AWG cable; used to connect the sensors to the DAQ system.
Flow Switch - water flow circuits	McDonnell & Miller [FS6-3/4]	Allows minimum flow rate of 0.12 gpm and maximum flow rate of 2.5 gpm.
Gear Pump Motor	Baldor. Reliance Super-E motors [CEM3545]	Input: 230/460 V, 2.8/1.4 A, 60 Hz, 3 phase, usage: 0.75 kW, 1 hp, 3450 rpm; used for refrigeration and injection gear pumps

Helical separator	Henry Technologies Inc. [S-5188]	Designed for 10 cfm for 10 tons refrigeration capacity, height: 19 in. (48.3 cm), diameter: 4 in. (10.2 cm). Internal float valve absent.
High Temperature Heater Tapes	OMEGA Engineering Inc. [FWH171-060]	Input: 120 V, usage: 624 W with 5.2 W/in ² , resists up to 900 °F (480 °C); used to heat the oil-refrigerant mixture in the oil reservoir and the oil level tank.
High-Pressure Safety Valves	McMaster-Carr [5825T21]	The brass safety valve is placed after the refrigerant gear pump (not shown in any figures), and is designed to relieve the pressure from the system if it exceeds 500 psig (34.5 bar).
Injection Gear Pump	Micropump	
Injection Oil Reservoir (Blue Tank), Oil Reservoir #1	Emerson Climate Technologies [AOR-4]	Capacity: 4 gallon (15.1 L), 2.5 ft. (0.88 m) tall; stores the oil to be injected using the injection gear pump.
In-Line Centrifugal Fan	Suncourt Inc. Centrax [TF104-CRD 4"]	Input: 120 V, 0.53 A, 60 Hz, 1 phase, usage: 60 W, 4 in. (10.2 cm) air inlet and outlet, 200 cfm, in-line centrifugal fan; used as a fan/blower on the air sampling device.
Needle Valve 1/4"	Parker Hannifin Corp. [4A-V4LR-B]	Opens 10% per 1/2 turn - total 5.125 turns; used on the pressure equalization and the oil injection lines.
Needle Valve 3/8"	Parker Hannifin Corp. [6A-V6LR-B]	Opens 10% per 1/2 turn - total 5.5 turns; used for refrigerant mass flow rate control.
Plate Heat Exchanger	GEA [GB400L-14]	14 plates, heat transfer area of 16 ft ² , and minimum heat transfer capacity of 15750 Btu/h
Refrigerant Filter-Dryer	Parker Hannifin Corp. Sporlan Division [C-032]	Size of 3 in ³ , removes moisture, dirt, acid, and sludge; initially was used on the refrigerant liquid line, then was transferred on oil line to filter it.
Refrigerant Filter-Dryer	Parker Hannifin Corp. Sporlan Division [C-083-S-HH 3/8]	Size of 8 in ³ , removes moisture, dirt, acid, and sludge; used after the refrigerant gear pump.

Refrigeration Gear Pump	Micropump [GC-M25.JVS]	0.48 gallon/1000-rev (1.82 ml/rev), maximum differential pressure: 125 psi (862 kPa)
Remote gas bulb control thermostat	Honeywell [L4008A]	Control thermostat with high temperature limit of 150°F (66°C); used on the Vapor Compression cycle system.
Service Manifold	Ritchie Engineering Co., Inc. YELLOW JACKET product division [Series 41]	Used to charge and recover the refrigerant from the system.
Sight glass	McMaster-Carr [1138K64]	Pipe size - 1/2 in; used to monitor the oil-refrigerant extraction at the oil separators, and also to ensure that liquid refrigerant enters the refrigerant gear pump (not shown in any figures)
Sight Glass Tube/ Level Indicator	McMaster-Carr [1106K76]	Designed for maximum pressure of 240 psi, viewing glass of 18 in. length; it is graduated and connected to oil level tank to measure the volume of the extracted oil-refrigerant mixture.
Suction Line Accumulator	Grainger Inc. [6AXD3]	Placed on the suction line to prevent any liquid refrigerant to enter the compressor.
Suction line Filter-Dryer	Parker Hannifin Corp. Sporlan Division Catch-All [C-417-S-T-HH]	Separates moisture, dirt, acid, sludge doing to the compressor
Variable frequency Drive	Baldor Electric Company [VS1SP21-1B]	Input: 230 V, 4.2 A, 60 Hz, 3 phase, usage: 0.75 kW, 1hp; Configured for the motors of the refrigerant gear pump and the injection gear pump.
Variable Transformer	Superior Electric [3PN116C]	Input: 120 V, 50/60 Hz, 1 phase, 1.4 KVA, output: 0 - 120V; variac for the heater tapes.

4.6.1 Temperature Measurements

The temperature sensors on the air side were resistance temperature detector-type (RTD). RTD works based on the effect of temperature on the electrical resistance of material, in this case, platinum. Platinum is chosen in place of nickel or copper on account of its inertness, and also because its temperature and resistance relation is repeatable over a large temperature ranges. In this study, RTDs were used to measure dry and wet bulb

temperatures at the inlet and outlet of the air flow across microchannel heat exchanger. It was also used to measure the temperature of air at the inlet other nozzle bank ($T_{N,i}$). The specification is listed in Table 4.6.

Table 4.6 Specifications of Resistance Temperature Detectors

Item	Item Specification
Model	P-M-1/3-1/8-6-0-T-3
Type	Pt100
Range	-148 to 752°F (-100 to 400°C)
Accuracy	Accuracy 1/3 DIN (-50 ±0.18°C, 0 ±0.1°C, 100 ±0.27°C); ±0.1°F (±0.05°C) after calibration.
Description	100 Ω at 0°C; temperature coefficient of resistance = 0.00385 Ω/Ω/°C; 6" length, 1/8" diameter
Manufacturer	Omega Engineering, Inc.

A thermocouple (TC) works on the principle of the thermoelectric effect, more precisely the Seebeck effect; where a junction (TC) of two dissimilar metals produces voltage when there is a temperature difference between the junction and the voltmeter. The voltage generated across the TC is then calibrated with the help of a reference cold junction to produce an accurate temperature reading. Thermocouples are used on air side, oil side and refrigeration side. The specifications of the TCs are shown in Table 4.7.

Table 4.7 Specifications of the Thermocouples

Item	Item Specification
Type	T-type
Model: Inline Thermocouple	TMQSS-125G-6
Model: Thermocouple Wire	TT-T-24-SLE-1000, the wire needs to be welded.
Range	-40 to 130°F (-40 to 54°C)
Accuracy	±0.5°F (0.3°C); ±0.1°F (±0.05°C) after calibration.
Manufacturer	Omega Engineering, Inc.

Inline thermocouples are installed to measure the temperatures at the refrigerant gear pump inlet ($T_{pump,i}$), the preheater inlet ($T_{pre,in}$), the microchannel evaporator inlet ($T_{mchx,i}$), and the microchannel evaporator

outlet ($T_{mchx,o}$). They are also used to measure the temperature of the injected oil-refrigerant mixture ($T_{oil-ref,i}$). These inline thermocouples are placed in the stream of oil and refrigerant using compression fittings to prevent any possible leaks.

A grid of 18 welded TCs is used on the air supply side of the microchannel heat exchanger. This grid helps in calculating the heat transfer to the air on selected sections of the microchannel heat exchanger slab. A TC is also placed at the inlet of the nozzle in parallel with the RTD, for cross-referencing. A welded TC is attached to the fin of the microchannel heat exchanger when capturing the infrared images in order to calibrate the camera.

Calibration of the TCs and the RTDs is done in a temperature bath with reference to a NIST (National Institute of Standards and Technology) traceable thermometer having an accuracy of $\delta T_a = \pm 0.36^\circ\text{F}$ ($\pm 0.2^\circ\text{C}$). The software by National Instruments, Measurement & Automation Explorer (MAX) is used along with the NI-DAQ to record the data points at a sampling rate of 1 millisecond (1 kHz) during the calibration. These TCs and RTDs are calibrated to an uncertainty of $\delta T_b = \pm 0.05^\circ\text{F}$ ($\pm 0.03^\circ\text{C}$) with respect to the thermometer. Adding the errors in the thermometer and the calibrated TCs or RTDs in quadrature (Taylor 1996), gives the net error or uncertainty δT of 0.36°F ($\pm 0.2^\circ\text{C}$) in temperature measurements. Temperature measurements using the RTDs and TCs followed and exceeded the ANSI/ASHRAE Standard 41.1 (2013).

4.6.2 Oil and Refrigerant Pressure Measurements

Absolute pressure transducers are installed to measure the pressures at the refrigerant gear pump inlet ($P_{pump,i}$), the preheater inlet ($P_{pre,in}$), the microchannel evaporator inlet ($P_{mchx,i}$), and the microchannel evaporator outlet ($P_{mchx,o}$) to measure pressure of the injected oil-refrigerant mixture ($P_{oil+ref,i}$) using the transducer at the oil reservoir. The specifications of the absolute pressure transducer are shown in Table 4.8. For refrigerant and oil lines having less than 5/8 in. (15.8 mm) outer diameter, the tubing to the pressure transducers is of the same size, while for higher diameter copper lines, the tubing are kept as small as possible to avoid turbulence at the sensor, which could measure total pressure instead of static pressure. All the

pressure measurements on the refrigerant, oil, and air side are done according to ANSI/ASHRAE Standard 41.3 (2014).

Table 4.8 Specifications of the Absolute Pressure Transducers

Item	Item Specification
Model	206
Pressure Range	7 to 500 psia (50 to 3450 kPa)
Accuracy	± 0.65 psi (± 4.5 kPa)
Output	24 VDC Nominal
Excitation	0-5 VDC
Manufacturer	Setra System, Inc.

A set of differential pressure transducers (for more information see Table 4.9) were placed between the inlet and the outlet lines outside the psychrometric chamber connecting the microchannel evaporator slab. It measures the pressure drop experienced by the refrigerant or the oil-refrigerant mixture when flowing through the resisting ports of the micro-channels. The specifications of the differential pressure transducer are shown in Table 4.9.

Table 4.9 Specifications of the Differential Pressure Transducers

Item	Item Specification
Model	P55D-4-N-4-40-S-4-A
Pressure Range	8 to 12.5 psi (55 to 86 kPa), actually it can measure as low as 0 psi.
Accuracy	$\pm 0.25\%$ of full scale; ± 0.03 psi
Output	4 to 20 mA
Excitation	9-55 VDC
Manufacturer	Validyne Engineering

4.6.3 Air Humidity Measurements

The relative humidity (ϕ or RH) values of the ambient air and the air supplied by the microchannel heat exchanger are measured and then used along with the dry bulb temperatures to determine the density of the air flowing across the heat exchanger. The specifications are shown in Table 4.10.

Table 4.10 Specifications of the Relative Humidity Sensors

Item	Item Specification
Model	HX71-MA
Operating temperature range	-13 to 185°F (-25 to 85°C)
Accuracy	$\pm 3.5\%$ from $\phi = 15\%$ to $\phi = 85\%$; $\pm 4\%$ below $\phi = 15\%$; and $\pm 4\%$ above $\phi = 85\%$ when measured at 73.4°F (23°C).
Manufacturer	Omega Engineering, Inc.

4.6.4 Air Flow Measurements

The airflow nozzles are arranged in parallel at the nozzle bank to have a pressure drop in the airflow path. Pressure drop measurements are used to calculate the air flow rates (*CFM*). This *CFM* value is then used for the air side calculations, to check the heat balance with the refrigerant side calculations. All the air flow measurements are done according to the ANSI/ASHRAE Standard 41.2 (1987). The specifications of the nozzles are shown in Table 4.11.

Table 4.11 Specifications of the Air flow Nozzles

Item	Item Specification
Model	Elliptical nozzle
Metal	Aluminum
Bore Diameter	8" (203 mm), 7" (178 mm), and 0.5" (12.7 mm)
Operating range	150 to 2,000 cfm (0.07 to 1 m ³ /s)
Accuracy	$\pm 0.4\%$ of flow rate (using Setra 264 pressure transducer and precise calculation of uncertainty propagation); Tightest Tolerance $\pm 0.001''$ (± 0.0254 mm) = error in bore diameter.
Manufacturer	Helander Metal Spinning Company

Very low differential pressure measurement of air was performed by a unidirectional differential pressure transducers, 2641-003WD, measure the air pressure drop across the nozzle bank ($\Delta P_{air,N}, \Delta P2$) and the microchannel heat exchanger ($\Delta P_{air,mchx}, \Delta P1$), while 2641-2R5WD measures the static pressure of the Psychrometric test room ($P_{air,amb}, P1$) in which the microchannel heat exchanger is placed. The bidirectional differential pressure transducer, 2641-1R5WB, measures the static pressure before the nozzle bank ($P_{air,N,i}, P2$). The specifications are shown in Table 4.12. Simple Pitot tubes are used to measure the pressure inside the air ducts; they are either purchased or constructed from small size copper tubes. As recommended, these Pitot tubes have holes of 1/16 in. (1.6 mm) diameter perpendicular to the direction of the air flow.

Table 4.12 Specifications of the Very Low Differential Pressure Transducers

Item	Item Specification
Model	264
Manufacturer	Setra System, Inc.
1.) Unidirectional Transducer	2641-003WD
Pressure Range	0 to 3 in. W.C. (0 to 747 Pa)
Accuracy	$\pm 0.25\%$ of full scale; ± 0.0075 in. W.C.
Output	24 VDC Nominal
Excitation	0-5 VDC
2.) Unidirectional Transducer	2641-2R5WD
Pressure Range	0 to 2.5 in. W.C. (0 to 623 Pa)
Accuracy	$\pm 0.25\%$ of full scale; ± 0.00625 in. W.C.
Output	0-5 VDC Nominal
Excitation	9-30 VDC
3.) Bidirectional Transducer	2641-1R5WB
Pressure Range	± 1.5 in. W.C. (± 373 Pa)
Accuracy	$\pm 0.25\%$ of full scale; ± 0.0075 in. W.C.
Output	24 VDC Nominal
Excitation	0-5 VDC

Table 4.13 Specifications of the Refrigerant Mass Flow Meter

Item	Item Specification
Model	(CMF025) CMF025M319NRAAEZZZ
Type	Coriolis Flow and Density Meter
Transmitter	2700C12BBAEZZZ
Flow rate range	4800 lbm/h (2180 kg/h)
Flow rate accuracy	±0.10% of the flow rate
Zero stability	0.06 lbm/h (0.027 kg/h)
Density range	312 lbm/ft ³ (5000 kg/m ³) or (5 g/cm ³)
Density accuracy	±0.0312 lbm/ft ³ (±0.5 kg/m ³)
Temperature range	300°F (148°C)
Temperature accuracy	±2°F (±1°C)
Output	4 to 20 mA
Pressure rating for sensor	1500 psig (10.4 MPa)
Manufacturer	Micro Motion Inc.

4.6.5 Oil flow and refrigerant flow measurements

The mass flow rate of the refrigerant (\dot{m}_{ref}) and the injected oil-refrigerant mixture ($\dot{m}_{oil-ref,inj}$), are measured using the Coriolis flow meter. The mass of the oil injected at the microchannel evaporator inlet ($m_{oil,in}$) is measured by integrating the value of the mass flow rate of injected oil with the time-period of the test. The Coriolis meter can be used to measure either liquid or gas mass flow rate, but it is only employed to measure liquid mass flow rates. The specifications for the mass flow meters are shown in Table 4.13 and Table 4.14, respectively. The mass flow meter CMF025 is placed between the refrigerant gear pump and the preheaters to measure the pumped refrigerant mass flow rate. One mass flow meter CMF010M is placed at

the oil injection gear pump on the injection line to measure the injected oil-refrigerant mixture's mass flow rate.

Table 4.14 Specifications of the Oil-Refrigerant Mixture Injection and Extraction Mass Flow Meter

Item	Item Specification
Model	(CMF010M) CMF010M323NRAAEZZZ
Type	Coriolis Flow and Density Meter
Transmitter	2700C12BBAEZZZ
Flow rate range	240 lbm/h (108 kg/h)
Flow rate accuracy	±0.10% of the flow rate
Zero stability	0.0045 lbm/h (0.002 kg/h)
Density range	312 lbm/ft ³ (5000 kg/m ³) or (5 g/cm ³)
Density accuracy	±0.0312 lbm/ft ³ (±0.5 kg/m ³)
Temperature range	300°F (148°C)
Temperature accuracy	±2°F (±1°C)
Output	4 to 20 mA
Pressure rating for sensor	1813 psig (12.6 MPa)
Manufacturer	Micro Motion Inc.

According to the manufacturer, the rated accuracy of the mass flow meter is ±0.10% of the flow rate. But, if the actual flow rate is less than $\frac{\text{zero stability}}{0.001}$, then the accuracy is $\pm \left(\frac{\text{zero stability}}{\text{flow rate}} 100 \right) \%$ of the flow rate. The oil-refrigerant mass flow rate in the system varied from 3 to 20 lbm/h. The $\frac{\text{zero stability}}{0.001} = \frac{0.0045}{0.001} = 4.5$ lbm/h, which means that the flow rate from 3 to 4.5 lbm/h has the uncertainty greater than ±0.10% of the flow rate. If calculated, the uncertainty at 3 lbm/h is ±0.15% of the flow rate. Comparing the percentage of the net region of 4.5 to 20 lbm/h with the region of 3 to 4.5 lbm/h it will be reasonable to choose the uncertainty as ±0.10% of the flow rate. This is illustrated in Figure 4.33. The refrigerant mass flow rate in the system is

always greater than 300 lbm/h, while the $\frac{\text{zero stability}}{0.001} = \frac{0.06}{0.001} = 60 \text{ lbm/h}$, which is very small compared to the flow rate of the refrigerant in the system. Hence, the uncertainty in the refrigerant flow rate is $\pm 0.10\%$ of the flow rate.

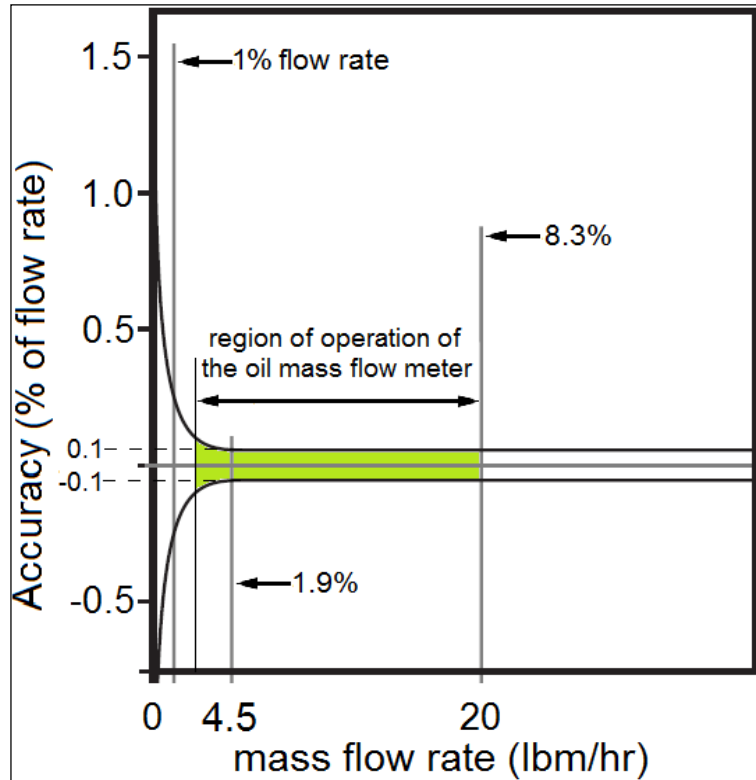


Figure 4.33: Relation between the flow meter accuracy and the mass flow rate (Deokar, 2013)

A weighing scale is used to measure the weight of the oil-refrigerant samples collected at the end of each injection test to determine the solubility of the refrigerant in the oil using the gravimetric method. The specifications of the weighing scale are shown in Table 4.15.

Table 4.15 Specification of the Weighing Scale

Item	Item Specification
Model	SAW-L
Capacity	50 lb (22 kg)
Resolution	0.0005 lb (0.2 g)
Accuracy	$\pm 0.01\%$ of full scale; $\pm 0.005 \text{ lb}$ ($\pm 2.2 \text{ g}$)
Manufacturer	Arlyn scales

CHAPTER V

5. DATA REDUCTION AND UNCERTAINTY ANALYSIS

5.1 Data Reduction

5.1.1 Oil retention in microchannel evaporators calculation

The amount of oil carried over with the refrigerant in the microchannel heat exchanger was referred to as the oil mass fraction (OMF) and it was defined as follows:

$$OMF = \frac{\dot{m}_{oil}}{\dot{m}_{oil} + \dot{m}_{ref}} \times 100 \quad (5-1)$$

where \dot{m}_{oil} was the measured flow rate of the oil released to the test section and \dot{m}_{ref} was the measured flow rate of refrigerant in the test setup. Oil was injected at the inlet of the test section with OMF of x wt.%. Once the travel time for the oil to go from S1 to S2 was estimated, the corresponding OMF of $(x - \delta x)$ wt.% for the injection at the outlet of the test section was also found. It should be notice that for the δx was small and for some of the tests it was zero. For these two OMFs identified, the oil travelled in the pipeline downstream the test section with the same velocity. The oil retention was calculated as follow:

$$OR_{mass@OMF=x \text{ wt.\%}} = M_{a@OMF=x \text{ wt.\%}@inlet} - M_{pipeline} \quad (5-2)$$

$$M_{pipeline} = M_{(A-B)@OMF=x \text{ wt.\%}@inlet} + M_{(C-D)@OMF=(x-\delta x) \text{ wt.\%}@outlet} \\ + M_{(D-E)@OMF=(x-\delta x) \text{ wt.\%}@outlet} \quad (5-3)$$

Where,

$$M_{a@OMF=x \text{ wt.\%@inlet}} = \int_{t_{0,in}}^{t_{2,in}} \dot{m}_{oil,injected@inlet} dt = M_{(A-E)} [grams] \quad (5-4)$$

$$M_{(A-B)} = \frac{OMF}{100} \cdot \rho_{oil@68^\circ F} \cdot V_{a-b} = M_{(A-B)} [grams] \quad (5-5)$$

$$M_{(C-D)@OMF=(x-\delta x)\text{wt.\%@outlet}} = \partial \cdot D \cdot L \cdot \rho_l \cdot \omega = M_{(C-D)} [grams] \quad (5-6)$$

Here ∂ is annular liquid film thickness in the pipeline and ω is local oil concentration in liquid film. These two parameters are estimated based on empirical correlations available in literature. The procedure for calculation of ω and ∂ is discussed in section 5.1.1.1 through section 5.1.1.3.

$$M_{(D-E)@OMF=(x-\delta x)\text{wt.\%@outlet}} = \int_{t_{0,out}}^{t_{1,out}} \dot{m}_{oil,injected@outlet} dt = M_{(D-E)} [grams] \quad (5-7)$$

And where $\dot{m}_{oil,injected} = \frac{\dot{m}_{oil,injection}}{(1+S)}$ was the mass flow rate of oil injected at the inlet and at the outlet by subtracting the amount of refrigerant dissolved in the oil. The time $t_{0,in}$ and $t_{0,out}$ were the times at which the oil was first released to the inlet and outlet of the test section. The time $t_{2,in}$ and $t_{2,out}$ were the times at which the oil was detected at the sight glass S2 for oil injection at the inlet and outlet of the test section. The final oil retention mass in the test section was calculated as follows:

$$ORmass@OMF=x \text{ wt.\%} = M_{(B-C)} = M_{(A-E)} - M_{(A-B)} - M_{(C-D)} - M_{(D-E)} \quad (5-8)$$

And the oil retention volume in the test section was calculated as follows:

$$ORvolume@OMF=x \text{ wt.\%} [cm^3] = \frac{ORmass@OMF=x \text{ wt.\%} [grams]}{\rho_{oil@68^\circ F} [grams/cm^3]} \quad (5-9)$$

Where ρ_{oil} was the density of the oil at reference temperature of 68 °F (20 °C). The oil retention inside the microchannel heat evaporators was normalized with respect to the estimated internal volume of the heat exchanger, that is, internal volume of the tubes plus the internal volume of the headers:

$$ORV_{N,@OMF=x \text{ wt.\%}} [-] = \frac{ORvolume@OMF=x \text{ wt.\%}}{V_{total,internal \ volume}} \quad (5-10)$$

The ORV_N was a dimensionless number that varied from 0 for the case of no oil retained in the heat exchanger to 1, if the heat exchanger was completely filled up with oil. In the experiments ORV_N varied from 0.01 to 0.15, that is, the oil retained in the heat exchanger ranged from 1 up to 15 percent of the estimated internal volume of the heat exchanger. An example of the above data reduction procedure was provided in section 4.3.1.6 of this report.

It should be noted that the length of Pipeline A-B and Pipeline C-D was less than 0.5 m for microchannel evaporator A. Due to shorter pipe lengths, the sum of oil mass retention in ‘pipeline A-B’ and ‘pipeline C-D’ of evaporator A were less than or equal to 2.5% of total oil mass retention in microchannel evaporator A. Therefore for evaporator A, the oil mass retention in those pipelines are negligible. But for microchannel evaporator B the length of Pipeline A-B and Pipeline C-D was 2.5 m. The sum of oil mass retention in pipeline A-B and pipeline C-D connected to microchannel evaporator B was less than or equal to 18% of total oil mass retention in microchannel evaporator B. The following section 5.1.1.1 through section 5.1.1.3, discusses the procedure to estimate annular oil film thickness and local oil concentration in Pipeline D-E (see Figure 4.19).

5.1.1.1 Estimation of flow pattern

To estimate amount of oil mass retention in the pipeline that is located between outlet of the test section and outlet injection port (Pipeline C-D in Figure 4.19), it is generally necessary to know the flow pattern for calculation of oil film thickness. The modified Baker’s map (Baker, 1954) was used for estimating two phase flow pattern of R410A/POE mixture and R134a/POE mixture in that pipeline. The map was originally developed for two phase flow of air-water in horizontal pipelines. However, equations (5-11) and (5-12) can be used to account for different fluid properties and apply it for different fluids. In this map, y-axis represents corrected core vapor mass flux (Y) in the pipeline and x-axis represents corrected ratio of liquid mass flux (X). The data from all experiments are plotted in the map of figure where circles represents R410A-POE data

and squares represents R134a-POE data. For same shape, the closed symbol represents low mass flux of refrigerant and open symbols represents high mass flux of refrigerant.

$$\lambda = \sqrt{\left(\frac{\rho_g}{\rho_a}\right) \left(\frac{\rho_l}{\rho_w}\right)} \quad (5-11)$$

$$\psi = \left(\frac{\sigma_w}{\sigma_l}\right) \left[\left(\frac{\mu_l}{\mu_w}\right) \left(\frac{\rho_w}{\rho_l}\right)^2\right]^{\frac{1}{3}} \quad (5-12)$$

$$X = \left(\frac{G_l}{G_g}\right) \lambda \psi \quad (5-13)$$

$$Y = \frac{G_g}{\lambda} \quad (5-14)$$

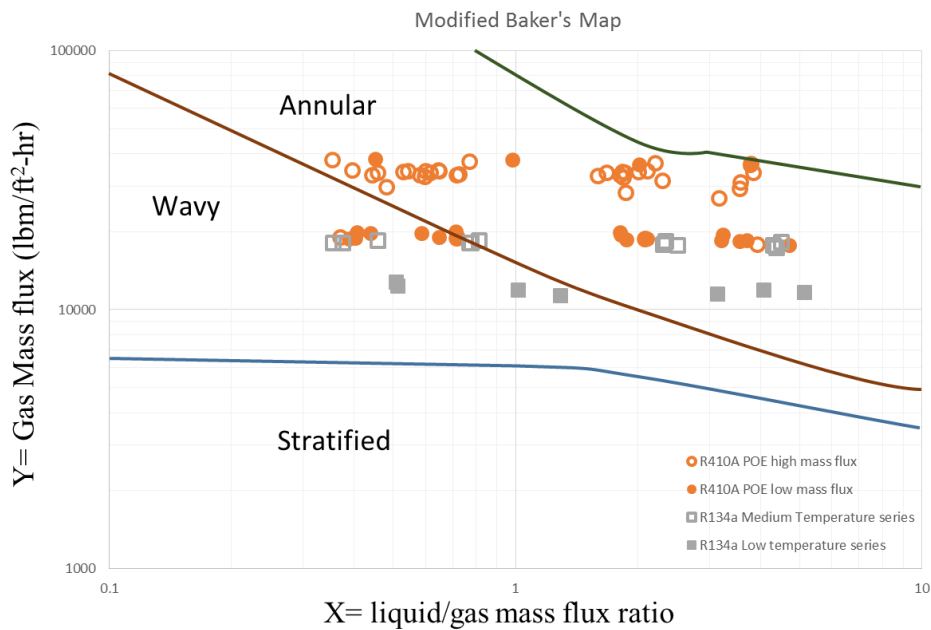


Figure 5.1: Modified (Baker, 1954) map adopted from (Radermacher et al., 2006)

In Figure 5.1, most of the data points falls under annular flow regime. For low mass flux series and OMF less than 1 wt.%, the flow of refrigerant and oil mixture at evaporator outlet pipeline falls under wavy flow regime. Due to complexity involved in calculating oil retention in wavy flow patterns, and absence of interfacial friction factor in literature, forced us to assume the flow pattern for those cases to be annular.

5.1.1.2 Estimation of Local oil concentration:

The liquid film in two phase flow at evaporator outlet is not pure oil and because some amount of un-evaporated refrigerant is always dissolved in the oil. The amount of refrigerant dissolved in the oil depends on temperature and pressure at the outlet of evaporator. Takaishi & Oguchi, 1987 suggested following empirical correlation to predict bubble point temperature for R-22 and oil mixture.

$$\ln(P_{sat}) = \left(\frac{A}{T_{bub}} \right) + B \quad (5-15)$$

$$\text{Where } A = a_o + a_1 \cdot w + a_2 \cdot w^3 + a_3 \cdot w^5 + a_4 \cdot w^7 \quad (5-16)$$

$$B = b_o + b_1 \cdot w + b_2 \cdot w^3 + b_3 \cdot w^5 + b_4 \cdot w^7 \quad (5-17)$$

Values of empirical constants are:

$$a_o = -2394.5 \quad b_o = 8.07236$$

$$a_1 = 182.52 \quad b_1 = -0.72212$$

$$a_2 = -724.21 \quad b_2 = -2.3914$$

$$a_3 = 3868 \quad b_3 = -13.779$$

$$a_4 = -5268.9 \quad b_4 = 17.066$$

(Thome, 1995) proposed that this method could be applied to other refrigerants and zeotropic mixture by changing empirical constants a_o and b_o while keeping other empirical constants unchanged. Following procedure was suggested by him:

1. Substitute $w=0$ in equation (5-16) and (5-17)
2. Substitute $A = a_o$ and $B = b_o$ values in equation (5-15)

3. Substitute pure refrigerant pure refrigerant saturation temperature and corresponding saturation pressure (P_{sat1}, T_{sat1}) , (P_{sat2}, T_{sat2}) in equation (5-15). Which gives two equations and two unknowns
4. Solve both equations for a_o and b_o .

a_o and b_o were individually calculated for R410A and R134a. For a given oil injection test, evaporator outlet temperature and pressure were used for determining local oil concentration ' ω ' in liquid film.

5.1.1.3 Estimation of Oil film thickness

This section describes semi-empirical models from literature that was used in this research for estimation of oil mass retention for annular two phase flow in horizontal and vertical pipeline C-D. Following assumptions were made to calculate oil film thickness for R410A/POE oil mixture and R134a/POE oil mixture measurements.

- Fully developed flow
- Axisymmetric flow
- Presence oil droplets in vapor was ignored
- Liquid film thickness was uniform throughout the pipe
- Flow assumed to be separated annular flow

Radermacher et al., 2006 and Sethi, 2011 applied Navier-Stokes equation on liquid film in suction lines to obtain velocity profile. Later the velocity profile was integrated over the liquid film to obtain liquid mass flow rate. The obtained liquid mass flow rate was function of interfacial shear stress, pressure drop gradient along the axis of pipeline, and oil film thickness.

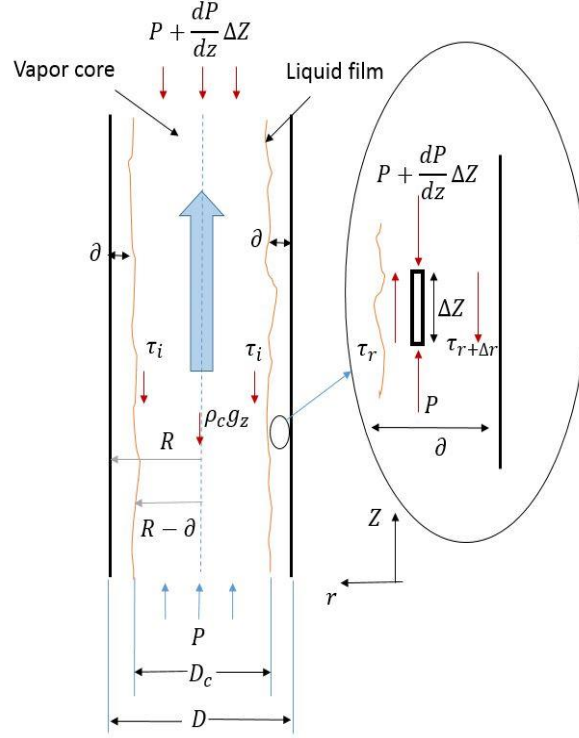


Figure 5.2: Liquid film entrainment model (adopted from Sethi, 2011)

The derivation of liquid mass flow rate in two phase annular flow was explained in detailed manner in Radermacher et al., 2006 and Sethi, 2011. The following is expression for liquid mass flow rate

$$\dot{m}_{oil,injected} = \frac{2\pi\rho_l}{\mu_l} \left[\left(\tau_i(R - \delta) + \left(\frac{(R - \delta)^2}{2} \left(\frac{dP}{dz} + \rho_l g_z \right) \right) \right) \left(\frac{(R^2 - (R - \delta))^2}{4} - \frac{(R - \delta)^2}{2} \ln \left(\frac{R}{R - \delta} \right) \right) - \frac{\pi\rho_l}{8\mu_l} \left(\frac{dP}{dz} + \rho_l g_z \right) (R^2 - (R - \delta))^2 \right] \quad (5-18)$$

Where $\dot{m}_{oil,injected} = \frac{\dot{m}_{oil,injection}}{(1+S)}$ was the mass flow rate of pure oil injected at the outlet. The force balance on refrigerant core is shown in Figure 5.2. Following expression is result of force balance on refrigerant core.

$$\frac{dP}{dz} + \rho_l g_z + \frac{\tau_i \pi D_c}{A_c} = 0 \quad (5-19)$$

Here A_c is cross sectional area occupied by core refrigerant vapor in annular two phase flow. A_c can be estimated based on void fraction in annular two phase flow model.

$$\alpha = \frac{A_c}{A} = \left(\frac{D_c}{D}\right)^2 = \left(\frac{D - 2\delta}{D}\right)^2 \quad (5-20)$$

In equation (5-21), the interfacial shear stress τ_i can be approximated as follows:

$$\tau_i = \frac{1}{2} f_i \rho_l u_c^2 \quad (5-21)$$

An additional equation is required to obtain closure of the system of equation from equation (5-18) to equation (5-21). The interfacial friction factor ' f_i ' is important term missing in the system of equations. It generally depends on liquid film thickness, properties of vapor and liquid, and flow regime of two phase flow. In literature there are abundant correlation for friction factor in two phase flow. The empirical correlation for interfacial friction factor suggested by Sethi, 2011 was used in this research to obtain oil mass in the pipeline at microchannel evaporator outlet for R134a and POE oil mixture. Following is expression for interfacial friction factor proposed by him:

$$\frac{f_i}{f_s} = 1 + 0.0784 Re_v^{-0.3} \delta_v^{+1.4} Re_l^{-0.3} \quad (5-22)$$

Where,

$$\delta_v^+ = \frac{\delta}{u_v} \sqrt{\frac{\tau_i}{\rho_v}} = \text{dimensionless film thickness parameter} \quad (5-23)$$

$$f_s = 0.046 Re_v^{-0.2} \quad (5-24)$$

For R410A and POE oil mixture empirical correlation suggested by Zoellick, 2010 was used for estimating interfacial friction factor. He suggested separate equations for vertical and horizontal pipelines. Following are expressions for calculating interfacial friction factor for two phase flow R410A and POE oil mixture:

$$f_i = 0.005 \left(1 + 300 \left(\frac{\delta}{D} \right) \right) \quad (5-25)$$

$$\frac{\delta_o}{v_l} \sqrt{\left(\frac{\tau_i}{\rho_l} \right)} = 0.69 Re_l^{0.54} \quad (\text{Horizontal tubes}) \quad (5-26)$$

$$\frac{\delta_o}{v_l} \sqrt{\left(\frac{\tau_i}{\rho_l} \right)} = 0.88 Re_l^{0.53} \quad (\text{Vertical tubes}) \quad (5-27)$$

Where

$$G = \left(\frac{m_{ref} + m_{oil, injected @ (x-\delta x)\%}}{A} \right) = \text{Total mass flux} \quad (5-28)$$

$$x = 1 - \frac{OMF}{100 * w} = \text{Vapor quality at evaporator outlet} \quad (5-29)$$

$$Re_l = \frac{G(1-x)D}{4\mu_l} = \text{Liquid reynolds number} \quad (5-30)$$

$$Re_v = \frac{GxD}{\mu_v} = \text{Vapor reynolds number} \quad (5-31)$$

$$u_v \text{ or } u_c = \frac{Gx}{\rho_v \alpha} = \text{core vapor velocity} \quad (5-32)$$

$$u_l = \frac{G(1-x)}{\rho_l(1-\alpha)} = \text{liquid velocity} \quad (5-33)$$

Using equations from (5-18) through (5-32), we can estimate oil film thickness for two phase annular flow. The refrigerant and lubricant mixture viscosity μ_l was calculated from data obtained from Honeywell for R410A/ POE ISO 32 mixture and for R134a/ POE ISO 32 mixture, empirical correlations from Henderson, 1994 were used.

5.1.2 HTF and PDF calculations

The amount of oil retention in the microchannel heat exchanger offers an additional resistance to refrigerant flow. If the OMF increases, oil retention in the test section increases as well. Consequently the pressure drops depend upon the refrigerant flow rate and on the OMF in the circulating refrigerant-oil mixture (Cremaschi

et al., 2005). The oil effect on pressure drop was estimated by measuring the pressure drop in the test section at specific mass flow rates and OMFs. The refrigerant side pressure drop at the measured OMF, $\Delta p_{with\ oil}$ was compared to the corresponding pressure drop across the test section at the same total mass flow rate but with no oil present, $\Delta p_{without\ oil}$. The pressure drop factor (PDF) was used to represent the effect of the oil and it is defined as follows:

$$PDF = \frac{\Delta p_{with\ oil}}{\Delta p_{without\ oil}} \quad (5-34)$$

The PDF is a cumulative factor that account for both acceleration and friction pressure drop components e.g. alteration of two-phase flow regime, increase in the liquid phase viscosity and the reduction of the free-flow area available to the refrigerant flow due to the oil retention.

Similarly, the microchannel heat exchanger heat transfer capacity factor, HTF, was calculated based on the heat transfer capacity measured during test with oil and the corresponding operating conditions without oil, as follows:

$$HTF = \frac{\dot{Q}_{air,with\ oil}}{\dot{Q}_{air,without\ oil}} \quad (5-35)$$

\dot{Q}_{air} is the heat transfer rate measured from the air side of the microchannel evaporator at given test condition by using the following equation :

$$Q_{air} = \rho_{air} \cdot CFM \cdot 60 \cdot c_p \cdot (T_{air,out} - T_{air,in}) \quad (5-36)$$

The volume flow rate of the air, CFM , through the microchannel heat exchanger was calculated from the pressure difference across the flow nozzle in agreement with the ANSI/ASHRAE Standard 41.2 (Ashrae, 1987). The properties of air were estimated by using ASHRAE Handbook – Fundamentals (ASHRAE 2001). The dry bulb temperature of the inlet air ($T_{air,in}$), the dry bulb temperature of the outlet air ($T_{air,out}$) from the microchannel heat exchanger, and the volume flow rate (CFM) were measured. The density of the air (ρ_{air}) was estimated based on the temperature of the air stream at the flow nozzle and the specific heat was

$c_p = 0.2405 \text{ Btu/lbm}\cdot^\circ\text{F}$, and it did not change significantly between two pair of tests with and without oil. Since the air flow rate was also constant between two pair of tests with and without oil, the HTF can be reduced to the following result:

$$HTF \approx \frac{\rho_{air,with\ oil} \cdot (T_{air,out\ with\ oil} - T_{air,in})}{\rho_{air,without\ oil} \cdot (T_{air,without\ oil} - T_{air,in})} \quad (5-37)$$

Where the variations in specific heat at constant pressure of the air were neglected because they were small. Equation (5-36) shows that the HTF is basically dependent only on temperature measurements. Thus, the experimental uncertainty on the HTF was fairly small.

An example of HTF calculation during evaporator tests, the saturation temperature at Microchannel Evaporator A inlet was controlled to about 48°F , and the mass flow rate was 200 lb/hr . The superheat at microchannel evaporator outlet was controlled to 10°F . An example for the main variables in this case are as follows:

$m_r = 200 \text{ lb}_m/\text{hr}$ (Mass flow rate of refrigerant for no oil condition)

$m_{oil} = 10.2 \text{ lb}_m/\text{hr}$ (Mass flow rate of oil during injection)

$m_{tot,OMF=5\ wt.\ \%} = m_r + m_{oil} = 210.2 \text{ lb}_m/\text{hr}$ (Mass flow rate of refrigerant and oil mixture)

Therefore during oil injection period, the total mass flow rate of the mixture was about 210 lb/hr , the measured heat transfer capacity was $\dot{Q}_{with\ oil} = 16,580 \text{ Btu/hr}$ and the measured refrigerant side pressure drop was $\Delta p_{with\ oil} = 1.023 \text{ psid}$. Performance mapping tests were conducted at refrigerant mass flow rate of $200 \text{ lb}_m/\text{hr}$ (referred in this example with the notation “*without oil low*”) and $212 \text{ lb}_m/\text{hr}$ (referred to as “*without oil high*”) and at the same refrigerant saturation temperature of 48°F , and degree of superheat of refrigerant vapor at the microchannel evaporator A outlet of about 10°F (5.5°C). These performance mapping tests provided four neighboring points for the heat transfer rate ($\dot{Q}_{without\ oil,low} = 18,264 \text{ BTU/hr}$, $\dot{Q}_{without\ oil,high} = 18,917 \text{ BTU/hr}$.) and pressure drop ($\Delta p_{without\ oil,low} = 0.75 \text{ psid}$, $\Delta p_{without\ oil,high} = 0.9 \text{ psid}$) of the

microchannel evaporator A when no oil was present and when the refrigerant flow rate ranged from 200 to 212 lb_m/hr. Then, the actual heat transfer rate ($\dot{Q}_{without\ oil} = 18,842\ BTU/hr$) and pressure drop ($\Delta p_{without\ oil} = 0.882\ psid$) for the corresponding baseline case of no oil at the refrigerant flow rate of 210 lb/hr was estimated from linear interpolation between each two pairs of the mapping points (i.e. the two neighboring points for $\dot{Q}_{without\ oil}$ and the two neighboring points for $\Delta p_{without\ oil}$). The HTF and PDF factors resulted as follows:

$$HTF = \frac{\dot{Q}_{with\ oil}}{\dot{Q}_{without\ oil}} = \frac{16,580}{18,842} = 0.88$$

$$PDF = \frac{\Delta p_{with\ oil}}{\Delta p_{without\ oil}} = \frac{1.023}{0.882} = 1.16$$

It should be noted that during the evaporator tests, the absolute pressure varied by less than 3 psia in microchannel evaporator A and 4 psia in Microchannel Evaporator B when oil was injected in the refrigerant loop. This variation was small enough to be neglected for the estimation of $\dot{Q}_{without\ oil}$ and $\Delta p_{without\ oil}$. In other words, for most of the evaporation tests, a linear interpolation was used to calculate $\dot{Q}_{without\ oil}$ and $\Delta p_{without\ oil}$ from two points at different flow rates. But there were few exceptions where pressure change during oil injection period in the microchannel evaporator B was 5 to 6 psia. For those tests the calculations of the corresponding baseline values of $\dot{Q}_{without\ oil}$ and $\Delta p_{without\ oil}$ were done by considering double interpolation on four mapping points measured without oil and that spanned the neighborhood of saturation pressures and flow rates during the oil injection periods. The interpolation (or double interpolation) approach eliminated any source of systematic error that could potentially skew the results for HTF and PDF due to the fact that during the experiments the oil slightly altered the pressure and flow rate of the system. With this approach, the effect of oil in the microchannel heat exchanger was isolated in the experimental results and the comparison of heat transfer rate and pressure drop between the case with oil and the case without oil was more meaningful. The HTF and PDF calculated with the data reduction method of the present work were

representative of the degradation of the refrigerant-side heat transfer rate and of the increase of the refrigerant-side pressure drop due to the oil retained in the heat exchangers.

5.2 Uncertainty Analysis

Based on the technical approach described in the previous sections, a preliminary uncertainty analysis was conducted according to the uncertainty propagation method suggested by Taylor & Kuyatt, 1994a. The accuracies of the main instrumentations used in this project are listed in Table 5.1. These values will be used to calculate the uncertainty of the important parameters based on uncertainty propagation analysis described in the following section.

This section discusses further the uncertainty error in OMF, ORV_N , HTF, and PDF for microchannel evaporators. The uncertainty analysis for calculating the experimental uncertainty of HTF for Microchannel Evaporator A, required further details when the saturation temperature ranged from 10° F to 0° F (-12.2° C to -17.8° C) during the low temperature series of R134a and POE oil mixture. For these low temperature tests, the air inlet temperature was below freezing point.

Table 5.1 Accuracy of the main instrumentation for the project

Sensor	Manufacturer	Model / Type	Nominal range	Accuracy
Refrigerant Mass flow meter	Micromotion	CFM025 Elite series	6 to 19 lb/min (45 to 143 g/s)	±0.1% of reading
Oil Mass flow meter	Micromotion	CFM010 Elite series	0.01 to 0.8 lb/min (0.08 to 6 g/s)	±0.5% of reading if flow <0.04 lb/min; ±0.1% of reading if flow > 0.04 lb/min
Air flow rate	Helander	Elliptical nozzle	150 to 2,000 cfm (0.07 to 1 m ³ /s)	±2.2% of flow rate (using Setra 264 pressure transducer)
Temperature	Omega	T-type	-40 to 130 °F (-40 to 54 °C)	±0.5°F (0.3°C)
High accuracy barometer	Vaisala	PX02	26-32 inHg (88 – 108 kPa)	±0.25% of full scale
Air pressure transducer	Setra	Model 264	0 ~ 3 in WC (0 to 747 Pa)	±0.25% of full scale
Precision Temperature	Omega	RTD (Pt-100)	-40 to 130 °F (-40 to 54 °C)	±0.2°F (0.1°C)
Refrigerant Saturation Pressure	Setra	Model C206	7 to 500 psia (50 to 3,450 kPa)	±0.65psi (4.5 kPa)
Differential pressure	Validyne	Diaphragm Typer	0 to 50 psi (0 to 350 kPa)	±0.25 psi (1.8 kPa)
Watt Transducer	Omega	OM11	6,800 to 38,000 Btu/hr (2 to 11 kW)	0.2% of reading

5.2.1 Uncertainty in Oil Mass Fraction (OMF):

The uncertainties in the *OMF* values depended on propagation of small errors due to measurement in mass flow rates of refrigerant and mass flow rate of injected oil. The uncertainties in the solubility values were

propagated to the errors in the *OMF*. It should be noted that the Coriolis mass flow meters had very good accuracies for the range of flow rates were above 2 lbm/hr, which resulted in small uncertainties of the measured mass flow rates. This means that when flow rates were above 2 lbm/hr, the uncertainties in the solubility dominated the propagation of experimental error for the *OMF*. When refrigerant mass flow rate was 200 lbm/hr, and *OMF* was 0.5 wt.% then the mass flow rate of injecting oil was set to 1 – 1.5 lbm/hr. As shown in the Figure 4.33, the uncertainty in mass flow rate increased from 0.1 % to 0.25% of flow rate.

5.2.2 Uncertainty in Oil Mass Retention:

The uncertainty in measurements of oil retention in microchannel evaporators was depended on the oil mass difference at the inlet port and at the outlet port, and oil masses in pipeline A-B and pipeline C-D.

$$OR_{mass} = M_a - M_{pipeline} \quad (5-38)$$

$$OR_{mass} = M_{(B-C)} = M_{(A-E)} - M_{(A-B)} - M_{(C-D)} - M_{(D-E)} \quad (5-39)$$

Oil retention in microchannel evaporators was predominantly depended on the oil mass injected at the inlet port of test section ($M_{(A-E)}$) and the oil mass injected at the outlet of test section ($M_{(D-E)}$). Where $M_{(A-E)}$ and $M_{(D-E)}$ were result of a time integral. They are expressed as follow

$$M = \int_{t_0}^{t_2} \dot{m}_{oil, injected} dt \quad (5-40)$$

And using above time integral for inlet and outlet ports of the test section, the oil mass $M_{(A-E)}$ and $M_{(D-E)}$ are obtained. The uncertainty calculation of oil retention mass includes uncertainty propagation of solubility of the refrigerant dissolved in the oil. The uncertainty of oil mass retention also involves the human operator error in estimating the time t_0 and t_2 of the above time integral of the flow rate. In a conservative way, based on our experience we estimated the human operator error in detecting the time at which the oil passes through the sight glass to as ± 2 seconds. Figure 5.3 shows the uncertainty bars in the calculated oil retention volume if the error in the time of oil detection at the sight glasses is ± 2 seconds. For *OMF* at or below 3 wt. % this

human error does not affect significantly the reported ORV_N because the time of integration is long, that is, of several minutes. For OMF higher than 3 wt.%, the error bars in the ORV_N resulted ± 0.01 , which could be significant. In order to achieve an error of within ± 2 seconds in the time of detection of oil at the sight glasses, video recordings of the flow at the sight glasses were taken and synchronized during the oil retention tests. The digital images provided the time at which the oil arrived to the sight glass and covered its glass surfaces. Oil had a dye in it and it appeared as yellowish and greenish in color as opposed to refrigerant, which appeared as transparent fluid inside the sight glass. During a tests, video recordings of the sight glasses with actual time indicators (i.e., a digital chronometers) next to them were taken, as shown in Figure 5.4.

Then, the recordings were synchronized in time, labeled, and archived. After the test was completed, the video recordings were played back at 3 time slower rate than real time. The digital frames of the sight glasses and chronometers indicated the instant in which the oil appeared first in a sight glass until the instant in which the oil covered the full length of the sight glass surfaces. The images of the digital chronometer, once synchronized, provided the exact times (within ± 2 seconds) at which the oil arrived approximately at the end of the sight glass. The overall theoretical uncertainty plus the uncertainty due to human operator on the ORV_N was estimated to ± 0.01 . For normalized oil retention volumes in the range of 0.05 to 0.1, this experimental uncertainty on the oil retention was 10 to 20 percent.

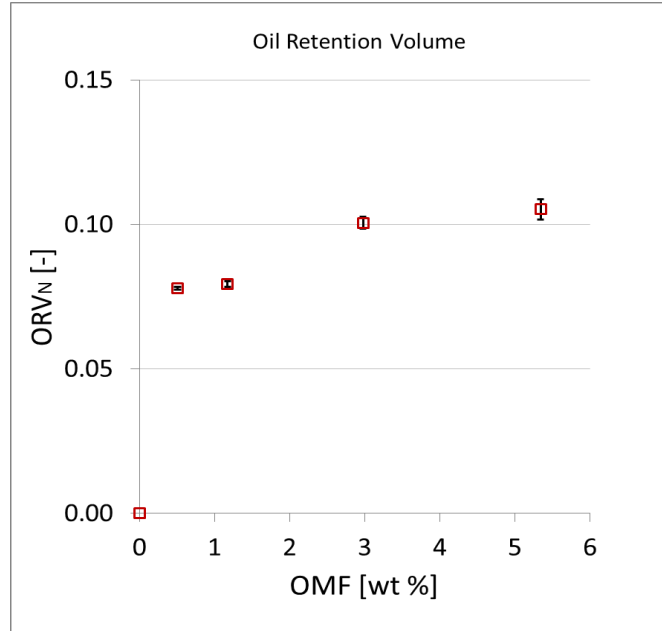


Figure 5.3: Uncertainty of ORV with $t \pm 2$ seconds

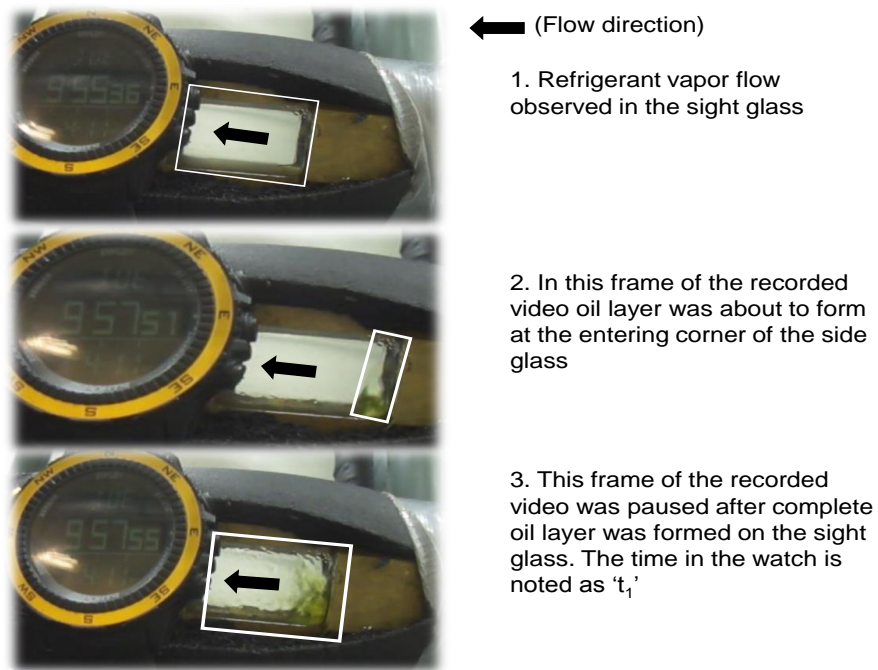


Figure 5.4: Oil layer observed for various OMFs

5.2.3 Uncertainty in Heat Transfer rate and HTF:

If the variables of the air side heat transfer rate, that is, ρ_{air} , CFM , $\Delta T_{air} = (T_{air,out} - T_{air,in})$ have random experimental uncertainties of $\delta\rho_{air}$, δCFM , and $\delta\Delta T_{air}$ and these uncertainties are also independent from

each other, then the theoretical experimental uncertainty of the heat transfer rate, δQ_{air} , was calculated by using the Taylor series uncertainty propagation equation:

$$\delta Q_{air} = \sqrt{\left[\left(\frac{\partial Q_{air}}{\partial \rho_{air}} \delta \rho_{air}\right)^2 + \left(\frac{\partial Q_{air}}{\partial CFM} \delta CFM\right)^2 + \left(\frac{\partial Q_{air}}{\partial \Delta T_{air}} \delta \Delta T_{air}\right)^2\right]} \quad (5-41)$$

The uncertainty error propagation to the Heat Transfer Factor (*HTF*) is calculated as following:

$$\delta HTF_{-Q_{air}} = \sqrt{\left[\left(\frac{1}{Q_{air@OMF=0}} \delta Q_{air@OMF}\right)^2 + \left(\frac{-Q_{air@OMF}}{Q_{air@OMF=0}^2} \delta Q_{air@OMF=0}\right)^2\right]} \quad (5-42)$$

The uncertainty above is the uncertainty in *HTF* based on the heat transfer calculation. While calculating the δHTF , the uncertainty $\delta Q_{air@OMF=0}$ was taken to be similar to the experimental uncertainty $\delta Q_{air@OMF}$. This was reasonable because the heat transfer rates with and without oil were measured by using the same instrumentation and in the same period. The measured values for $Q_{air@OMF=0}$ and $Q_{air@OMF}$ were also close to each other and thus it is logical to assume that $\delta Q_{air@OMF}$ and $\delta Q_{air@OMF=0}$, were also close to each other. Equation (5-42) was simplified to:

$$\delta HTF = \sqrt{\left[\left(HTF \frac{\delta Q_{air}}{Q_{air@OMF}}\right)^2 + \left(HTF^2 \frac{\delta Q_{air}}{Q_{air@OMF}}\right)^2\right]} \quad (5-43)$$

Equation (5-43) simplification leads to Equation (5-44), which expresses the fractional uncertainty of *HTF* as a function of the fractional uncertainty of $Q_{air@OCR}$.

$$\frac{\delta HTF}{HTF} = \sqrt{1 + HTF^2} \cdot \frac{\delta Q_{air}}{Q_{air@OMF}} \quad (5-44)$$

The uncertainty in the *HTF* for microchannel evaporator for the medium temperature evaporator tests and it was of $\pm 4.5\%$. For the low temperature evaporator tests, a thermocouple grid of 5 T-type thermocouples was installed in front of microchannel evaporators and the dry bulb temperature of the air at the inlet of the evaporator was an average between these 5 T-type thermocouple sensors. The theoretical uncertainty on the *HTF* increased slightly to $\pm 5\%$ for the low temperature evaporator tests.

5.2.4 Uncertainty in Pressure Drop and PDF:

Four different differential pressure transducers were used based on the magnitude of the pressure drop across the microchannel evaporator. Each pressure transducer had a different full scale. For high mass flux tests, the pressure drop measured between microchannel evaporator inlet and outlet ranged from 5 psid to about 10 psid. Thus, for these cases, a differential pressure transducer of 15 psid full scale range or of 8 psid full scale range were used. For low mass flux tests, the differential pressure transducer with 3 psid full scale range or 5 psid full scale range were used in order to improve the accuracy of the pressure drop measurements.

Similar to *HTF* uncertainty analysis, applying the theory of uncertainty propagation by Taylor & Kuyatt, 1994b to the Pressure Drop Factor (*PDF*) Equation (5-35) gives the Equation (5-45) to calculate the uncertainty on the pressure drop factor, δPDF .

$$\delta PDF = \sqrt{\left[\left(\frac{1}{\Delta P_{@OMF=0}} \delta \Delta P_{@OMF} \right)^2 + \left(\frac{-\Delta P_{@OMF}}{\Delta P_{@OMF=0}^2} \delta \Delta P_{@OMF=0} \right)^2 \right]} \quad (5-45)$$

The uncertainty $\delta \Delta P_{@OMF=0}$ of the mapping data and the uncertainty $\delta \Delta P_{@OMF}$ of the pressure drop for tests with $OMF > 0\%$ were same because same differential pressure transducer was used for measuring $\Delta P_{@OMF=0}$ and $\Delta P_{@OMF}$. Equation (5-45) was simplified accordingly to get a new Equation (5-46).

$$\delta PDF = \sqrt{\left[\left(PDF \frac{\delta \Delta P_{@OMF}}{\Delta P_{@OMF}} \right)^2 + \left(PDF^2 \frac{\delta \Delta P_{@OMF}}{\Delta P_{@OMF}} \right)^2 \right]} \quad (5-46)$$

The fractional uncertainty of *PDF* as a function of the fractional uncertainty of $\Delta P_{@OMF}$.

$$\frac{\delta PDF}{PDF} = \sqrt{1 + PDF^2} \cdot \frac{\delta \Delta P_{@OMF}}{\Delta P_{@OMF}} \quad (5-47)$$

CHAPTER VI

6. EXPERIMENTAL RESULTS AND DISCUSSION

This chapter discusses the experimental results of oil retention measurements in microchannel evaporators in terms of normalized oil retention volume (ORV_N), pressure drop factor (PDF) and heat transfer factor (HTF). The definitions of these three variables are given in Equations (5-10), (5-34) and (5-35). When oil was present in the evaporator, the heat transfer rate and refrigerant-side pressure drop were compared to those of the oil free case at same total mass flow rate, same saturation pressure, and similar degree of vapor superheated at the outlet of the evaporator.

6.1 Oil retention volume in the evaporators

This section discusses the oil retention in microchannel evaporator A and evaporator B with R410A and POE oil and R134a and POE oil and for two mass flux and several saturation temperatures, and several degree of vapor superheat at test section outlet. The oil retention volume was measured by using the timing and video recording method of the oil flow entering and existing the test section; this method was discussed in section 4.3.1.6. The information of test conditions and the legend for the symbols used for the test series of R410A and POE oil and R134a and POE oil during the tests on evaporators are given in Table 6.1, Table 6.2 and Table 6.3. An example of the calculation of mass flux inside each microchannel tube is provided below for test series represented by the letter G and the solid round black symbol in Table 6.1. The mass flow rate during the test of series G was 200 lb_m/hr (90.7 kg/hr). This was the total mass flow rate, i.e., the refrigerant mass flow rate if OMF = 0 wt. % or the total mixture (refrigerant plus oil) flow rate if OMF > 0 wt. %. For evaporator A, the overall cross sectional area of each microchannel tube was 0.01953 in² (or 0.126 cm²), that

is, 0.000135625 ft². Since there were 98 tubes for microchannel evaporator A, the overall cross sectional flow area resulted:

$$A_{cross,overall,Evap A} = 0.000135625 ft^2 \cdot 98 = 0.013291 ft^2$$

Then, the total mass flux for the series G for the evaporator A resulted

$$m''_{G,Evap A} = \frac{\text{mass flow rate}}{\text{flow area}} = \frac{200 (lb/hr)}{(0.013291 ft^2 \cdot 3600 S/hr)} = 4.2 \frac{lb_m}{ft^2 - s} \text{ or } 20.4 \frac{kg}{m^2 - s}$$

Evaporator B, overall cross sectional area of each microchannel tube was 0.0341 in² (or 0.22 cm²), that is, 0.000236806 ft². Since there were 50 tubes for microchannel evaporator B, the overall cross sectional flow area resulted

$$A_{cross,overall,Evap B} = 0.000236806 ft^2 \cdot 50 = 0.011840301 ft^2$$

Then, the total mass flux for the series G for the evaporator B resulted







$$m''_{G,Evap B} = \frac{\text{mass flow rate}}{\text{flow area}} = \frac{200 (lb/hr)}{(0.011840301 ft^2 \cdot 3600 S/hr)} = 4.7 \frac{lb_m}{ft^2 - s} \text{ or } 23 \frac{kg}{m^2 - s}$$

It should be emphasized in here that this is the total mass flux in each microchannel tube, i.e., the refrigerant mass flux if OMF = 0 w.t. % or the total mixture (refrigerant plus oil) mass flux if OMF > 0 w.t. %.

6.1.1 Oil retention volume in the evaporators for R410A and POE oil mixture

From section 6.1.1.1 to 6.1.1.2 the experimental results of oil retention volume (ORV_N) in evaporator A and evaporator B with refrigerant R410A and POE oil are discussed. The information of test conditions and the legend for the symbols used for the test series of R410A and POE oil are given in Table 6.1. For series G, H, I, J, K, and L in Table 6.1 the microchannel evaporator outlet degree of vapor superheat was maintained constant at 10°F (5.5°C). In section 6.1.1.1 and 6.1.1.2, the effect of oil mass fraction, refrigerant mass flux on oil mass retention volume (ORV_N) are discussed.




Table 6.1 Legend of the letters and symbols used in the figures reporting the tests results of microchannel evaporators with R410A and POE

Symbol	Letter	T_{sat}		$*G_{Evaporator A}$		$*G_{Evaporator B}$		SH	
		$^{\circ}F$ ($^{\circ}C$)	lb_m/ft^2-s (kg/m^2-s)	lb_m/ft^2-s (kg/m^2-s)	lb_m/ft^2-s (kg/m^2-s)	$^{\circ}F$ ($^{\circ}C$)			
	G	33 (0.5)	4.2 (20.4)	4.7 (23)	10 (5.5)				
	H	38 (3.3)	4.2 (20.4)	4.7 (23)	10 (5.5)				
	I	48 (9)	4.2 (20.4)	4.7 (23)	10 (5.5)				
	J	33 (0.5)	7.5 (36.7)	7.7 (37.8)	10 (5.5)				
	K	38 (3.3)	8.4 (41.0)	8.4 (41.0)	10 (5.5)				
	L	48 (9)	8.4 (41.0)	8.4 (41.0)	10 (5.5)				

*G is the mass flux inside each microchannel tubes. It was calculated from the total mass flow rate entering the evaporator divided by the total cross sectional area of microchannel tubes in each evaporator ($G_{Evaporator A}$ and $G_{Evaporator B}$). *SH is degree of superheat of vapor refrigerant at evaporator outlet

From section 6.1.1.3 to 6.1.1.4 the experimental results of oil retention volume (ORV_N) in evaporator A and evaporator B with refrigerant R410A and POE oil for several degree of superheat at evaporator outlet are discussed. The information of test conditions and the legend for the symbols used for the test series of R410A and POE oil for several degree of superheat at evaporator outlet are given in Table 6.2. In section 6.1.1.3 and section 6.1.1.4, the effect of degree of vapor superheat at microchannel evaporator outlet on oil retention volume are discussed.

Table 6.2 Legend of the letters and symbols used in the figures reporting the tests results of microchannel evaporators with R410A and POE, for several degree of superheat

Symbol	Letter	*SH °F (°C)	*G _{Evaporator A} lb _m /ft ² -s (kg/m ² -s)	*G _{Evaporator B} lb _m /ft ² -s (kg/m ² -s)
	S	5 (2.8)	7.5 (36.7)	8.4 (41.0)
	T	15 (8.3)	7.5 (36.7)	8.4 (41.0)
	U	25 (13.9)	7.5 (36.7)	8.4 (41.0)

*G is the mass flux inside each microchannel tubes. It was calculated from the total mass flow rate entering the evaporator divided by the total cross sectional area of microchannel tubes in each evaporator (G_{Evaporator A} and G_{Evaporator B}). *SH is degree of superheat maintained at outlet of microchannel evaporators.

6.1.1.1 Microchannel evaporator A with R410A and POE oil at constant exit superheat

The experimental results of oil retention volume (ORV_N) in evaporator A with refrigerant R410A and POE oil at constant superheat are summarized in Figure 6.1. This figure shows the oil retention volume in the microchannel evaporator A on the y-axis and the oil mass fraction (OMF) of POE oil in refrigerant R410A on the x-axis. The oil retention volume normalized, ORV_N, was the ratio of the oil retention volume over the internal volume of the evaporator A, including the headers internal volume. The effect of mass flux is represented as void and solid symbols and corresponding letters. Low mass flux series are represented by the solid symbols (G, H, and I) while high mass flux tests are represented as void symbols (J, K and L series) (for details see Table 6.1). Each saturation temperature is given with a void and a solid symbol with same color and shape of the symbol. For example, the black circle data points in Figure 6.1 represent saturation temperature of 33°F (~0.5°C) but the solid circle points (series G) are for low mass flux while the void circle points (series J) are for high mass flux. From a quick glance on those two series, it is evident that if the mass flux doubled then the oil retention in the evaporator was reduced by half. This result was observed when OMF was from 0 to 3 w.t. %.

The experimental results of ORV_N suggested that the amount of oil retained in the microchannel evaporator was strongly depended on the OMF and the oil retention in the microchannel increased as OMF increased. In the evaporator, oil existed in the liquid mixture because the entering fluid was a mixture of saturated refrigerant liquid and POE oil and the evaporation of liquid refrigerant along the microchannel tubes created refrigerant vapor in which the oil droplets entrainment was small. This assumption is supported by a Cremaschi et al., 2005 work on refrigerant and oil flow visualization in air conditioning evaporators. During evaporation of the refrigerant along the length of microchannel tubes, the local concentration of oil in liquid mixture increased. Therefore the viscosity of liquid mixture increased along the length of microchannel tube, that is, along the direction of the refrigerant flow. For example, for OMF of 0.5 wt. %, the viscosity of liquid mixture in the microchannel tube increased by up to 40 times. In other words, the viscosity of the liquid mixture of saturated liquid refrigerant and POE at the inlet of the tube was 40 times lower than the viscosity of the liquid mixture of POE oil and refrigerant dissolved in it at the outlet of the tube (most of the refrigerant was superheated vapor at the outlet of the microchannel tube but a small amount of refrigerant was still dissolved in the oil because of POE and refrigerant R410A are soluble and miscible at those temperatures and pressures). For OMF of 5 wt. % the liquid mixture viscosity increased by 7 times from inlet to outlet of the microchannel tube. The increase in the refrigerant R410A and POE oil mixture viscosity augmented the shear stress required to remove the oil, particularly the shear stress at the liquid-wall interface. Thus, oil increased its resistance to flow with and to be carried with the refrigerant vapor along the microchannel tube. It was sound to assume that oil tended to form a film layer around the wall, that is, to wet the internal walls of the microchannel tubes and of the outlet header. However, since the tests were conducted on a full size microchannel heat exchanger, this hypothesis was not verified in the present work and flow visualization experiments of refrigerant and oil mixtures in microchannel tubes are potential future work on this topic. In Figure 6.1, when OMF increased from 0 wt. % to 5 wt. % the oil retention volume in evaporator A also increased and it was measured up to 12.5 % of internal volume of evaporator A. The trends in Figure 6.1 are clearly not linear. At OMF below 2 wt.%, the magnitude of the ORV_N for low mass flux cases (series G, H, and I) were different from that of high mass flux cases (J, K and L). For low mass flux series (G, H, and I),

the amount of oil retention volume in evaporator A increased significantly as OMF increased from 0 to 1 wt.%. This finding was intriguing and the effect of potential systematic errors on the measured oil retention volume in the heat exchanger was further investigated. We recall the test methodology details described in section 4.3.1. The methodology was based mainly on timing and video recording method of the oil flow when oil appeared at sight glasses. If we assume an operator error of ± 2 seconds on detecting such time instances, the results varied to within the experimental uncertainty of the oil retention measurements, which are shown in Figure 6.2 as an example. For OMF of 0.5 and 1 wt.% the actual time that the oil took to travel from inlet to outlet of the evaporator was of several minutes (that is, about 10 minutes or more). Thus, a human operator of 2 seconds on detecting the instant at which the oil appeared on the sight glasses had an impact on the ORV_N that was within the experimental uncertainty reported for one representative point in Figure 6.1. It should be noted that the experimental uncertainty bars reported for only one representative point in Figure 6.1 to Figure 6.7 applies to all data points of the figures. The bars were intentionally omitted for the other points to avoid compromising the readability and quality of the plots.

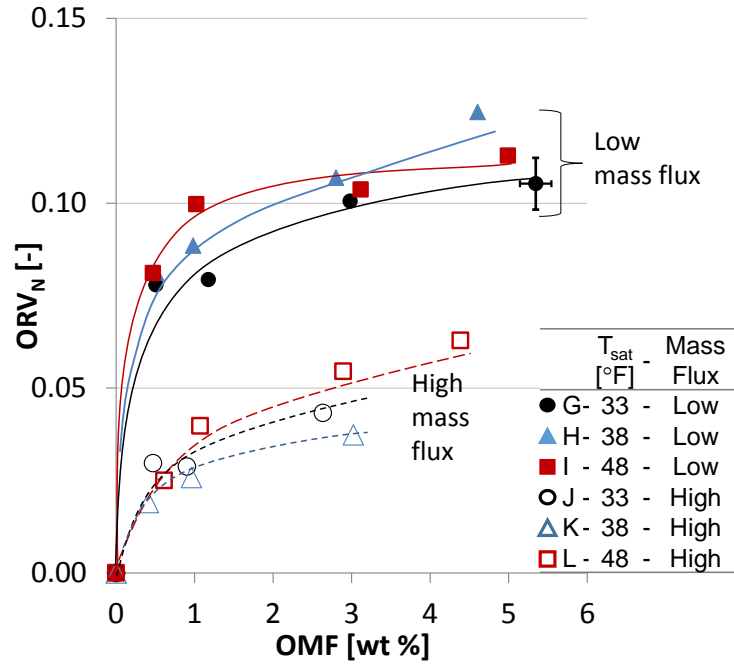


Figure 6.1: Oil retention volume (ORV_N) in microchannel evaporator A with R410A and POE oil

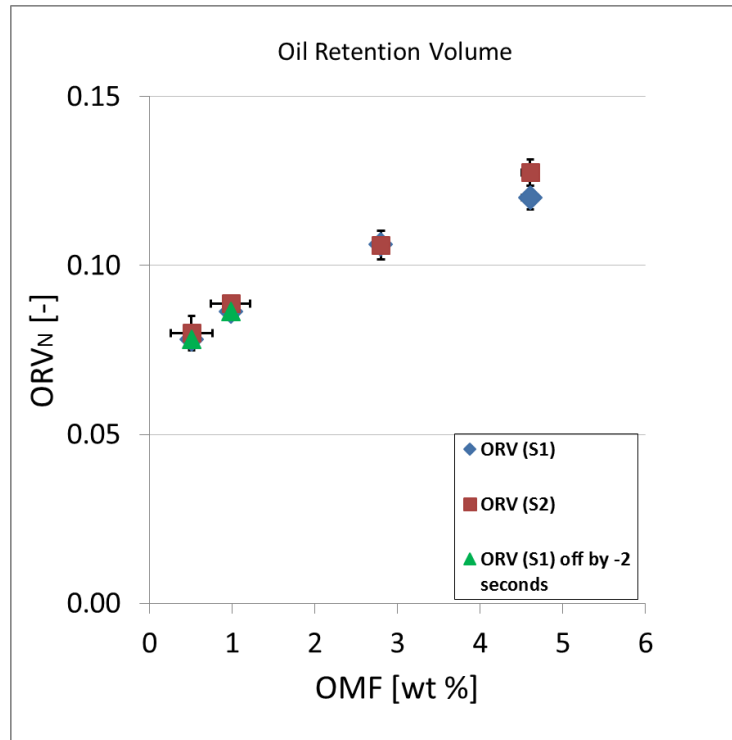


Figure 6.2: Oil retention volume (ORV_N) in microchannel evaporator A with respect to sight glass S1, sight glass S2, and effect of the variation of the observed time by 2 seconds (the results for series H)

Referring to Figure 6.2, the data in blue solid diamonds represent the actual measurements of oil retention in evaporator A for the series H. The green solid triangle data points represent the measured oil retention volume if the time of appearance at the sight glasses were to be shifted by ± 2 seconds with respect to the original time measured. This figure also shows the brown square solid data points, which represent the measured oil retention volume in the evaporator A if a second sight glass S2 was used to measure the oil travel time. The second sight glass was downstream S1 with respect to the direction of the refrigerant flow. The comparison of the ORV_N for the S1 series and S2 series indicates that the measured oil retention volume was independent of the location of the sight glass used to measure the oil travel time. This was because the oil retention volume in the evaporator was obtained from a difference between two volumes, i.e., the volume retained from inlet injection port to the sight glass and volume retained from outlet inject port of the evaporator to the sight glass. Moving the sight glass downstream simply altered those two measured volumes by the same quantity but their difference (which was the oil retention volume in the evaporator) did not change. Nevertheless, we verified that the oil retention volume was independent on the sight glass location for several tests of the evaporator and we used the second sight glass as redundant method to confirm the measurements obtained from the first sight glass.

Even for small OMFs of 0.5 and 1 wt.%, the oil retained in the evaporator was quite significant and it was already 77 to 95 % of the oil retention volume measured when OMF was 3 wt.%. This result suggested that the geometry of the evaporator trapped a certain amount of oil regardless of the OMF in the main flow. Because only liquid mixture was present at the inlet of the evaporator, we concluded that the oil traps were most likely at the outlet header of the evaporator. In our experiments, recalling that the refrigerant flow inside the heat exchanger was vertical upward and that superheated refrigerant vapor was present at the outlet of the microchannel heat exchanger, we speculated that the oil was trapped in the valleys created between the microchannel tubes inserts into the outlet header. As the refrigerant and oil mixture flowed through the microchannel heat exchanger, the refrigerant evaporated leaving behind a liquid phase richer in POE oil. The oil-rich liquid mixture then filled the outlet header valleys until it flooded them. For these cases, the ORV_N

increased sharply with OMFs and lower mass flux augmented significantly the filling time. This could explain the remarkable difference in ORV_N in Figure 6.1 for low and high mass fluxes when OMF was below 1 wt.%. Once the minimum threshold volume defined by the volume of the valleys in the outlet header was filled with oil, then any additional oil was carried with the refrigerant vapor out from the evaporator header. For these cases, the ORV_N increase slowly with OMFs and the additional oil retention volume measured in the evaporator at OMF above 1 wt.% is mainly due to refrigerant and oil solubility. A similar phenomena was reported in the literature by Jin & Hrnjak, 2014 but for condensers, where oil separated at the inlet header of the condenser and started to fill the bottom channels first. Furthermore, in the present evaporator A, the superheated vapor velocity at microchannel tubes decreased from around 2000 ft/s to 2.4 ft/s in the outlet header. Low vapor velocity inside outlet header reduced the vapor refrigerant and oil rich liquid layer interfacial shear force, which was responsible to carry the oil. This further promoted oil retention in the outlet header. At higher mass flux of refrigerant and oil mixture, the shear stress at the vapor-liquid interface was also high when compared to that of low mass flux. The interfacial shear stress was depended upon the difference between the refrigerant gas velocity and liquid oil film velocity (Lee, 2002). Thus, at higher mass flux, hence higher vapor velocity, more oil was carried over with the refrigerant vapor out form the evaporator and the oil retention volume decreased.

At the same saturation temperature, lower mass flux caused oil retention volume to increase between 5% and 3 times that for OMF ranging from 0.5 to 5 wt.%. It should be noted that for typical air conditioning applications, OMF is equal or less than 1 wt.%. From the experiments of the present work, the ORV_N at OMF of 1 wt.% was less than 4% of internal volume for high mass flux series of J, K and L (represented as void symbols in Figure 6.1) and the ORV_N was up to 10% of internal volume of evaporator A for low mass flux series G, H, and I (represented as solid symbols in Figure 6.1).

6.1.1.2 Microchannel evaporator B with R410A and POE oil at constant exit superheat

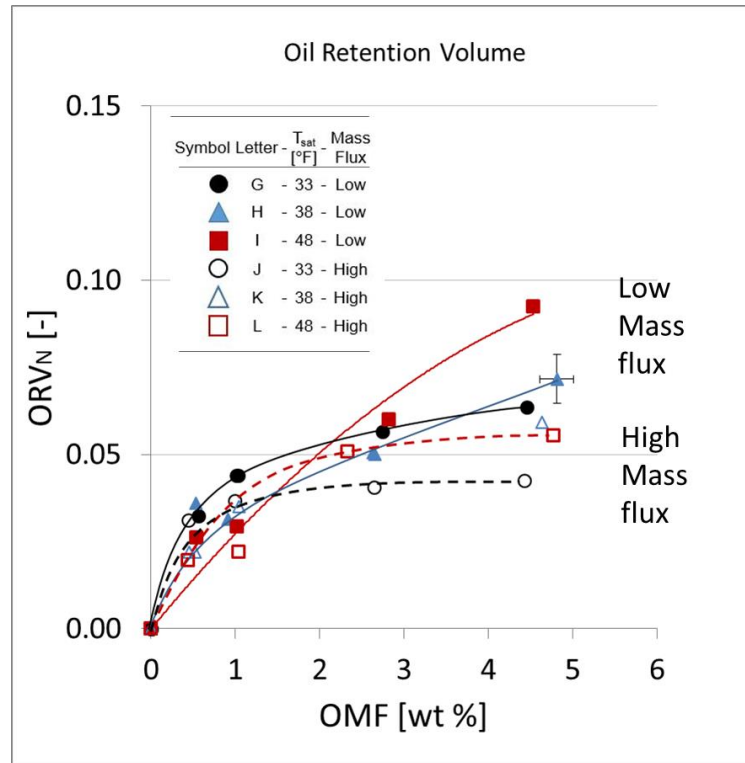


Figure 6.3: Oil retention volume (ORV_N) in microchannel evaporator B with R410A and POE oil

The experimental measurements of oil retention volume (ORV_N) for the single pass and double vertical microchannel slabs of evaporator B are summarized in Figure 6.3. The results indicated that the oil retained in evaporator B was depended on oil mass fraction (OMF) but, in contrast to the ORV_N of evaporator A, the increase of oil retention volume with OMF was smoother. For example, at OMF of 1 wt.%, the ORV_N for evaporator B was about 0.04 (series H in Figure 6.3) while the ORV_N for evaporator A for the same test conditions was about double (series H in Figure 6.1). Then, if OMF increased from 1 to 5 wt.%, ORV_N for evaporator B increased from 0.03 to 0.07 and it was measured up to 10 % of internal volume of evaporator B. At OMFs of 0.5 to 3 wt.%, there was not any difference in the measured oil retention for the series at high mass flux and low mass flux when testing the evaporator B. We recall here that evaporator B had both inlet and outlet headers at the bottom of the heat exchanger, that is, the refrigerant circulated vertically upward in the first microchannel slab, bended by 180 degree, and circulated vertically downward in the second

microchannel slab. The tubes in the second slab entered the outlet header from the top, eliminating the valleys of potential oil traps in between the tube inserts inside the outlet header of evaporator B. The result of the configuration of evaporator B was a markedly reduced oil retention when OMF is 1 wt.% with respect to the configuration used in evaporator A (recall that evaporator A was a single pass and single vertical microchannel slab with refrigerant entering at the bottom and existing at the top). This result also confirmed that the valleys in between the microchannel tube inserts in the outlet header of the evaporator A were responsible of the high ORV_N measured for evaporator A at OMF of 1 wt.%. Such valleys were potential locations for trapping the oil inside the evaporator due to reduced refrigerant vapor velocity, separation of the oil from the bulk stream, and accumulation of the oil in the valleys due to gravity.

For residential air conditioning applications with OMF typically less than or equal to 1 w.t. %, the oil retention volume was measured up to 5 % of internal volume of evaporator B. The effect of OMF on ORV_N in evaporator B seemed to follow similar trend in all series (G to L) for OMF from 0 to 1 wt. %. For series G to L the ORV_N increased smoothly as OMF increased from 0 to 1 wt. %. When OMF increased from 1 wt.% to 5 wt.%, the trend in oil retained was slightly different for the low mass flux series (G, H, and I) compared to high mass flux series (J, K and L). For low mass flux series (G, H, and I in Figure 6.3), if OMF increased from 1 wt.% to 5 wt.% there was a smooth but measurable increase in the oil retention volume. A significant increase was observed for the series I at saturation temperature of about 48 °F (9 °C). For high mass flux series (J, K and L in Figure 6.3) if OMF increased from 1 to 5 wt.%, the increase in oil retention volume was very small and almost within the experimental uncertainty, which was reported in the error bars for one representative data point in Figure 6.3 (the same experimental uncertainty bars are valid for all the remaining data points in the figure).

At the same saturation temperature and OMF, the effect of mass flux was not measurable if OMF ranged between 0.5 to 3 wt. %. In this OMF range, the mass flux affected the oil retention volume within the experimental uncertainty of the measurements, which is reported in the error bars for one representative data

point in Figure 6.3. Only when OMF was above 3 wt. % an increase of the mass flux decreased the oil retention volume by up to 60%.

For OMFs between 0.5 to 3 wt. % the effect of saturation temperature for both low mass flux series (G, H, and I) and high mass flux series (J, K and L) were also small. Only when OMF was above 3 wt. % an increase of the saturation temperature in the evaporator increased oil retention volume for the low mass flux series. For example, at 5 wt.% of oil, the ORV_N for saturation temperature 48°F (9°C) (series I in Figure 6.3) was 0.10 while the ORV_N for saturation temperature 33°F (~0.5°C) (series G) was about 0.06. This meant 40% less oil due to a decrease of evaporation saturation temperature from 48 to 33°F (9 to 0.5°C) when the mass flux was low in evaporator B. A different result was observed when the mass flux was high and the series J and L had approximately the same oil retention volume, that is, within the experimental uncertainty of the measurements, regardless of the saturation temperature of evaporation.

6.1.1.3 Microchannel evaporator A with R410A and POE oil at several degree of exit superheat

The experimental results of oil retention volume (ORV_N) in evaporator A with refrigerant R410A and POE oil at three different superheats are summarized in Figure 6.4. The oil retention volume normalized, ORV_N , was the ratio of the oil retention volume over the internal volume of the evaporator A, including the headers internal volume. To isolate the effect of superheat on oil retention volume at given oil mass fraction (OMF), the mass flux was maintained constant at 7.5 lbm/ft²-s (36.7 kg/m²-s) and saturation temperature of R410A was maintained constant at 39° F (3.9° C) throughout the series S, T and U. Tests were carried out for three different superheat and two different oil mass fractions (OMFs). Each degree of superheat is given with a solid symbol with different color and shape of the symbol in Figure 6.4. For example, the black circle data points in Figure 6.4 represent 5°F (~2.8°C) superheat or low superheat series. From a quick glance on those three series, it is evident that if the superheat at the microchannel evaporator outlet increased from 5° F to 25° F (2.8°C to 13.9° C) then the oil retention volume in microchannel evaporator A doubled at constant oil mass fraction. This trend was observed when OMF was from 0.9 w.t. % to 3 w.t. %.

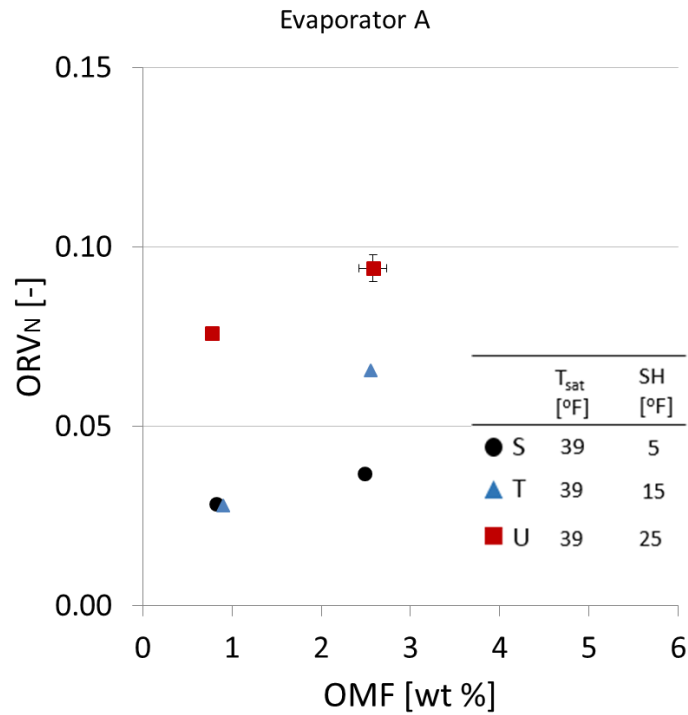


Figure 6.4: Oil retention volume (ORV_N) in microchannel evaporator A with R410A and POE oil for several degree of superheat

The experimental results of ORV_N for low, medium and high degree of superheat series (Series S, T, and U in Figure 6.4) suggested that at given exiting superheat the amount of oil retained in the microchannel evaporator was strongly depended on the OMF, and ORV_N increased as OMF increased. These findings were consistent with the oil retention volume results reported in section 6.1.1.1. For low superheat series (series S), the oil retention volume was measured up to 3.7 % of internal volume of evaporator A. For low superheat series (series U in Figure 6.4) and medium superheat series (series T in Figure 6.4) as OMF increased from 0 to 1 wt. %, the ORV_N increased from 0 % to 2.6 % of internal volume of evaporator A. Therefore increase in ORV_N for low and medium superheat series (series S and series T) was smoother which is confirmed by findings of high mass flux series (J, K and L) in Figure 6.1. For high superheat series (series U) as OMF increased from 0 to 0.9 wt. %, the ORV_N was up to 7.5 % of internal volume of evaporator A. Therefore there is sudden increase in oil retention volume for high superheat series (series U) which is similar to the findings of low mass flux series (series G, H and I in Figure 6.1). In evaporators as degree of exit superheat increases

the amount of refrigerant dissolved in liquid film decreases at constant pressure, which leads to increase in viscosity of the liquid film in high quality region and superheat section of micro channels and outlet header of evaporator A. This assumption is supported by Youbi-Idrissi et al., 2003 work on effect of refrigerant–oil solubility on an evaporator performances. They showed that Non-Evaporated refrigerant quantity (NEQ) at evaporator outlet decreased as superheat increased but becomes stable at higher superheats. That means viscosity of liquid mixture that exits evaporator at higher degree of superheat is high when compared to low degree of superheat. In additional, the oil was potentially trapped in the valleys created between the microchannel tubes inserts into the outlet header due to insufficient interfacial friction between vapor and liquid layer. This further promoted oil retention in the outlet header.

6.1.1.4 Microchannel evaporator B with R410A and POE oil at several degree of exit superheat

The experimental results of oil retention volume (ORV_N) in evaporator B with refrigerant R410A and POE oil exiting with three different superheats are summarized in Figure 6.6. To isolate the effect of exit superheat on oil retention volume, the mass flux of refrigerant was maintained constant at $8.4 \text{ lb}_m/\text{ft}^2\text{-s}$ ($41.0 \text{ kg}/\text{m}^2\text{-s}$), and saturation temperature at 39° F (3.9° C) for all three series (series S, T and U in Figure 6.6). The effect of superheat is represented as solid symbols and corresponding letters (for details see Table 6.2). From Figure 6.6, it is evident that if the superheat at the evaporator B outlet increased from 5° F to 25° F (2.8° C to 13.9° C) then oil retention volume increased nearly 2.5 times for same oil mass fraction. For residential air conditioning applications with OMF typically less than or equal to 1 w.t. %, the oil retention volume was measured up to 2.9 % of internal volume of evaporator B when degree of superheat was 5° F (2.8° C) and it was measured up to 9.8% of internal volume of evaporator B when degree of superheat was 25° F (13.9° C).

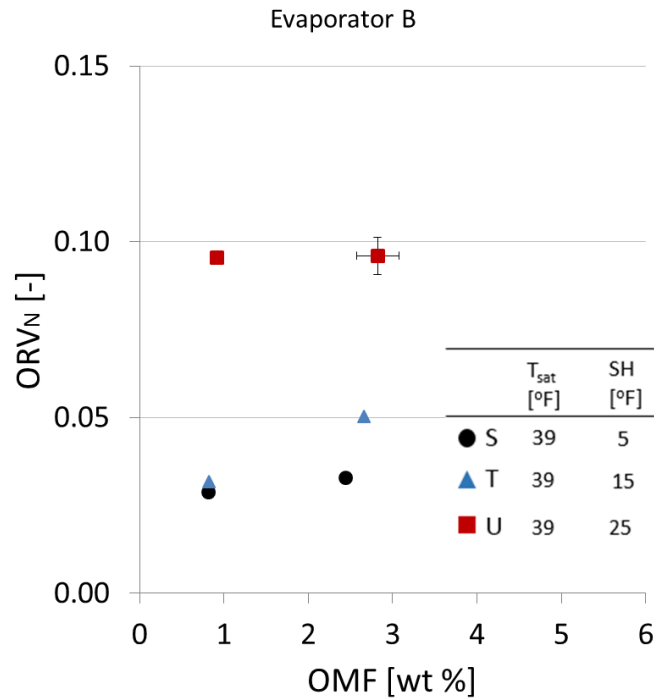


Figure 6.5: Oil retention volume (ORV_N) in microchannel evaporator B with R410A and POE oil for several degree of superheat

The effect of OMF on oil retention volume at given superheat in evaporator A and evaporator B followed similar trends in all three series (S to U) for OMF from 0 to 2.9 wt. %. For example, at OMF of 0.9 wt.%, the ORV_N for evaporator B was about 0.029 (series ‘S’ in Figure 6.6) while the ORV_N for evaporator A for the same test conditions was almost same (series S in Figure 6.4). For high superheat series (series U), as OMF increased from 0 to 0.9 wt.% the ORV_N increased up to 9.8 % of the total volume of evaporator B. The sudden increase in ORV_N for high degree of superheat at OMF 0.9 wt.% was also observed in evaporator A (see Figure 6.4) . In order to explain the sudden increase in ORV_N in evaporator B for high superheat series (series U in Figure 6.6) when compared to low superheat series (series S in Figure 6.6), following illustration of cross section of microchannel evaporator B is shown in Figure 6.6, which is similar to the schematic shown in Figure 4.2.

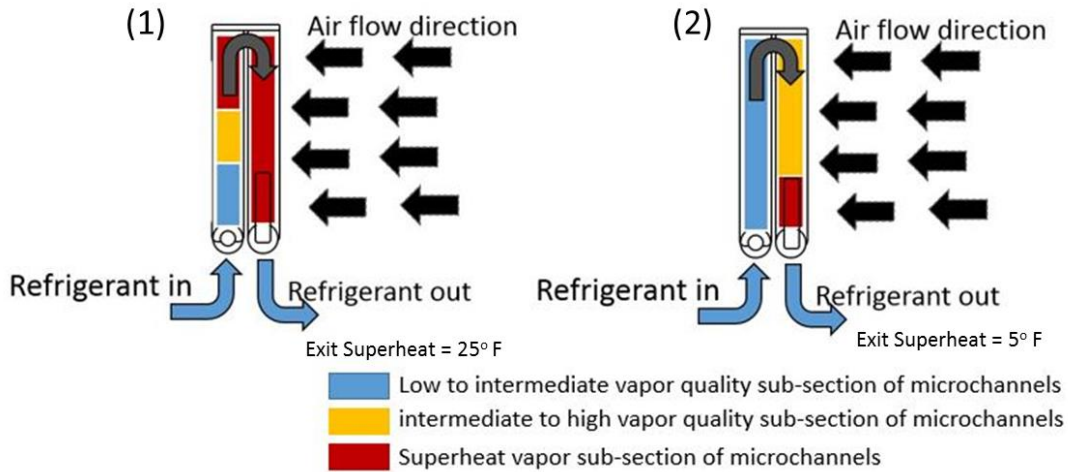


Figure 6.6: Schematic representation two phase evaporation length along the microchannels for various exiting degree of superheat







The Figure 6.6 is an approximate representation of section of microchannels in evaporator B which is occupied by two phase and superheat sections during in-tube evaporation. The first schematic of evaporator B on the left side in Figure 6.6 shows refrigerant vapor exits at superheat 25° F (13.9° C). Similarly the second schematic in Figure 6.6 shows refrigerant vapor exits at superheat 5° F (2.8° C). It is intuitive that for same inlet conditions in microchannel evaporator B, the length of two phase evaporation decreases as superheat at outlet increases. In Figure 6.6, it is shown that when exit superheat was 25° F (13.9° C), the high quality and superheat vapor region is present in the first microchannel slab where refrigerant is circulated vertically upward against gravity. In this case when oil is circulated in the refrigerant, the local oil concentration in liquid mixture can reach up to 20 % when OMF is 1 wt. %. Therefore refrigerant vapor needs to overcome the gravitational force to drag viscous liquid mixture. On contrary, when vapor exits at superheat 5° F (2.8° C), it is possible that first microchannel slab of evaporator B was occupied by low to intermediate vapor quality. In this case, the liquid mixture viscosity is considerably less because it is diluted with liquid refrigerant where local oil concentration in liquid mixture can range from 1.5 % to 2 %, when OMF is 1 wt.%. Radermacher et al., 2006 showed that in evaporator heat exchanger model, the oil retention is minimum at intermediate qualities (0.4 – 0.6) and they argued that it was due to the combination of liquid refrigerant evaporated and local oil concentration was low. In addition, high quality and superheated refrigerant vapor

will occupy second microchannel slab of evaporator B where refrigerant is circulated downward (see Figure 6.8). Thus amount of oil retained in low superheat series (series S in Figure 6.8) is less when compared to that of high superheat series (series U in Figure 6.8). Also further as superheat increases the viscosity of liquid mixture also increase which increased amount of oil retained in evaporator B. This hypothesis explains why there is sudden increase in oil retention in evaporator B even though there is no possible valleys filling effect as discussed in section 6.1.1.1.

6.1.2 Microchannel evaporator A with R134a and POE oil

This section discusses the experimental results of oil retention volume in microchannel evaporator A with refrigerant R134a and POE oil mixture. The experiments were carried out for saturation temperature of R134a at below and above freezing temperatures, i.e. 32 °F (0 °C). The series with saturation temperatures of evaporation below 32 °F (0 °C) are referred as low temperature series (letter M, N, and O) and the series for saturation temperature of evaporation above 32 °F (0 °C) are referred as medium temperature series in this report. Details of the test conditions at low and medium temperatures are given in Table 6.3. For low temperature series (M, N, and O) the oil retention experiments were carried out at mass flow rate of 150 lbm/hr, and saturation temperature was varied from 0 to 10 °F (-17.7 °C to -12.2 °C) in three stages. For medium temperature series (P, Q, and R) the oil retention experiments were carried out at slightly higher mass flow rate of about 200 lbm/hr, and the saturation temperature was also varied in three stages ranging from 33 to 48 °F (0.5 °C to 9.5 °C).

Table 6.3: Legend of the letters and symbols used in the figures reporting the tests results of microchannel evaporator A with R134a and POE

Symbol	Letter	T_{sat}	$G_{Evaporator A}$	SH
		$^{\circ}F (^{\circ}C)$	$lb_m/ft^2-s (kg/m^2-s)$	$^{\circ}F (^{\circ}C)$
	M	0 (-18)	4.2 (20.4)	10 (5.5)
	N	7 (-14)	4.2 (20.4)	10 (5.5)
	O	10 (-12)	4.2 (20.4)	10 (5.5)
	P	33 (0.5)	3 (15)	10 (5.5)
	Q	38 (3.3)	3 (15)	10 (5.5)
	R	48 (9)	3 (15)	10 (5.5)

*G is the mass flux inside each microchannel tube. It was calculated from the total mass flow rate entering evaporator A divided by the total cross sectional area of all the microchannel tubes of the evaporator A ($G_{Evaporator A}$). *SH is degree of superheat of vapor refrigerant at evaporator outlet

The results of oil retention volume (ORV_N) in evaporator A with refrigerant R134a and POE oil mixture for low temperature series (M, N, and O) and medium temperature series (P, Q, and R) are given in Figure 6.7. The results indicated that the oil retention in evaporator A was strongly depended on the OMF and the oil retention volume increased if OMF increased. For low temperature series (letters M, N, and O), for which the saturation temperatures were varied within common ranges for vending machines, wine and water coolers, and refrigeration systems, the oil retention volume was measured up to 15 % of internal volume of evaporator A. For medium temperature series (letter P, Q, and R), the oil retention volume was measured up to 7.5 % of internal volume of evaporator A. The medium temperatures are representative of air conditioning applications.

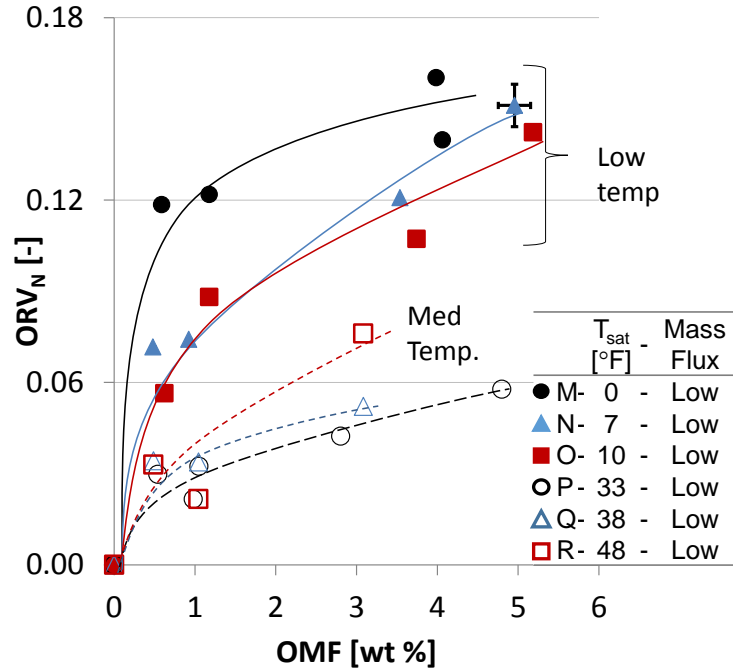


Figure 6.7: Oil retention volume for R134a+POE oil in microchannel evaporator A

For low temperature series (M, N, and O), if OMF varied from 0 to 1 % there was sudden increase in oil retention volume, especially for the lowest saturation temperature at 0°F (-18°C, series M). The increase in ORV_N was about 5.8 % and up to 12 % of internal volume of evaporator A for low temperature series when OMF varied from 0.5 wt. % to 1 wt. %. For medium saturation temperature series as OMF increased from 0 to 1 wt. %, the ORV_N was up to 3 % of internal volume of evaporator A. In other words, the ORV_N for medium temperature was significantly lower than the ORV_N for the low temperature series at similar OMFs. This finding indicated that the resulting viscosity of the liquid mixture at temperatures below freezing impaired the transport of oil and, thus, promoted the retention of oil in the evaporator.

The effect of saturation temperature was clearly visible when comparing the low temperature series (M, N and O) and the medium temperature series (P, Q and R) for oil mass fraction of 3 wt.%. At OMF of 3 wt.%, the ORV_N was 0.06 for the above freezing temperatures and it doubled for below freezing temperatures. It increased further to 0.14 for the lowest saturation temperature of 0°F (-18°C, series M).

6.2 Heat transfer factors (HTFs) for microchannel evaporators

This section discusses the results of effect of oil on heat transfer rate of microchannel evaporator A and evaporator B with refrigerant R410A and POE oil mixture and with refrigerant R134a and POE oil mixture. The tests were conducted for two mass fluxes, three saturation temperatures and three superheats. The test conditions and the legend for the symbols used to report the experimental results from these tests were given in Table 6.1, Table 6.2 and Table 6.3. The effect of oil on the heat transfer rate is provided in terms of heat transfer factor (HTF), which was the ratio of heat transfer rate measured from the air-side when oil was present over the heat transfer rate in oil-free conditions. Both heat transfer rates were evaluated at the same total mass flux, saturation pressure, and degree of superheated vapor at the outlet for given series. Thus, the HTF isolated and quantified the effect of oil on the refrigerant-side heat transfer capacity. The results are summarized in plots in which OMF is on the x-axis and the HTF is on the y-axis. Low mass flux is represented by solid symbols (series G, H, and I) while the high mass flux is represented by the void symbols (series J, K and L series). Each saturation temperature was evaluated at both high and low mass flux. To isolate the effect of superheat on heat transfer factors (HTFs) due to presence of oil, the mass flux and saturation temperatures were maintained constant in series S, T and U.

It should be emphasized in here that the refrigerant was well distributed across the microchannel tubes of the evaporators. Since we purposely decided to control the inlet conditions of the microchannel evaporators to slightly sub-cooled (or near saturated) liquid, the distribution of the refrigerant and oil mixture across the microchannel tubes was uniform during the tests of the present work. The flow distribution was only qualitatively observed by using thermal images of the evaporators during the tests. Since the thermal image (see Figure 4.17) colors of the evaporator were uniform everywhere along the front face of the heat exchanger, we concluded that all the microchannel tubes received approximately the same flow rate of refrigerant (or of refrigerant and oil mixture). The condition of saturated liquid at the inlet of the evaporator was not necessarily representative of real life evaporator applications but, in the present study, it avoided the challenge of non-uniform flow distribution of the refrigerant and oil mixture when oil was injected to the evaporator. As a

result of the testing conditions imposed for the evaporators in the present work, the HTFs presented for the evaporators do not account for the effect that oil might have on the refrigerant flow distribution across the microchannel tubes and they do not account for the flow change, if any, inside the inlet headers of the microchannel heat exchangers. These effects, which are still due to the presence of oil in the mixture, might result in additional sources of heat transfer rate degradation in microchannel evaporators and their investigation could be part of future studies of this work.

6.2.1 HTF of microchannel evaporator A with R410A and POE oil

From section 6.2.1.1 to 6.2.1.2 the experimental results of heat transfer factor (HTF) in evaporator A and evaporator B with refrigerant R410A and POE oil at constant degree of superheat at outlet are discussed. The information of test conditions and the legend for those tests are given in Table 6.1. From section 6.2.1.3 to 6.2.1.4 the experimental results of heat transfer factor (HTF) in evaporator A and evaporator B with refrigerant R410A and POE oil at several degree of superheat at outlet are discussed. The information of test conditions and the legend for those tests are given in Table 6.2.

6.2.1.1 HTF of Microchannel evaporator A with R410A and POE oil at constant exit superheat

The experimental results of heat transfer factor (HTF) in evaporator A with refrigerant R410A and POE oil at constant superheat are summarized in Figure 6.8. This figure shows the HTF of the microchannel evaporator A on the y-axis and the oil mass fraction (OMF) of POE oil in refrigerant R410A on the x-axis. When OMF is 0 (i.e., no oil is present inside the evaporator), the HTF resulted 1 by its own definition and it decreased if OMF increased as shown in Figure 6.8. The effect of mass flux is represented as void and solid symbols and corresponding letters in the legend of the figures. Low mass flux series are represented by the solid symbols (G, H, and I) while high mass flux tests are represented as void symbols (J, K and L series) (for details about the legend, see Table 6.1). Each saturation temperature is given with a void and a solid symbol with same color and shape of the symbol. For example, the black circle data points in Figure 6.8 represent saturation temperature of 33° F (~0.5° C); the solid circle points (series G) are for low mass flux

while the void circle points (series J) are for high mass flux. The results indicate that if the oil mass fraction (OMF) increased, the heat transfer factor of microchannel evaporator A decreased from 1 to 0.87. This represents a reduction of the refrigerant-side heat transfer rate due to oil by about 13%. However, at OMF of 1 wt.%, the reduction of the refrigerant side heat transfer rate was within the experimental uncertainty of $\pm 4.5\%$. From Figure 6.8 it is clear that the effect of oil on heat transfer rate was to decrease the refrigerant-side heat transfer rate but the impact of oil was not significant if OMF ranged from 0.5 wt. % and 1 wt. %. The impact of oil on the heat transfer rate was measurable for OMFs of 3 wt. % and of 5 wt. % and the heat transfer rate decreased by about 8 to 13%. The HTFs given in Figure 6.8 represent only the effect of oil because each test with oil was compared with the corresponding reference without oil at the same inlet saturation pressure, total mass flow rate, and degree of superheated vapor at the outlet of the evaporator. The air inlet temperature and velocity were also constant between the tests with oil and the baseline reference tests with no oil provides the simulation results of the local refrigerant-side convective heat transfer coefficient of R410A and POE oil mixture along the direction of the refrigerant flow in a microchannel tube. Each tube was divided in 100 segments in order to compute 100 values (one for each segment) of the two phase flow boiling heat transfer coefficient inside the microchannel tube. The model used to obtain these results will be described in details in the next section but it is used here to highlight some insights on the convective heat transfer process inside the microchannel tube when oil was present. The simulation results indicate that the presence of oil in refrigerant R410A decreases the heat transfer coefficient when compared to refrigerant R410A heat transfer coefficient (blue series with legend 1-0OMF). This preliminary calculations show that oil tended to penalize the two phase flow heat transfer coefficient if refrigerant heat transfer coefficient correlations available in the literature were used for predicting the behavior of refrigerant and oil mixtures. This extrapolation of the heat transfer correlations might not be valid and should be carefully evaluated. However, developing local heat transfer coefficient correlations for refrigerant and oil mixtures was out of scope of the present work and might be potential future work.

The plots from Figure 6.10 to Figure 6.13 show the direct effect of oil on the heat transfer rate, $\dot{Q}_{evap,A}$, which was measured from the air-side of the evaporator A during the actual heat transfer experiments. $\dot{Q}_{evap,A}$ was measured directly from the measurements of air flow rate (which was constant at all time during the tests) and of air inlet and outlet dry bulb temperatures. These figures shows how the heat transfer rate varied in real time during the tests when the oil was injected in the evaporator. The green solid line in each Figure represent the oil injection period. If the oil flow was zero than the green line is also zero; if the oil flow is greater than zero then the green line becomes high value. The measured data of instantaneous heat transfer rate in Figure 6.10 to Figure 6.13 were sampled every 2 seconds and the brown solid lines had some scattering. However, from these figures it was evident that when oil was introduced in the evaporator, the heat transfer rate decreased. The effect of oil on heat transfer rate was not directly visible from the instantaneous measurements of heat transfer rate if OMF was 0.5 wt. % and 1 wt. % (see Figure 6.10 and Figure 6.11). But when OMF was 3 wt. % and 5 wt. %, there was a marked shift of the instantaneous heat transfer rate to below 15,000 Btu/hr (4.4 kW), shown in Figure 6.12 and Figure 6.13.

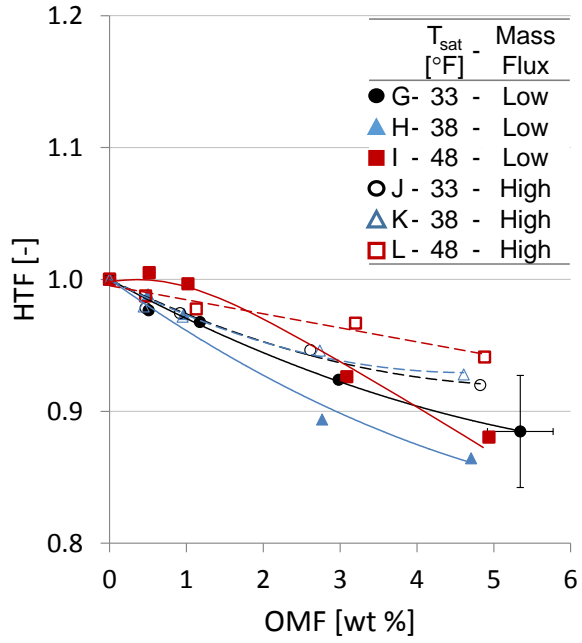


Figure 6.8: Heat transfer factor in microchannel evaporator A with R410A and POE oil

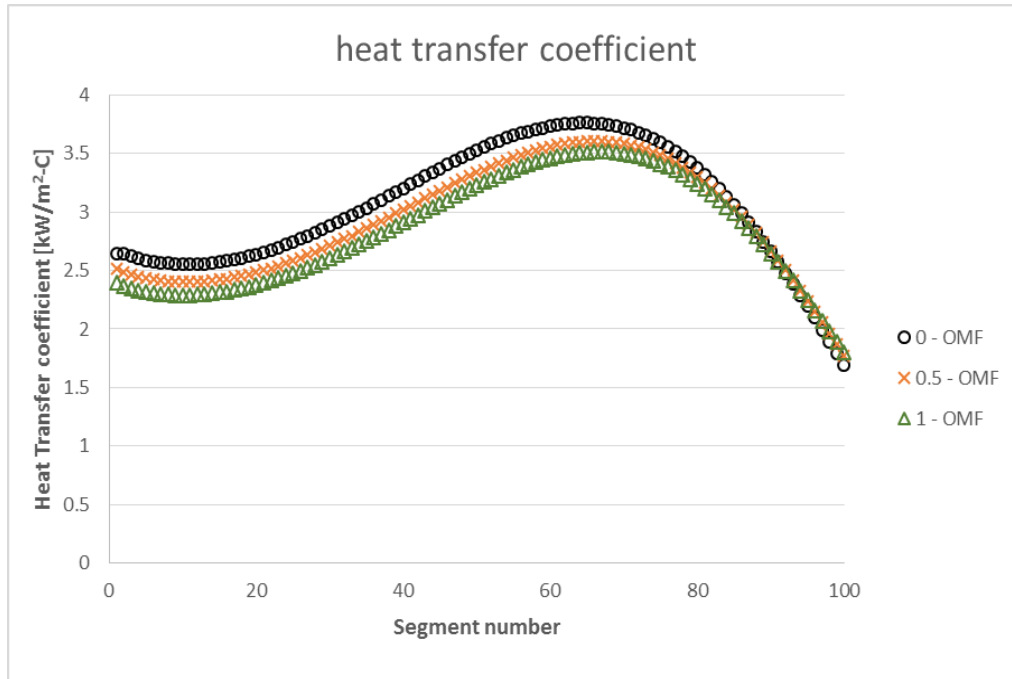


Figure 6.9: Simulation results of the local convective heat transfer coefficient in one microchannel tube of evaporator A with R410A and POE oil mixture

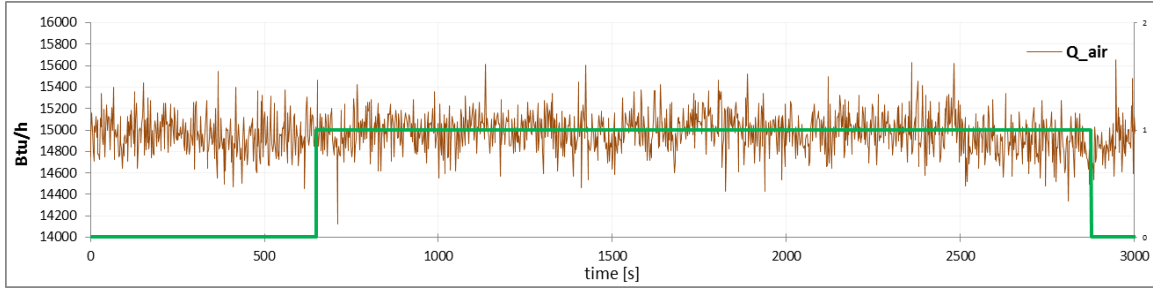


Figure 6.10: Heat transfer rate measured from the air-side ($\dot{Q}_{evap,A}$) in microchannel evaporator A with R410A and POE oil at OMF at 0.5%

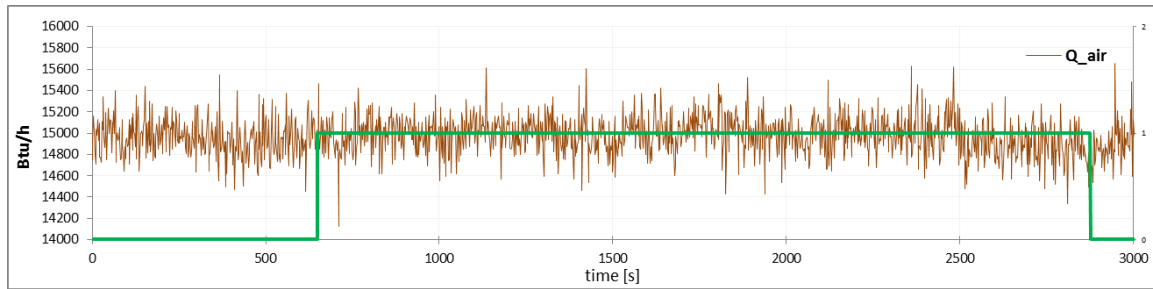


Figure 6.11: $\dot{Q}_{evap,A}$ in microchannel evaporator A with R410A and POE oil at OMF 1%

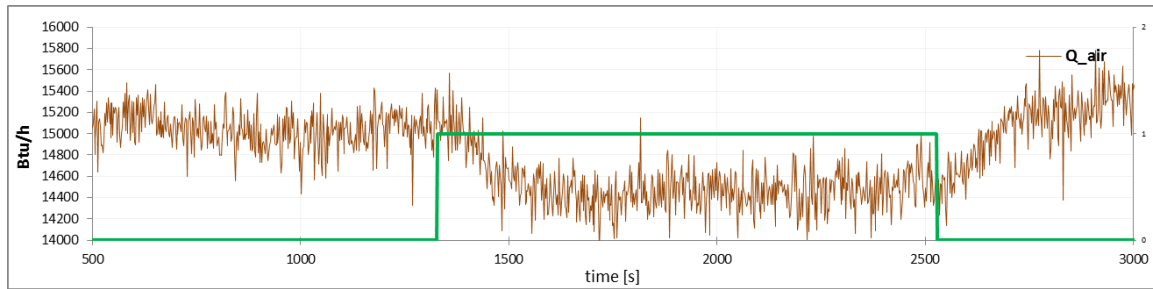


Figure 6.12: $\dot{Q}_{evap,A}$ in microchannel evaporator A with R410A and POE oil at OMF 3%

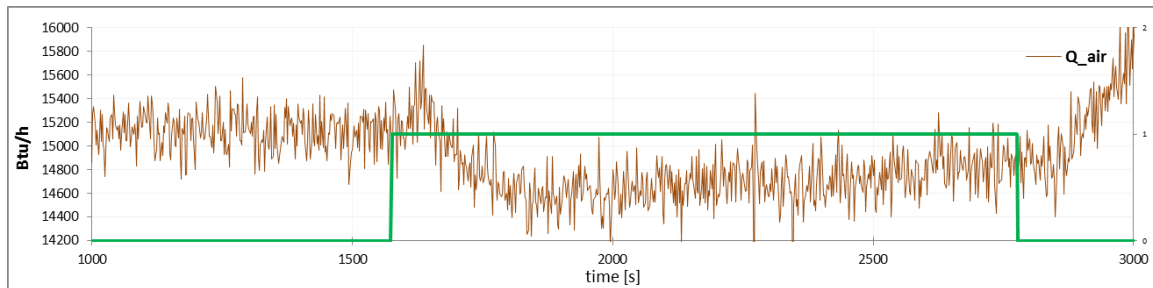


Figure 6.13: $\dot{Q}_{evap,A}$ in microchannel evaporator A with R410A and POE oil at OMF 5%

The worst case of decrease in HTF of the microchannel evaporator A in Figure 6.8 was measured at OMF of 5 wt. % and at low mass flux (series H) where HTF was reduced by 13 % when compared to no oil conditions.

For air-conditioning applications, when OMF is typically less than 1 wt. %, the decrease in heat transfer rate was less than 4%. The oil decreased the heat transfer rate and its impact was also depended on the mass flux. The HTFs were close to 1 for OMF less than 1 wt. % and for both high and low mass flux. For OMF higher than 1 wt. %, the impact of mass flux on HTF was measurable. For example, at OMF of 3 wt.%, a reduction of mass flux from high mass flux of 8.4 lb_m/ft²-s (20.4 kg/m²-s, series K) to low mass flux of 4.2 lb_m/ft²-s (20.4 kg/m²-s, series H) decreased the HTF from 0.96 (series K in Figure 6.8) to 0.90 (series H) for the same saturation temperature of 38°F (~3.3°C). Hu et al. (2011) conducted heat transfer experiments to study the heat transfer coefficient of R410A and POE oil mixture during flow boiling in a 7 mm diameter smooth tube. Their analysis showed that decreasing the mass flux of R410A/POE mixture at particular quality and oil concentration resulted in diminished local heat transfer coefficient. Their finding was in agreement with the experimental results of Figure 6.8, in which the HTFs for low mass flux series (letters G, H, and I) tended to be slightly lower than the HTFs for the high mass flux series (J, K and L). Furthermore, we recall that for the same OMF and saturation temperature, oil retention in the low mass flux series (G, H, and I) was higher when compared to that of high mass flux series (J, K and L). Due to high oil retention for low mass flux series (G, H, and I) there could be additional resistance added to heat transfer process in microchannel tubes. Finally, for evaporator A, the saturation temperature did not have a marked effect on HTF. This might be due to the normalization of the heat transfer rate with oil over the corresponding heat transfer rate with no oil at the same saturation temperature. The low mass flux series (G, H, and I) in Figure 6.8 were close to each other and the high mass flux series (J, K and L) were close to each other. For each group, the HTFs were within the experimental uncertainties of ± 4.5% for HTF, shown by the error bars for one representative data point in Figure 6.8 (the same experimental uncertainty bars applied to all data points of the figure).

6.2.1.2 HTF of Microchannel evaporator B with R410A and POE oil POE oil constant exit superheat

The results for effect of oil on HTF for the microchannel evaporator B with refrigerant R410A and POE oil for conditions that are applicable to air conditioning systems are given in Figure 6.14. The HTFs in Figure 6.14 represent only the effect of oil because each test with oil was compared with the reference without oil at

the same inlet saturation pressure and total mass flow rate. The air inlet temperature and velocity were also constant between each tests with oil and the corresponding baseline references with no oil. The results indicate that HTFs of microchannel evaporator B decreased by 12% if the OMF increased from 0 to 5 wt.% and for low mass flux and saturation temperature of 38°F (3.3°C) (series H).

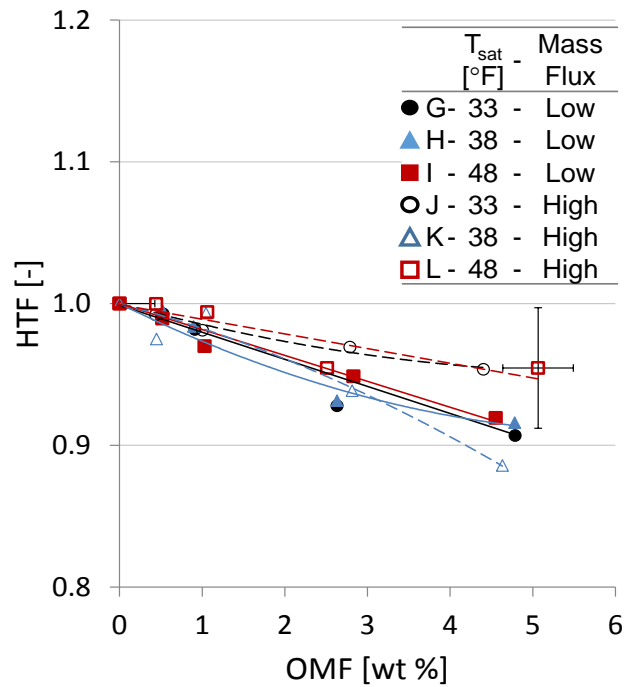


Figure 6.14: Heat transfer factor in microchannel evaporator B with R410A and POE oil

In air conditioning applications, in which the OMF is typically at or below 1 wt. %, the decrease in heat transfer rate was about 1 to 4 % when compared to the case of oil free conditions in the evaporator B. The trends in Figure 6.14 suggest that the increase of oil from 0 to 5 wt.% in the refrigerant R410A flow decreased the heat transfer rate of the evaporator almost linearly. The effect of mass flux on HTF was evident when OMF was higher than 3 wt. %. This was also the case for the microchannel evaporator A. A reduced mass flux resulted in lower HTF, especially for OMF of 3 wt. % and 5 wt. %. For similar saturation temperatures, the HTF decreased up to 5% when mass flux was low. Interestingly the effect of mass flux was not observed in the series H and K, whose saturation temperature was 38°F (3.3°C). For this saturation temperature the heat transfer factor decreased in a very similar manner from 1 to 0.9 regardless of the mass flux.

6.2.1.3 HTF of Microchannel evaporator A with R410A and POE oil at several degree of exit superheat

The experimental results of heat transfer factor (HTF) in evaporator A with refrigerant R410A and POE oil at three different degree of superheat at outlet are summarized in Figure 6.15. This figure shows the HTF of the microchannel evaporator A on the y-axis and the oil mass fraction (OMF) of POE oil in refrigerant R410A on the x-axis. When OMF is 0 (i.e., no oil is present inside the evaporator), the HTF resulted 1 by its own definition and it decreased if OMF increased as shown in Figure 6.8. The effect of superheat on HTF due to presence of oil in refrigerant was isolated by maintaining saturation temperature at 39° F (3.9° C) and mass flux at 7.5 lbm/ft²-s (36.7 kg/m²-s) for all three series (series S, T and U) (for details about the legend, see Table 6.2). The results indicate that for constant superheat if the oil mass fraction (OMF) increased, the heat transfer factor of microchannel evaporator A decreased from 1 to 0.95. This represents a reduction of the refrigerant-side heat transfer rate due to oil by about 5%. This findings were in agreement with results discussed in 6.2.1.1 for series K. The worst case of decrease in HTF of the microchannel evaporator A in Figure 6.15 was measured at OMF of 3 wt. % and at low superheat (series S in Figure 6.15) and medium superheat series (series T in Figure 6.15) where HTF was reduced by 5 % when compared to no oil conditions. For air-conditioning applications, when OMF is typically less than 1 wt. %, the decrease in heat transfer rate was less than 3% for all three superheat (series S, T and U in Figure 6.15).

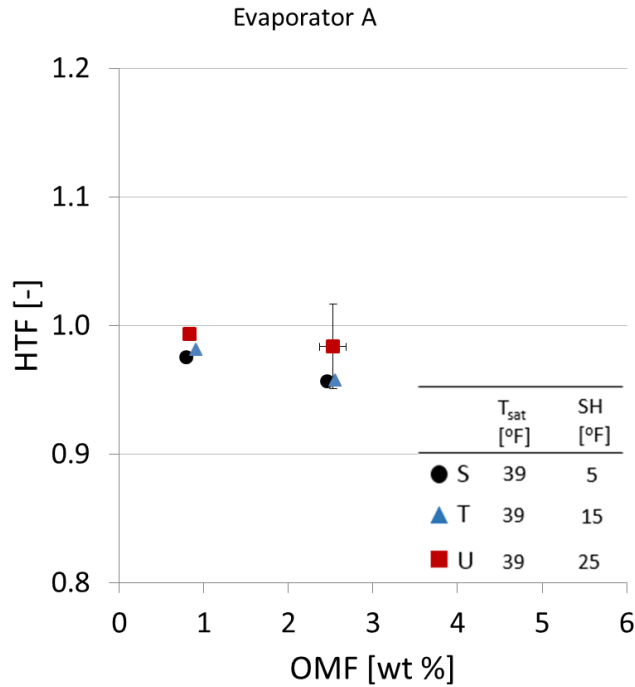


Figure 6.15: Heat transfer factor in microchannel evaporator A with R410A and POE oil several degree of exit superheat

From Figure 6.15 it is clear that the HTF increases slightly as superheat increases from 5° F to 15° F (2.8°C to 8.3°C) at constant OMF. If the superheat at microchannel evaporator A outlet increases then the amount of refrigerant dissolved in liquid film for similar OMF decreases. In other words, the non-evaporated quantity of liquid refrigerant at microchannel evaporator A outlet for superheat 5 series is more than that of superheat 15° F series (series T). This assumption is supported by Youbi-Idrissi et al., 2003 work on effect of refrigerant–oil solubility on an evaporator performances. They showed that Non-Evaporated refrigerant quantity (NEQ) at evaporator outlet decreased as superheat increased but becomes stable at higher superheats. McMullan et al., 1988b studied evaporator heat transfer rate for various degree of superheat (°C) for oil free and with oil conditions. Their results suggested that for high degree of superheat the effect of oil on heat transfer rate had negligible effect. They also showed that at OMF 1.9 wt.% when superheat at evaporator outlet decreased below 4°C the heat transfer performance of the evaporator became worse. These findings in literature are in agreement with results in Figure 6.15.

6.2.1.4 HTF of Microchannel evaporator A with R410A and POE oil at several degree of exit superheat

The results for effect of oil on HTF for the microchannel evaporator B with refrigerant R410A and POE oil for three different degree of superheat at outlet are given in Figure 6.16.

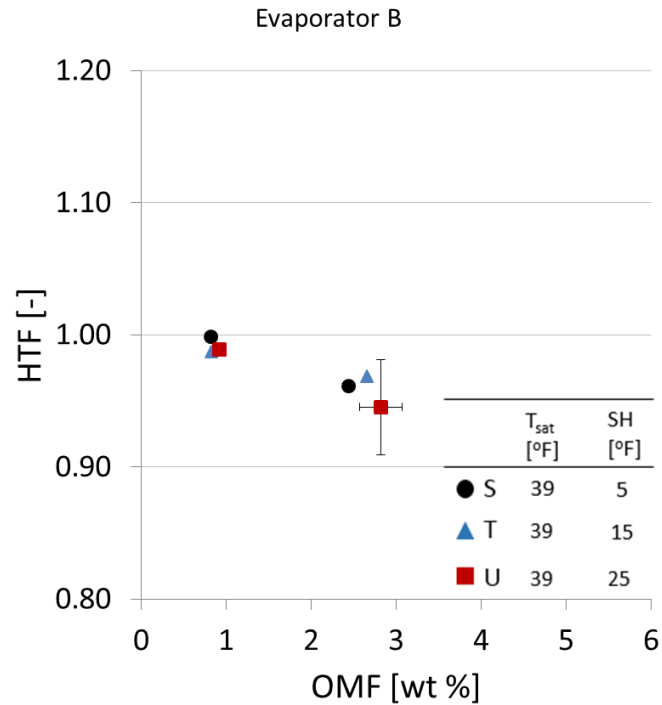


Figure 6.16: Heat transfer factor in microchannel evaporator B with R410A and POE oil

To isolate the effect of exit superheat on HTF, the mass flux of refrigerant was maintained constant at 8.4 lb_m/ft²-s (41.0 kg/m²-s), and saturation temperature at 39° F (3.9° C) for all three series (series S, T and U in Figure 6.16). The effect of superheat is represented as solid symbols and corresponding letters (for details see Table 6.2). The results indicate that HTFs of microchannel evaporator B decreased by 6 % if the OMF increased from 0 to 3 wt.% (series U in Figure 6.16). In Figure 6.16 the effect of superheat on HTF at OMF 0.9 wt.% was negligible for all 3 different superheat. Therefore for residential air-conditioning application when OMF is 0.9 wt.% the effect of oil is negligible on heat transfer rate of evaporator B and increase or decrease in exit superheat will not affect the heat transfer rate.

6.2.2 HTF for microchannel evaporator A with R134a and POE oil mixture

This section discusses the experimental results of effect of oil on heat transfer factor in microchannel evaporator A with refrigerant R134a and POE oil mixture. For this part of research, experiments were carried out for saturation temperature of R134a below and above freezing temperature, i.e. 32 °F (0 °C). For the saturation temperatures below 32 °F (0 °C) is referred as low temperature series and for above 32° F (0° C) is referred as medium temperature series. For the low temperature series experiments, the mass flow rate was 150 lb_m/hr, and the saturation temperature varied from 0 to 10°F (-17.7° C to -12.2° C). For medium temperature series experiments, the mass flow rate was 200 lb_m/hr, and the saturation temperature varied from 33° F to 48° F (0.5° C to 9.5° C). The mass fluxes and test conditions are provided in Table 4.3.

The HTFs in Figure 6.17 represent only the effect of oil because each test with oil was compared with the reference without oil at the same inlet saturation pressure, total mass flow rate, and degree of vapor superheated at the outlet of the evaporator. The air inlet temperature and velocity were also constant between the cases of tests with oil and the baseline references with no oil. The results indicates that the presence of oil decreased the heat transfer capacity of microchannel evaporator A with refrigerant R134a. For few exceptions it was observed that presence of oil slightly increased the heat transfer rate of the evaporator compared to case of oil free conditions. For OMF ranging from 0 wt.% to 5 wt.%, the HTF of microchannel evaporator A decreased up to 12%. For refrigeration applications in which the OMF is typically less than 1 wt. % the HTF was about 0.96, which indicates a maximum decrease of heat transfer rate of 4% when compared to oil free conditions. These were the results for series O, P, Q and R in Figure 6.17. For series M and N the HTF results indicated that there was a slight increase in heat transfer rate of microchannel evaporator A when the OMF was 0.5 and 1 wt.%. Then, for OMF above 3 wt.%, the heat transfer rate started to decrease. For low temperature series M, N, and O the effect of saturation temperature was clearly evident for OMF 3 and 5 wt. %. When saturation temperature decreased from 10° F to 0° (-12.2° C to -17.7° C), the HTF further decreased up to 5%.

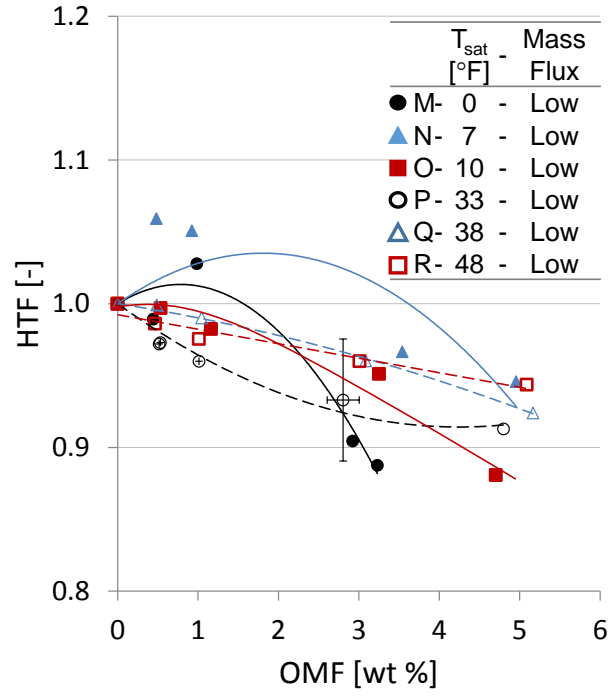


Figure 6.17: Heat transfer factor in microchannel evaporator A with R134a and POE oil

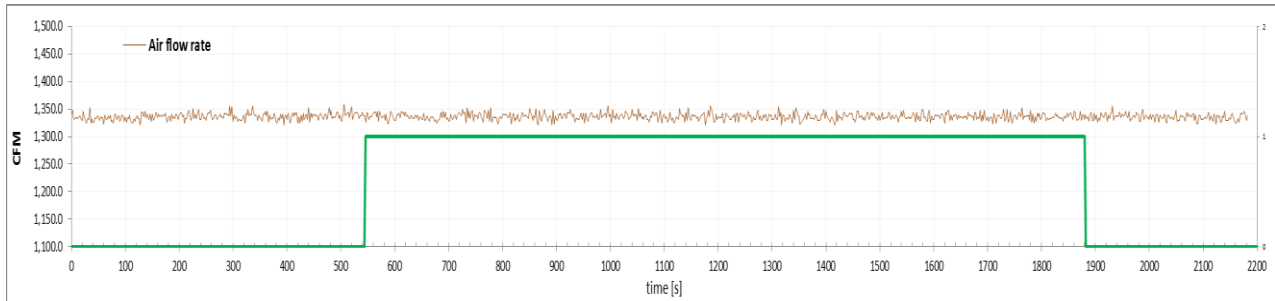


Figure 6.18: Air flow rate (CFM) for microchannel evaporator A with R134a and POE oil at saturation temperature 7° F (series N) and OMF 1 wt. %. This figure shows air flow rate did not change

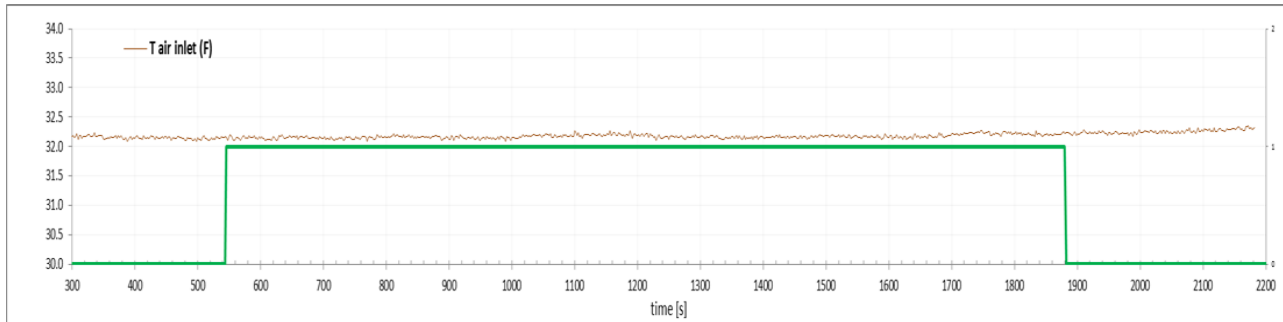


Figure 6.19: Air inlet temperature (° F) for microchannel evaporator A with R134a and POE oil at saturation temperature 7° F (series N) and OMF 1 wt. %. This figure shows air inlet temperature was constant

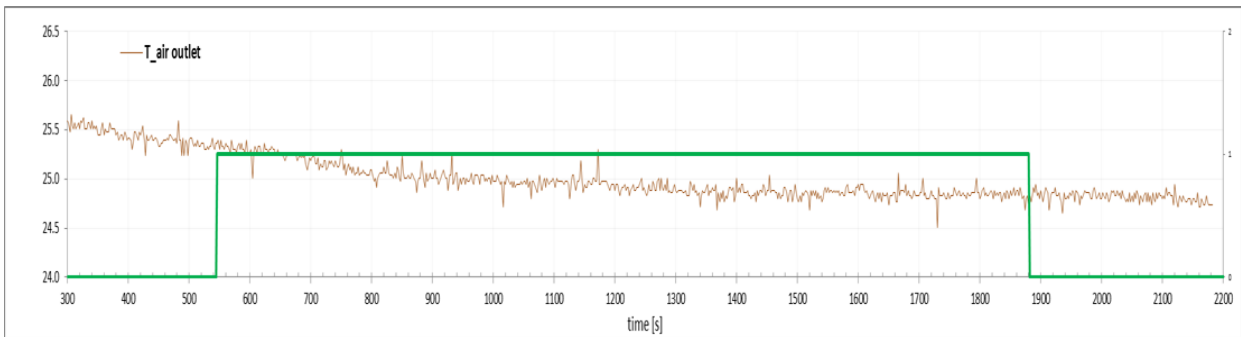


Figure 6.20: Air outlet temperature (° F) for microchannel evaporator A with R134a and POE oil at saturation temperature 7° F (series N) and OMF 1 wt. %. This figure shows air outlet temperature decreases during injection

During the evaporator tests, when high amount of oil was injected in the microchannel evaporator, the decrease in capacity of the microchannel evaporator was visible from the instantaneous real time measurements of the air side heat transfer rate. Figure 6.18 to Figure 6.20 provides instantaneous real time live measurements of the air side flow rate and air inlet-outlet temperature difference during a test with the

evaporator A and for refrigerant R134a and POE oil mixture. First it is observed that in Figure 6.18, the volumetric flow rate of the air did not change during the period in which the oil was metered to the evaporator. This result indicated that there was not any frost accumulation on the microchannel evaporator A for this test. While the air inlet temperature was controlled to be constant during the tests, as shown in Figure 6.19, the air outlet dry bulb temperature in Figure 6.20 was the result of the heat transfer process in the evaporator. In Figure 6.19, the temperature of air at the inlet test section was very stable and constant before, during, and after the injection period of oil. However, the dry bulb temperature of the airstream at the outlet of the evaporator A was not completely stable, as shown in Figure 6.20. The air outlet temperature was slowly but gradually decreasing, even though it was considered as quasi-steady state for the purpose of the experiment. When oil was metered to the evaporator, a gradual decrease of the air outlet temperature was observed, as shown between 550 and 1000 seconds in Figure 6.20. This decrease of the outlet air temperature was interpreted as increase of heat capacity of the evaporator and thus, HTF resulted higher than 1. Similar trends of the air outlet temperature were observed for OMF 1 wt. % in series M, and for OMFs 0.5 (and 1 wt. %) in series N. Thus, their HTFs in Figure 6.17 resulted slightly higher than 1. However, it was not clear if the decreases of air outlet temperature was due to the presence of oil in the evaporator or due to some non-steady state instability phenomena or disturbances in their air stream during these three tests. For this reason we concluded that the apparent increase of HTFs at OMFs below 1 wt.% in Figure 6.17 were basically within the experimental uncertainty of the HTF for the low temperature tests.

6.3 Pressure drop factor of microchannel evaporators

This section discusses the results of the effect of oil on the refrigerant side pressure drop for microchannel evaporator A and evaporator B with refrigerant R410A and POE oil mixture and with refrigerant R134a and POE oil mixture. The tests were conducted for two mass fluxes and at several saturation temperatures. The test conditions and the legend for the symbols used to report the experimental results from these tests are given in Table 6.1, Table 6.2 and Table 6.3. The effect of oil on the pressure drop is provided in terms of pressure drop factor (PDF), which was the ratio of pressure drop measured across the refrigerant side of the

microchannel evaporator when oil was present over the pressure drop in oil-free conditions (see again definition of PDF in Equation (5-35)). Both pressure drops were measured at the same total mass flux, saturation pressure, and degree of superheated vapor at the outlet. Thus, the PDF isolated and quantified the effect of oil on the refrigerant-side pressure drop. The results were summarized in plots in which OMF was on the x-axis and the PDF was on the y-axis. Low mass flux was represented by solid symbols (series G, H, and I) while the high mass flux was represented by the void symbols (series J, K and L series). Each saturation temperature was evaluated at both high and low mass flux. In addition, to isolate the effect of superheat on heat transfer factors (HTFs) due to presence of oil, the mass flux and saturation temperatures were maintained constant in series S, T and U.

It should be emphasized in here that the refrigerant was well distributed across the microchannel tubes of the evaporators. The PDFs presented in this work did not account for the effect that oil might have on the refrigerant flow distribution across the microchannel tubes and they did not account for the flow change, if any occurred, inside the inlet headers of the microchannel heat exchangers. These effects, which are still due to the presence of oil in the mixture, might results in additional sources of pressure drop augmentation in microchannel evaporators and their investigation could be part of future studies of this work.

6.3.1 PDF of Microchannel evaporator A with R410A and POE oil

From section 6.3.1.1 to 6.3.1.2 the experimental results of pressure drop factor (PDF) in evaporator A and evaporator B with refrigerant R410A and POE oil for constant degree of superheat at evaporator outlet are discussed. The information of test conditions and the legend for the symbols used for the test series of R410A and POE oil for constant degree of superheat at evaporator outlet are given in Table 6.1. From section 6.3.1.3 to 6.3.1.4 the experimental results of pressure drop factor (PDF) in evaporator A and evaporator B with refrigerant R410A and POE oil for several degree of superheat at evaporator outlet are discussed. The information of test conditions and the legend for the symbols used for the test series of R410A and POE oil for several degree of superheat at evaporator outlet are given in Table 6.2.

6.3.1.1 PDF of Microchannel evaporator A with R410A and POE oil constant exit superheat

The experimental results of pressure drop factor (PDF) in evaporator A with refrigerant R410A and POE oil are summarized in Figure 6.21. This figure shows the PDF of the microchannel evaporator A on the y-axis and the oil mass fraction (OMF) of POE oil in refrigerant R410A on the x-axis. When OMF is 0 (i.e., no oil is present inside the evaporator), the PDF resulted 1 by its own definition and it increased if OMF increased as shown in Figure 6.21. The effect of mass flux is represented as void and solid symbols and corresponding letters in the legend of the figures. Low mass flux series were represented by the solid symbols (G, H, and I) while high mass flux tests were represented as void symbols (J, K and L series) (for details about the legend, see Table 6.1). Each saturation temperature was given with a void and a solid symbol with same color and shape of the symbol. For example, the black circle data points in Figure 6.21 represent saturation temperature of 33° F (~0.5° C); the solid circle points (series G) are for low mass flux while the void circle points (series J) are for high mass flux. The results indicate that if the oil mass fraction (OMF) increased, the pressure drop factor of microchannel evaporator A increased from 1 to 1.47. This represents an augmentation of the refrigerant-side pressure drop due to oil by about 47%. From Figure 6.21 it is clear that the effect of oil on pressure drop was to increase the refrigerant-side pressure drop. The impact of oil was still significant even when OMF ranged from 0.5 wt. % and 1 wt. %. The PDFs given in Figure 6.21 represent only the effect of oil because each test with oil was compared with the corresponding reference without oil at the same inlet saturation pressure, total mass flow rate, and degree of superheated vapor at the outlet of the evaporator. The air inlet temperature and velocity were also constant between the tests with oil and the baseline reference tests with no oil. The increase in pressure drop can be attributed to the increase in viscosity of liquid mixture of refrigerant and lubricant in the microchannels. Hu et al., 2009 reported that the presence of lubricant enhances two phase pressure drop, where penalty factor ranges from 1.0-1.9 for 3.0 mm O.D. tube. As the amount of oil in refrigerant increased the penalty factor also increased.

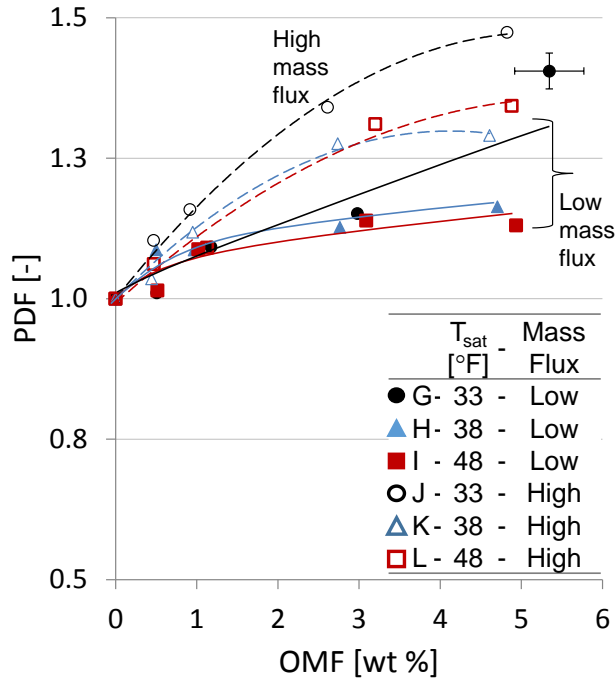


Figure 6.21: Pressure drop factor in microchannel evaporator A with R410A and POE oil

The worst case of increase in PDF of the microchannel evaporator A in Figure 6.21 was measured at OMF of 5 wt. % and at high mass flux (series J) where PDF was augmented by 47 % when compared to no oil conditions. For air-conditioning applications, when OMF is typically less than 1 wt. %, the increase in pressure drop was less than 20%. The PDFs were slightly above 1 for OMF less than 0.5 wt. % and for both high and low mass flux. At OMF of 3 wt.%, increase of mass flux from low mass flux of 4.2 lb_m/ft²-s (20.4 kg/m²-s, series H) to high mass flux of 8.4 lb_m/ft²-s (20.4 kg/m²-s, series K) increased the PDF from 1.15 (series H in Figure 6.21) to 1.32 (series K) for the same saturation temperature of 38°F (3.3°C). Hu et al., 2008b measured and correlated two phase frictional pressure of R410A/POE mixture flow boiling inside 7 mm diameter tube. Their experimental parameters include the evaporation temperature of 5 °C for two mass flux, the heat flux from 7.56 to 15.12 kW/m², the inlet vapor quality from 0.2 to 0.7, and nominal oil concentration from 0 % to 5 %. Their results indicated that the frictional pressure drop of R410A/ POE oil mixture increases as mass flux increases for similar vapor quality. And frictional pressure drop was high in regions of high vapor quality due to high viscosity oil rich liquid mixture. Their findings are in agreement

with the experimental results of Figure 6.21, in which the PDFs for high mass flux series (letters J, K, and L) tended to be significantly higher than the PDFs for the low mass flux series (letters G, H and I) and OMF above 1 wt.%.

For similar OMF and mass flux, the impact of saturation temperature on pressure drop was less significant for OMF less than 1 wt. % and the results for these conditions were within uncertainty range of experimental instruments. For same mass flux and OMF higher than 3 wt. %, pressure drop was highest for saturation temperature of 33 °F (0.5 °C) for each OMF, represented by the series G and J. As saturation temperature increased from 33 to 38 °F (0.5 to 3.3 °C), the pressure drop factor decreased. Although change in liquid mixture viscosity at particular quality and saturation temperature from 33 to 38 °F (0.5 to 3.3 °C) was negligible, there was significant decrease in liquid mixture density by 2.56 % for R410A+POE oil mixture at 5 wt. % POE oil. Furthermore, there was considerable decrease in surface tension of R410A+POE oil at the same concentration by approximately 22 % as temperature decreased from 33 to 38° F (0.5 to 3.3° C) (Wei et al., 2007). The decrease in surface tension could lead to decrease in wall shear stress which can lead to lesser pressure drop factor during evaporation in the microchannels. These two effects coupled together could explain the high pressure drop factor at saturation temperature 33 °F (0.5 °C) with respect to the pressure drop factor measured at 38°F (3.3°C) in the present work. As saturation temperature increased from 38 to 48 °F (3.3 to 9 °C) there was no measurable effect on pressure drop, for similar mass flux and OMF. The reason behind this was due to decrease in density approximately by 1 %, surface tension decreased by approximately 5 % as saturation temperature increased from 38 to 48 °F (3.3 to 9 °C)(Wei et al., 2007).

6.3.1.2 PDF of Microchannel evaporator B with R410A and POE oil at constant exit superheat

The results for effect of oil on PDF for the microchannel evaporator B with refrigerant R410A and POE oil for conditions that are applicable to air conditioning systems are given in Figure 6.22. The PDFs in Figure 6.22 represent only the effect of oil because each test with oil was compared with the reference without oil at the same inlet saturation pressure and total mass flow rate. The air inlet temperature and velocity were also

constant between each tests with oil and the corresponding baseline references with no oil. The results indicated that PDFs of microchannel evaporator B increased by 77% if the OMF increased from 0 to 5 wt.% and for high mass flux and saturation temperature of 38° F (3.3° C) (series K). The results shows that PDF was dependent of OMF. PDF increased as OMF increased. Hu et al. (2009) reported that the presence of lubricant enhances two phase pressure drop, where penalty factor ranges from 1.0-1.9 for 3.0 mm O.D. tube. As amount of oil in refrigerant increased the penalty factor also increased. Similarly, Hu et al (2007) suggested that two phase frictional pressure drop was more evident in higher vapor qualities in flow boiling inside 7 mm diameter tube. Furthermore, preliminary calculations showed that at vapor quality of 0.8, for OMF ranged between 0.5 wt. percent to 5 wt. % the local oil concentration in the liquid mixture ranged between 2.5% to 20%. For this range of local oil concentration, the local viscosity of liquid mixture ranged roughly from 0.2 cSt to 2 cSt. This explained higher pressure drop at higher OMF.

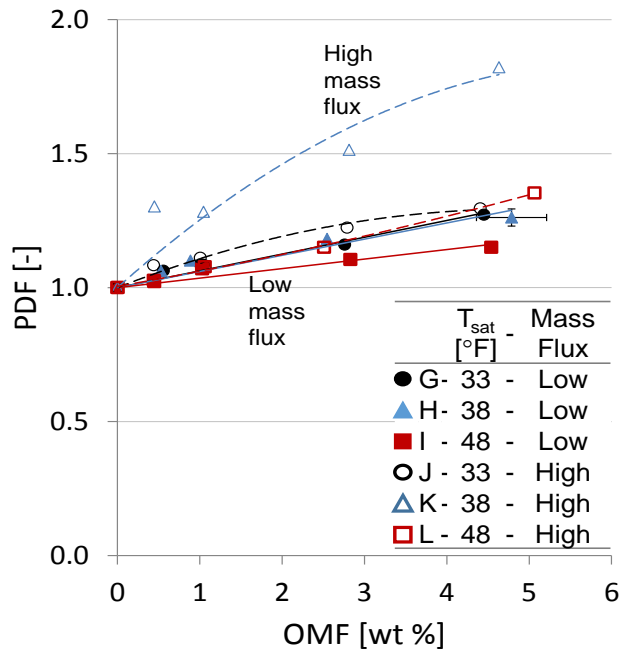


Figure 6.22: Pressure drop factor in microchannel evaporator B with R410A and POE oil

In air conditioning applications, in which the OMF is typically at or below 1 wt. %, the increase in pressure drop was from 1 to 27 % when compared to the case of oil free conditions in the evaporator B. The trends in

Figure 6.22 suggested that the increase of oil from 0 to 5 wt.% in the refrigerant R410A flow increased the pressure drop of refrigerant in the evaporator almost linearly. While the mass flux had an measurable effect on the PDFs results for evaporator A, the same effects of mass flux on the PDFs for evaporator B were not significant; not even when OMFs were higher than 3 wt. % (except for series H and K). A possible reason might be that the effect of oil on the refrigerant side pressure drop was depended on the geometry of the microchannel tubes and header configurations. Interestingly the effect of mass flux was observed in the series H and K, whose saturation temperature was 38°F (3.3°C). For this saturation temperature an increase in mass flux from 4.7 lb_m/ft²-s (23 kg/m²-s) to 8.4 lb_m/ft²-s (41.2 kg/m²-s) in the microchannel evaporator, augmented the PDF from 1.2 to 1.5 if OMF was 3 wt.%.

6.3.1.3 PDF of Microchannel evaporator A with R410A and POE oil with several degree of superheat

The experimental results of pressure drop factor (PDF) in evaporator A with refrigerant R410A and POE oil are summarized in Figure 6.23. This figure shows the PDF of the microchannel evaporator A on the y-axis and the oil mass fraction (OMF) of POE oil in refrigerant R410A on the x-axis. When OMF is 0 (i.e., no oil is present inside the evaporator), the PDF resulted 1 by its own definition and it increased if OMF increased as shown in Figure 6.23. The effect of superheat is represented as corresponding letters in the legend of the figures (for details about the legend, see Table 6.2). To isolate the effect of superheat on PDF the saturation temperature 39° F (3.9° C) and mass flux at 7.5 lbm/ft²-s (36.7 kg/m²-s) for all three series (S, T and U) were maintained constant. The results indicate that for constant superheat if the oil mass fraction (OMF) increased, the pressure drop factor of microchannel evaporator A increased from 1 to 1.53. This represents an augmentation of the refrigerant-side pressure drop due to oil by about 53%. For constant superheat, the effect of OMF on PDF is consistent with PDF in Figure 6.21. For air-conditioning applications, when OMF is typically less than 1 wt. %, the increase in pressure drop was less than 25%. From Figure 6.23 it is clear that the effect of superheat at evaporator A outlet on PDF was not significant at given OMF, and PDFs for all three superheat at same OMF were within the range of instrumentation uncertainty.

Interestingly I did not measured any effect of exit superheat on pressure drop in presence of oil. A possible reason might be that pressure drop increment in the superheat section of microchannels and the outlet header is negligible when compared to increment in pressure drop that occurs in the two phase region of microchannels. However, since the tests were conducted on a full size microchannel evaporators, this hypothesis was not verified in the present work. Pressure drop experiments of refrigerant and oil mixtures at different superheat of refrigerant vapor in a dedicated microchannel tubes are potential future work on this topic.

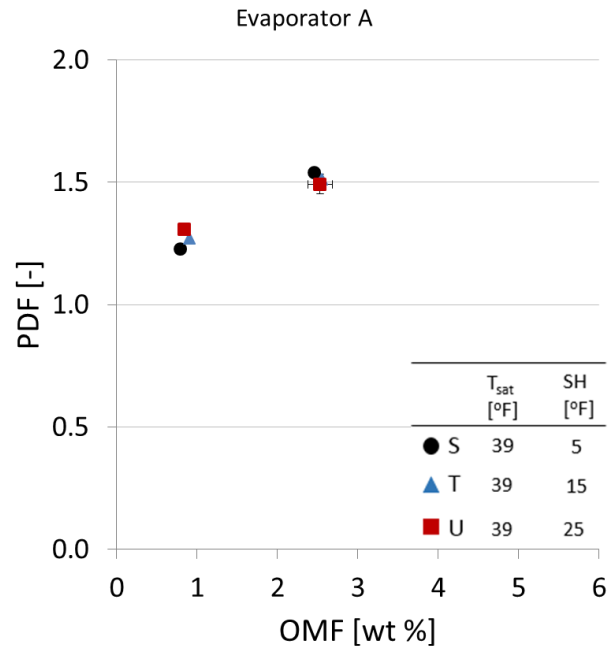


Figure 6.23: Pressure drop factor in microchannel evaporator A with R410A and POE oil

6.3.1.4 PDF of Microchannel evaporator B with R410A and POE oil with several degree of superheat

The results for effect of oil on PDF for the microchannel evaporator B with refrigerant R410A and POE oil for three different superheat are given in Figure 6.24. The PDFs in Figure 6.24 at constant superheat, represent only the effect of oil because each test with oil was compared with the reference without oil at the same inlet saturation pressure and total mass flow rate. The air inlet temperature and velocity were also constant between

each tests with oil and the corresponding baseline references with no oil. To isolate the effect of exit superheat on PDF, the mass flux of refrigerant was maintained constant at 8.4 lb_m/ft²-s (41.0 kg/m²-s), and saturation temperature at 39° F (3.9° C) for all three series (series S, T and U in Figure 6.24). The results indicate that for constant superheat if the oil mass fraction (OMF) increased, the pressure drop factor of microchannel evaporator B increased from 1 to 1.25. The trends observed in Figure 6.24 are similar to trends observed in Figure 6.23. From a quick glance on those three series, it is evident that if the superheat at the microchannel evaporator outlet increased from 5° F to 25° F (2.8° C to 8.3° C) then the PDF at given OMF does not change significantly. For example, as superheat increased from 5° F to 25° F (2.8° C to 8.3° C) for OMF 0.9% the increase in PDF was negligible and it was within the range of experimental uncertainty.

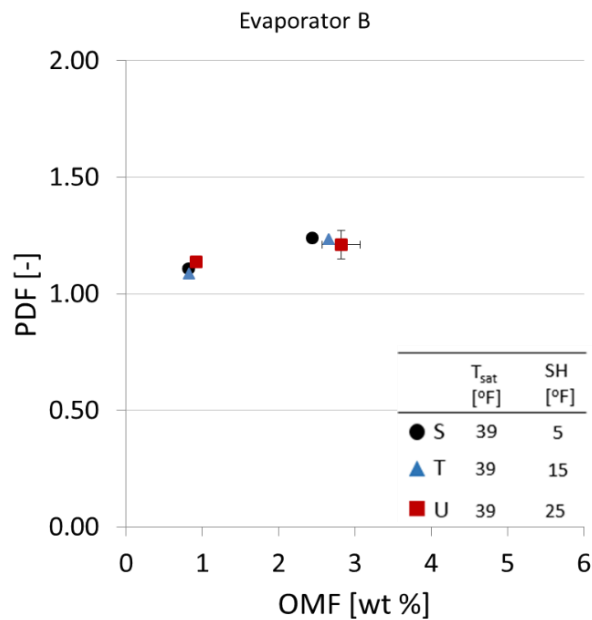


Figure 6.24: Pressure drop factor in microchannel evaporator A with R410A and POE oil

6.3.2 PDF of Microchannel evaporator A with R134a and POE oil mixture

This section discusses the experimental results of effect of oil on pressure drop factor in microchannel evaporator A with refrigerant R134a and POE oil mixture. For this part of research, experiments were carried out for saturation temperature of R134a below and above freezing temperature, i.e. 32 °F (0 °C). For the

saturation temperatures below 32 °F (0 °C) is referred as low temperature series and for above 32° F (0° C) is referred as medium temperature series. For the low temperature series experiments, the mass flow rate was 150 lb_m/hr, and the saturation temperature varied from 0 to 10°F (-17.7° C to -12.2° C). For medium temperature series experiments, the mass flow rate was 200 lb_m/hr, and the saturation temperature varied from 33° F to 48° F (0.5° C to 9° C). The mass fluxes, test conditions, and the legend for the symbols in Figure 6.25 are provided in Table 6.3.

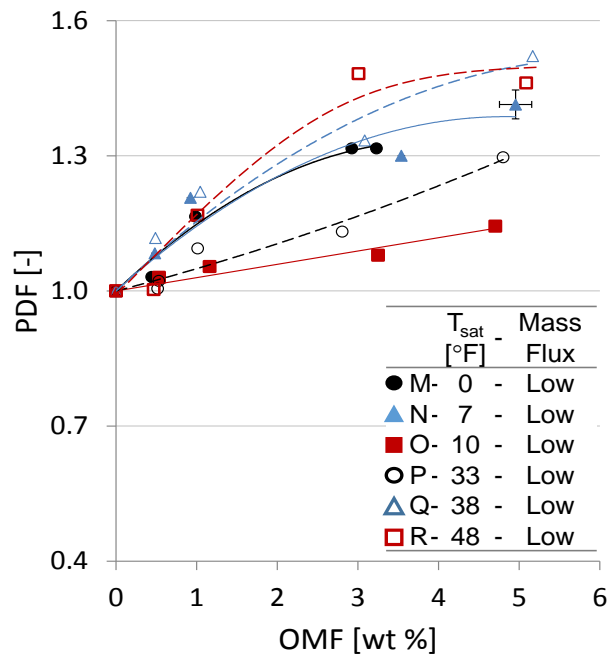


Figure 6.25: Pressure drop factor in microchannel evaporator A with R134a and POE oil

The PDFs in Figure 6.25 represent only the effect of oil because each test with oil was compared with the reference without oil at the same inlet saturation pressure, total mass flow rate, and degree of vapor superheated at the outlet of the evaporator. The air inlet temperature and velocity were also constant between the cases of tests with oil and the baseline references with no oil. The results indicates that the presence of POE oil increased the refrigerant-side pressure drop in microchannel evaporator A when refrigerant R134a was used. For OMF ranging from 0 wt.% to 5 wt.%, the PDF of microchannel evaporator A increased up to

57%. For refrigeration applications in which the OMF is typically less than 1 wt. % the PDF was about 1.2, which indicates a maximum increase of pressure drop of 20% when compared to oil free conditions.

The series M, N and O were conducted for mass flow rate of 150 lb_m/hr and P, Q and R series were conducted at mass flow rate 200 lb_m/hr. For these low temperature series (M, N and O) the decrease in saturation temperature increased pressure drop for each OMF. This was attributed to an increase in the viscosity of oil rich and refrigerant mixture when temperature decreased. In other words, as the saturation temperature decreased from 10° to 0° F (-12 to -18°C), the pressure drop augmented by at least 15% for each OMF (higher than 1wt%). For high temperature series (series P, Q and R), the pressure drop increased by 35% only when the saturation temperature increased from 33° to 38° F (0.5 to 3.3°C, series P and Q) while there was no significant increase in pressure drop when the saturation temperature increased from 38° F to 48° F (3.3 to 9°C, series Q and R).

6.4 Thermodynamic and heat transfer analysis of the experimental results of HTF for the microchannel evaporator A

As mentioned in section 6.2.2.3 for R134a and POE mixture, the results for heat transfer capacity when oil was present varied among the oil mass fractions and saturation temperatures investigated in the present work. With reference to Figure 6.17, some of the HTFs were higher than 1 when oil was present at OMFs less than 1 wt.%, which meant that small amount of oil retained in the microchannel evaporator A augmented its heat transfer capacity. This was an intriguing and counterintuitive finding and this section discusses further analysis of the effects of oil retention on the saturation temperature, flow regime, and free flow area of the microchannel evaporator A.

It was reported that presence of oil in refrigerant changes the saturation temperature of working fluid (Takaishi & Oguchi, 1987; Wei et al., 2008). The saturation temperature of the refrigerant R134a and POE mixture was calculated by using the correlation developed by Thome, 1995 and it is reported in the last column of Table 6.4, for an example. By comparing the values in the last column of Table 6.4 with the

corresponding values of the thermodynamic saturation temperature of refrigerant R134a at each pressure (given in the adjacent column of Table 6.4), it was concluded that for OMFs 0.5 and 1 wt. % there was not a significant change in the saturation temperature of evaporation for R134a due to presence of oil that could justified an increase of heat transfer capacity. In other terms, any change of saturation temperature of evaporation of the refrigerant and oil mixture when small amount of oil was retained in the microchannel evaporator A was not a factor that could have supported an increase of the HTF in the observed data of Figure 6.17.

Table 6.4 Variation of the saturation temperature of the refrigerant R134a and POE oil mixture during evaporation with OMF of 0.5 and 1 wt.%

OMF (wt.%)	Vapor Quality of R134a	Local oil concentration, ω_{local} (wt.%)	Saturation Pressure (kPa)	Saturation temperature of R134a (K)	Saturation Temperature from Thome (K)
0.5	0.1	0.55	145.6	255.3	255.4
0.5	0.2	0.62	145.6	255.3	255.4
0.5	0.3	0.71	145.6	255.3	255.4
0.5	0.4	0.83	145.6	255.3	255.4
0.5	0.5	0.99	145.6	255.3	255.4
0.5	0.6	1.24	145.6	255.3	255.4
0.5	0.9	4.78	145.6	255.3	255.4
0.5	0.99	33.44	145.6	255.3	255.7
1	0.1	1.11	145.6	255.3	255.4
1	0.2	1.24	145.6	255.3	255.4
1	0.3	1.42	145.6	255.3	255.4
1	0.4	1.65	145.6	255.3	255.4
1	0.5	1.98	145.6	255.3	255.4
1	0.6	2.46	145.6	255.3	255.4
1	0.9	9.17	145.6	255.3	255.4
1	0.99	50.25	145.6	255.3	256.5

The flow regime of refrigerant and oil mixture at the microchannel evaporator outlet was determined using superficial velocity of liquid component and superficial velocity of vapor component. For OMF ranging from 0.5 to 5% it was found that the flow was annular at microchannel evaporator outlet for both no-oil and oil cases. Mandhane, 1974 flow map was used for determining the flow regime of the refrigerant R134a and POE oil mixture in the test conditions of the microchannel evaporator A of the present work.

Figure 6.26 shows the convective heat transfer coefficient of refrigerant R134a and of refrigerant R134a and POE oil mixture in the microchannels at OMFs ranging from 0.5 to 5 wt. %. These calculations showed that the convective heat transfer coefficient of R134a and POE oil mixture decreased for quality of 0.7 and below. At quality above 0.7 the convective heat transfer coefficient of the mixture increased when oil was present in the mixture. At first, one might be tempted to conclude that the increase of the refrigerant-side heat transfer coefficient showed in Figure 6.26 explains why the HTFs were observed to be slightly higher than 1 in some of the data of Figure 6.17. However, after a deeper analysis, the contribution of the refrigerant-side convective heat transfer resistance on overall (total) thermal resistance of the microchannel evaporators was estimated. The total thermal resistance included the resistances due to the refrigerant in-tube two phase flow boiling, microchannel tube conduction, and the convective resistance of the air side on the fin, which was the dominant resistance. Although there was an overall change in the refrigerant side in-tube two phase flow boiling resistance (as shown in Figure 6.26), the total thermal resistance of the microchannel evaporator A decreased by less than 0.1% when oil was retained inside the evaporator at OMF of 1 wt.%. Therefore there must be some other mechanism that increased the HTF when oil was present in small quantities. Such mechanism was not captured by the heat transfer coefficient correlations used for two phase flow of refrigerant and oil mixtures in microchannel tubes and further investigation on the local heat transfer behavior of refrigerant and oil mixture flow boiling in microchannel tubes might be part of future work. Further thermodynamic and heat transfer analysis was conducted by using the model developed in the present work. While the model will be presented in chapter 7, the simulations were used to provide some insights in the HTF data of the microchannel evaporator and the main observations are highlighted in next section.

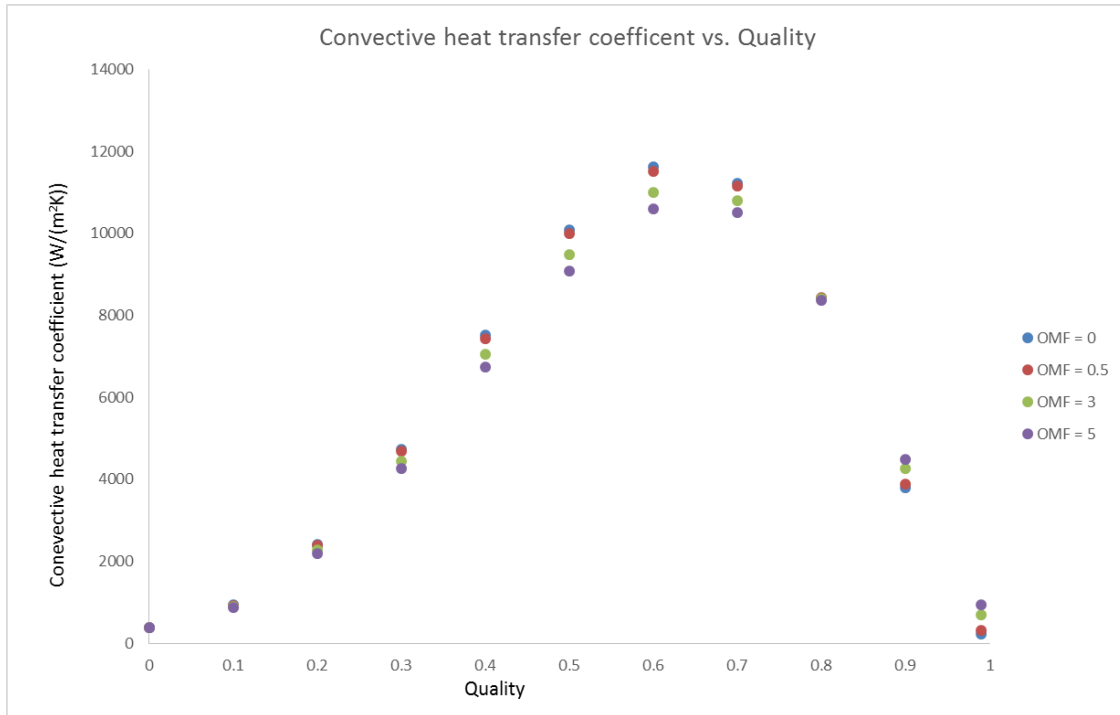


Figure 6.26: Local heat transfer coefficient (from modeling results) of refrigerant R134a and of refrigerant R134a and POE oil mixture in the microchannels at OMFs ranging from 0.5 to 5 wt. %

6.5 Thermodynamic and heat transfer analysis of the evaporator A by using the present simulation tool in order to test several hypotheses of why of the possible increase of HTFs

The HTF data for the evaporator A indicated that for same saturation temperatures the presence of oil at OMFs less than 1 wt.% increased the evaporator heat transfer capacity with respect to the no oil retention conditions. A thermodynamic and heat transfer analysis of the evaporator A was conducted by using the simulation program developed in the separate work in order to tests some possible hypotheses that might explain the observed increase in heat transfer capacity. Table 6.5 provides a comparison between simulation results and the experimental data in order to provide some insights on the HTF for the microchannel evaporator A. In Table 6.5, the simulations were conducted for the Evaporator A and the mass flow rate was constant at 200 lb_m/hr (0.025 kg/s) and the saturation temperature of evaporation was constant at 48°F (9°C) for all the cases. The simulations had the same inlet conditions as that of the corresponding experiments. The case no 1 in Table 6.5, provides the baseline reference case for heat transfer capacity and pressure drop of the

evaporator when no oil was present, i.e, in oil free conditions. Case no 2 and 3 served to validate the model and assess the simulation results sensitivity and the uncertainty in the experimental data.

Table 6.5 Comparison of the simulation results and experimental data to provide some insights on the HTF and PDF for the microchannel evaporator A.

No	Simulation Description*	OMF [wt.%]	Experimental Data		Simulation Results	
			HTF _{Exp}	PDF _{Exp}	HTF _{sim}	PDF _{sim}
1	Baseline case no oil	0	1	1	1	1
2	Validation at low oil level	0.5	1.005	1.015	0.995	1.001
3	Validation at medium oil level	1	0.996	1.088	0.993	1.002
4	HTC ref/oil mixture is 50% higher than that provided by the correlations (i.e. assume correlations under predicted the HTC)	1	--	---	1.045	1.000
5	oil is assumed to cause 25% flow blockage in the microchannel tubes	1	---	--	0.998	1.052
6	No. 5 and No. 6 combined	1	---	---	1.050	1.051

*The mass flow rate was constant at 200 lbm/hr (0.025 kg/s) and the saturation temperature of evaporation was constant at 48°F (9°C)

Three hypotheses were tested to explain a possible increase of the heat transfer capacity of the microchannel evaporator when oil was present in low and medium concentration of 0.5 to 1 wt.% and they are summarized as follows:

Case 4: the first hypothesis was that the two phase flow boiling refrigerant mixture heat transfer coefficient (HTC) was about 50% higher than the value provided by the correlations in the literature. While the presence of oil in small quantities increased the in-tube flow boiling heat transfer coefficient by 50%, the mechanisms that caused such intensification were not captured by the existing correlations in the literature and thus, we assume that the correlations might have under predicted the in-tube convective heat transfer coefficient.

Case 5: the second hypothesis tested was that the oil might have caused a flow restriction for the mixture circulating inside the microchannel tubes and the flow blockage was up to 25% of the free flow area. The blockage in microchannel tubes due to the presence of oil increased the mass flux and the simulations were conducted with assumption that the flow in microchannel tubes were partially blocked due to presence of oil film layer wetting and stretching the internal walls.

Case 6: the third hypothesis was a combination of the two cases 4 and 5 above and it is reported in the last row of Table 6.5 with the simulation no. 6.

The simulation results showed that the model for microchannel evaporator A was able to predict the HTF quite well. However, while the model predicted a gradual decrease of HTF if OMF increased from 0 to 3 wt.%, the experimental data sometimes showed a maximum HTF of over 1.1 when the OMF was about 0.5 to 1 wt.%. This meant that oil increased the heat transfer capacity by as much as 10% with respect to the oil free conditions. To investigate this phenomena we considered simulations no. 4, 5, and 6 in Table 6.5. Even if the correlations from the literature under predicted the in-tube microchannel tube heat transfer coefficient by 50% and the flow restriction created by the oil was 25% of the free flow area, the HTF increased to 1.04 and up to 1.05. Thus, an accuracy of the correlations might be able to explain a 5% increase of the heat transfer capacity but not over this value. In addition, an increase of 5% in the heat transfer capacity of the microchannel evaporator A was accompanied by an increase of the pressure drop of 5%.

All cases were simulated for refrigerant R410A and POE oil mixture in the microchannel evaporator A and for the conditions represented in Table 6.5; the simulation results are plotted in Figure 6.27. The x-axis represents the segment number along the length of microchannel heat exchanger. The first segment (0th segment in the plot) was the entrance of microchannel tube and the last segment (100th segment in the plot) was where refrigerant exited the microchannel tube and flowed into the outlet header at the top of the evaporator. The y-axis represents the in-tube two phase flow boiling heat transfer coefficient of the refrigerant and of the refrigerant and oil mixture inside the microchannel tubes. The notations and symbols used in Figure 6.27 is provided in the first column of Table 6.5. The heat transfer coefficient of the refrigerant and oil mixture for OMF 0.5% and 1% (legends sim-2 and sim-3 in Figure 6.27) was lower than heat transfer coefficient for refrigerant (series sim-1 in in Figure 6.27) at any segment of the microchannel tube. The decrease of the two phase flow heat transfer coefficient due to oil is particularly evident in the segments from 45 to 85, shown in the zoom out at the bottom of Figure 6.27.

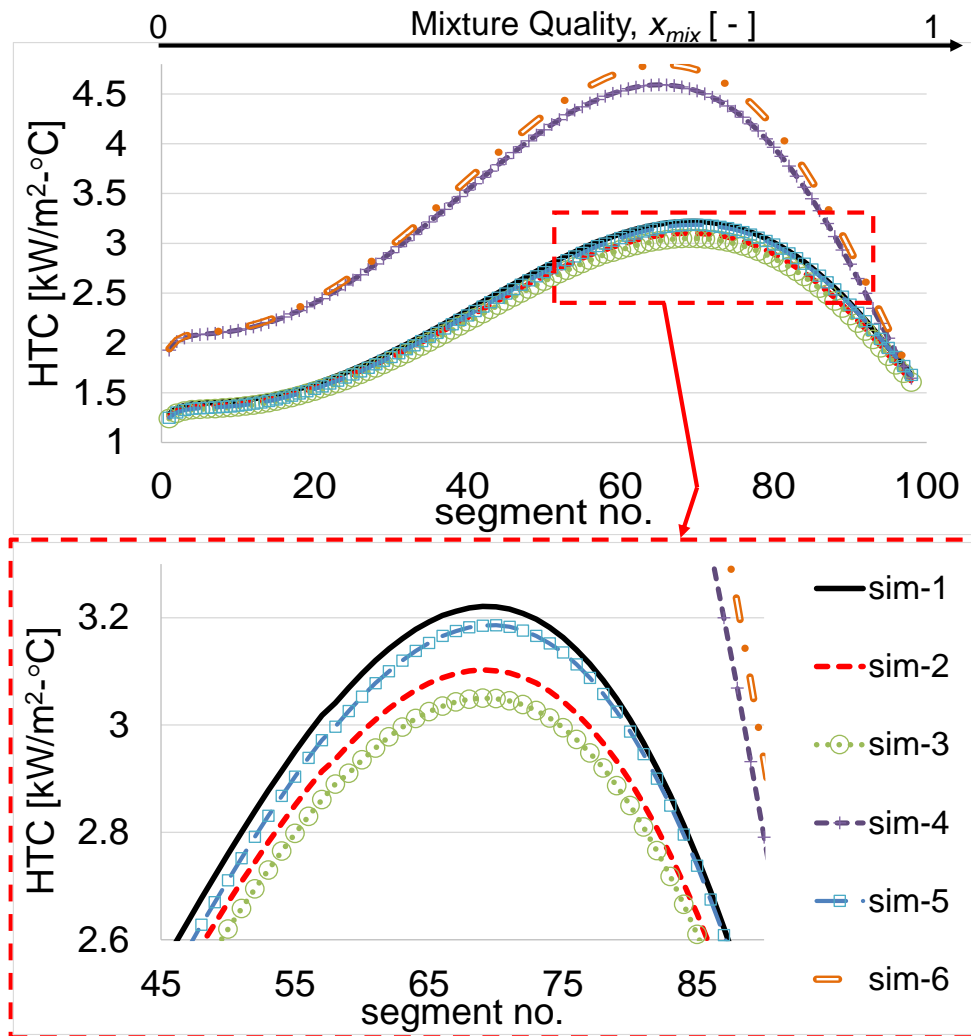


Figure 6.27: Effect of oil on local heat transfer coefficient (htc) for (sim-1) OMF=0, (sim-2) OMF = 0.5, (sim-3) OMF =1, (sim-4) OMF = 1 and (h=value from htc correlation*1.5), (sim-4) OMF = 1 and 25% flow blockage, and (sim-6) OMF = 1 and 25% flow blockage and (h=value from correlation*1.5).

If OMF increased from 0 (i.e. no oil) to 0.5 wt.%, the decrease of HTC was from 3.2 to 3.1, which represents about 3.1% decrease of the HTC. If OMF increased further from 0.5 to 1 wt%, the HTC decreased from 3.1 to 3.05, which represents 1.6% decrease of the maximum HTC observed between segment 65 and 75.

The simulation results of flow blockage by 25% of the free flow area and for OMF 1 wt. % (sim-5 in Figure 6.27) showed that the heat transfer coefficient increased slightly when compared to the no blockage scenario with the same OMF 1 wt. %. In other words, the results for sim-5 in Figure 6.27 showed slightly higher heat transfer coefficient than sim-3 but they are still below the case of no oil (see sim-1 and sim-5 in Figure 6.27).

The heat transfer coefficients for cases 4 and 6, were also plotted in Figure 6.27 and they are represented by the sim-4 and sim-6. Since we artificially increased the predicted heat transfer coefficient values from the existing correlations from the literature by 50%, the results showed that the HTC for sim-4 and sim-6 are significantly higher than all the other ones. Again, the difference between sim-4 and sim-6 is not much, supporting the hypothesis that flow blockage alone was not responsible for the heat transfer capacity enhancements observed in some of the experimental results.

Given the variations of the in-tube convective heat transfer coefficient shown in Figure 6.27 for the cases of Table 6.5, the overall HTF for the entire evaporator A were calculated by the simulation model and the results of the predicted HTF are summarized in Figure 6.28. The main insights from the simulation results were as follows:

- i. The predicted HTF of the entire microchannel evaporator calculated for the case of 25% flow blockage when oil was retained in the microchannel evaporator A was slightly higher when compared to no oil conditions but it did not support an increase of HTF over 3%.
- ii. The predicted HTF calculated for the case 4 of Table 6.5, suggested that the HTF of the coil could increase by up to 9.7 % when compared to no oil conditions. Although this simulation was carried out on refrigerant R410A, it is likely that the heat transfer coefficient of R134a and POE mixture might have increased as well in the case of low temperature series if a similar assumption to that of case 4 of Table 6.5 is made. This result support a small increase in the HTF of the evaporator A for low temperature series (series M and N in Figure 6.17).
- iii. The predicted HTF calculated for case 6 indicated that the heat transfer factor further increased and the heat transfer capacity of the microchannel evaporator A was up to 10.4% higher when small amount of oil was retained in the evaporator A with respect to oil conditions. In other words, in order to support a 10.4% increase of the microchannel evaporator A heat transfer capacity when small amount of oil was retained in the evaporator, two phenomena must occur simultaneously: the oil has to induce a 25% flow restriction (i.e. 25% flow blockage of the overall free flow area of the microchannel tubes) and the refrigerant-side

heat transfer coefficient has to be at least 50% higher than what is currently predicted by the existing correlations in the literature. Both phenomena were considered highly unlikely to occur but they were theoretically possible. They supported the intriguing data of HTFs of the present work and the fact that for some saturation temperatures and flow conditions in the microchannel tubes, the HTFs increased to 1.05 and 1.1 (that is it was slightly higher than 1 by about 5 to 10%) when the OMFs were 1 wt.%.

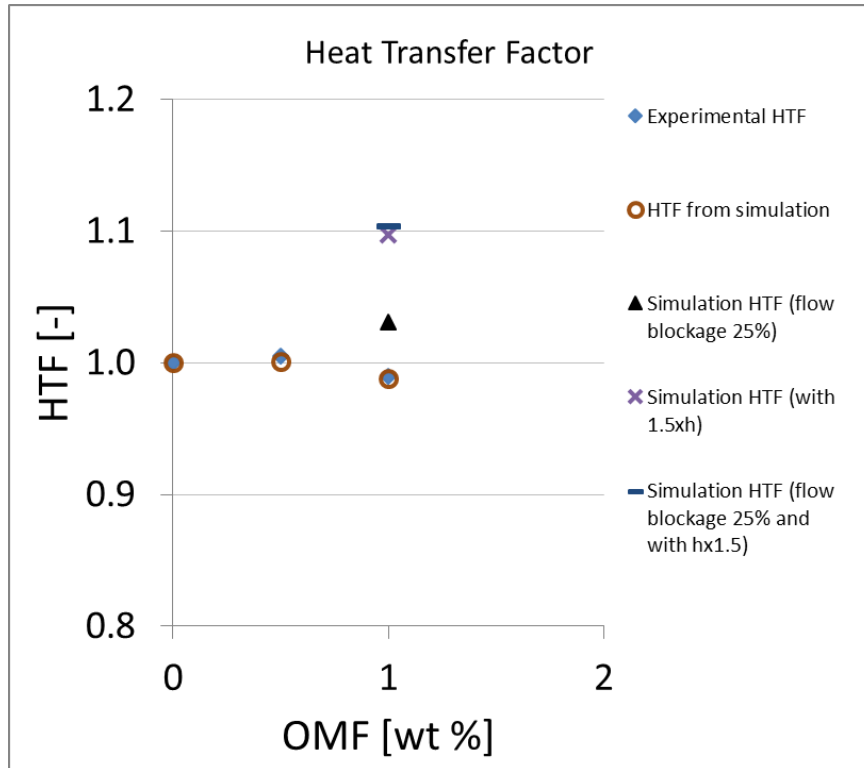


Figure 6.28: Comparison of the HTFs of the microchannel evaporator A between the model simulation results and the experimental data in order to tests 3 hypothesis for possible increase of heat transfer capacity when small amount of oil was retained in the evaporator

CHAPTER VII

7. OIL RETENTION MODEL VALIDATION

In a separate study carried by Andrea Bigi, Stefano Dell'Orto and Dr. Lorenzo Cremaschi developed a model to predict the performance of microchannel type of evaporators when oil was present in the refrigerant flow and the model was experimentally validated. The present model calculated the oil retention, the overall heat capacity, and pressure drop for microchannel evaporator A. This section discusses briefly the summary of the model, and its validation with the data of the present work.

7.1 Summary of the Model for Microchannel Evaporators

A model of a microchannel evaporator was developed and compared with experimental data. The model was based on the segmentation approach. Local properties were calculated for each control volume. The capacity of each volume was calculated using the ϵ -NTU method, and the pressure drop was calculated with semi-empirical correlations. The model was able to predict the capacity of the coil within $\pm 4\%$ and pressure drop was predicted with an error of 20 to 50%. The developed physics based model predicted well the effects of the presence of oil in the heat exchanger on the heat transfer capacity and pressure drops of the microchannel evaporators. The oil decreased the heat transfer capacity of the coil and increased the pressure drop. The results from the simulation agreed with the experimental data and the simulations showed similar trend as the behavior of the data. The amount of oil retained in the system was generally under predicted because the oil retention in the headers was estimated based on several simplifying assumption. Thus, an improved model of the headers might be part of future work of this research topic.

7.2 Experimental Validation of the Microchannel Evaporator Model

7.2.1 Validation of the Model for Microchannel Evaporator A with no Oil

The model developed in the present work was validated with the experimental data of this work. Figure 7.1 shows the comparison between experimental data and predicted results for the heat transfer capacity (Figure 7.1a) and pressure drop (Figure 7.1b) of the microchannel evaporator A with refrigerant R410A but with no oil (i.e. in oil free conditions of the baseline R410A tests).

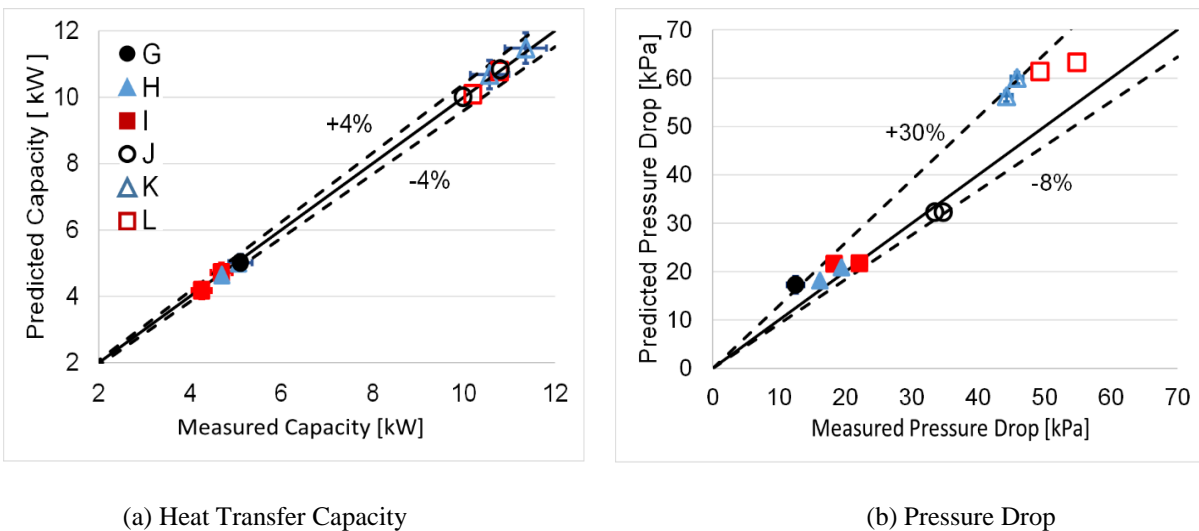
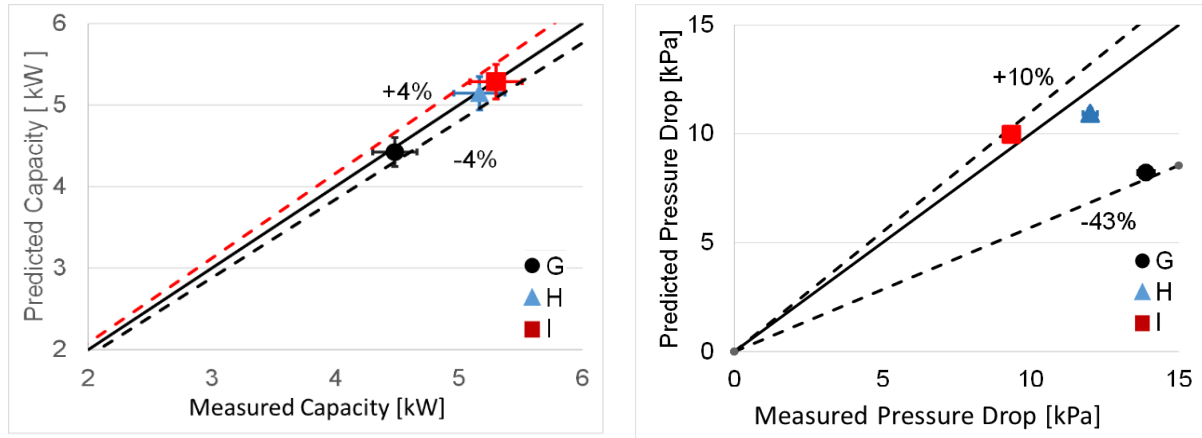


Figure 7.1: Comparison between experimental data and predicted results for the heat transfer capacity (a) and pressure drop (b) of the microchannel evaporator A with refrigerant R410A but with no oil (i.e. in oil free conditions of the baseline R410A tests)

The heat transfer capacity was predicted within $\pm 4\%$ with respect to the experimental data and the pressure drop was predicted from -8 to +30% with respect to the measured pressure drop across the evaporator A. It should be noticed that for comprehensibility and for avoiding confusion, the uncertainty error bars are provided in only for few representative data points in the plots of Figure 7.1 but similar uncertainty error bars applied to all the experimental data points in the plot (a) and (b).

Figure 7.2 summarizes the comparison between experimental data and predicted results for the heat transfer capacity (Figure 7.2a) and pressure drop (Figure 7.2b) of the microchannel evaporator A with refrigerant R134a but with no oil (i.e. in oil free conditions of baseline R134a tests). The heat transfer capacity was predicted to within $\pm 4\%$ and the pressure drop was predicted from -43 to +10% with respect to the measured

pressure drop across the evaporator A. The main error in Figure 7.2 was observed because the measured pressure drops were small, that is, less than 22 kPa. For these cases, the experimental uncertainty in the differential pressure transducer was at the highest.

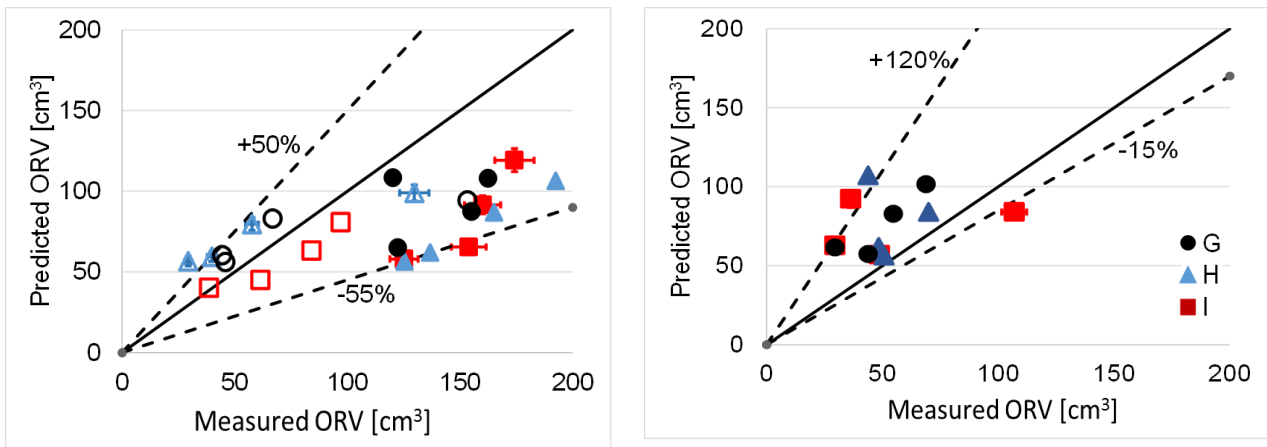


(a) Heat Transfer Capacity (b) Pressure Drop
Figure 7.2: Comparison between experimental data and predicted results for the heat transfer capacity (a) and pressure drop (b) of the microchannel evaporator A with refrigerant R134a but with no oil (i.e. oil free conditions for baseline R134a tests)

7.2.2 Validation of the Model for Microchannel Evaporator A with Oil

The model developed in the present work was also validated with the experimental data of this work when oil was retained in the microchannel evaporator A. Figure 7.3 shows the comparison between experimental data and predicted results for the oil retention volume (ORV) of the microchannel evaporator A with refrigerant R410A and POE oil mixture (Figure 7.3a) and with refrigerant R134a and POE mixture (Figure 7.3b). There is some scattering of the data in Figure 7.3a and the ORV was predicted from -55 to +50% with respect to the experimental data for R410A and POE mixture. Figure 7.3b provides the summary of the comparison between experimental data and predicted results for the oil retention volume (ORV) of the microchannel evaporator A with refrigerant R134a and POE oil mixture. Again there is some scattering of the data in Figure 7.3b and the ORV was predicted from -15 to +120% with respect to the experimental data. The main reason for the discrepancy was due to the estimation of the oil retained in the outlet header and in the final length of the microchannel tubes, in which refrigerant was superheated vapor. We observed that these sections of the evaporator A retained a significant portion of the total oil retained in the entire heat

exchanger and sometimes they were dominant with respect to the oil miscible with the liquid phase of the refrigerant and oil mixture during two phase flow evaporation. It is important to emphasize here that the sections of the evaporator A headers and microchannel tubes in which refrigerant was in thermodynamic superheated vapor state, were assumed to retain oil in the form of a layer of oil rich mixture film that stretched and wetted the internal walls and that filled the valleys in between the protrusions of the microchannel tubes inside the outlet header. While these assumptions were sound the thickness of the liquid oil rich mixture film was estimated from the velocity of the vapor refrigerant and it was assumed constant among the various saturation temperatures. It was also assumed that the thickness varied linearly from 0 to a maximum value if the OMF increased from 0 to 5 wt.%. These assumptions might be the reason of the large error in the prediction of the ORV for some of the data points. However, overall the model provide the same order of magnitude of the oil retention that was measured during the tests. It should be finally noticed that for comprehensibility and for avoiding confusion, the uncertainty error bars are provided in only for few representative data points in the plots of Figure 7.3 but similar uncertainty error bars applied to all the experimental data points in the plot (a) and (b).

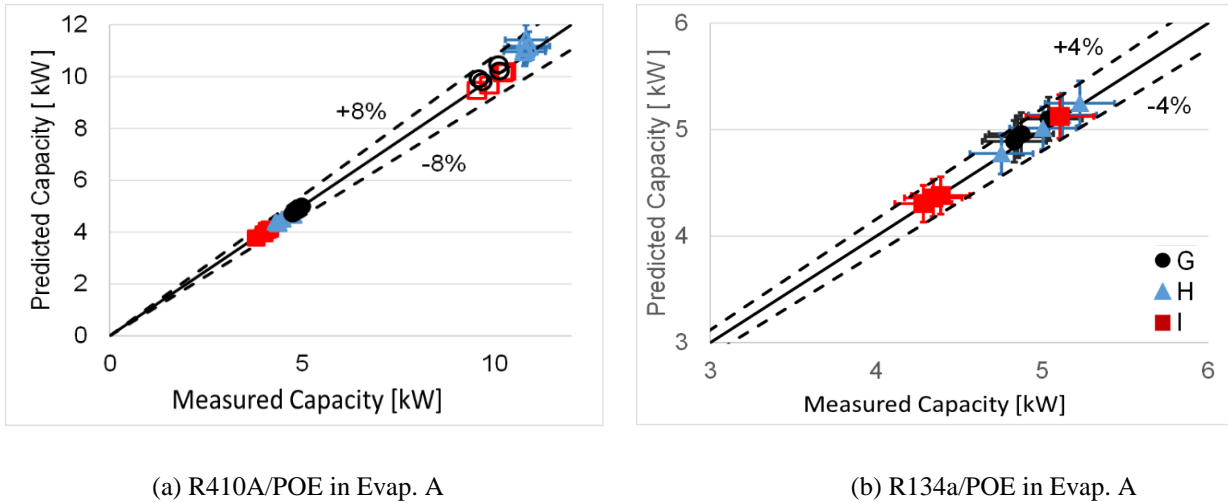


(a) R410A/POE in Evap. A

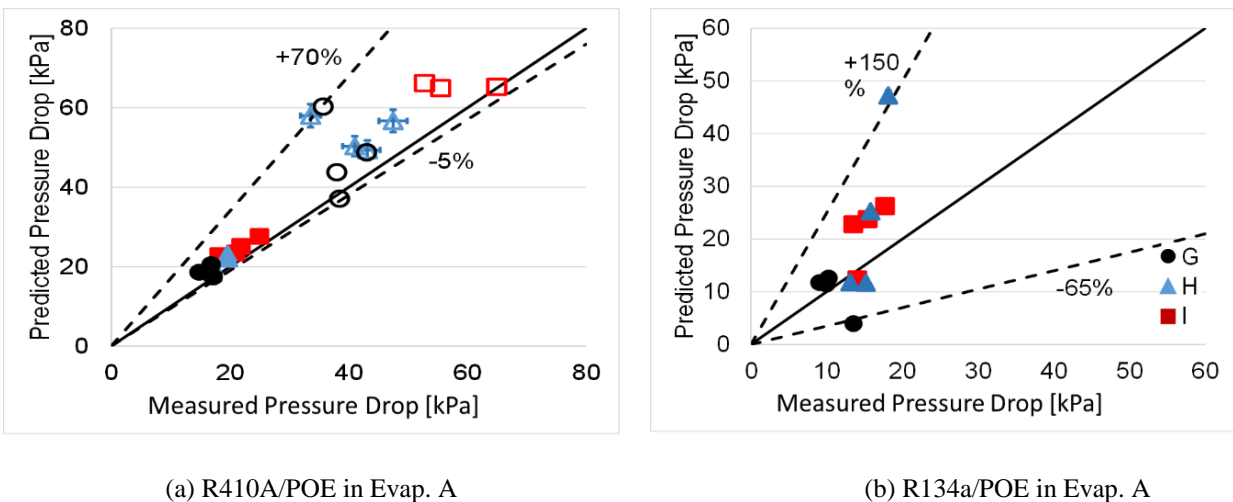
(b) R134a/POE in Evap. A

Figure 7.3: Comparison between experimental data and predicted results for the oil retention volume (ORV) of the microchannel evaporator A with refrigerant R410A and POE oil mixture (a) and with refrigerant R134a and POE mixture (b)

Figure 7.4 shows the model validation for heat transfer capacity when oil is retained in the evaporator A and Figure 7.5 shows the model validation for the pressure drop across the microchannel type evaporator A for the refrigerant and oil mixtures.



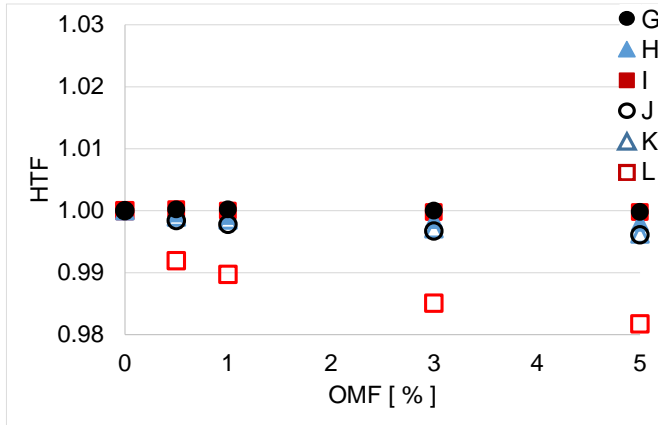
(a) R410A/POE in Evap. A (b) R134a/POE in Evap. A
Figure 7.4: Comparison between experimental data and predicted results for the heat transfer capacity (Q) of the microchannel evaporator A with refrigerant R410A and POE oil mixture (a) and with refrigerant R134a and POE mixture (b)



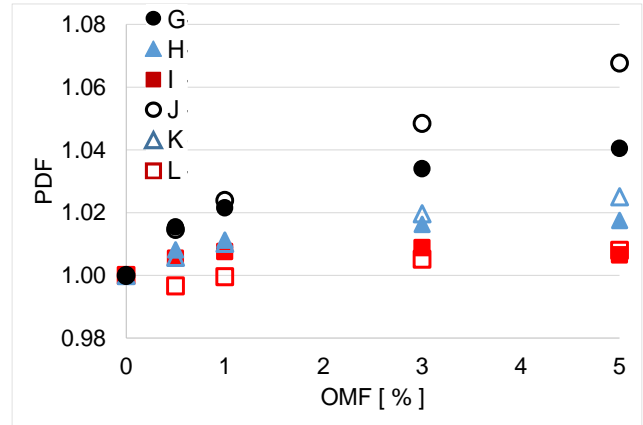
(a) R410A/POE in Evap. A (b) R134a/POE in Evap. A
Figure 7.5: Comparison between experimental data and predicted results for the pressure drop (Δp) of the microchannel evaporator A with refrigerant R410A and POE oil mixture (a) and with refrigerant R134a and POE mixture (b)

Figure 7.6 provides an example of the simulation results for the HTF (Figure 7.6a) and PDF (Figure 7.6b) of the microchannel evaporator A with refrigerant R410A and POE oil mixture at saturation temperature ranging from 33 to 48°F (0 to 9°C). The symbols and letters in Figure 7.6 are described in Table 6.1. Similarly Figure 7.7 provides an example of the simulation results for the HTF (Figure 7.7a) and PDF (Figure 7.7b) of the

microchannel evaporator A with refrigerant R134a and POE oil mixture at saturation temperature ranging from 33 to 48°F (0 to 9°C). The symbols and letters in Figure 7.7 are also described in Table 6.1. The simulation results predicted a drop of heat transfer capacity of the evaporator A and an increase of pressure drop when oil was retained in the microchannel heat exchanger. The agreement with the experimental findings was quite good and the model captured well the effects of oil on the heat transfer capacity and pressure drops.

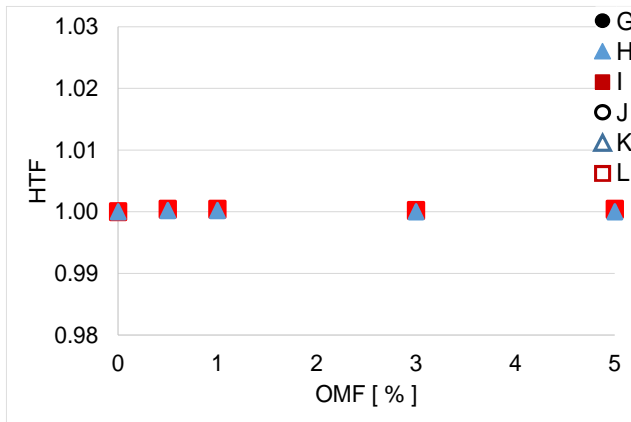


(a) HTF (R410A/POE in Evap. A)

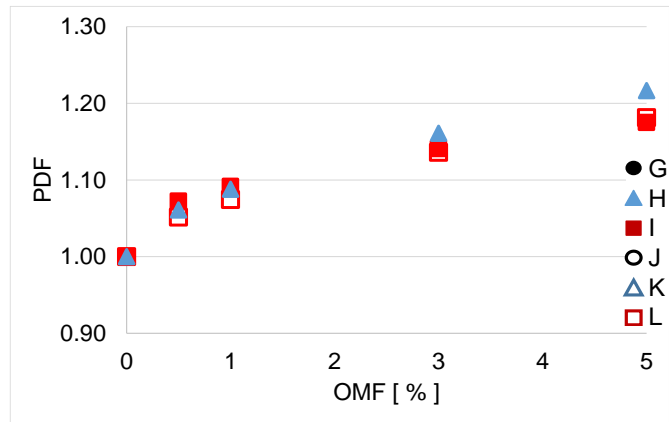


(b) PDF (R410A/POE in Evap. A)

Figure 7.6: Simulation results for the HTF (a) and PDF (b) of the microchannel evaporator A with refrigerant R410A and POE oil mixture at saturation temperature ranging from 33 to 48° F (0 to 9° C) (see Table 6.1 for details on symbols and letters)



(a) HTF (R134a/POE in Evap. A)



(b) PDF (R134a/POE in Evap. A)

Figure 7.7: Simulation results for the HTF (a) and PDF (b) of the microchannel evaporator A with refrigerant R134a and POE oil mixture at saturation temperature ranging from 33 to 48° F (0 to 9° C) (see Table 6.1 for details on symbols and letters)

CHAPTER VII

8. CONCLUSIONS AND RECOMMENDATIONS FOR FUTURE WORK

8.1 Conclusions from the thesis work

In vapor compression cycles, the oil circulating with the refrigerant flow can deposit in heat exchangers and degrade its performance by increasing pressure losses and adding additional resistance to heat exchange process. In this thesis work the oil retention and its effects on heat transfer and pressure drop of refrigerants and oil mixtures in microchannel type evaporators were investigated. The present work used two different louvered-fin aluminum microchannel heat exchangers: working in evaporator mode. The following conclusions could be drawn from the experimental work discussed in this thesis.

- i. Experimentally investigated the oil retention in microchannel evaporators as function of oil mass fraction circulating in the heat exchangers, refrigerant flow rates, refrigerant saturation temperatures, and exit degree of superheat. The oil retention volume in the microchannel evaporators was measured up to 13 % of estimated internal volume of evaporators. For typical air conditioning application, OMF is less than 1 wt.%, and the oil retention volume varied from 3 to 10% of internal volume, depending on the configuration of the outlet header and direction of the refrigerant flow at the outlet of the evaporator.
- ii. Oil retention volume in microchannel evaporators depended on oil mass fraction, and it increased if oil mass fraction increased. The trend of increment depended on microchannel evaporator geometry, refrigerant mass flux, and degree of superheat at the microchannel evaporator outlet.

- iii. When the microchannel tubes in the evaporator entered the outlet header vertically from the bottom and the refrigerant flow was vertical upward, then the valleys in between the 'tube inserts' inside the outlet header were potential traps for oil accumulation. If interfacial friction between oil and refrigerant is not enough then oil separates from the flow and potentially gets trapped in the valleys due to gravity. This phenomena was speculated for low mass flux conditions which explains sudden increase in oil retention volume for oil mass fraction less than 1 wt. %.
- iv. When the microchannel tubes in the evaporator entered the outlet header vertically from the top and the refrigerant flow was vertical downward, then the valleys in between the tube inserts inside the outlet header were not potential traps for oil accumulation. The result of this tube/header configuration was a markedly reduced oil retention when OMF was 1 wt.% with respect to the opposite configuration, that is, vertical upward flow with microchannel tube entering the outlet header from the bottom.
- v. If refrigerant mass flux increased, the oil retention volume decreased in microchannel evaporators. Oil retention in microchannel evaporator was reduced up to 50% when mass flux was nearly doubled.
- vi. The effect of saturation temperature was clearly visible when comparing the low evaporation temperature series used in refrigeration systems applications and the medium evaporation temperature series used in air conditioning systems applications. If the saturation temperature decreased from medium temperature to low temperature then there was a significant increase in oil retention volume up to 3 to 4 times.
- vii. For same inlet conditions and oil mass fractions, when superheat at microchannel evaporator outlet increased from 5° F to 25° F (2.8°C to 13.9° C) then oil retention volume increased up to 150%. This findings was observed in both evaporator A and evaporator B.
- viii. Oil affected the heat transfer rate of the microchannel evaporators and it penalized the heat transfer capacities by as much as 14% if the oil mass fraction was 5 wt.%. For air-conditioning

applications and water and wine cooler applications, when OMFs were equal to or less than 1 wt. %, the decrease in heat transfer rates were within 4 %.

- ix. The oil decreased the heat transfer rate and its impact was also depended on the mass flux. The heat transfer factors (HTFs) were close to 1 for OMF less than 1 wt. % and for both high and low mass flux. For OMF higher than 1 wt. %, the impact of mass flux on HTF was measurable. For example, at OMF of 3 wt.%, a reduction of mass flux by half, that is from high mass flux of 8.4 lbm/ft²-s (20.4 kg/m²-s) to low mass flux of 4.2 lbm/ft²-s (20.4 kg/m²-s), decreased the HTF from 0.96 to 0.90. This represented a decrease of 6% in the heat transfer rate for the same evaporation saturation temperature of 38°F (3.3°C) in the microchannels due to the decrease of mass flux from that of full load to part load conditions. These findings confirmed that the presence of oil in the evaporator was more marked at part load conditions.
- x. The effect of oil on the heat transfer factors (HTFs) were negligible when superheat was 25° F (13.9° C). For given oil mass fraction, increase in superheat at microchannel evaporator outlet increased the heat transfer factor slightly. This findings was observed in evaporator A.
- xi. The refrigerant-side pressure drop across the microchannel evaporators increased by 10 to 25 percent when oil was present inside the heat exchangers and when the OMF was in the range of typical of air conditioning systems and refrigeration systems.
- xii. When saturation temperature, oil mass fraction and exit superheat maintained constant then increase in mass flux increased the refrigerant side pressure drop.
- xiii. The effect of superheat on pressure drop due to presence of oil was negligible.

In separate study a model to predict the performance of microchannel evaporator A when oil was present in the refrigerant flow was developed. The model was experimentally validated with the data from the current study. The model predicted the thermal performance of the microchannel evaporator A and the refrigerant-side operating conditions with and without oil (as well as the air-side conditions).

- i. The model was able to capture correctly the trends and the magnitude of the penalization due to the oil on the heat transfer capacities and pressure drops of the microchannel heat exchangers at various oil mass fractions.
- ii. The predicted oil retention volume was often lower than the measured oil retention volume. The main reason for the discrepancy was due to the estimation of the oil retained in the headers and in the length of the microchannel tubes, in which refrigerant was superheated vapor.
- iii. Simulation results of the microchannel type evaporators predicted the heat transfer capacities and the pressure drop with and without oil. The model predictions of the heat transfer capacities were in general quite good and had an error of about ± 5 to $\pm 8\%$ with respect to the experimental data of the present work. The pressure drop were estimated by the newly developed model with an error that range from ± 20 to $\pm 50\%$ and the error increased significantly for some of the tests when oil was retained in the heat exchangers.

8.2 Recommendations for Future Work on this Research Topic

The present work carried out oil retention measurements and effect of oil on heat transfer capacity and refrigerant side pressure drop by to considering the entire heat exchanger, that is, the microchannel tubes and the inlet and outlet headers all together. While this approach had the advantages of being feasible and accurate for the measurements of oil retention volume, heat transfer rate, and pressure drop, and it also had certain limitations such as the determination of local heat transfer coefficient and local flow conditions. Based on the experiences with the current tests and results, some recommendations on the future works are proposed.

1. Future work can be extended to additional microchannel heat exchangers with different geometrical aspects of microchannels. Following are various geometrical aspects of microchannels
 - i. Various shapes of microchannels (circular, square, triangular) with same hydraulic diameter.
 - ii. Number of channels in each microchannel tubes
 - iii. Length of microchannel tubes

2. The present work can extend to additional microchannel heat exchangers with different headers internal geometries and refrigerant flow configurations in the headers. The inlet and outlet (and intermediate headers for heat exchangers with multiple passes) are important elements that affect the oil retained in a microchannel heat exchanger and oil retention studies in the headers are recommended in future work on this research topic.
3. The present work can be extended to additional refrigerant and oil mixtures to study the parametric effect of change in viscosity of mixture on oil retention and its effects on pressure drops and heat transfer rate of microchannel evaporators.
4. The present work can be extended to study the effects of refrigerant and oil miscibility property on oil retention and its effects on pressure drops and heat transfer rate of microchannel evaporators.
5. In this thesis work the inlet of microchannel evaporator was maintained near saturated liquid conditions to avoid the distribution effects on oil retention. The present work can be extended to study the effects of maldistributions on oil retention in microchannel heat exchangers. This can be achieved by increasing vapor quality at inlet above 0.2.
6. The oil retention model in the present works tended to underestimate the oil hold up in the heat exchangers. This was due to the lack of modeling of the microchannel headers internal geometries details. Literature showed (and the experimental work of this project confirmed) that oil accumulated in the headers, that is, in the valleys created by the tube inserts. Not only this accumulation might change the refrigerant flow distribution across the microchannel tubes but a model of the oil filling process of these valleys is missing. Future work might focus on modeling the oil retention in the headers of microchannel type heat exchangers in order to improve the accuracy of the oil retention mode

NOMENCLATURE

A	area, m ² (ft ²)
CFC	chlorofluorocarbon
COP	coefficient of performance, dimensionless
c	Core refrigerant vapor
c _p	specific heat capacity, J/kg.K (Btu/lbm.°F)
D	inner microchannel diameter, mm (inches)
EF	enhancement factor
evap	evaporator
f	friction factor
g	gravity acceleration, m ² /s (ft ² /hr)
G	mass flux, kg/m ² -s (lb _m /hr-ft ²)
h	heat transfer coefficient, W/m ² .K (Btu/hr-ft ² .°F) or enthalpy J/kg (Btu/lb)
HFC	hydrofluorocarbons
HTF	heat transfer factor, dimensionless
j	superficial phase velocity, m/s (fpm)

Ja	Jacob number
l	length of microchannel tubes, cm (inches)
m	mass, grams (or lbm) \dot{m} mass flow rate, grams/s or (lbm/min)
MO	mineral oil
MCHX	microchannel heat exchanger
NEQ	Non-evaporated refrigerant quantity
NTU	number transfer unit
OCR	oil circulation ratio, same as OMF
OMF	oil mass fraction, wt. %
ORV _N	oil retention volume normalized, dimensionless
P	pressure, Pa (psi) or perimeter, m (ft)
PAG	polyalkylene glycol
PDF	pressure drop factor
PF	penalty factor
POE	polyolester
\dot{Q}	heat transfer rate, kW (Btu/hr)
r	Refrigerant
R	thermal resistance, m ² .K/W (hr-ft ² .°F/Btu)

RH	relative humidity, %
Re	Reynolds number, dimensionless
s	solubility of refrigerant and oil mixture, % wt./wt.
S	sight glass
SUS	Saybolt universal second viscosity measurement method
t	time, second
T	temperature, °C (°F)
u	absolute uncertainty
v	velocity, m/s (fpm)
V	volume, cm ³ (or inch ³)
VG	viscosity grade
VFD	variable frequency drive
We	Weber number, dimensionless

Greek symbols

ΔP	refrigerant side pressure drop, kPa (psi)
α	heat transfer coefficient, W/m ² .K (Btu/hr-ft ² .°F)
ε	void fraction or efficiency, %
β	velocity ratio

δ	difference or uncertainty
ρ	density, grams/cm ³ (lb/inch ³)
σ	surface tension, N/m
μ	dynamic viscosity, Pa-s
ν	kinematic viscosity, cSt
$\tilde{\nu}$	viscosity ratio, dimensionless
γ	refrigerant-oil miscibility, dimensionless
ω	oil concentration by weight
λ	thermal conductivity, W/m.K (Btu/hr-ft.°F)

Subscripts

evap	Evaporator
f, L	liquid phase,
g	gas phase
hx	heat exchanger
I	inlet
in	inlet
LO	liquid only
mchx	microchannel heat exchanger
min	minimum

mix	mixture
N	nozzle
NcB	nucleate boiling
oil	oil
out	outlet
OR	oil retention
r	refrigerant
ref	Refrigerant
g, v	gas phase
sat	saturation
w	wall
tp	two phase
x	vapor quality

REFERENCES

- Alonso, M., Jassim, E. W., & Newell, T. A. 2010. Experimental Measurement of Oil Hold-up During Refrigerant Condensation and Evaporation in Two Phase Flow. International Refrigeration and Air Conditioning Conference, West Lafayette, Indiana.
- ANSI/ASHRAE 41.2-1987, Standard methods for laboratory airflow measurements (1987).
- ASHRAE. (1988). ANSI/ASHRAE Standard 37-1988: Methods of testing for rating unitary air-conditioning and heat pump equipment (pp. 25). Atlanta, GA, USA: ASHRAE.
- ASHRAE. (1996). Standard Method for Measurement of Proportion of Lubricant in Liquid Refrigerant (ANSI approved) ANSI/ASHRAE Standard 41.4-1996 (RA 2006). USA: ASHRAE.
- ASHRAE. (2013). Standard 41.1-2013 -- Standard Method for Temperature Measurement.
- ASHRAE. (2014). 41.3 Standard Methods for Pressure Measurement.
- Baker, O. (1954). Simultaneous flow of oil and gas. *The Oil and Gas Journal*, 53, 185–195.
- Bigi, A. A. M., Cremaschi, L., & Fisher, D. E. 2014. Modeling of Lubricant Effects in a Microchannel Type Condenser. International Refrigeration and Air Conditioning Conference, West Lafayette, Indiana. Paper 1429
- Cavestri, R. C. (1993). Measurement of viscosity, density, and gas solubility of refrigerant blends in selected synthetic lubricants ARTI MCLR Project Number 650-51400: Blends: Air-Conditioning and Refrigeration Technology Institute, USA.
- Cavestri, R. C. (1995). Measurement of viscosity, density, and gas solubility of refrigerant blends in selected synthetic lubricants ARTI MCLR Project Number 650-51400: Blends: Air-Conditioning and Refrigeration Technology Institute, USA.
- Cavestri, R. C., & Schafer, W. R. (2000). Measurement of solubility, viscosity, and density of R-410A refrigerant/lubricant mixtures.
- Choi, J., Kim, M., Shin, J.-S., Oh, S.-K., Chung, B.-Y., & Kim, M. (2009). A numerical study on oil retention and migration characteristics in the heat pump system. *Journal of Mechanical Science and Technology*, 23(7), 1858-1865.
- Cremaschi, L. (2004). Experimental Investigation of oil retention in vapor compression systems. (Ph.D), University of Maryland.
- Cremaschi, L., Hwang, Y., & Radermacher, R. (2005). Experimental investigation of oil retention in air conditioning systems. *International Journal of Refrigeration*, 28(7), 1018-1028.
- Cremaschi, L., & Lee, E. (2008). Design and Heat Transfer Analysis of a New Psychrometric Environmental Chamber for Heat Pump and Refrigeration Systems Testing. *ASHRAE transactions*, 114(2), 619-631.
- Crompton, J. A., Newell, T. A., & Chato, J. C. (2004). Experimental Measurement and Modeling of Oil Holdup ACRC TR-226. University of Illinois, Urbana, Illinois: Air Conditioning and Refrigeration Center.
- Deokar, P. S. (2013). Development of an experimental methodology for measurement of oil retention and its effect on the Microchannel Heat Exchanger. (Master of Science), Oklahoma State University, Stillwater, Oklahoma.
- Ding, G., Hu, H., Huang, X., Deng, B., & Gao, Y. (2009). Experimental investigation and correlation of two-phase frictional pressure drop of R410A–oil mixture flow boiling in a 5 mm microfin tube. *International Journal of Refrigeration*, 32(1), 150-161.

- Fung, K. K., & Sundaresan, S. G. 1994. Study of Oil Return Characteristics in a Display Case Refrigeration System. International Refrigeration and Air-conditioning Conference, West Lafayette, Indiana.
- Hambraeus, K. (1995). Heat transfer of oil-contaminated HFC134a in a horizontal evaporator. *International Journal of Refrigeration*, 18(2), 87-99.
- Hasan, M. I., Rageb, A. A., Yaghoubi, M., & Homayoni, H. (2009). Influence of channel geometry on the performance of a counter flow microchannel heat exchanger. *International Journal of Thermal Sciences*, 48(8), 1607-1618.
- Henderson, D. R. (1994). Solubility, Viscosity and Density of Refrigerant/Lubricant Mixtures ARTI MCLR Project Number 655-51200 (pp. 144). Stockbridge, GA: Spauschus Associates, Inc.
- Hu, H.-T., Ding, G.-L., Huang, X.-C., Deng, B., & Gao, Y.-F. (2011). Experimental investigation and correlation of two-phase heat transfer of R410A/OIL mixture flowboiling in a 5-MM microfin tube. *Journal of Enhanced Heat Transfer*, 18(3), 209-220.
- Hu, H., Ding, G., Huang, X., Deng, B., & Gao, Y. (2009). Measurement and correlation of flow-boiling heat transfer of a R-410A/Oil mixture inside a 4.18 mm straight smooth tube. *HVAC and R Research*, 15(2), 287-314.
- Hu, H., Ding, G., & Wang, K. (2008a). Heat transfer characteristics of R410A–oil mixture flow boiling inside a 7 mm straight microfin tube. *International Journal of Refrigeration*, 31(6), 1081-1093.
- Hu, H., Ding, G., Wei, W., Wang, Z., & Wang, K. (2008b). Heat transfer characteristics of R410A-oil mixture flow boiling inside a 7 mm straight smooth tube. *Experimental Thermal and Fluid Science*, 32(3), 857-869.
- Hu, H., Peng, H., Ding, G., Zheng, Y., & Gao, Y. 2014. Influence of Oil on Heat Transfer Characteristic of R410A Flow Boiling in Conventional and Small Size Microfin Tubes. International Refrigeration and Air Conditioning Conference, West Lafayette, Indiana. Paper No.1452
- Hughes, D. W., McMullan, J. T., Mawhinney, K. A., Morgan, R., & Sutcliffe, B. L. 1980. Lubricant Related Problems with Heat-Pumps. International Compressor Engineering Conference, West Lafayette, Indiana. Paper 325
- Jacobs, M. L., Scheideman, F. C., Kazem, S. M., & Macken, N. A. (1976). Oil Transport by Refrigerant Vapor. *ASHRAE transactions*, 82(2), 318-329.
- Jiang, Y., & Garimella, S. 2001. Compact air-coupled and hydronically coupled microchannel heat pumps. ASME International Mechanical Engineering Congress and Exposition.
- Jin, S., & Hrnjak, P. 2014. An Experimentally Validated Model for Predicting Refrigerant and Lubricant Inventory in MAC Heat Exchangers. SAE 2014 World Congress & Exhibition, Michigan, USA.
- Kattan, N., Thome, J. R., & Favrat, D. (1998). Flow Boiling in Horizontal Tubes: Part 2—New Heat Transfer Data for Five Refrigerants. *Journal of Heat Transfer*, 120(1), 148-155.
- Kesim, S. C., Albayrak, K., & İleri, A. (2000). Oil entrainment in vertical refrigerant piping. *International Journal of Refrigeration*, 23(8), 626-631.
- Kruse, H. H., & Schroeder, M. (1985). Fundamentals of lubrication in refrigerating systems and heat pumps. *International Journal of Refrigeration*, 8(6), 347-355.
- Lee, J.-P., Hwang, Y., Radermacher, R., & Mehendale, S. S. 2001. Experimental Investigations on Oil Accumulation Characteristics in a Vertical Suction Line. ASME International Mechanical Engineering Congress and Exposition, New York, NY.
- Lee, J. P. (2002). Experimental and Theoretical Investigation of Oil Retention in Carbon Dioxide Air-Conditioning System. (Ph.D.), University of Maryland, College Park, MD (USA).
- Li, H., & Hrnjak, P. 2014a. Lubricant Effect on Performance of R134a MAC Microchannel Evaporators. SAE Technical Paper.
- Li, H., & Hrnjak, P. S. 2014b. An Experimentally Validated Model for Microchannel Heat Exchanger Incorporating Lubricant Effect. International Refrigeration and Air Conditioning Conference, West Lafayette, Indiana. Paper 1375
- Lottin, O., Guillemet, P., & Lebreton, J.-M. (2003a). Effects of synthetic oil in a compression refrigeration system using R410A. Part I: modelling of the whole system and analysis of its response to an increase in the amount of circulating oil. *International Journal of Refrigeration*, 26(7), 772-782.

- Lottin, O., Guillemet, P., & Lebreton, J. M. (2003b). Effects of synthetic oil in a compression refrigeration system using R410A. Part II: quality of heat transfer and pressure losses within the heat exchangers. *International Journal of Refrigeration*, 26(7), 783-794.
- Mandhane, J. M., Gregory, G. A., Aziz, K. (1974). A Flow Map for Gas-Liquid Flow in Horizontal Pipes. *Int. J. Multiphase Flow*, 1, 537-553.
- Manwell, S. P., & Bergles, A. E. (1994). Gas-liquid flow patterns in refrigerant-oil mixtures. *ASHRAE transactions*, 100 (2), 456-464.
- Marsh, K. N., & Kandil, M. E. (2002). Review of thermodynamic properties of refrigerants + lubricant oils. *Fluid Phase Equilibria*, 199(1-2), 319-334.
- Martz, W. L., & Jacobi, A. M. (1994). Refrigerant-Oil Mixtures and Local Composition Modeling *Air Conditioning and Refrigeration Center TR-68* (pp. 123).
- McMullan, J. T., Murphy, N., & Hughes, D. W. (1988a). The effect of oil on the performance of heat pumps and refrigerators—II. Experimental results. *Heat Recovery Systems and CHP*, 8(2), 95-124.
- McMullan, J. T., Murphy, N., & Hughes, D. W. (1988b). The effect of oil on the performance of heat pumps and refrigerators—part one. Experimental test facility. *Heat Recovery Systems and CHP*, 8(1), 53-68.
- Mehendale, S. S., & Radermacher, R. (2000). Experimental and Theoretical Investigation of Annular Film Flow Reversal In a Vertical Pipe: Application To Oil Return In Refrigeration Systems. *HVAC&R Research*, 6(1), 55-74.
- Neto, M. M., & Barbosa, J. 2012. A Departure Function-Based Method to Determine the Effect of the Oil Circulation Ratio on the Performance of Vapor Compression Refrigeration Systems. International Refrigeration and Air Conditioning Conference. Paper 1178
- Nidegger, E., Thome, J. R., & Favrat, D. (1997). Flow Boiling and Pressure Drop Measurements for R-134a/Oil Mixtures Part 1: Evaporation in a Microfin Tube. *HVAC&R Research*, 3(1), 38-53.
- Park, C. Y., & Hrnjak, P. (2008). Experimental and numerical study on microchannel and round-tube condensers in a R410A residential air-conditioning system. *International Journal of Refrigeration*, 31(5), 822-831.
- Pérez-Lombard, L., Ortiz, J., & Pout, C. (2008). A review on buildings energy consumption information. *Energy and Buildings*, 40(3), 394-398.
- Peuker, S., & Hrnjak, P. S. 2010. Experimental Techniques to Determine Oil Distribution in Automotive A/C Systems. International Refrigeration and Air Conditioning Conference, West Lafayette, Indiana. Paper 1011
- Qi, Z., Zhao, Y., & Chen, J. (2010). Performance enhancement study of mobile air conditioning system using microchannel heat exchangers. *International Journal of Refrigeration*, 33(2), 301-312.
- Radermacher, R., Cremaschi, L., & Schwentker, R. A. (2006). Modeling of Oil Retention in the Suction Line and Evaporator of Air-Conditioning Systems. *HVAC&R Research*, 12(1), 35-56.
- Ramakrishnan, A. (2012). Investigation of oil retention and pressure drop in suction lines using R1234yf, R134a and R410A with POE ISO 100. (Master of Science), University of Illinois Urbana, Illinois.
- Schlager, L. M., Pate, M. B., & Bergles, A. E. (1987). A survey of refrigerant heat transfer and pressure drop emphasizing oil effects and in-tube augmentation. *ASHRAE transactions*, Vol. 93(Part 1), 392-415.
- Sethi, A. (2011). Oil Retention and Pressure Drop of R1234yf and R134a with POE ISO 32 in Suction Lines. (Master of Science), University of Illinois at Urbana-Champaign, Urbana, Illinois
- Sunami, M., Takigawa, K., & Suda, S. 1994. New Immiscible Refrigeration Lubricant for HFCs. International Refrigeration and Air Conditioning Conference. Paper 237
- Sundaresan, S. G., Judge, J., Chu, W., & Radermacher, R. 1996. A Comparison of the Oil Return Characteristics of R-22/Mineral Oil, and Its HFC Alternatives (R-407C & R-410A) with Mineral Oil and POE in a Residential Heat Pump. International Refrigeration and Air Conditioning Conference, West Lafayette, Indiana. Paper 340
- Takaishi, Y., & Oguchi, K. (1987). Measurements of Vapor Pressures of R22/Oil Solutions. 18th international Congress of Refrigeration, Vienna.

- Taylor, B. N., & Kuyatt, C. E. (1994a). Guidelines for Evaluating and Expressing the Uncertainty of NIST Measurement Results. Gaithersburg, MD: National Institute of Standards and Technology.
- Taylor, B. N., & Kuyatt, C. E. (1994b). Guidelines for evaluating and expressing the uncertainty of NIST measurement results. (GovDoc: C 13.46:1297/994; GPO Item No: 0249-A (MF)). U.S. Dept. of Commerce, Tech. Adm., NIST, Gaithersburg, MD, USA.
- Thome, J. (2007). Engineering data book III. 10-11 10-29.
- Thome, J. R. (1995). Comprehensive Thermodynamic Approach to Modeling Refrigerant-Lubricating Oil Mixtures. *HVAC&R Research*, 1(2), 110-125.
- Tichy, J. A., Macken, N. A., & Duval, W. M. B. (1985). An experimental investigation of heat transfer in forced convection condensation of oil-refrigerant mixtures *ASHRAE transactions*, 91(A), 297-309.
- Tuckerman, D. B., & Pease, R. F. W. (1981). High-performance heat sinking for VLSI. *Electron Device Letters, IEEE*, 2(5), 126-129.
- Wei, W., Ding, G., Hu, H., & Wang, K. (2007). Influence of lubricant oil on heat transfer performance of refrigerant flow boiling inside small diameter tubes. Part I: Experimental study. *Experimental Thermal and Fluid Science*, 32(1), 67-76.
- Wei, W., Ding, G., Hu, H., & Wang, K. (2008). Models of thermodynamic and transport properties of POE VG68 and R410A/POE VG68 mixture. *Frontiers of Energy and Power Engineering in China*, 2(2), 227-234.
- Wongwises, S., Wongchang, T., Kaewon, J., & Wang, C.-C. (2002). A Visual Study of Two-Phase Flow Patterns of HFC-134a and Lubricant Oil Mixtures. *Heat Transfer Engineering*, 23(4), 13-22.
- Wujek, S. S., Peuker, S., Mai, H., Bower, J., & Koffler, M. 2010. Method for Measuring Oil Contained in Air-Conditioning Components. International Refrigeration and Air Conditioning Conference, West Lafayette, Indiana. Paper 1035
- Yatim, A. S. (2015). Oil Retention and its effects on pressure drop and heat transfer in microchannel heat exchangers of air conditioning and refrigeration system. (PhD), Oklahoma State University, Stillwater, Oklahoma.
- Yatim, A. S., Cremaschi, L., & Fisher, D. E. 2014. Measurements of Oil Retention in a Microchannel Condenser for AC Systems. International Refrigeration and Air Conditioning Conference, West Lafayette, Indiana. West Lafayette
- Yokozeiki, A., Takigawa, k., & Sandler, S. I. 2000. Solubility and Viscosity of Hydrofluorocarbon/Alkylbenzene Oil Mixtures. International Refrigeration and Air Conditioning Conference, West Lafayette, Indiana. Paper 488
- Yokozeiki, A. M. 1994. Solubility and Viscosity of Refrigerant-Oil Mixtures. International Compressor Engineering Conference, West Lafayette, Indiana. Paper1002
- Youbi-Idrissi, M., Bonjour, J., Marvillet, C., & Meunier, F. (2003). Impact of refrigerant-oil solubility on an evaporator performances working with R-407C. *International Journal of Refrigeration*, 26(3), 284-292.
- Youbi-Idrissi, M., Bonjour, J., Terrier, M. F., Marvillet, C., & Meunier, F. (2004). Oil presence in an evaporator: experimental validation of a refrigerant/oil mixture enthalpy calculation model. *International Journal of Refrigeration*, 27(3), 215-224.
- Zhao, Y., Molki, M., Ohadi, M. M., Franca, F. H. R., & Radermacher, R. (2002). Flow boiling of CO(2) with miscible oil in microchannels. *ASHRAE transactions*, 108.
- Zoellick, K. F. (2010). Oil Retention and Pressure Drop in Horizontal and Vertical Suction Lines with R410A / POE ISO 32. University of Illinois, Urbana, Illinois.
- Zürcher, O., Thome, J. R., & Favrat, D. (1997). Flow Boiling and Pressure Drop Measurements for R-134a/Oil Mixtures Part 2: Evaporation in a Plain Tube. *HVAC&R Research*, 3(1), 54-64.
- Zürcher, O., Thome, J. R., & Favrat, D. (1998). In-Tube Flow Boiling of R-407C and R-407C/Oil Mixtures Part I: Microfin Tube. *HVAC&R Research*, 4(4), 347-372.

APPENDICES

Appendix A Oil retention volume results summary

The table below represents results of ORV_N and corresponding oil retention volume (ml) in microchannel evaporator A for all series given in Table 6.1, Table 6.2 and Table 6.3.

Series	Test No.	Mass flow rate	Refrigerant	Ref. saturation temperature (°F)	OMF	ORV_N	Oil Retention Volume (ml)
G	1	202.05	R410A	29.35	0.00	0.000	0.00
	2	200.33	R410A	29.54	0.51	0.078	118.88
	3	199.73	R410A	30.09	1.17	0.079	121.08
	4	199.57	R410A	29.85	2.98	0.101	153.44
	5	193.26	R410A	30.81	5.34	0.105	160.65
H	11	200.00	R410A	38.25	0.00	0.000	0.00
	12	197.14	R410A	38.39	0.51	0.081	123.98
	13	202.07	R410A	38.23	0.98	0.089	135.15
	14	200.70	R410A	38.59	2.80	0.107	163.20
	15	194.87	R410A	38.90	4.60	0.125	190.27
I	21	200.00	R410A	47.33	0.00	0.000	0.00
	22	200.78	R410A	47.67	0.47	0.081	123.77
	23	198.96	R410A	47.79	1.02	0.100	152.17
	24	202.23	R410A	48.16	3.12	0.104	158.26
	25	201.30	R410A	48.01	4.99	0.113	172.25
J	6	360.00	R410A	32.19	0.00	0.000	0.00
	7	361.40	R410A	32.66	0.47	0.030	45.34
	8	359.91	R410A	31.93	0.90	0.029	43.99
	9	360.64	R410A	32.36	2.63	0.043	66.11
	10	360.84	R410A	32.87	5.12	0.099	151.61
K	16	400.00	R410A	39.10	0.00	0.000	0.00
	17	401.20	R410A	37.70	0.41	0.019	29.04
	18	400.55	R410A	39.29	0.96	0.026	39.40
	19	400.23	R410A	38.45	3.02	0.037	57.02
	20	398.49	R410A	39.04	4.63	0.084	128.28

Series	Test No.	Mass flow rate	Refrigerant	Ref. saturation temperature (°F)	OMF	ORV _N	Oil Retention Volume (ml)
L	26	400.00	R410A	48.81	0.00	0.000	0.00
	27	400.27	R410A	49.38	0.61	0.025	38.18
	28	399.54	R410A	49.49	1.07	0.040	60.69
	29	383.04	R410A	49.56	2.89	0.055	83.21
S	30	389.67	R410A	49.93	4.39	0.063	95.99
	32	358.90	R410A	39.13	0.82	0.029	43.52
	33	360.57	R410A	39.26	2.48	0.037	56.26
T	34	360.30	R410A	39.37	0.00	0.000	0.00
	35	357.64	R410A	39.49	0.90	0.028	42.60
	36	359.33	R410A	39.16	2.55	0.065	99.93
U	37	360.25	R410A	39.57	0.00	0.000	0.00
	38	357.56	R410A	39.79	0.78	0.076	115.83
	39	358.27	R410A	39.20	2.58	0.094	143.51
M	40	139.893	R134a	-0.6347	0	0	0
	41	148.469	R134a	-0.8641	0.589576	0.11847	180.7813152
	42	144.693	R134a	-0.7933	1.177363	0.12182	185.8933339
	43	151.2969	R134a	-0.8936	3.986538	0.1602	244.4724536
	44	142.369	R134a	-1.236	4.063449	0.13978	213.3036133
N	45	156.3596	R134a	7.589	0	0	0
	46	148.9693	R134a	6.893	0.480681	0.07167	109.370029
	47	151.3973	R134a	6.5893	0.922861	0.0742	113.2295964
	48	145.933	R134a	7.3169	3.538329	0.12078	184.3063268
	49	149.3697	R134a	7.15696	4.954994	0.15112	230.6153569
O	50	145.6893	R134a	10.269	0	0	0
	51	147.5863	R134a	10.8931	0.62328	0.0564	86.07371626
	52	151.3969	R134a	9.5698	1.178481	0.08808	134.4054598
	53	146.3694	R134a	9.8943	3.745535	0.10716	163.5254248
	54	145.6936	R134a	10.1239	5.187389	0.14221	217.0091915
P	55	200.131	R134a	32.821	0	0	0
	56	200.253	R134a	32.974	0.54	0.02975	45.39490245
	57	200.495	R134a	33.01	0.98	0.02162	32.98604984
	58	200.091	R134a	33.2156	1.048983	0.03244	49.5019471
	59	201.062	R134a	33.12565	2.804004	0.0423	64.54388493
	60	200.23665	R134a	32.5698	4.798929	0.0578	88.19860591
Q	61	200.051	R134a	38.989	0	0	0
	62	199.687	R134a	38.1559	0.486813	0.03419	52.17948648
	63	200.293	R134a	39.3959	1.044121	0.03384	51.63657163

	64	200.091	R134a	38.1859	3.084157	0.05211	79.51316099
	65	200.091	R134a	38.6979	5.166386	0.04152	63.36591881
R	66	202.073	R134a	47.892	0	0	0
	67	200.779	R134a	47.693	0.486813	0.03293	50.25160652
	68	201.021	R134a	48.1756	1.044121	0.02161	32.97050205
	69	200.698	R134a	47.51756	3.084157	0.07608	116.0922818
	70	203.771	R134a	47.6546	5.166386	0.03666	55.93733324

The table below represents results of ORV_N and corresponding oil retention volume in microchannel evaporator B for all series given in Table 6.1, and Table 6.2.

Series	Test No.	Mass flow rate	Refrigerant	Ref. saturation temperature (°F)	OMF	ORV_N	Oil Retention Volume (ml)
G	1	200.85	R410A	31.97	0.00	0.000	0.00
	2	207.98	R410A	32.90	0.56	0.032	61.56
	3	208.87	R410A	33.22	1.03	0.044	83.64
	4	207.17	R410A	33.65	2.74	0.057	107.62
	5	210.61	R410A	33.44	4.46	0.064	120.75
H	11	201.35	R410A	37.25	0.00	0.000	0.00
	12	206.16	R410A	37.83	0.53	0.036	68.58
	13	205.71	R410A	38.20	0.92	0.031	59.52
	14	208.62	R410A	38.07	2.63	0.051	96.20
	15	207.94	R410A	38.54	4.81	0.072	136.05
I	21	200.82	R410A	48.87	0.00	0.000	0.00
	22	199.00	R410A	47.00	0.53	0.026	49.99
	23	200.70	R410A	46.79	1.01	0.029	55.71
	24	198.92	R410A	47.33	2.82	0.060	114.23
	25	199.97	R410A	47.75	4.53	0.092	175.55
J	6	333.56	R410A	32.36	0.00	0.000	0.00
	7	308.02	R410A	32.89	0.44	0.031	59.37
	8	338.35	R410A	33.12	0.99	0.037	69.60
	9	300.06	R410A	31.96	2.64	0.041	77.03
	10	288.29	R410A	32.57	4.42	0.043	80.90
K	16	353.73	R410A	37.30	0.00	0.000	0.00
	17	351.66	R410A	37.11	0.52	0.022	42.00
	18	347.29	R410A	36.10	1.04	0.035	66.82
	19	347.45	R410A	37.15	2.65	0.050	95.26
	20	349.27	R410A	37.89	4.63	0.059	112.63

L	26	349.69	R410A	48.00	0.00	0.000	0.00
	27	346.24	R410A	48.24	0.43	0.020	37.39
	28	347.01	R410A	48.59	1.04	0.022	42.26
	29	349.55	R410A	49.48	2.32	0.051	96.57
	30	316.48	R410A	48.92	4.77	0.056	105.51
S	31	354.36	R410A	39.79	0.00	0.000	0.00
	32	355.23	R410A	39.65	0.82	0.033	49.74
	33	354.57	R410A	39.58	2.44	0.039	59.61
T	34	356.36	R410A	39.87	0.00	0.000	0.00
	35	355.29	R410A	39.48	0.82	0.036	55.22
	36	355.89	R410A	39.76	2.66	0.058	88.50
U	37	357.86	R410A	38.98	0.00	0.000	0.00
	38	356.70	R410A	38.76	0.92	0.101	154.14
	39	357.36	R410A	39.22	2.82	0.103	156.79

Appendix B PDF and HTF results summary

The table below represents results of PDF and HTF results of microchannel evaporator A for all series given in Table 6.1, Table 6.2 and Table 6.3.

Series	Test No.	Mass flow rate	Refrigerant	Ref. saturation temperature (°F)	OMF	PDF	HTF
G	1	202.05	R410A	29.35	0.00	1.000	1.00
	2	200.33	R410A	29.54	0.51	1.011	0.98
	3	199.73	R410A	30.09	1.17	1.092	0.97
	4	199.57	R410A	29.85	2.98	1.152	0.92
	5	193.26	R410A	30.81	5.34	1.405	0.88
H	11	200.00	R410A	38.25	0.00	1.000	1.00
	12	197.14	R410A	38.39	0.51	1.087	0.99
	13	202.07	R410A	38.23	0.98	1.087	0.97
	14	200.70	R410A	38.59	2.80	1.127	0.89
	15	194.87	R410A	38.90	4.60	1.164	0.86
I	21	200.00	R410A	47.33	0.00	1.000	1.00
	22	200.78	R410A	47.67	0.47	1.015	1.01
	23	198.96	R410A	47.79	1.02	1.088	1.00
	24	202.23	R410A	48.16	3.12	1.139	0.93
	25	201.30	R410A	48.01	4.99	1.131	0.88
J	6	360.00	R410A	32.19	0.00	1.000	1.00
	7	361.40	R410A	32.66	0.47	1.104	0.98
	8	359.91	R410A	31.93	0.90	1.159	0.97
	9	360.64	R410A	32.36	2.63	1.341	0.95
	10	360.84	R410A	32.87	5.12	1.474	0.92
K	16	400.00	R410A	39.10	0.00	1.000	1.00
	17	401.20	R410A	37.70	0.41	1.035	0.98
	18	400.55	R410A	39.29	0.96	1.118	0.97
	19	400.23	R410A	38.45	3.02	1.276	0.95
	20	398.49	R410A	39.04	4.63	1.291	0.93
L	26	400.00	R410A	48.81	0.00	1.000	1.00
	27	400.27	R410A	49.38	0.61	1.062	0.99
	28	399.54	R410A	49.49	1.07	1.091	0.98
	29	383.04	R410A	49.56	2.89	1.311	0.97
	30	389.67	R410A	49.93	4.39	1.343	0.94

Series	Test No.	Mass flow rate	Refrigerant	Ref. saturation temperature (°F)	OMF	PDF	HTF
S	31	359.66	R410A	38.83	0.00	1	1.00
	32	358.90	R410A	39.13	0.82	1.231	0.98
	33	360.57	R410A	39.26	2.48	1.541	0.96
T	34	360.30	R410A	39.37	0.00	1	1.00
	35	357.64	R410A	39.49	0.90	1.271	0.98
	36	359.33	R410A	39.16	2.55	1.513	0.96
U	37	360.25	R410A	39.57	0.00	1	1.00
	38	357.56	R410A	39.79	0.78	1.308	0.99
	39	358.27	R410A	39.20	2.58	1.492	0.98
M	40	139.893	R134a	-0.6347	0	1	1
	41	148.469	R134a	-0.8641	0.589576	1.03147	0.989268
	42	144.693	R134a	-0.7933	1.177363	1.16563	1.027963
	43	151.2969	R134a	-0.8936	3.986538	1.31679	0.90455
	44	142.369	R134a	-1.236	4.063449	1.31676	0.887576
N	45	156.3596	R134a	7.589	0	1	1
	46	148.9693	R134a	6.893	0.480681	1.08369	1.059274
	47	151.3973	R134a	6.5893	0.922861	1.20689	1.050819
	48	145.933	R134a	7.3169	3.538329	1.30039	0.966569
	49	149.3697	R134a	7.15696	4.954994	1.41413	0.945887
O	50	145.6893	R134a	10.269	0	1	1
	51	147.5863	R134a	10.8931	0.62328	1.03008	0.997048
	52	151.3969	R134a	9.5698	1.178481	1.05426	0.982429
	53	146.3694	R134a	9.8943	3.745535	1.07948	0.951206
	54	145.6936	R134a	10.1239	5.187389	1.1438	0.880771
P	55	200.131	R134a	32.821	0	1	1
	56	200.253	R134a	32.974	0.54	1.00519	0.972
	57	200.495	R134a	33.01	0.98	1.02257	0.972952
	58	200.091	R134a	33.2156	1.048983	1.09456	0.96
	59	201.062	R134a	33.12565	2.804004	1.13211	0.933
	60	200.23665	R134a	32.5698	4.798929	1.29718	0.913
Q	61	200.051	R134a	38.989	0	1	1
	62	199.687	R134a	38.1559	0.486813	1.11778	0.999186
	63	200.293	R134a	39.3959	1.044121	1.22041	0.990188
	64	200.091	R134a	38.1859	3.084157	1.3345	0.960275
	65	200.091	R134a	38.6979	5.166386	1.52151	0.924
R	66	202.073	R134a	47.892	0	1	1
	67	200.779	R134a	47.693	0.486813	1.00312	0.986181
	68	201.021	R134a	48.1756	1.044121	1.16796	0.975485
	69	200.698	R134a	47.51756	3.084157	1.48259	0.960019
	70	203.771	R134a	47.6546	5.166386	1.46182	0.943707

The table below represents results of PDF and HTF results of microchannel evaporator B for all series given in Table 6.1, and Table 6.2.

Series	Test No.	Mass flow rate	Refrigerant	Ref. saturation temperature (°F)	OMF	PDF	HTF
G	1	200.85	R410A	31.97	0.00	1.000	1.00
	2	207.98	R410A	32.90	0.56	1.063	0.99
	3	208.87	R410A	33.22	1.03	1.085	0.98
	4	207.17	R410A	33.65	2.74	1.161	0.93
	5	210.61	R410A	33.44	4.46	1.272	0.91
H	11	201.35	R410A	37.25	0.00	1.000	1.00
	12	206.16	R410A	37.83	0.53	1.062	0.99
	13	205.71	R410A	38.20	0.92	1.101	0.98
	14	208.62	R410A	38.07	2.63	1.182	0.93
	15	207.94	R410A	38.54	4.81	1.262	0.92
I	21	200.82	R410A	48.87	0.00	1.000	1.00
	22	199.00	R410A	47.00	0.53	1.022	0.99
	23	200.70	R410A	46.79	1.01	1.070	0.97
	24	198.92	R410A	47.33	2.82	1.105	0.95
	25	199.97	R410A	47.75	4.53	1.150	0.92
J	6	333.56	R410A	32.36	0.00	1.000	1.00
	7	308.02	R410A	32.89	0.44	1.084	0.99
	8	338.35	R410A	33.12	0.99	1.111	0.98
	9	300.06	R410A	31.96	2.64	1.224	0.97
	10	288.29	R410A	32.57	4.42	1.296	0.95
K	16	353.73	R410A	37.30	0.00	1.000	1.00
	17	351.66	R410A	37.11	0.52	1.303	0.98
	18	347.29	R410A	36.10	1.04	1.283	0.99
	19	347.45	R410A	37.15	2.65	1.514	0.94
	20	349.27	R410A	37.89	4.63	1.823	0.89
L	26	349.69	R410A	48.00	0.00	1.000	1.00
	27	346.24	R410A	48.24	0.43	1.027	1.00
	28	347.01	R410A	48.59	1.04	1.077	0.99
	29	349.55	R410A	49.48	2.32	1.150	0.95
	30	316.48	R410A	48.92	4.77	1.353	0.95

Series	Test No.	Mass flow rate	Refrigerant	Ref. saturation temperature (°F)	OMF	PDF	HTF
S	31	354.36	R410A	39.79	0.00	1.000	1.00
	32	355.23	R410A	39.65	0.82	1.110	1.00
	33	354.57	R410A	39.58	2.44	1.242	0.96
T	34	356.36	R410A	39.87	0.00	1.000	1.00
	35	355.29	R410A	39.48	0.82	1.087	0.99
	36	355.89	R410A	39.76	2.66	1.234	0.97
U	37	357.86	R410A	38.98	0.00	1.000	1.00
	38	356.70	R410A	38.76	0.92	1.138	0.99
	39	357.36	R410A	39.22	2.82	1.211	0.95

VITA

Sarath Kumar Mulgurthi

Candidate for the Degree of

Master of Science

Thesis: OIL RETENTION AND ITS EFFECTS ON PRESSURE DROP AND HEAT TRANSFER IN MICROCHANNEL EVAPORATORS OF AIR CONDITIONING AND REFRIGERATION SYSTEMS

Major Field: Mechanical and Aerospace Engineering

Biographical: Born in Bhimavaram, Andhra Pradesh, India

Education:

Completed the requirements for the Master of Science in Mechanical and Aerospace Engineering at Oklahoma State University, Stillwater, Oklahoma in December, 2015.

Completed the requirements for the Bachelor of Technology in Mechanical Engineering at Vellore Institute of Technology, Vellore, India in 2012.

Experience:

- Graduate Research Assistant at Oklahoma State University Psychrometric Chamber laboratory.
- Graduate Teaching Assistant at Mechanical and Aerospace Engineering, Oklahoma State University

Professional Memberships:

- American Society of Heating, Refrigeration and Air-conditioning Engineers (ASHRAE).